

# REPORT DOCUMENTATION PAGE

Form Approved  
OMB No. 0704-0188

Public reporting burden for this collection of information is estimated to average 1 hour per response, including the time for reviewing instructions, searching existing data sources, gathering and maintaining the data needed, and completing and reviewing the collection of information. Send comments regarding this burden estimate or any other aspect of this collection of information, including suggestions for reducing this burden, to Washington Headquarters Services, Directorate for Information Operations and Reports, 1215 Jefferson Davis Highway, Suite 1204, Arlington, VA 22202-4302, and to the Office of Management and Budget, Paperwork Reduction Project (0704-0188), Washington, DC 20503.

1. AGENCY USE ONLY (Leave blank)		2. REPORT DATE <i>9 Dec 96</i>	3. REPORT TYPE AND DATES COVERED	
4. TITLE AND SUBTITLE <i>Numerical Studies of the Georgia Coast Sea Breeze</i>			5. FUNDING NUMBERS	
6. AUTHOR(S) <i>Douglas A. Tunney</i>				
7. PERFORMING ORGANIZATION NAME(S) AND ADDRESS(ES) <i>Florida State University</i>			8. PERFORMING ORGANIZATION REPORT NUMBER <i>96-083</i>	
9. SPONSORING / MONITORING AGENCY NAME(S) AND ADDRESS(ES) DEPARTMENT OF THE AIR FORCE AFIT/CI 2950 P STEET, BLDG 125 WRIGHT-PATTERSON AFB OH 45433-7765			10. SPONSORING / MONITORING AGENCY REPORT NUMBER	
11. SUPPLEMENTARY NOTES				
12a. DISTRIBUTION / AVAILABILITY STATEMENT <i>Unlimited</i>			12b. DISTRIBUTION CODE	
13. ABSTRACT (Maximum 200 words)				
14. SUBJECT TERMS			15. NUMBER OF PAGES <i>166</i>	
			16. PRICE CODE	
17. SECURITY CLASSIFICATION OF REPORT	18. SECURITY CLASSIFICATION OF THIS PAGE	19. SECURITY CLASSIFICATION OF ABSTRACT	20. LIMITATION OF ABSTRACT	

## GENERAL INSTRUCTIONS FOR COMPLETING SF 298

The Report Documentation Page (RDP) is used in announcing and cataloging reports. It is important that this information be consistent with the rest of the report, particularly the cover and title page. Instructions for filling in each block of the form follow. It is important to *stay within the lines* to meet *optical scanning requirements*.

### Block 1. Agency Use Only (Leave blank).

**Block 2. Report Date.** Full publication date including day, month, and year, if available (e.g. 1 Jan 88). Must cite at least the year.

**Block 3. Type of Report and Dates Covered.** State whether report is interim, final, etc. If applicable, enter inclusive report dates (e.g. 10 Jun 87 - 30 Jun 88).

**Block 4. Title and Subtitle.** A title is taken from the part of the report that provides the most meaningful and complete information. When a report is prepared in more than one volume, repeat the primary title, add volume number, and include subtitle for the specific volume. On classified documents enter the title classification in parentheses.

**Block 5. Funding Numbers.** To include contract and grant numbers; may include program element number(s), project number(s), task number(s), and work unit number(s). Use the following labels:

<b>C</b> - Contract	<b>PR</b> - Project
<b>G</b> - Grant	<b>TA</b> - Task
<b>PE</b> - Program Element	<b>WU</b> - Work Unit Accession No.

**Block 6. Author(s).** Name(s) of person(s) responsible for writing the report, performing the research, or credited with the content of the report. If editor or compiler, this should follow the name(s).

**Block 7. Performing Organization Name(s) and Address(es).** Self-explanatory.

**Block 8. Performing Organization Report Number.** Enter the unique alphanumeric report number(s) assigned by the organization performing the report.

**Block 9. Sponsoring/Monitoring Agency Name(s) and Address(es).** Self-explanatory.

**Block 10. Sponsoring/Monitoring Agency Report Number.** (If known)

**Block 11. Supplementary Notes.** Enter information not included elsewhere such as: Prepared in cooperation with...; Trans. of...; To be published in.... When a report is revised, include a statement whether the new report supersedes or supplements the older report.

**Block 12a. Distribution/Availability Statement.** Denotes public availability or limitations. Cite any availability to the public. Enter additional limitations or special markings in all capitals (e.g. NOFORN, REL, ITAR).

**DOD** - See DoDD 5230.24, "Distribution Statements on Technical Documents."

**DOE** - See authorities.

**NASA** - See Handbook NHB 2200.2.

**NTIS** - Leave blank.

**Block 12b. Distribution Code.**

**DOD** - Leave blank.

**DOE** - Enter DOE distribution categories from the Standard Distribution for Unclassified Scientific and Technical Reports.

**NASA** - Leave blank.

**NTIS** - Leave blank.

**Block 13. Abstract.** Include a brief (*Maximum 200 words*) factual summary of the most significant information contained in the report.

**Block 14. Subject Terms.** Keywords or phrases identifying major subjects in the report.

**Block 15. Number of Pages.** Enter the total number of pages.

**Block 16. Price Code.** Enter appropriate price code (*NTIS only*).

**Blocks 17. - 19. Security Classifications.** Self-explanatory. Enter U.S. Security Classification in accordance with U.S. Security Regulations (i.e., UNCLASSIFIED). If form contains classified information, stamp classification on the top and bottom of the page.

**Block 20. Limitation of Abstract.** This block must be completed to assign a limitation to the abstract. Enter either UL (unlimited) or SAR (same as report). An entry in this block is necessary if the abstract is to be limited. If blank, the abstract is assumed to be unlimited.

THE FLORIDA STATE UNIVERSITY  
COLLEGE OF ARTS AND SCIENCES

NUMERICAL STUDIES OF THE GEORGIA COAST SEA BREEZE

By

DOUGLAS A. TUNNEY

A Thesis submitted to the  
Department of Meteorology  
in partial fulfillment of the  
requirements for the degree of  
Master of Science

Degree Awarded:  
Summer Semester, 1996

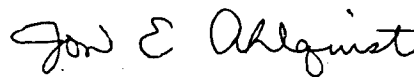
19961212 052

The members of the Committee approve the thesis of Douglas A. Tunney  
defended on June 4, 1996.



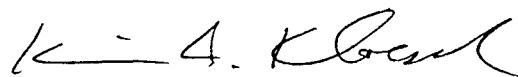
---

Paul H. Ruscher  
Professor Directing Thesis



---

Jon E. Alhquist  
Committee Member



---

Kevin A. Kloesel  
Committee Member

## ACKNOWLEDGMENTS

I would like to express my sincere gratitude to my major professor, Dr. Paul H. Ruscher, for his guidance and support throughout this research project. I would also like to thank my committee members, Dr. Kevin A. Kloesel and Dr. Jon E. Alhquist for their advice and suggestions.

I would like to thank the National Center for Atmospheric Research for super-computing support and for putting up with a graduate student who may have been a little too resourceful in getting computer time. Also, thanks goes to Florida State University's Academic Computing and Network Services for providing computer time for both model executions and post-processing; JT Johnson at the Peachtree City NWS for providing the mesonet data, and Steve Rinard, chief of the Marine Olympic Support Forecast Center, for allowing me to experience first-hand the seaward components of the Wassaw Sound sea breeze.

A special thanks goes to Dr. Chris G. Herbster for putting up with my relentless questioning about the model, computers, meteorology, and life in general. Without his guidance, there would not have been any modeling results to present. He patiently took the time to answer my every question, no matter how ridiculous, and helped make graduate school an enjoyable experience.

I would especially like to thank the U.S. Air Force for providing me the chance to go to graduate school. It *is* a great way of life!

Finally and most importantly, I would like to thank my wife, Kara, and children, Troy and Ashley, for their love, patience, and support throughout this project.

## TABLE OF CONTENTS

	<b>Page</b>
<b>List of Tables</b>	vii
<b>List of Figures</b>	ix
<b>Abstract</b>	xvi
<b>Chapter</b>	
1 <b>Introduction</b>	1
Introduction.....	1
Background.....	2
This Project.....	4
Related Works.....	7
2 <b>Model Description and Set-Up</b>	14
Background.....	14
Model Description.....	14
Model Physics.....	20
Model Set-Up.....	27
Model Runs.....	35
3 <b>Model Results</b>	36
Introduction.....	36
Calm Initialization.....	38
Average Initialization.....	61
Offshore Initialization.....	72
Onshore Initialization.....	79
Alongshore Initialization.....	90
13 August 1995 Initialization.....	103
Discussion.....	126

4	Conclusions	132
	Summary.....	132
	Significant Results.....	139
	Project Short-Comings.....	140
	Future Work.....	141
	<b>Appendix</b>	143
	<b>References</b>	161
	<b>Biographical Sketch</b>	166



## LIST OF TABLES

Table	Page
2.1	Model domain summary..... 29
2.2	Sample FORTRAN output of the average sounding computed from 1082 soundings. Pressure is in mb, temperature is in °C, u and v wind components are in m s <sup>-1</sup> , ddd is in degrees from true north, and ff is in knots. Missing data are indicated by -9999..... 31
2.3	Number and percent of input soundings matching flow criteria. NE is northeast (alongshore), SE is southeast (onshore), SW is southwest (alongshore), and NW is northwest (offshore)..... 33
4.1	Table 4.1. Land breeze finding summary. Avg indicates the average idealization; NW (northwest) the offshore idealization; SE (southeast) the onshore idealization; SW (southwest) and NE (northeast) the alongshore idealizations; and 13 Aug the 13-15 August 1995 simulation. Onset time is defined as the time at which the winds over the Wassaw Sound first have an offshore component. Directions (dir) are degrees from true north and speeds (spd) are in m s <sup>-1</sup> . Initiation point is defined as the point at which the winds first had an offshore competent. Max refers to the time, direction and speed of the strongest land breeze. Landward (seaward) extents are in km and land-spd (sea-spd) is the maximum rate of advance in km hr <sup>-1</sup> of the boundaries of the circulation. Depth is the maximum height to the top of the land breeze in meters and offshore is the depth of the offshore competent of the circulation measured at the shoreline. Decay is defined as the time at which the winds across the Wassaw Sound lose their offshore component. Duration is the total time in hours the circulation existed. A indicates that the event had not occurred by the end of the model run. B indicates the winds backed to assume the land or sea breeze character. D indicates the circulation did not develop. E indicates the land breeze did not develop into a full circulation but still effected the large-scale flow across the area. M indicates the feature was masked by the background flow. V indicates the winds veered to assume the sea or land breeze character..... 136

4.2 Sea breeze finding summary. As in Table 4.1 except onset time is defined as the time at which the winds over the Wassaw Sound first have an onshore component. Initiation point is defined as the point at which the winds first had an onshore component. Max refers to the time, direction and speed of the strongest sea breeze. Decay is defined as the time at which the winds across the Wassaw Sound lose their onshore component.....

## LIST OF FIGURES

Figure	Page
<p>1.1 a (top): Savannah, Georgia's sea breeze season as defined when the mean monthly maximum temperature (solid line) is greater than the mean monthly SST (dashed line) off the Savannah coast. The season lasts from March through October. b (bottom): Savannah's sea breeze window in July as defined when the average hourly temperature (solid line) is greater than the monthly mean SST (dashed line). The window lasts from approximately 0900 through 1900 local time. Derived from the Marine Climatic Atlas of the World (Naval Oceanography Command Detachment Asheville 1992) and the International Station Meteorological Climate Summary (Naval Oceanography Command Detachment Asheville 1992).....</p>	5
<p>1.2 a: Southeastern U.S. showing location of Savannah, Georgia. b: Wassaw Sound, located southeast of Savannah, Georgia, site of the 1996 Summer Olympic Games sailing competition. Race courses are indicated by the hatched circles and dots indicate National Data Buoy Center (NDBC) buoy locations.....</p>	6
<p>1.4 Hourly position of the sea breeze front on 19 March 1968. Solid lines are isochrones (lines of equal time) depicting the location of the sea breeze front at each hour. SAV is Savannah; SVN is Hunter Army Airfield; SSI is Saint Simons Island; NEA is Brunswick; and LIY is Ft Stewart. From Williams 1969.....</p>	10
<p>1.5 As in Figure 1.4 except isochrones depict the average passage times of the sea breeze front across the Project Theo domain computed from 36 sea breeze events from March through May 1968. From Williams 1969..</p>	11
<p>2.1 MM5 modeling system flow chart with arrows representing data flow. Main programs are boxed and data sets represent input into a main program. FDDA is four-dimensional data analysis. DATAGRID inputs coarse resolution analyses from the National Center for Environmental Prediction (NCEP), the Tropical Ocean and Global Atmosphere (TOGA)</p>	

	data set, the European Center for Medium-range Weather Forecasts (ECMWF), or from Unidata. After Grell et al. 1994.....	15
2.2	Representation of the terrain following coordinate system of the MM5. Solid lines represent full sigma-levels and dashed lines represent half-sigma levels. Vertical velocities ( $\bar{\sigma}$ ) are defined on the full-sigma levels while the scalars (a) are defined on the half-sigma levels. K is the layer number, s is the sigma layer, $p_t$ and $p_s$ are the pressure levels at the top and surface of the model. From Grell et al. 1994.....	17
2.3	Representation of the horizontal coordinate system of the MM5. Scalars are defined on the cross points (X) and vectors on the dot points (•). The smaller, inner mesh is representative of a 3:1 coarse to fine grid distance ratio. From Grell et al. 1994.....	18
2.4	Example of MM5 nesting configuration showing four domains with differing levels of nesting and overlap. After Chen et al. 1995 .....	19
2.5	Domain and nest configuration used for all model runs. Domain 1 (D01) has a 36-km mesh, domain 2 (D02) a 12-km mesh, and domain 3 (D03) a 4-km mesh. Sizes are given in Table 2.1.....	28
2.6	Wassaw Sound, Georgia. Arrows depict wind direction for onshore flow (130°), offshore flow (310°), and alongshore flows (40° and 220°) used develop to soundings representative of those regimes.....	32
3.1	a: Thermodynamic profile used to initialize the calm and average idealizations. Wind barbs are in knots. For the calm run, the wind field was set to zero. b: Solid line depicts the location of the cross-sectional analysis used in the 4-km domain. The line bisects the Wassaw Sound as it crosses the shoreline.....	39
3.2	a: As in Figure 3.1b, except for the 12-km domain. b: As in Figure 3.1b, except for the 36-km domain.....	40
3.3	a: 01/03 UTC wind field from the lowest sigma level (0.995, 40 m above MSL) of the model for the 4-km domain. Wind strength is indicated by relative size of the vector. Solid lines are isotachs with a contour interval of 2.5 m s <sup>-1</sup> . Embedded numbers in the field indicate wind speed maxima and minima. b: 01/03 UTC cross-sectional analysis along the solid line depicted in Figure 3.1a. View is towards the northeast; land is to the left and water is to the right, with the shoreline located at the midpoint of the horizontal axis. Vertical axis is pressure in mb, solid lines are contours of mixing ratio (isohumes) in g kg <sup>-1</sup> with an interval of two,	

	arrows represent circulation vectors in the cross-sectional plane with strength indicated by relative size, and the line below figure is a representative distance of 100 km.....	41
3.4	a: As in Figure 3.3a except for 01/12 UTC. b: As in Figure 3.3b except for 01/12 UTC.....	42
3.5	a: As in Figure 3.3a except for 01/13 UTC. b: As in Figure 3.3b except for 01/13 UTC.....	44
3.6	a: As in Figure 3.3a except for 01/14 UTC. b: As in Figure 3.3b except for 01/14 UTC.....	45
3.7	a: As in Figure 3.3a except for 01/15 UTC. b: As in Figure 3.3b except for 01/15 UTC.....	46
3.8	a: As in Figure 3.3a except for 01/17 UTC. b: As in Figure 3.3b except for 01/17 UTC.....	48
3.9	a: As in Figure 3.3a except for 01/19 UTC. b: As in Figure 3.3b except for 01/19 UTC.....	50
3.10	a: As in Figure 3.3a except for 01/21 UTC. b: As in Figure 3.3b except for the 12-km domain at 01/21 UTC along the solid line depicted in Figure 3.2a.....	51
3.11	a: As in Figure 3.3a except for the 12-km domain at 01/21 UTC. b: 01/22 UTC cross-sectional analysis along the solid line depicted in Figure 3.2a. Arrows represent circulation vectors in the cross-sectional plane with strength indicated by relative size and lines are isotachs of wind speed tangential to the cross section. Solid (dashed) lines are offshore (onshore) flow with a contour interval of $1 \text{ m s}^{-1}$ .....	52
3.12	a: As in Figure 3.3a except for 02/08 UTC.....	54
3.13	a: As in Figure 3.3a except for 02/10 UTC. b: As in Figure 3.3b except for 02/10 UTC.....	55
3.14	a: As in Figure 3.3a except for 02/15 UTC. b: As in Figure 3.3b except for 02/15 UTC.....	56
3.15	a: As in Figure 3.3a except for 02/17 UTC. b: As in Figure 3.3a except for 02/20 UTC.....	57

3.16	a: As in Figure 3.10b except for 02/20 UTC. b: As in Figure 3.11b except for 02/22 UTC.....	59
3.17	a: Pressure and temperature analysis for the 36-km domain at 01/20 UTC. Solid lines are pressure with a contour interval of 2 mb and dashed lines are temperature with a contour interval of 2 °C. b: As in Figure 3.17a except for 02/10 UTC.....	60
3.18	a: As in Figure 3.3a except for 01/12 UTC. b: As in Figure 3.3b except for 01/12 UTC.....	63
3.19	a: As in Figure 3.3a except for 01/15 UTC. b: As in Figure 3.3a except for 02/16 UTC.....	64
3.20	a: As in Figure 3.17a except for the calm idealization at 01/15 UTC. b: As in Figure 3.17a except for the average idealization at 01/15 UTC...	66
3.21	a: As in Figure 3.3a except for 01/21 UTC. b: As in Figure 3.10b except for 01/20 UTC.....	67
3.22	a: As in Figure 3.3a except for 36-km domain at 01/23 UTC. b: As in Figure 3.3a except for 02/10 UTC.....	68
3.23	a: As in Figure 3.17a except for the 4-km domain at 01/12 UTC with a pressure contour interval of 0.25 mb and a temperature contour interval of 0.25 °C . b: As in Figure 3.24a except for 02/12 UTC.....	70
3.24	a: As in Figure 3.3a except for 02/16 UTC. b: As in Figure 3.3b except for 02/16 UTC.....	71
3.25	a: Thermodynamic and wind profile used to initialize the offshore idealization. Wind barbs are in knots. b: As in Figure 3.3a except for 01/00 UTC.....	73
3.26	a: As in Figure 3.17a except for 01/11 UTC. b: As in Figure 3.23a except for 01/11 UTC.....	75
3.27	a: As in Figure 3.23a except for 01/15 UTC. b: As in Figure 3.3a except for 01/15 UTC.....	76
3.28	a: As in Figure 3.3a except for 01/21 UTC. b: As in Figure 3.10b except for 01/20 UTC.....	77

3.29	a: As in Figure 3.11b except for 01/20 UTC. b: As in Figure 3.3a except for 02/17 UTC.....	78
3.30	a: As in Figure 3.23a except for 02/17 UTC. b: As in Figure 3.3b except for 02/19 UTC.....	80
3.31	a: As in Figure 3.3b except for 02/20 UTC. b: Precipitation in cm across the 4-km domain for day one of the simulation.....	81
3.32	a: As in Figure 3.25a except for onshore idealization. b: As in Figure 3.3a except for 01/00 UTC.....	82
3.33	a: As in Figure 3.17a except for 01/11 UTC. b: As in Figure 3.23a except for 01/11 UTC.....	84
3.34	a: As in Figure 3.23a except for 01/16 UTC. b: As in Figure 3.3b except for 01/16 UTC.....	85
3.35	a: As in Figure 3.11b except for the 4-km domain at 01/18 UTC. b: As in Figure 3.10b except for 01/20 UTC.....	86
3.36	a: As in Figure 3.23a except for 02/11 UTC. b: As in Figure 3.35a except for 02/11 UTC.....	88
3.37	a: As in Figure 3.3b except for 02/11 UTC. b: As in 3.3a except for 02/21 UTC.....	89
3.38	a: As in Figure 3.25a except for southwest alongshore initialization. b: As in Figure 3.25a except for northeast alongshore initialization.....	91
3.39	a: As in Figure 3.3a except for 01/00 UTC. b: As in Figure 3.23a except for 01/11 UTC.....	92
3.40	a: As in Figure 3.35a except for 01/12 UTC. b: As in Figure 3.3b except for 01/12 UTC.....	94
3.41	a: As in Figure 3.3a except for 01/20 UTC. b: As in Figure 3.10b except for 01/20 UTC.....	95
3.42	a: As in Figure 3.23a except for 02/11 UTC. b: As in Figure 3.3a except for 02/17 UTC.....	97
3.43	a: As in Figure 3.3a except for 02/20 UTC. b: As in Figure 3.10b except for 02/21 UTC.....	98

3.44	a: As in Figure 3.3a except for 01/00 UTC. b: As in Figure 3.23a except for 01/11 UTC.....	99
3.45	a: As in Figure 3.3b except for 01/12 UTC. b: As in Figure 3.3a except for 01/20 UTC.....	101
3.46	a: As in Figure 3.10b except for 01/22 UTC. b: As in Figure 3.3a except for 02/11 UTC.....	102
3.47	a: As in Figure 3.35a except for 02/11 UTC. b: As in Figure 3.11b except for 02/22 UTC.....	104
3.48	Observational mesonet sites found within the approximate bounds of the 4-km domain. Numbers refer to site locations given in the Appendix.....	106
3.49	a: 500 mb chart for 13 August 1995 at 0000 UTC. b: Surface chart for 13 August 1995 at 0000 UTC.....	107
3.50	a: 500 mb chart for 15 August 1995 at 0000 UTC. b: Surface chart for 15 August 1995 at 0000 UTC.....	108
3.51	a: As in 3.25a except for CHS on 13 August 1995 at 0000 UTC. b: As in Figure 3.3a except for 13/00 UTC.....	110
3.52	a: As in Figure 3.3a except for 13/12 UTC. b: As in Figure 3.3a except for 13/12 UTC.....	111
3.53	a: Modeled 13 August 1995 1200 UTC sounding for CHS. b: Observed 13 August 1995 1200 UTC sounding for CHS.....	112
3.54	a: As in Figure 3.3a except for 13/15 UTC. b: As in Figure 3.3a except for 13/16 UTC.....	114
3.55	a: As in Figure 3.3a except for 13/20 UTC. b: As in Figure 3.3b except for 13/21 UTC.....	115
3.56	As in Figure 3.35a except for 13/21 UTC.....	116
3.57	a: As in Figure 3.53a except for 14 August 1995 at 0000 UTC. b: As in Figure 3.53b except for 14 August 1995 at 0000 UTC.....	119
3.58	a: As in Figure 3.3a except for 14/12 UTC. b: As in Figure 3.3b except for 14/11 UTC.....	120



3.59	a: As in Figure 3.53a except for 14 August 1995 at 1200 UTC. b: As in Figure 3.53b except for 14 August 1995 at 1200 UTC.....	122
3.60	a: As in Figure 3.3a except for 14/17 UTC. b: As in Figure 3.3a except for 14/18 UTC.....	123
3.61	a: As in Figure 3.23a except for 14/15 UTC. b: As in Figure 3.23a except for 13/16 UTC.....	124
3.62	a: As in Figure 3.3a except for 14/21 UTC. b: As in Figure 3.35a except for 14/21 UTC.....	125

## ABSTRACT

This study presents a numerical examination of the land and sea breeze system (LSBS) that develops in the Wassaw Sound, located southeast of Savannah, Georgia and site of the 1996 Summer Olympic Games sailing competition. The project used the Pennsylvania State University/National Center for Atmospheric Research Mesoscale Model version 5 to simulate the diurnal circulations that evolve in the Wassaw Sound under varying flow regimes. Model runs were designed to examine the initiation, development, intensity, duration, and decay of the LSBS, with emphasis on the seaward component of the circulation.

Thermodynamic and wind profiles used for model initialization were compiled from 1082 Charleston, South Carolina soundings from 1946 to 1992 for the period 15 July through 15 August. Idealized model runs were conducted with all domains initialized to represent either calm, average, onshore, offshore, or alongshore wind profiles developed from the sounding data.

Idealized model output showed that under weak forcing, there is a clear transition from the land breeze to the sea breeze and that as the land breeze decays, it migrates seaward as the sea breeze forms at the shoreline. Under stronger forcing that does not allow the full development of the land breeze, winds either veer or back to assume sea

breeze character. As the sea breeze matures, the return flow and its associated subsidence region compact the marine planetary boundary layer. Seaward, the boundary of the circulation advances faster than the landward edge.

The modeled average land breeze initiated by 1000 UTC at the shoreline blowing at less than 1 meters per second ( $\text{m s}^{-1}$ ), reached a maximum speed of slightly greater than  $1 \text{ m s}^{-1}$  from 320 degrees by 1200 UTC, had an offshore depth of 150 meters (m), a maximum depth of 1000 m, a seaward extent of 6 kilometers (km), a landward extent of 9 km, and decayed after 1300 UTC. The modeled average sea breeze initiated by 1600 UTC at the shoreline with a speed of  $2.5 \text{ m s}^{-1}$  flowing from 150 degrees, reached a maximum speed of  $6.5 \text{ m s}^{-1}$  from  $160^\circ$  by 2000 UTC, had an onshore depth of 400 m, a maximum depth of 2300 m, a landward extent of 75 km, a seaward extent of 110 km, and decayed after 0100 UTC.

To test the model set-up, a real case model run was conducted to simulate LSBS that developed across the Wassaw Sound 13-15 August 1995. Available observations from across the area agreed well with model output.

# CHAPTER 1

## INTRODUCTION

### Introduction

The sea breeze is a well known, often studied mesoscale meteorological phenomenon. This is primarily due to the repetitive nature of the event, occurring almost daily during the summer months at most coastal locations. This makes it relatively easy to study and gather data because it is geographically tied to the land-water boundaries and its signature is usually readily distinguishable in the data.

Instrumented observational studies of the sea breeze date back to the late 1800s when Sherman measured the height and strength of the sea breeze from a manned hot-air balloon over Coney Island, New York for a two week period in July and August, 1879 (Sherman 1880). Numerical studies date back to the 1950s when Pearce (1955) used a 2D, nonlinear model to examine the sea breeze circulation in an isothermal, statically-stable atmosphere with differential heating along a straight coastline. Today, modern observational researchers do not have to rely on manned balloons to gather data. Instead they have access to Doppler radar output, high resolution satellite imagery, upper air soundings, and station observations to perform their studies. Numerical modelers now have a choice of models

to use. Modern mesoscale models allow tailoring of the physics package, permit nonhydrostatic runs and produce realistic outputs. These outputs can then be verified using the observational data mentioned above.

## **Background**

### **Early Modelers**

Many researchers have used numerical models to examine the sea breeze since Pearce in 1955. As computing power and knowledge grew, successive modelers improved upon the previous by adding more parameters to the model or making models more realistic. For example, Estoque (1961) performed several modeling studies using a 2D, two-layer model to study the sea breeze under idealized conditions. In 1962, he improved the model and studied the sea breeze under various flow regimes with differing thermal stratifications. MacPherson (1970) further improved Estoque's model by extending it into three dimensions and Lambert (1974) again used the model but decreased the grid spacing and shortened the time step. A list of early modelers is provided in Pielke (1984).

### **Modern Modelers**

Modern modelers use multileveled, 2D or 3D models with complex physics packages to allow them to realistically model the sea breeze. For example, Pielke (1974) used a 3D, eight-level model to simulate the sea breeze over South Florida. He then compared his outputs to both radar plots and satellite shots and found that the sea breeze induced convergence was the primary control mechanism for the observed cloud and precipitation patterns on synoptically undisturbed days.

Following Pielke, numerical researchers investigated many aspects of the sea breeze. For example, they have examined the sea breeze front (Neumann and Mahrer 1974), the effect of coastal shape on the evolution of the sea breeze (Abbs 1986; Herbster 1996), the interaction between the sea breeze and convection (Nicholls et al 1991), the influence of large-scale winds on the sea breeze circulation (Bechtold et al 1991; Arritt 1993), the effects of wind shear (Cautenet and Rosset 1989), the interaction between two sea breezes (Itoh and Sugimura 1989), the effects of varying SST on the sea breeze (Mahrer 1985), the influence of coastal topography and complexity on the sea breeze (Mahrer and Pielke 1977; Steyn and McKendrt 1988; Zhong and Takle 1993), the sea breeze effects on coastal pollution transport (Lu and Turco 1993; Segal et al 1982), the effect of latitude on the sea breeze (Yan and Anthes 1987), the inland penetration of the sea breeze (Physick 1980), and the effects of land width on the development of the sea breeze (Xian and Pielke 1991). Both Pielke (1984) and Simpson (1994) present a review of modern sea breeze modeling.

The results of this intense numerical modeling have greatly increased our understanding of the sea breeze circulation. To date though, most numerical and observational studies have concentrated on the landward portion of the sea breeze circulation. Little attention has been paid to the seaward portion of the circulation primarily due to the difficulty and expense in gathering over-water data for study and model verification. Yet it is this seaward portion of the sea breeze that often has a direct impact on transportation and circulation of pollution in coastal areas, directly affects shipping and sailing interests, and influences forecasting in coastal regions.

Further, perhaps the most favored location for sea breeze studies is the Florida peninsula (Gould 1993). Georgia, located just to its north, generally experiences the same large-scale flow patterns (Blanchard and Lopez 1985) but it offers only one coastal sea breeze to Florida's two. Georgia does have an active and long sea breeze season however (Figure 1.1), yet little research has been done on its circulations.

## **This Project**

### **Overview**

This project is a numerical modeling study of the land and sea breeze system (LSBS) that develops along the northern Georgia coast using the Penn State University/National Center for Atmospheric Research Mesoscale Model version 5 (PSU/NCAR MM5). This area was chosen because the 1996 Olympic Sailing Venue will be held in the coastal waters off Savannah, Georgia in July and August of 1996. As a result, this research will concentrate on that geographic area (Figure 1.2a) and the results produced will be used by the National Weather Service (NWS) at the Marine Olympic Support Forecast Center (Rinard 1996) during the 1996 Olympic Games.

### **Goals**

The intent of this modeling study is to develop an understanding of the initiation, development, intensity, duration, and decay of the LSBS in the vicinity of the Wassaw Sound (Figure 1.2b), where the sailing races will be held, with a particular emphasis on the seaward component of the circulation. This will aid the NWS in providing weather support for the sailing competition and increase our knowledge of the little studied, seaward portion of the circulation.

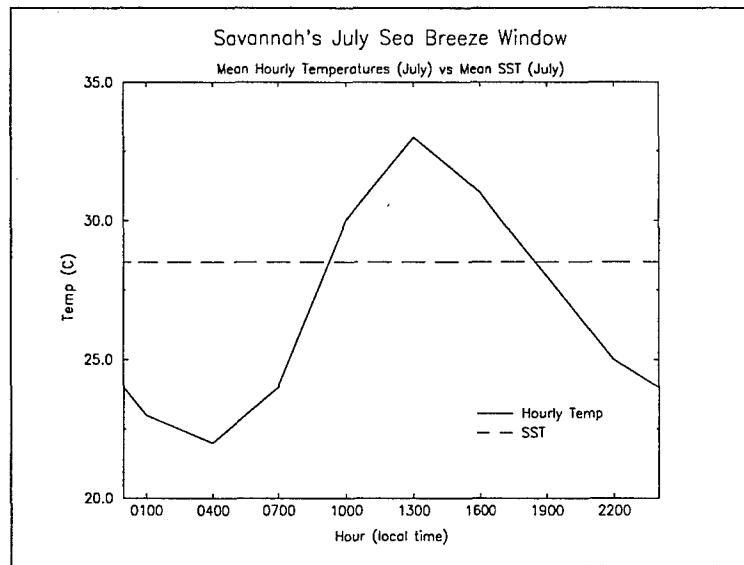
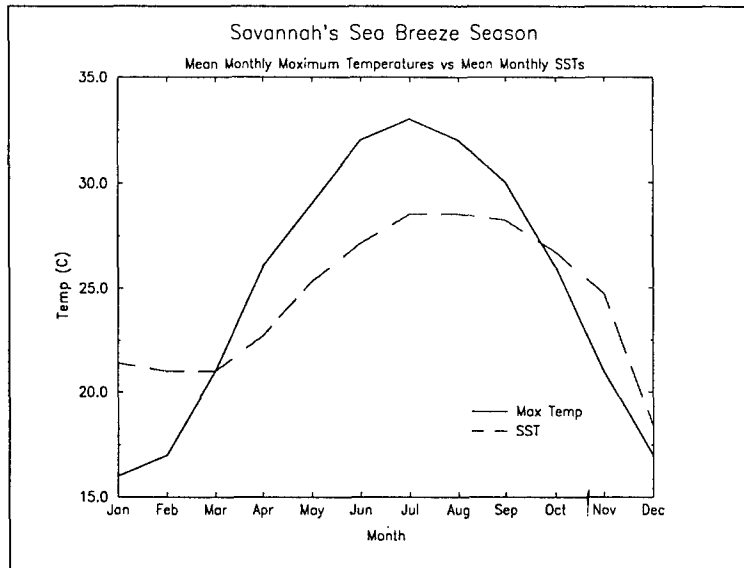


Figure 1.1. a (top): Savannah, Georgia's sea breeze season as defined when the mean monthly maximum temperature (solid line) is greater than the mean monthly SST (dashed line) off the Savannah coast. The season lasts from March through October. b (bottom): Savannah's sea breeze window in July as defined when the average hourly temperature (solid line) is greater than the monthly mean SST (dashed line). The window lasts from approximately 0900 through 1900 local time. Derived from the Marine Climatic Atlas of the World (Naval Oceanography Command Detachment Asheville 1992) and the International Station Meteorological Climate Summary (Naval Oceanography Command Detachment Asheville 1992).



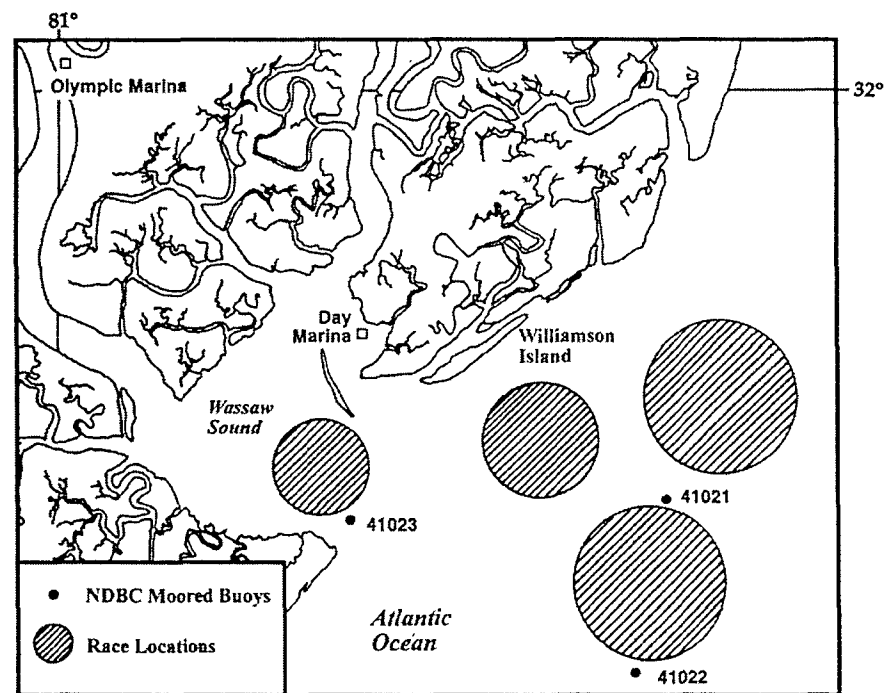
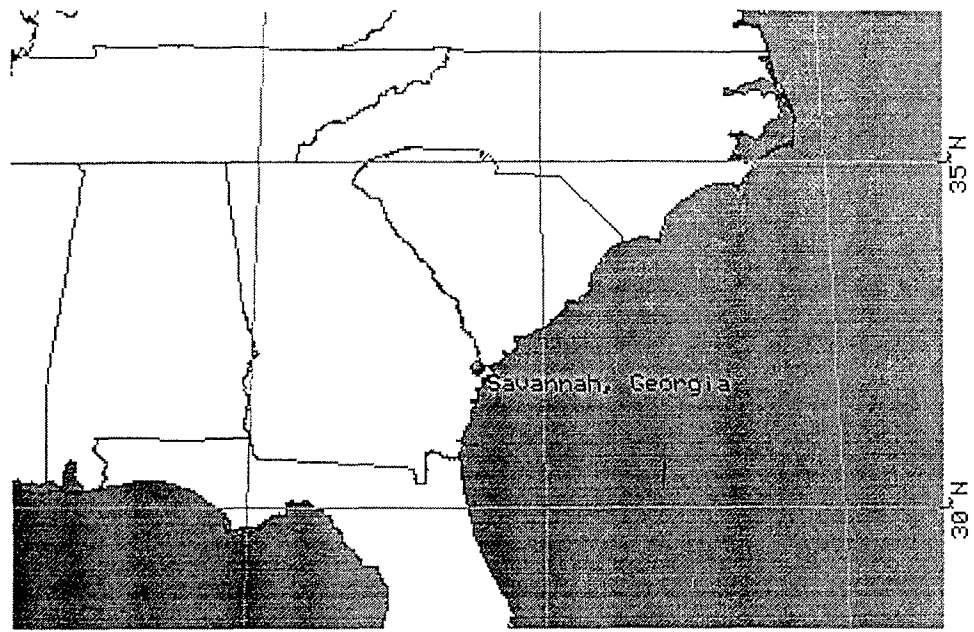


Figure 1.2. a: Southeastern U.S. showing location of Savannah, Georgia. b: Wassaw Sound, located southeast of Savannah, Georgia, site of the 1996 Summer Olympic Games sailing competition. Race courses are indicated by the hatched circles and dots indicate National Data Buoy Center (NDBC) buoy locations.

## **Methodology**

To gain this knowledge, the MM5 model was initialized with various flow regimes to simulate an average flow, onshore flow, offshore flow and alongshore flows. The model was executed with identical set-ups which should ensure the differing outputs observed are the results of varying the large-scale flow. In addition, the model was tested by performing a run to simulate the LSBS that developed on 13 August 1995. The model output was then compared to observed conditions. The model description, set-up, and initialization are discussed in the following chapter.

## **Related Works**

### **Observational Studies**

In general, few observational studies of the LSBS emphasize the seaward component. Most references to this portion of the circulation come from researchers whose primary work centered on the landward side of the circulation. Pielke (1984) does present a list of works that mention the seaward extension of the sea breeze.

In Wexler's (1946) discussion of the horizontal characteristics of the sea breeze circulation, he notes that the Southern California sea breeze has been detected 100 km offshore. He attributes this great distance to a combination of the sea breeze and strong valley winds. In England, the sea breeze was found to extend up to 15 km offshore and off the Baltic coast, it extended 8 km.

Meyer (1971) performed a radar study of the land breeze off the Virginia coast. From his analysis of radar data, the land breeze circulation extended offshore from 19-22 km, the land breeze front moved seaward at approximately  $3 \text{ km hr}^{-1}$ , and the total depth

of the circulation was approximately 1000 m. Meyer also noted the land breeze front can be the focus of nocturnal thunderstorms, and as the sea breeze returns the following day, the land breeze front recedes toward land and dissipates.

Lindsey et al. (1996) describe the LSBS that occurred over the northwestern Gulf of Mexico during the period April through October 1993 and its implications on the region's air quality. Using a network of wind profilers deployed inland, at the shoreline, and seaward off the southeast Texas and Louisiana coasts, they were able to determine the daily structure of the LSBS that developed. From these daily observations, they developed a conceptual model of the LSBS's diurnal cycle in this area of the Gulf. They identified six stages in their conceptual model. Stage 1 was a late afternoon sea breeze such that both offshore and onshore observing stations reported steady onshore flow. Stage 2 occurred early the following morning and was characterized by offshore winds at the inland and shoreline sites but with onshore winds still occurring at the seaward site. Stage 3 occurred when all stations reported offshore wind flow. Stage 4 marked the transition to the sea breeze, with onshore flow first observed at the shoreline site. Offshore flow continued at the stations inland as well as seaward. Stage 5 occurred when the inland stations began reporting onshore flow while the seaward stations still reported offshore flow. Stage 6 was when the seaward station finally reported onshore flow, thus representing the beginning of another stage 1.

Although not a study of the seaward component of the LSBS, Williams (1969) performed the only large-scale research project on the Georgia sea breeze known to this author and the personnel at the Savannah NWS. Williams analyzed data collected at

various U.S. Forest Service sites and reporting stations in southeastern Georgia during the period March through May of 1968. The purpose of his study was to determine timings for sea breeze passage through the area and the impacts of that passage on forest fire behavior for the Forest Service. Williams defined passage of a sea breeze front at a station as a shift in wind direction to the southeast, an increase in wind speed, a fall in temperature, and an increase in humidity. He tracked 36 sea breeze passages during the period and plotted their propagation with isochrones on an area chart (Figure 1.4). His analysis showed the sea breeze could remain offshore the entire day or move quickly through his entire area of study, depending upon the prevailing synoptic conditions. Williams computed the average time (Figure 1.5), the earliest time, and the latest time for passage of the sea breeze through various stations. He found the movement of the sea breeze front to be from  $110^\circ$  at speeds varying from 2 to 15 km hr<sup>-1</sup>.

### **Numerical Studies**

As with observational studies, the bulk of the modeling has concentrated on the landward portion of the sea breeze and again, no research has investigated the Georgia coast LSBS.

Arritt (1989) performed a numerical investigation of the offshore extent of the sea breeze. He used both a 2D and 3D nonlinear mesoscale model to try understand the effects of sea surface temperature, atmospheric stratification, latitude, large-scale forcing, and coastline shape on the offshore extent of the circulation.

First, Arritt varied the SSTs by up to 20 °C and found that the offshore extent of the sea breeze was considerably reduced when the underlying water temperature was

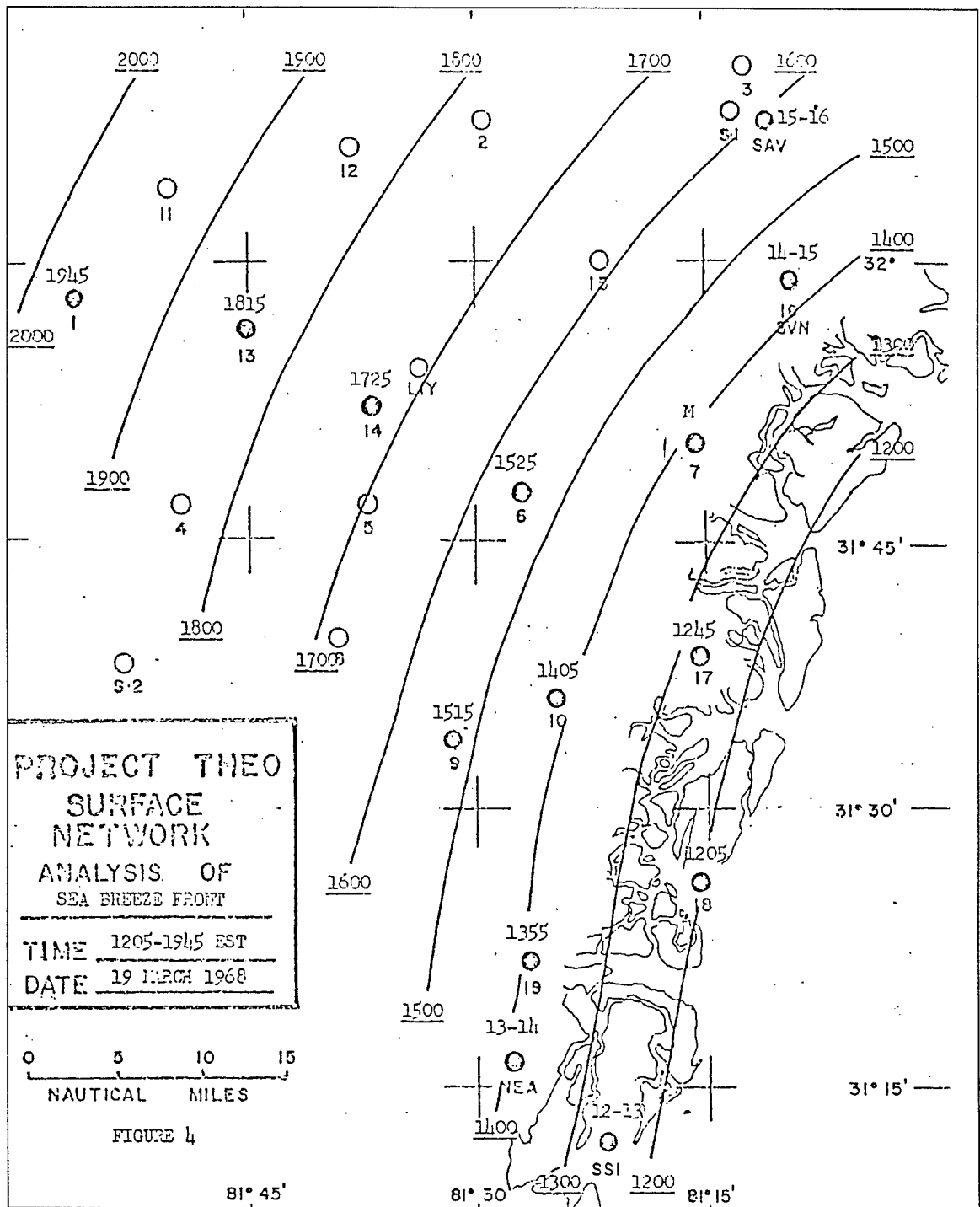


Figure 1.4. Hourly position of the sea breeze front on 19 March 1968. Solid lines are isochrones (lines of equal time) depicting the location of the sea breeze front at each hour. SAV is Savannah; SVN is Hunter Army Airfield; SSI is Saint Simons Island; NEA is Brunswick; and LIY is Ft. Stewart. From Williams 1969.

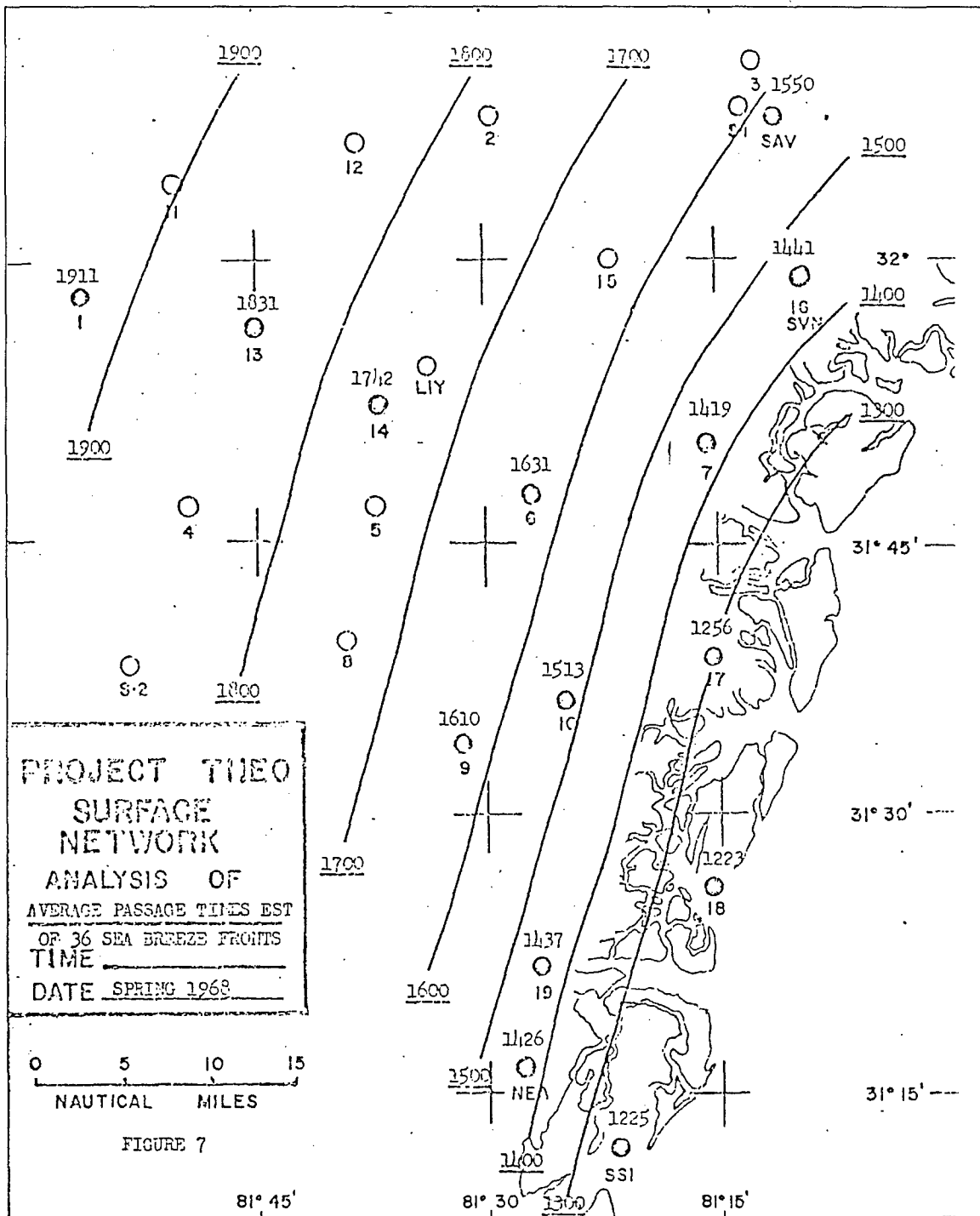


Figure 1.5. As in Figure 1.4 except isochrones depict the average passage times of the sea breeze front across the Project Theo domain computed from 36 sea breeze events from March through May 1968. From Williams 1969.

higher than the overlying air. Next, he examined the effects of low level inversions, like trade wind inversions, on the sea breeze. His results showed that the lower the inversion base, the less the offshore extent of the circulation. Arritt found that the sea breeze phenomenon was sensitive to latitude; the offshore extent was considerably greater at lower latitudes than higher latitudes due to the decrease in the Coriolis force. He also found that for cases of large-scale onshore winds, the seaward extent of the sea breeze was greatly suppressed and when the large-scale flow was offshore, the sea breeze influence was greatly extended. Finally, to consider the effects of a curved coastline, Arritt modeled both a convex and a concave coastal shape. He found that the offshore subsidence was enhanced for a concave coastline and reduced for a convex coastline if the length scale of the coastal irregularity is less than the length scale of the sea breeze circulation, allowing the sea breeze from different parts of the coast to interact.

### **Sailing Support Activities**

As with the observational and numerical studies, there have been few published meteorological studies done in support of regattas or sailing competitions. The NWS Forecast Office in Los Angeles prepared a detailed climatological analysis and made forecasts and observations available for all the race competitors during the 1984 Summer Olympic Games sailing events (Staff 1983). The NWS is again developing such a pamphlet (Garza et al. 1996) for the 1996 Summer Olympic Games sailing events.

Powell (1993) provided similar support for the US Sailing team at the 1991 Pan America Games held in the waters off Havana, Cuba. He did a wind climate analysis for the area, performed trail forecasts prior to the race, and provided race forecasts during the

competition. Powell (1996) is currently developing a similar wind analysis for the 1996 Summer Olympic Games sailing events.

Bedford and Davis (1987) published the only paper on modeling support for a sailing competition known to this author. They describe the modeling efforts used to assist the winning team in the 1987 America's Cup, held in the waters off Freemantle, Australia. Bedford and Davis describe the two models used during the competition: an analog model and a numerical model. The analog model was based on a two-year, large-scale climatology for the region. Forecasters examined the observed pattern and then using a scheme developed to classify flow fields, extracted a data set from the climatological data base that matched the current pattern. This extracted data was then compared to the early morning patterns and those that did not continue to match were removed. This left a data set that closely matched the current conditions. From this, the forecasters could produce an hourly forecast of wind speed and direction for the race.

To improve the resolution of the analog model, the forecasters ran a 2D model similar to Pielke's 1974 model with a 3-km grid spacing and a 60-second time step. This model was found on average to underpredict the wind speed and forecast the onset of the sea breeze too early, but it accurately predicted the wind direction.



## CHAPTER 2

### MODEL DESCRIPTION AND SET-UP

#### Background

This research project used the PSU/NCAR MM5. This model was originally developed at the Pennsylvania State University in the early 1970s and has undergone many changes and improvements at both PSU and NCAR. The current version (MM5v1) has been available for use since 1993 and is the version used for this study.

#### Model Description

The following is a brief overview of the major aspects of the MM5. The information below is summarized from Grell et al. (1994) and Chen et al. (1995), where a much more detailed description of the model is available.

#### MM5 Modeling System

The MM5 is a grid point model with finite differences centered in space and time. The MM5 modeling system consists of the mesoscale model and several additional programs that perform both the preprocessing and postprocessing of the input and output of the model (Figure 2.1). The TERRAIN program (referred to as a deck) is used to build model domains by utilizing archived land-use and terrain-height characteristics. The DATAGRID deck takes coarse resolution data sets such as those from the National

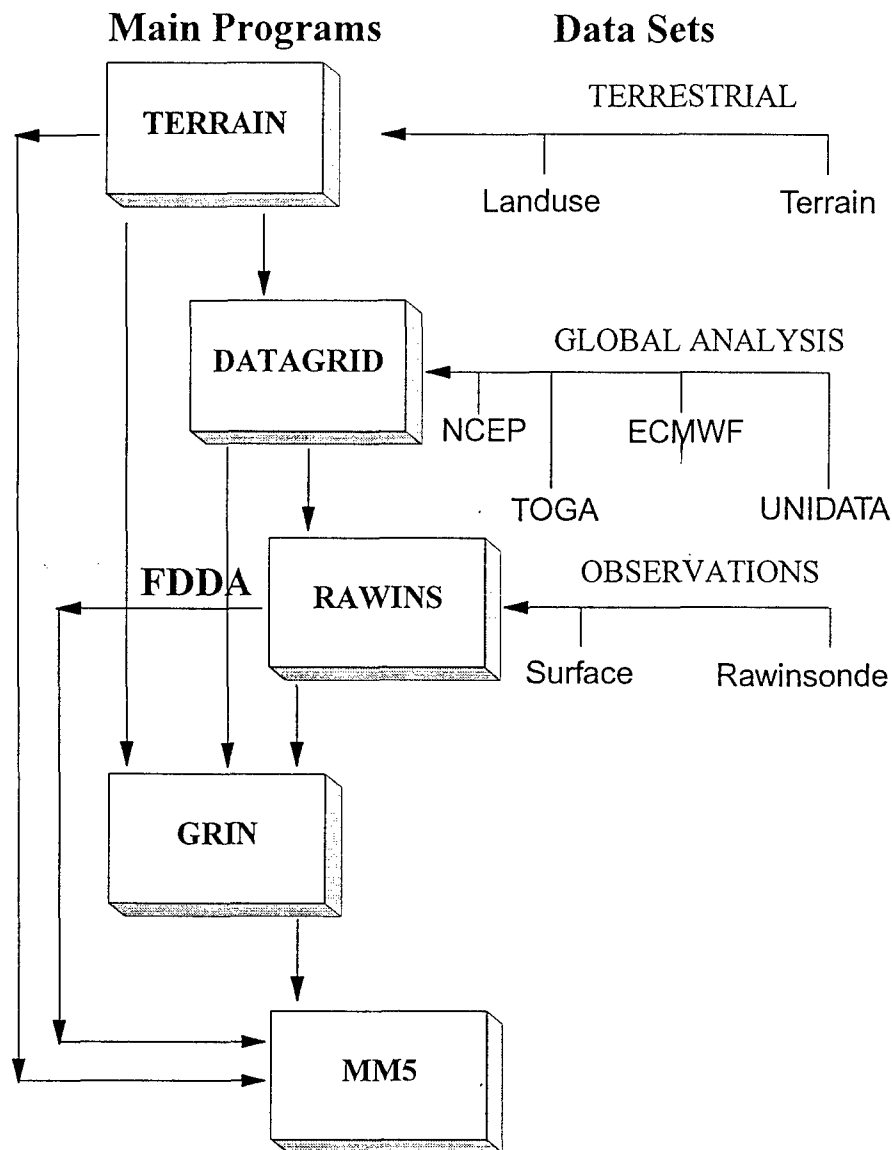


Figure 2.1. MM5 modeling system flow chart with arrows representing data flow. Main programs are boxed and data sets represent input into a main program. FDDA is four-dimensional data analysis. DATAGRID inputs coarse resolution analyses from the National Center for Environmental Prediction (NCEP), the Tropical Ocean and Global Atmosphere (TOGA) data set, the European Center for Medium-range Weather Forecasts (ECMWF), or from Unidata. After Grell et al. 1994.

Center for Environmental Prediction (NCEP) or real time forecasts and horizontally interpolates these analysis to the finer mesoscale grid developed in the TERRAIN deck. The RAWINS deck enhances the coarse grid analysis produced in DATAGRID by performing an objective analysis of the surface and upper-air observations. This produces useful data at regularly spaced data points from the input, irregularly-spaced observations. The GRIN deck takes the output from RAWINS and interpolates the pressure-level analysis to sigma levels, creating the input fields and boundary conditions for the model. Finally, the MM5 model takes these input fields and boundary conditions and produces the forecast. The GRAPH deck is then used to examine the MM5 output fields.

### **Coordinate Systems**

The model uses a terrain-following vertical coordinate system, meaning that the lower levels closely follow the terrain while the upper levels tend to flatten out.

A dimensionless quantity  $\sigma$  (sigma) is used to define the model levels where

$$\sigma = (p - p_t) / (p_s - p_t), \quad (1)$$

and  $p$  is pressure,  $p_t$  is the constant top pressure specified by the user (100 mb in this study), and  $p_s$  is the surface pressure. In this way, a vertical coordinate system is built such that  $\sigma = 1$  at the surface and  $\sigma = 0$  at  $p_t$  (Figure 2.2).

The horizontal grid uses an Arakawa-Lamb B scheme (Arakawa and Lamb 1977), staggering the velocity variables with respect to the scalar variables (Figure 2.3).

Velocity variables (u and v wind components) are defined at the corner of the grid square,

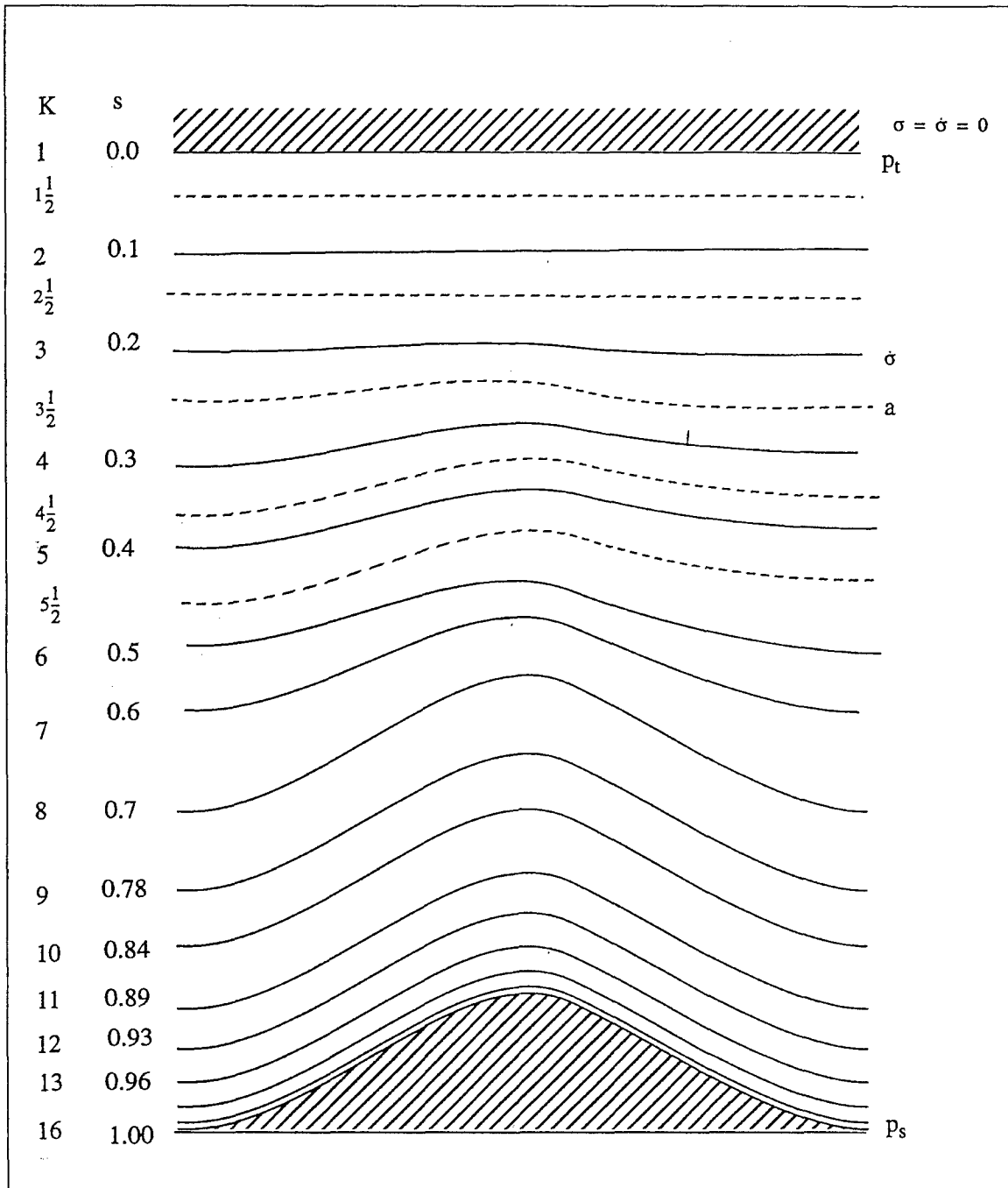


Figure 2.2. Representation of the terrain following coordinate system of the MM5. Solid lines represent full-sigma levels and dashed lines represent half-sigma levels. Vertical velocities ( $\dot{\sigma}$ ) are defined on the full-sigma levels while the scalars (a) are defined on the half-sigma levels. K is the layer number, s is the sigma layer,  $p_t$  and  $p_s$  are the pressure levels at the top and surface of the model. From Grell et al. 1994.

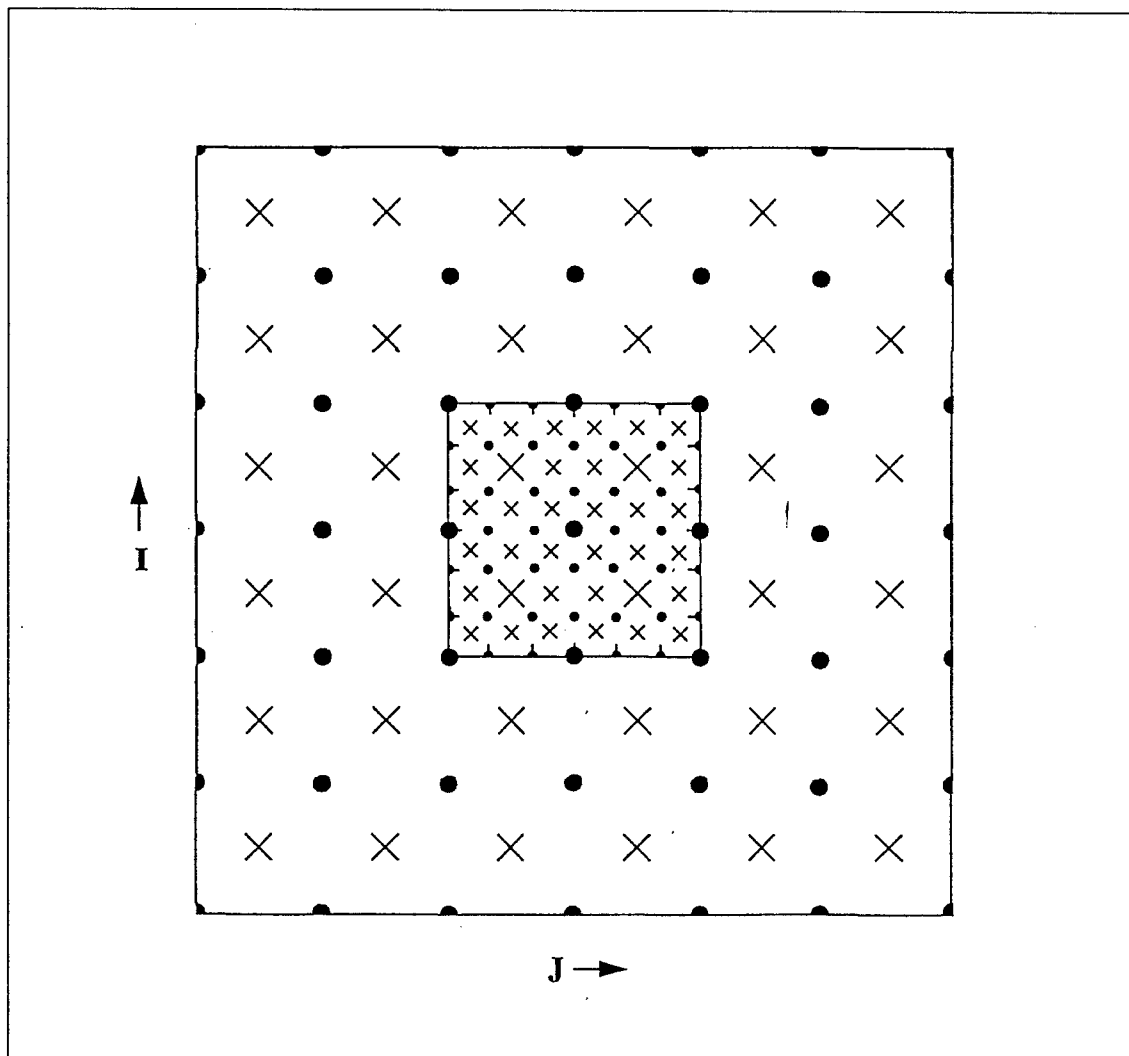


Figure 2.3. Representation of the horizontal coordinate system of the MM5. Scalars are defined on the cross points (X) and vectors on the dot points (•). The smaller, inner mesh is representative of a 3:1 coarse to fine grid distance ratio. From Grell et al. 1994.

referred to as dot points. The scalar variables (temperature, specific humidity) are defined in the center of the grid square, referred to as cross points. All of the horizontal variables are defined on the half-sigma layers. Vertical velocity is defined on the full-sigma levels.

### Nests

The MM5 model has the capability to embed several nests in the larger, coarse domain (Figure 2.4). Each nest is capable of having a two-way interaction meaning the smaller nests input comes via its boundaries with its mother domain while the feedback to the coarser domain occurs through interaction with the nest interior. A nest may be initialized on start-up or interpolated from its parent domain anytime during the model run.

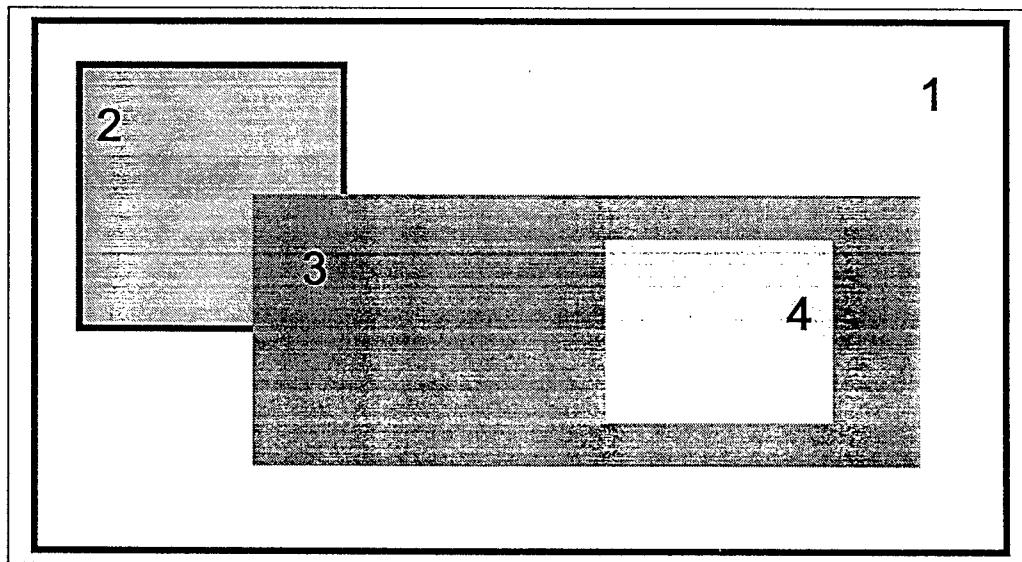


Figure 2.4. Example of MM5 nesting configuration showing four domains with differing levels of nesting and overlap. After Chen et al. 1995.

Nests in the MM5 are built using a 3:1 ratio. For example, if the coarse domain has a grid spacing of 12 km, the next internal nest would have 4-km grid spacing. To keep the solutions from diverging in the two or more nests, the fields in the finer mesh are fed back into the coarser domain every three time steps; the fine mesh takes three times steps and then the coarser mesh takes one. In this way, information is fed back into the larger domain from the smaller nest.

#### **Four Dimensional Data Assimilation**

The MM5 also has the capability to perform four-dimensional data assimilation (FDDA). This allows the model to be spun up and then have additional data inputted. This produces forcing terms which nudge the model toward the input observations or analysis, increasing data resolution and forecast accuracy. Stauffer and Seaman (1990) provide a historical overview and a description of this technique.

#### **Model Physics**

The MM5 has many options for tailoring physics packages to each individual project. Many choices involve choosing between explicit, where the model resolves the process, or nonexplicit, where the model does not resolve the process but parameterizes it. The explicit schemes typically require more memory and more computational time for execution, making the model more expensive to execute.

#### **Hydrostatic and Nonhydrostatic Modes**

The MM5 can be run either in a hydrostatic or nonhydrostatic mode with the determination usually being made by the aspect ratio of the phenomena being examined. If the horizontal scale of the phenomena is shorter than the vertical scale, the

nonhydrostatic version should be used. The nonhydrostatic option induces a vertical acceleration into the equations that contributes to the vertical pressure gradient, so the hydrostatic approximation is no longer valid.

In the nonhydrostatic mode, the model also includes the full 3D effects of the Coriolis force that are usually neglected. In addition to the traditional rightward deflection of horizontal flows in the northern hemisphere, the Coriolis force can lead to a small upward (downward) acceleration on westerly (easterly) flows and a westward (eastward) acceleration on upward (downward) flows.

The nonhydrostatic equations also permit sound waves, which can create numerical instabilities. Because sound waves travel much faster than typical meteorological features, they require a much shorter time step. To prevent numerical instability, the model separates the soundwave terms from those that are slowly varying. Shorter time steps are performed on this new reduced set of equations which only contain interactions between momentum and pressure. The remaining slowly varying equations containing temperature and moisture are updated less frequently as they contain no high frequency terms contributing to sound waves.

### **Moist Processes**

The model has several ways to explicitly resolve moist processes. A simple scheme can be used where supersaturation in a grid box is removed as precipitation. A more complicated scheme allows for the treatment of ice-phase processes. In areas where the temperature is below 0 °C, cloud water is allowed to be cloud ice and rain to become snow. The most sophisticated scheme is built on the above idea but it also adds a



mixed-phase ice scheme which allows supercooled water to exist below 0 °C and snow to exist at temperatures above 0 °C. For researchers not interested in the effects of moist processes, the model also offers the ability to remove the effects of moisture and latent heat release.

### **Cumulus Parameterization**

Cumulus parameterization schemes are necessary to resolve convective clouds smaller than the grid size of the model. With this approach, it is assumed that grid scale properties are different from the convective clouds, forcing the model to parameterize these clouds in terms of its resolvable scale. Incorporating convection is important because it is responsible for a large amount of the precipitation and the fluxes of heat, moisture and momentum that occur in the troposphere on the sub-grid scale. An implicit cumulus parameterization scheme is typically used for grid scales 3 km and larger. For resolutions between 3 and 20 km however, it is possible that the convection could be explicitly and implicitly resolved in the same grid box leading to a double counting of its effects (Pielke and Pearce 1994). This leads to the question of whether a cumulus scheme should be used for these resolutions.

The MM5 has three cumulus parameterization schemes that are used to resolve clouds: Grell, Arakawa-Schubert (AS), and Kuo. The Grell scheme is a simple cloud scheme with up and down drafts and compensating motion. Its main advantage is low computational overhead while its disadvantages are the lack of entrainment or detrainment along the cloud boundaries and all cloud water is converted to rain, which could lead to heavy rainfall. The AS scheme is the most sophisticated and resource

intensive. It offers much of the same features of the Grell scheme but it also allows for varying cloud heights, entrainment/detrainment, suspended liquid water in the clouds, and moist downdrafts. Its main disadvantage is high computational overhead.

The Kuo scheme is the cumulus scheme used in this modeling study. Reasons for its choice will be discussed later in this chapter under Model Set-Up. In this scheme, the amount of convection is determined by vertically integrating the moisture convergence. The Kuo scheme, while not as sophisticated as the AS, does offer entrainment and detrainment and liquid/vapor storage in the column. The Kuo scheme has been shown to yield good results but its main disadvantage is characteristic under-prediction of total precipitation in convective systems (Kuo and Anthes 1984; Grell 1993).

The Kuo scheme used in the MM5 is based on the one described in Anthes 1977. The basic procedure is to first determine the vertically integrated moisture convergence for the column. If that value is greater than the critical threshold value ( $3 \times 10^{-5} \text{ kg m}^{-2} \text{ s}^{-1}$ ), then the column's sounding is checked to see if convection is possible. If so, the cloud top and bottom are determined from the sounding and the amount of precipitation rained out is determined from the column's mean relative humidity. If the mean relative humidity of the column is greater than 50%, then a portion of the integrated moisture convergence is assumed to rain-out. Next, the vertical profiles of heat, moisture, and eddy flux are calculated for the environment inside the cloud. Finally, the cloud's effects on the rest of the grid box are calculated.

The MM5 also can allow shallow convection to occur, either in the planetary boundary layer (PBL) or in a shallow layer in the midtroposphere. This convection is

forced by PBL heat fluxes or by radiational cooling aloft, such as that associated with cloud-top radiational cooling. Shallow convection differs from normal convection in the model as these elements are nonprecipitating and have no convective scale downdrafts.

### **Planetary Boundary Layer Parameterizations**

In PBL, the model has parameterizations for resolving the surface energy balance. For net radiative flux, different schemes are used for clear and cloudy skies. The clear sky algorithm depends on the solar constant, the land's albedo, the sun's zenith angle and shortwave transmissivity to determine the amount of incoming radiation. For cloudy skies, the effects of clouds on both the incoming shortwave and reradiated outgoing longwave radiation are considered. Heat transfer due to molecular conduction is also calculated. Sensible heat and moisture fluxes are calculated in different ways depending on the choice of PBL scheme. The model has two PBL parameterization schemes: the bulk PBL and the Blackadar high-resolution PBL.

**Bulk PBL.** The bulk PBL has coarse resolution in the vertical and two stability regimes, stable and unstable, with the determination between the two being made using the Bulk Richardson number (Ri).

The Ri is given by

$$\text{Ri} = \frac{gz_a}{\theta_a} \frac{\theta_{va} - \theta_{vg}}{V^2} \quad (2)$$

where  $g$  is gravity;  $\theta$  is potential temperature; the subscripts  $v$ ,  $a$ , and  $g$  indicate virtual, lowest model layer, and ground respectively; and  $V$  is the horizontal wind speed. The Ri

is used because the model computes finite differences between discrete points in the PBL. Surface moisture availability is determined by the land-use category which largely determines the moisture flux. The surface heat fluxes are dependent on the lowest model layer's potential temperature and density, and the stability.

**Blackadar High-Resolution PBL.** The high-resolution Blackadar PBL is the most commonly used PBL scheme for the MM5. It has five layers in the lowest one km and four stability types: stable, mechanically-driven turbulence, unstable forced convection, and unstable free convection. Again, the distinction between the stability types is made using the Ri and the difference between the forced versus free convection is determined using the Monin-Obukhov length ( $L$ ) and the height of the PBL ( $h$ ).  $L$  is the height above the surface at which buoyancy factors first dominate over mechanical production of turbulence (Stull 1993). If this height is less than  $h$ , then forced convection can take place. If it is much less than  $h$ , then free convection can occur.

The surface heat and moisture fluxes are computed from similarity theory. Similarity theory uses the idea that a set of curves or relationships developed during one experiment can be generalized and applied to other experiments without having to remeasure or calculate all the variables again. It is often used to diagnose profiles of mean variables and turbulence statistics as a function of height or position. Similarity theory is zero-order closure meaning no prognostic equations are retained. The mean variables are all parameterized as a function of time and space (Stull 1993).

The Blackadar PBL has two regimes: nocturnal and free convection. The nocturnal regime is used for the first three stability types (stable, mechanically driven,

and unstable forced convection) and the free convection regime is used for the last stability type (unstable free convection). In the nocturnal regime, first order closure (which uses prognostic equations for zero order mean variables and variables such as  $\overline{u'v'}$  are approximated) is used to predict the model variables and the fluxes are computed using K-Theory.

K-Theory assumes that the turbulent flux of a variable flows down its gradient.

Fluxes are approximated by

$$\overline{u_j \xi'} = -K \frac{\partial \bar{\xi}}{\partial x_j} \quad (3)$$

where  $u_j$  represents the u (j=1), v (j=2), or w (j=3) component of the wind,  $\overline{u_j \xi'}$  represents a flux of the variable  $\xi$  by the respective wind component, and  $\frac{\partial \bar{\xi}}{\partial x_j}$  represents the gradient of the variable in the x (j=1), y (j=2), or z (j=3) direction. For positive  $K$ , equation (3) implies that the flux flows down the local gradient of  $\bar{\xi}$ , from high values of  $\xi$  to lower values of  $\xi$ .

In the free convection regime, the vertical fluxes are not determined by the local gradients, but by the thermal structure of the mixed layer and surface heat flux. This often results in counter-gradient flow, so the use of K-Theory is not recommended (Stull 1993). Instead of allowing the mixing to occur between adjacent layers as in K-Theory, mixing is permitted to occur between the lowest layer and each level in the mixed layer. This produces a more realistic model of a PBL that is being strongly heated from below, initiating buoyant plumes (Zhang and Anthes 1982).

**Free Atmosphere Processes.** Above the mixed layer, K-Theory is used to predict the vertical diffusion of the variables. The model can also include moist vertical

diffusion (moist-adiabatic processes in cloudy air).

**Radiation Schemes.** The MM5 has two atmospheric radiation schemes. The simple scheme has no cloud interactions or diurnal cycle and the cooling rate just depends on temperature. In the cloud radiation scheme, both longwave and shortwave radiation interactions with clouds and clear air water vapor are considered.

### **Model Set-Up**

The model set-up used for this study was intended to first realistically model the LSBS and second to minimize computational overhead. Over thirty test simulations were executed to examine the effects of various nest configurations, nest sizes, cumulus schemes, shallow convection routines, and boundary conditions. Examination of these test runs produced the set-up described below.

### **Terrain and Nests**

Based on the author's experience and that of other recent users, the model seems to perform best with embedded nests and having the largest domain's boundary, where the boundary conditions are reapplied and weighted into the domain, as far as possible from the area of interest. With this in mind, the nest configuration in Figure 2.5 was designed to keep the largest domain's boundaries far from the Wassaw Sound.

The largest domain is centered at 31.93 °N latitude and 81.10 °W longitude. The terrain and land-use matched well on the finest domain and required no nudging. Table 2.1 summarizes the set-up for the modeling domains.

### **Input Data**

For this study, instead of using an NCEP or real-time analysis as input, an

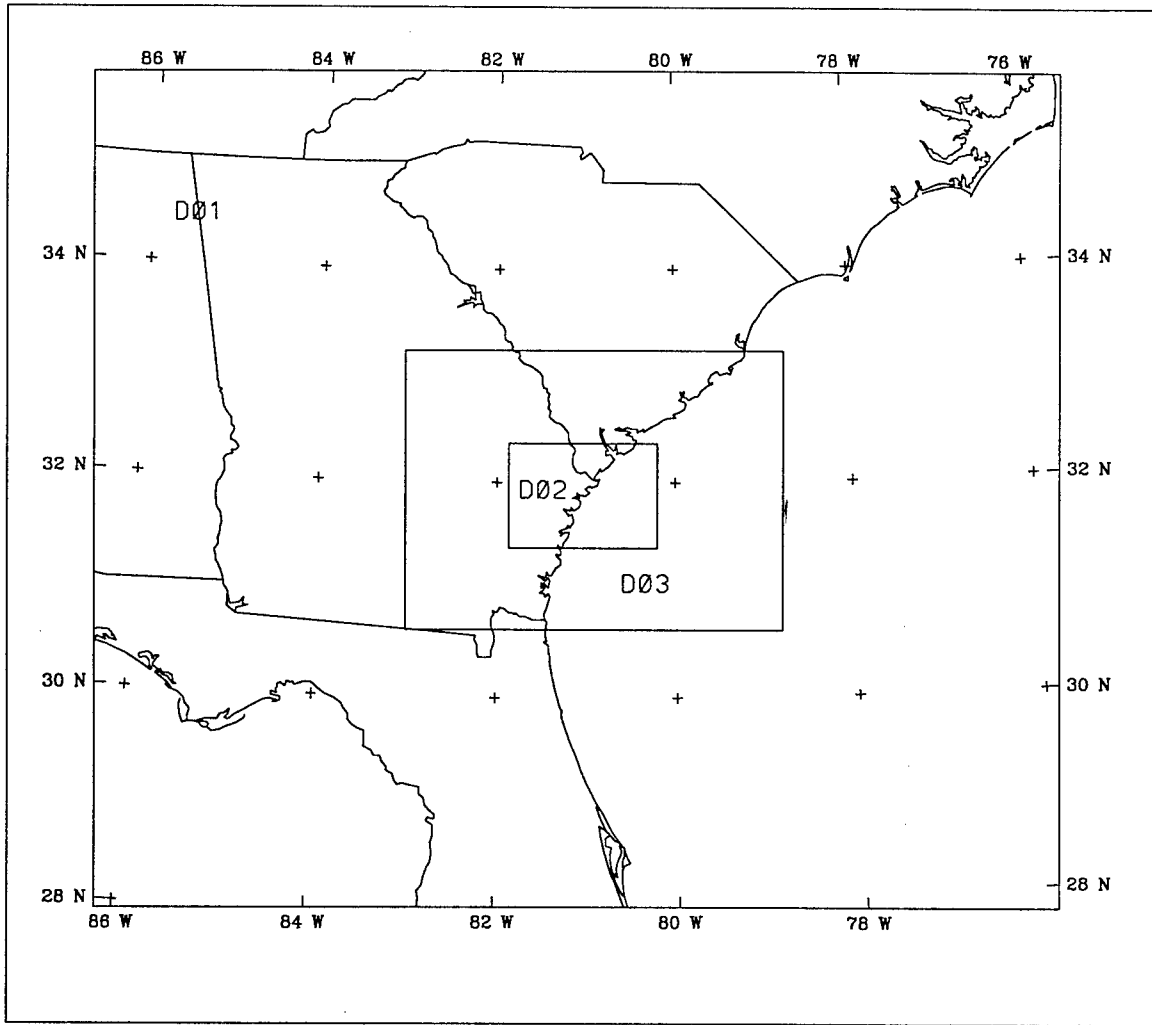


Figure 2.5. Domain and nest configuration used for all model runs. Domain 1 (D01) has a 36-km mesh, domain 2 (D02) a 12-km mesh, and domain 3 (D03) a 4 km-mesh. Sizes are given in Table 2.1.

averaged sounding was used to initialize the whole domain. This would allow the LSBS to develop in a synoptically undisturbed environment and permit the author to control the flow regimes being simulated. The RAWINS deck was modified by D. Stauffer from PSU to allow all the model domains to be initialized to one input sounding. This input sounding was centered in the coarsest domain.

Table 2.1. Model domain summary.

	Domain 1	Domain 2	Domain 3
Grid Spacing	36 km	12 km	4 km
X Dimensions Grid pts/km	29/1008 km	34/396 km	40/156 km
Y Dimensions Grid pts/km	25/864 km	25/288 km	28/108 km
Number of Pressure levels	26	26	26
Number of Sigma levels	23	23	23

### **Sounding Data**

The sounding data used for this study were extracted from the Radiosonde Data Set of North America (Forecast Systems Lab. 1993) on CD-ROM. This archive contains soundings from 1946 to 1992. For this investigation, the Charleston (CHS), South Carolina soundings, located 140 km to the northeast of the Wassaw Sound, were used. CHS is the closest sounding site to Savannah and is representative of the synoptic-scale conditions over the Wassaw Sound during the summer.



The CHS sounding data were used from the years 1946 to 1992, except for 1963 and 1966 which were missing, for the period 15 July through 15 August. This period was chosen because the 1996 Summer Olympic Games sailing competition will be held during this time frame. Only the 0000 UTC soundings were used because the model runs were initialized at 0000 UTC. This gave the model approximately 12 hours of spin-up time before the next full sea breeze cycle would initiate and eliminated the need to compensate for morning, radiational inversions in the sounding data. The total number of soundings used to construct the average was 1082.

### **Data Reduction**

The 1082 soundings were read into a FORTRAN program that averaged them and performed linear interpolation to compute u and v wind components and relative humidity at 26 pressure levels. Table 2.2 shows a sample FORTRAN output. This output would then be input into the RAWINS deck to initialize the MM5 domains to that sounding.

After the average sounding was calculated, the data were then reanalyzed to find soundings that would represent onshore, offshore and alongshore flows. Wind directions were chosen as shown in Figure 2.6 using the orientation of the Wassaw Sound and Williamson Island as the guide. The 850 mb and 700 mb wind directions were used to sort the data as they would generally represent flow above the boundary layer, free from surface effects. Thus, the data was stratified to portray the large-scale forcings uncontaminated by surface processes. As a result, the boundary layer winds could vary independent of the regime classification scheme.

Table 2.2. Sample FORTRAN output of the average sounding computed from 1082 soundings. Pressure is in mb, temperature is in °C, u and v wind components are in m s<sup>-1</sup>, ddd is in degrees from true north, and ff is in knots. Missing data are indicated by -9999.

Press	u	v	Temp	RH	ddd	ff
1014	-0.3	2.6	27.9	72.8	174	5.1
1000	0.1	3.1	26.7	75.3	179	6.1
975	0.4	3.4	25.1	75.4	187	6.6
950	0.9	3.2	23.8	75.4	195	6.5
925	1.3	2.5	22.2	73.6	207	5.5
900	1.6	1.8	20.8	72.8	222	4.7
880	1.9	1.4	19.5	71.8	233	4.6
860	2.1	1.1	18.3	71.2	244	4.4
850	2.1	0.7	17.8	71.8	251	4.3
840	2.1	0.7	17.1	69.6	251	4.3
820	2.2	0.6	15.9	67.5	256	4.3
800	2.2	0.4	14.8	65.9	259	4.3
775	2.4	0.4	13.1	64.1	261	4.7
750	2.4	0.3	11.6	62.7	262	4.8
725	2.5	0.4	10	61.5	261	4.9
700	2.5	0.4	8.3	61.9	261	4.9
650	2.6	0.6	4.9	58.2	258	5.2
600	2.6	0.4	1.3	56.6	262	5.1
550	2.7	-0.1	-2.5	51.8	272	5.3
500	3.1	-0.5	-6.7	48.2	279	6.2
400	3.9	-0.7	-17.4	42.8	280	7.6
300	4.5	-1	-32.6	38.6	282	8.9
250	4.9	-1.6	-42.7	37.4	288	9.9
200	5.1	-2.3	-54.6	-9999	295	10.6
150	3.5	-2.5	-66.1	-9999	306	8.3
100	-1.8	-1.5	-67.5	-9999	52	4.6

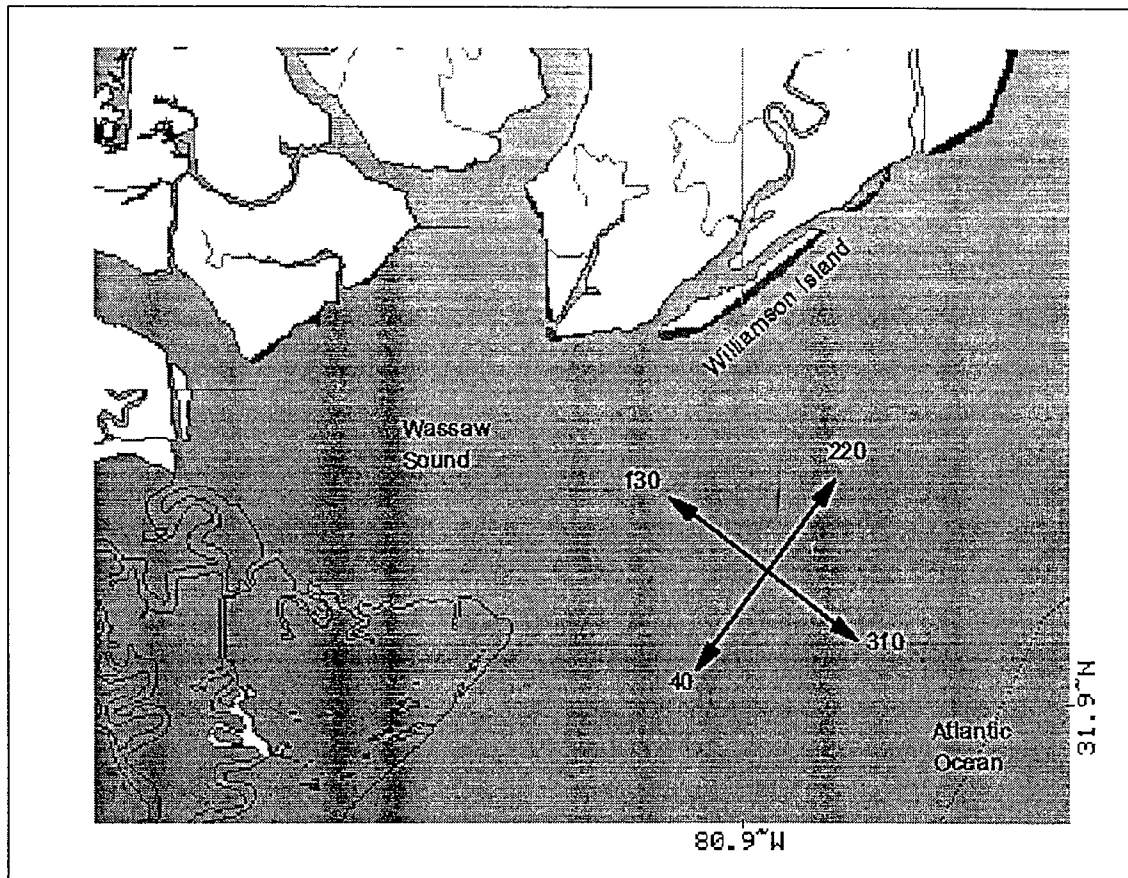


Figure 2.6. Wassaw Sound, Georgia. Arrows depict wind direction for onshore flow (130°), offshore flow (310°), and alongshore flows (40° and 220°) used to develop soundings representative of those regimes.

As the data were sorted, if it matched the given 850 mb and 700 mb wind directions within 20°, that sounding was saved and used to compute an average sounding representing that flow pattern. The results are summarized in Table 2.3. Figures for each soundings are presented in the following chapter, along with the discussion of the model output for that particular flow pattern.

An alternative regime classification scheme for the area is being developed by Powell (personal communication) using the position of the subtropical high across the region. This work is currently on-going and was unavailable for use in this study.

Table 2.3. Number and percent of input soundings matching flow criteria. NE is northeast (alongshore), SE is southeast (onshore), SW is southwest (alongshore), and NW is northwest (offshore).

	Average	NE Flow	SE Flow	SW Flow	NW Flow
850 and 700 mb Wind Criteria	N/A	20° - 60°	110° - 150°	200° - 240°	290° - 330°
Total Number of Soundings Considered	1,082	1,082	1,082	1,082	1,082
Number of Soundings Meeting Criteria	1,082	32	20	112	45
Percent Meeting Criteria	100	2.9	1.8	10.3	4.1

### Model Physics Used

All model runs were nonhydrostatic. With the intention of just modeling the LSBS, several of the simpler, less expensive schemes were chosen to reduce model overhead. The physics options were chosen to match those of Herbster (1996) except for

the cumulus parameterizations.

**Moist Processes.** Explicit moist processes were resolved using the simple ice-phase scheme.

**Cumulus Parameterizations.** Many of the test set-up runs were conducted to examine the effects of varying cumulus parameterizations schemes. All three schemes, Grell, AS, and Kuo were tested. First, each scheme was used in just the two largest domains (36 and 12-km grids). This produced excessive rainfall in the smallest domain in all three test runs. Next, each scheme was used in all three domains (36, 12, and 4-km grids). The Grell and AS parameterizations still produced excessive precipitation. Only the Kuo scheme produced realistic rainfall rates. To test if moving the boundary conditions further away would have any effect, the original domains were expanded 25%. Then the experiment using the cumulus parameterizations in all three domains were rerun with the same results. The Grell and AS schemes continued to produce heavy rainfall while the Kuo scheme produced realistic precipitation patterns.

Pielke and Pearce (1994) state that for midlatitude grid scales less than 5-10 km, the use of a cumulus parameterization scheme is recommended because once deep convection does develop in the midlatitude simulations, it tends to occur over too large an area producing excessive precipitation. Grell (1993) notes that it is difficult if not impossible to isolate errors caused by cumulus schemes from errors caused by other components of the model. Further, it "might even be more guessing work to decide why one parameterization has failed and another one worked." With these statements in mind and because this project is concerned with the study of the LSBS and not cumulus

parameterization schemes, the Kuo scheme was used in all three domains because it produced the most realistic output of all the test simulations.

Three of the test runs were designed to examine the effects of the shallow convection algorithm in the MM5. The initial test was with the shallow convection turned on in all domains first with no cumulus scheme in the smallest domain (4-km grid), then turned on simultaneously with the Grell scheme and then with the Kuo. Output showed no apparent difference with the algorithm on or off. As a result, the shallow convection algorithm was turned off in all domains to reduce computational overhead.

**PBL Parameterizations.** The Blackadar high-resolution PBL was used for all domains. This is the best PBL scheme available for the MM5 at present and the additional model overhead it requires is well worth the detailed, realistic output it produces.

**Radiation Schemes.** Although computationally expensive, the cloud radiation scheme was chosen because realistic diurnal temperature cycles and radiative interactions with clouds and water vapor are required to produce an accurate simulation of LSBS.

### **Model Runs**

All runs were executed on NCAR's Cray YMP or on Florida State University's Silicon Graphics Power Challenge (SGI-PC) platform. All postprocessing of the model data was done on the SGI-PC.

The idealized simulations were all initialized on 19 July 1995 at 0000 UTC. The day choice was dependent on the availability of data sets from the NCAR's archive to

initialize the DATAGRID deck. These inputs would eventually be overwritten during execution of the RAWINS deck, when the input sounding is used to initialize the entire model domain.

FDDA was not used and the nests remained stationary during the entire model run. The model was executed for 48 hours to provide output spanning at least one complete land and sea breeze cycle after the initial model spin up. The model's time step was 108 seconds.

Seven model runs were executed, one for each of the represented flow patterns (SE, SW, NW, and NE), the average flow, the calm initialization, and the test run for 13 August 1995. The calm initialization used the thermodynamic profile from the average sounding but with the wind field set to zero. Model outputs are discussed in the following chapter.

## CHAPTER 3

### MODEL RESULTS

#### Introduction

One of the disadvantages of a modeling study such as this is the enormous amount of data produced by the model makes it impractical to present a detailed examination of each model run. While the overall evolution of the circulation will be presented, the concentration will be on the seaward portion, as this will have the most impact on the 1996 Summer Olympic Games sailing competition and is also one of the least understood aspects of the LSBS.

All model runs were initialized at 0000 UTC and executed for 48 hours using the nest configuration shown in Figure 2.5. Local time, Daylight Savings time during the Olympic Games, is four hours behind UTC. Local sunrise occurs at approximately 1040 UTC and sunset at 0020 UTC during this period.

For each flow regime simulated (calm, average, onshore, offshore, alongshore, and 13 August 1995), the onset, initiation point, maximum intensity, wind direction, seaward extent, landward extent, duration, decay, and maximum circulation depth of both the sea and land breezes that develop will be determined. Note that some elements may not be defined when the large-scale flow coincides with the definition. For example, for



the onshore flow case, it may not be possible to determine the landward extent of the circulation as it may be masked by the prevailing flow. The test case (13 August 1995) will be compared against an independent data set.

### **Calm Initialization**

The first model run conducted was a calm initialization to examine how the LSBS would develop with no large-scale forcing. This run should yield a basic understanding of how the circulations in general will develop. All domains and boundary conditions in the model were initialized to calm winds and used the thermodynamic profile compiled from averaging 1082 CHS soundings (Figure 3.1a).

#### **Day One**

The calm initialization allows a rapid development of the circulations. By day one at 0300 UTC (here after, model date-time grouping will be day/UTC hour, thus day one at 0300 UTC will be referred to as 01/03 UTC), there is already evidence of a newly developed land breeze initiating at the coastline and blowing from  $310^\circ$ , perpendicular to the shoreline (Figure 3.3a). Cross-sectional moisture analysis (Figure 3.3b, cross section orientations are shown in Figures 3.1b, 3.2a, and 3.2b) shows a very shallow, but complete land breeze circulation centered over the shoreline. Over the next four hours, the land breeze intensifies and spreads inland 4 km and seaward 8 km.

By 01/12 UTC, the land breeze has reached a maximum speed slightly greater than  $1 \text{ m s}^{-1}$ , blowing from  $360^\circ$  (Figure 3.4a). Cross-sectional moisture analysis at the same time (Figure 3.4b) shows the entrainment of moist, maritime air upward within the narrow updraft of the land breeze circulation 11 km offshore, marked by the  $18.0 \text{ g kg}^{-1}$

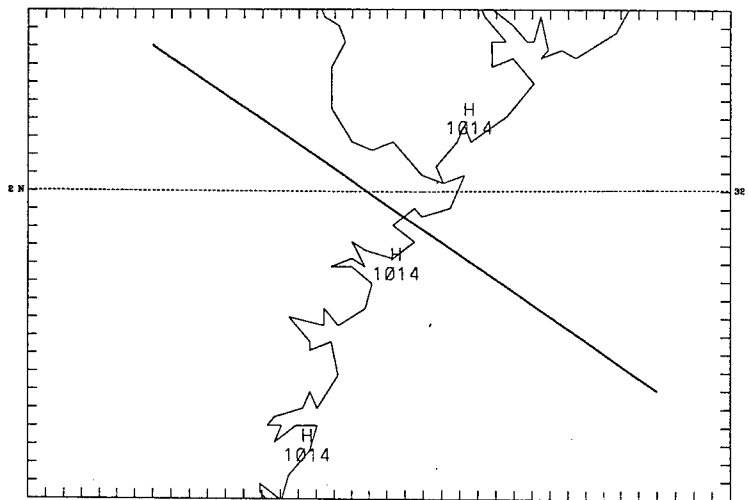
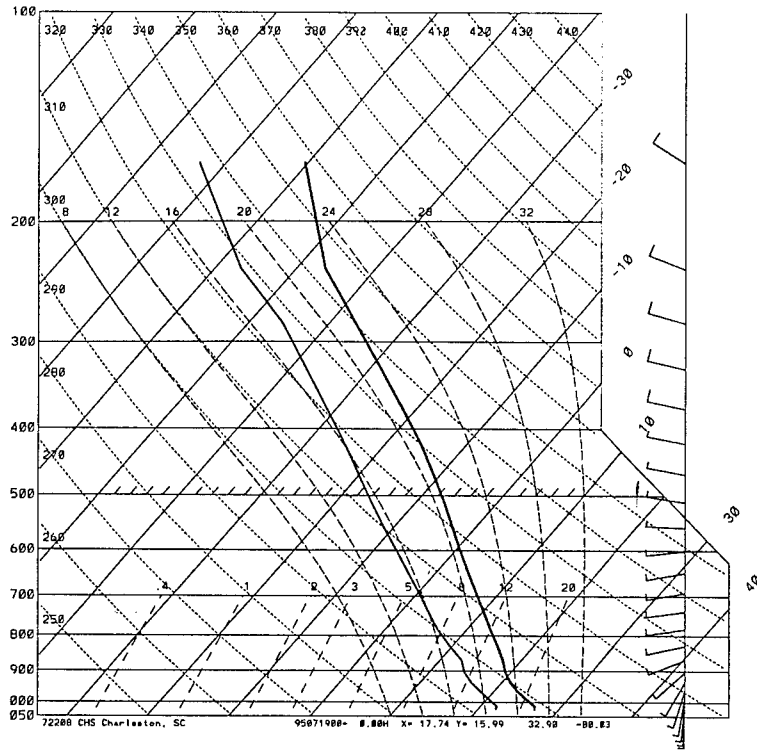


Figure 3.1. a: Thermodynamic profile used to initialize the calm and average idealizations. Wind barbs are in knots. For the calm run, the wind field was set to zero. b: Solid line depicts the location of the cross-sectional analysis used in the 4-km domain. The line bisects the Wassaw Sound as it crosses the shoreline.

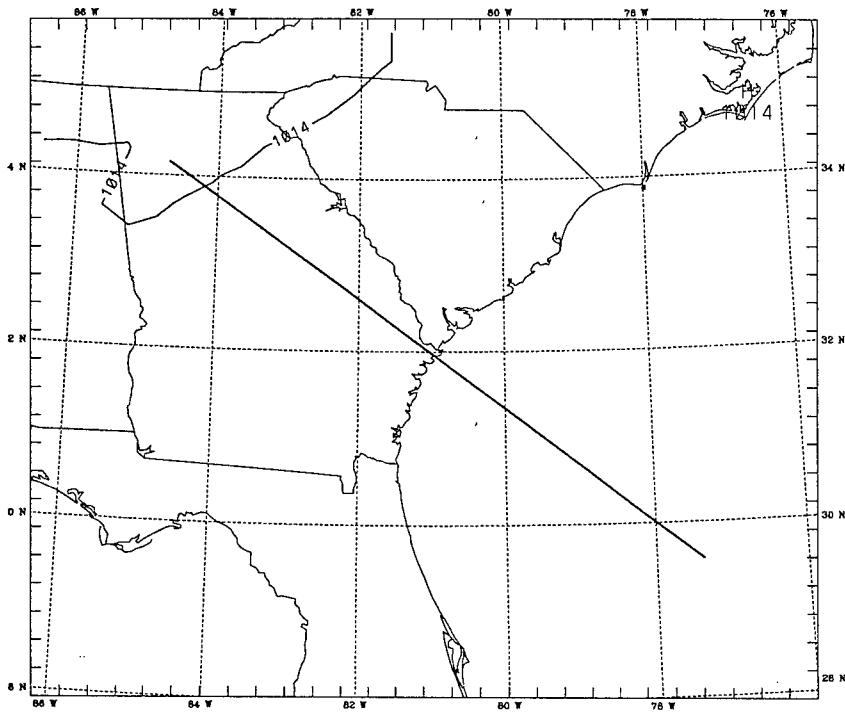
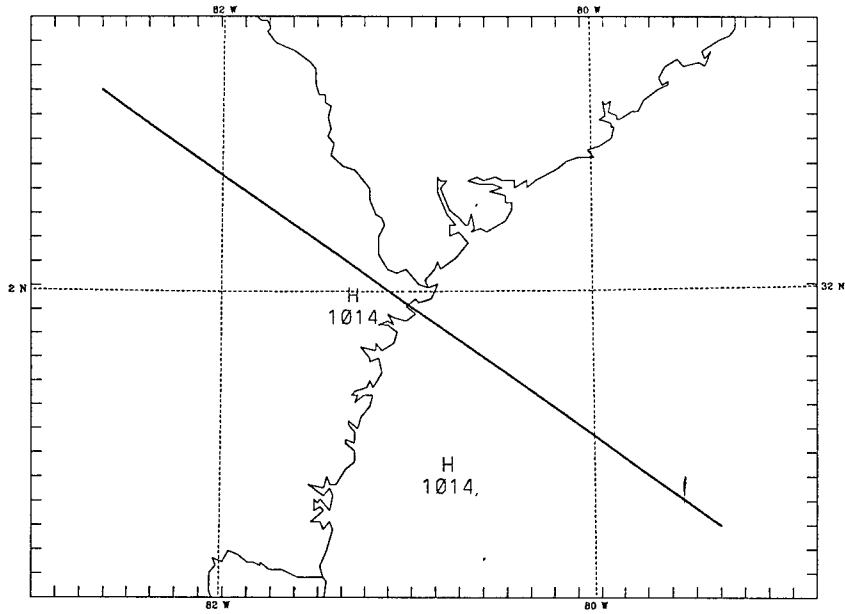


Figure 3.2. a: As in Figure 3.1b, except for the 12-km domain. b: As in Figure 3.1b, except for the 36-km domain.

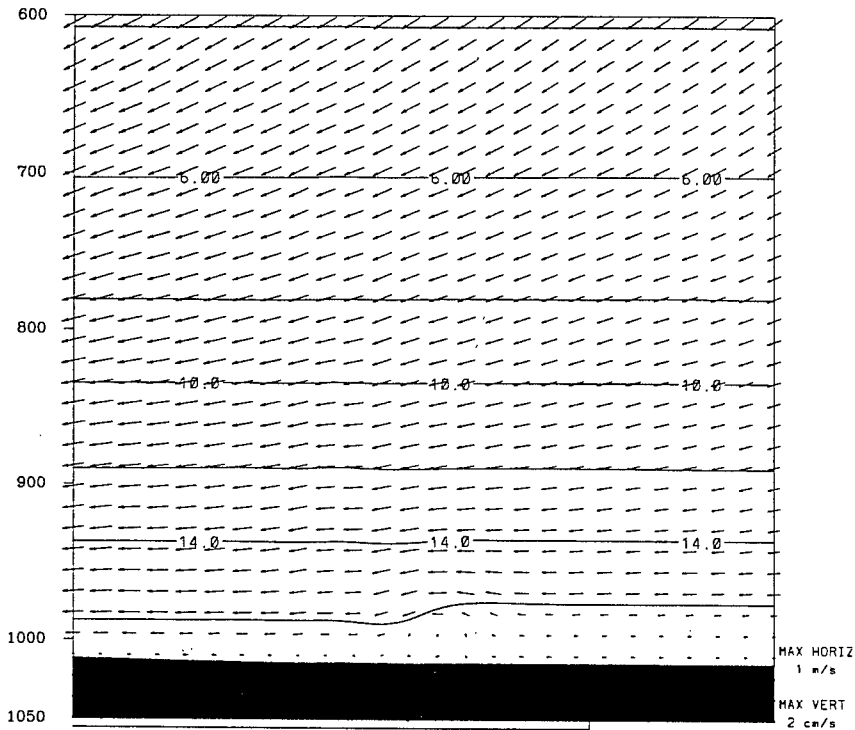
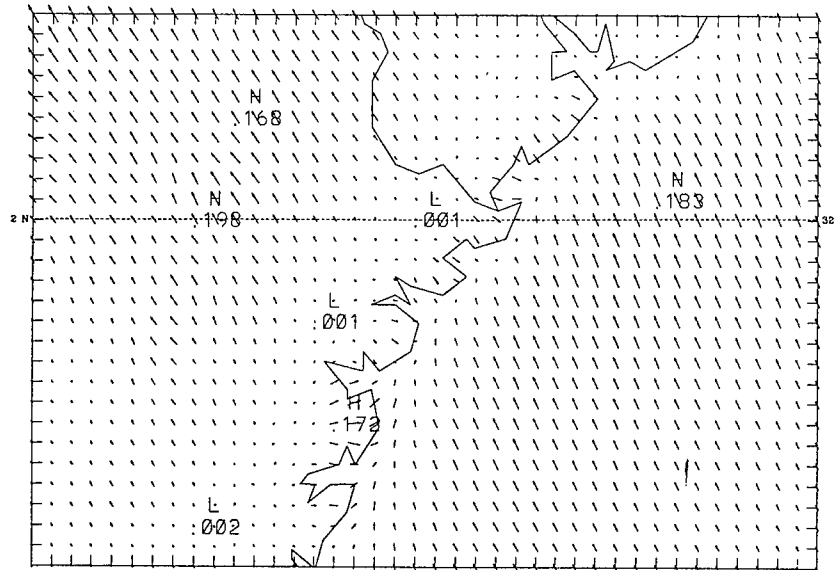


Figure 3.3. a: 01/03 UTC wind field from the lowest sigma level (0.995, 40 m above MSL) of the model for the 4-km domain. Wind strength is indicated by relative size of the vector. Solid lines are isotachs with a contour interval of  $2.5 \text{ m s}^{-1}$ . Embedded numbers in the field indicate wind speed maxima and minima. b: 01/03 UTC cross-sectional analysis along the solid line depicted in Figure 3.1a. View is towards the northeast; land is to the left and water is to the right, with the shoreline located at the midpoint of the horizontal axis. Vertical axis is pressure in mb, solid lines are contours of mixing ratio (isohumes) in  $\text{g kg}^{-1}$  with an interval of two, arrows represent circulation vectors in the cross-sectional plane with strength indicated by relative size, and the line below figure is a representative distance of 100 km.

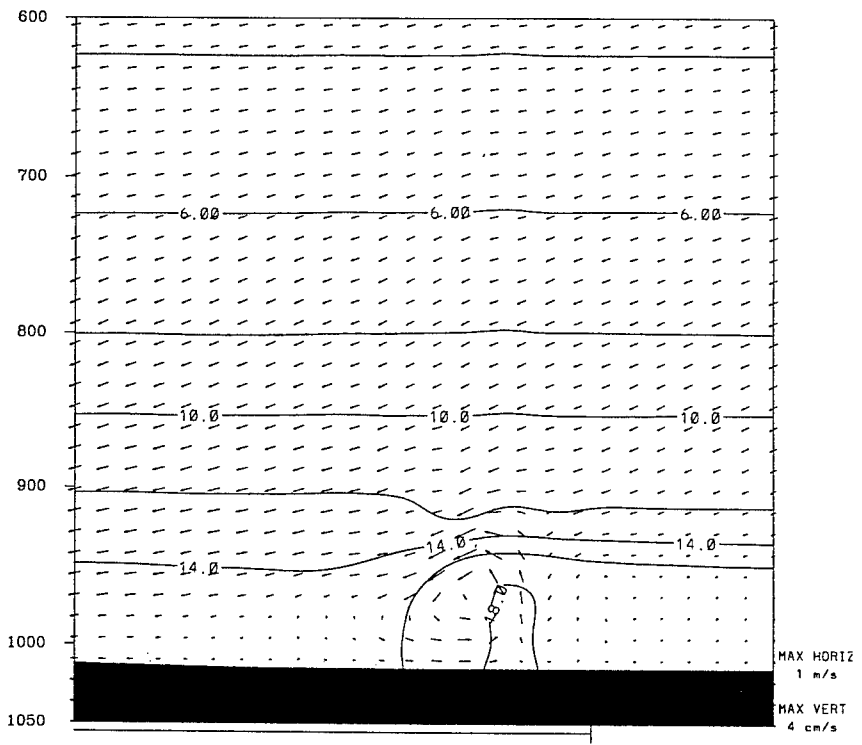
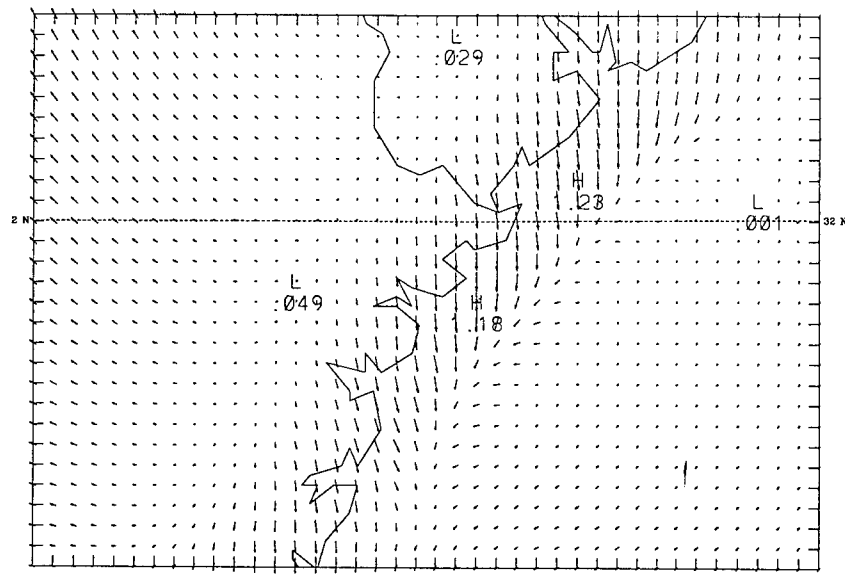


Figure 3.4. a: As in Figure 3.3a except for 01/12 UTC. b: As in Figure 3.3b except for 01/12 UTC.

isohume. A broader and weaker subsidence region extends 11 km inland, marking the landward extent of the land breeze. The circulation has reached a maximum depth of 110 mb (1100 m) with the offshore component less than 20 mb (200 m) deep.

The maximum depth is determined by examining the wind vectors in a column above the leading edge of the circulation to find the level at which the flow is the same as the background flow. The offshore depth is found by examining the winds in a column above the shoreline to find the top of the layer that represents the offshore flow.

After 01/12 UTC, the land breeze begins to decay from the land towards the sea. Over the next three hours, the entire circulation migrates seaward as it decreases in horizontal extent. The extreme seaward position stays approximately fixed as the landward portion of the circulation decays seaward to meet it. While at the shoreline, the transition from the land breeze to the sea breeze occurs.

By 01/13 UTC, the land breeze has begun to decay across the Wassaw Sound, with wind speeds becoming less than  $1 \text{ m s}^{-1}$  (Figure 3.5a). Cross-sectional moisture analysis at the same time (Figure 3.5b) shows the center of the circulation beginning to move seaward. In the next hour, the winds go almost calm over the shoreline (Figure 3.6a) while land breeze winds continue to blow 5-10 km offshore. This is in good agreement with the observational findings and conceptual model presented by Lindsey et al. (1996). Over the next hour, the circulation center continues to move seaward (Figure 3.6b). By 01/15 UTC, the sea breeze has begun, initiating at the coastline with wind speeds slightly greater than  $1 \text{ m s}^{-1}$  blowing from  $130^\circ$  (Figure 3.7a). The leading edge of the sea breeze at this time is marked by the  $16.0 \text{ g kg}^{-1}$  isohume on the cross-sectional

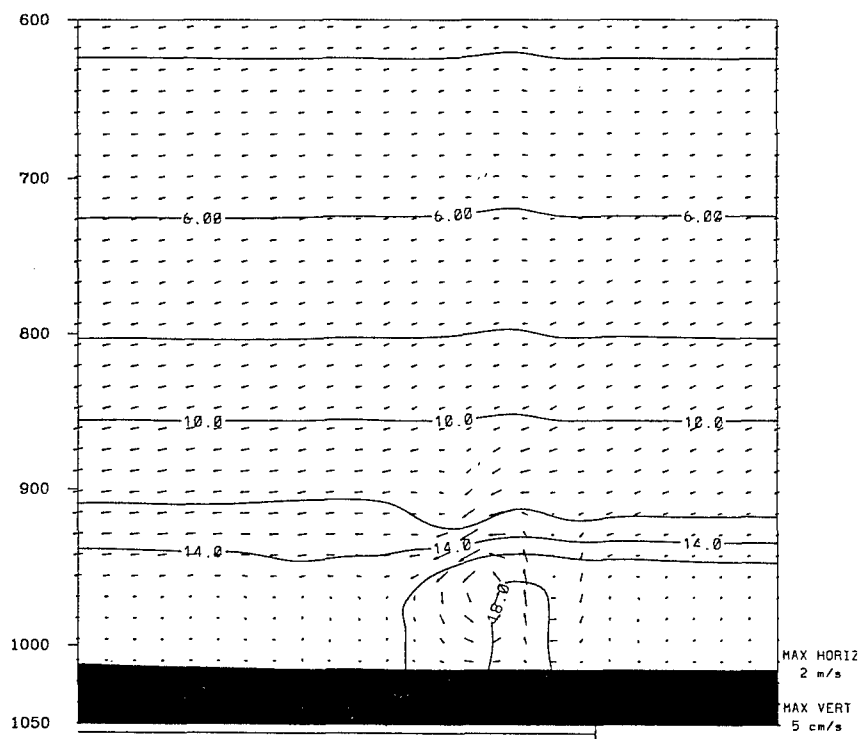
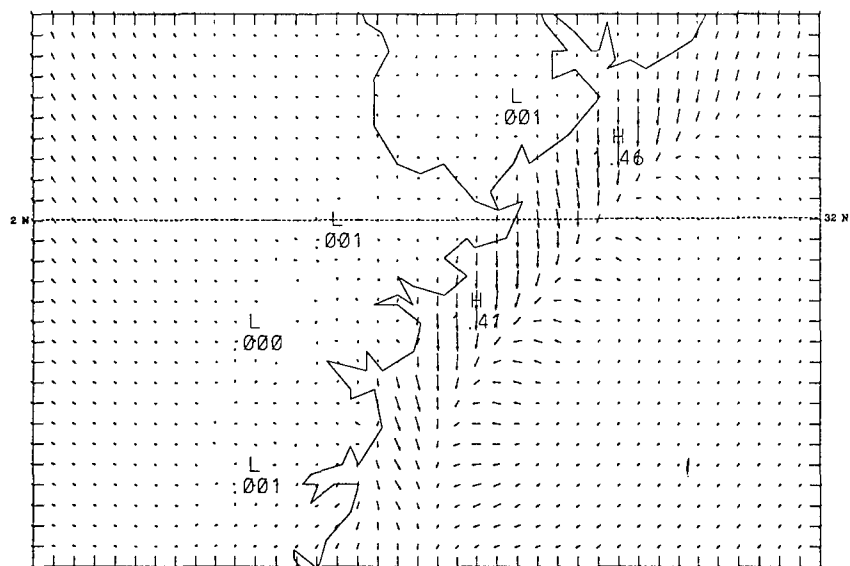


Figure 3.5. a: As in Figure 3.3a except for 01/13 UTC. b: As in Figure 3.3b except for 01/13 UTC.

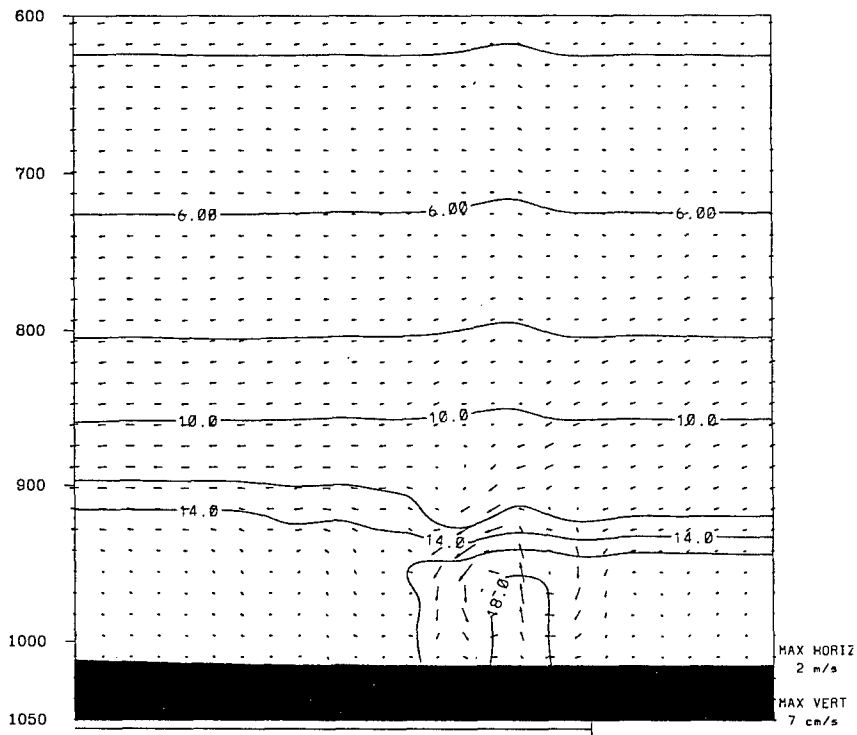
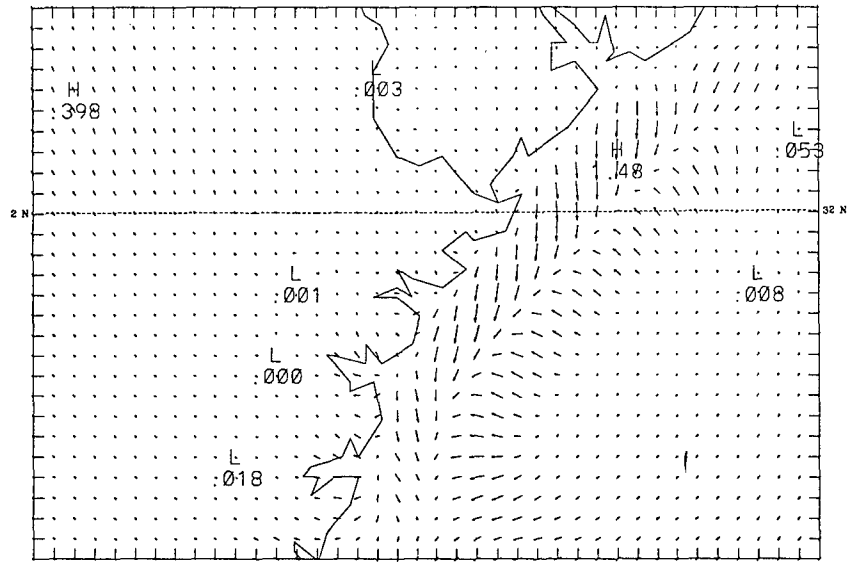


Figure 3.6. a: As in Figure 3.3a except for 01/14 UTC. b: As in Figure 3.3b except for 01/14 UTC.



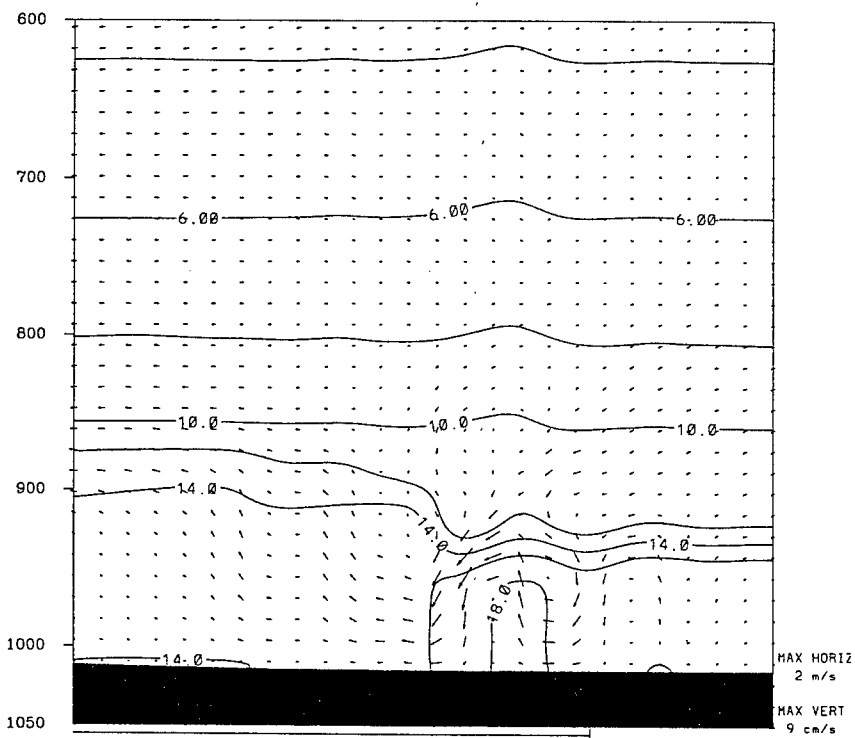
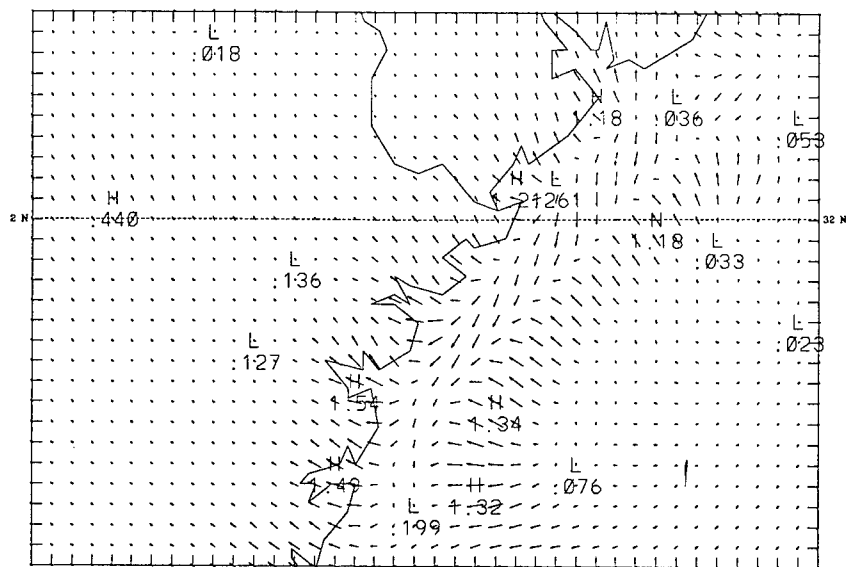


Figure 3.7. a: As in Figure 3.3a except for 01/15 UTC. b: As in Figure 3.3b except for 01/15 UTC.

moisture analysis (Figure 3.7b).

Over the next two hours, the sea breeze intensifies and begins to spread both landward and seaward. By 01/17 UTC, coastal wind speeds are now greater than  $3 \text{ m s}^{-1}$  and still flowing from  $130^\circ$  (Figure 3.8a). The extent of the sea breeze is expanding both inland and seaward at speeds up to  $15 \text{ km hr}^{-1}$ , in good agreement with movement speeds presented in Simpson (1994) and by Williams (1969).

Propagation speeds are determined by tracking the inland movement of the isohume that represents the sea breeze front using cross-sectional moisture analysis. The seaward extent is tracked following Arritt (1989) by defining the seaward boundary of the circulation as an onshore velocity of at least  $1 \text{ m s}^{-1}$ . Cross-sectional analysis of tangential wind speeds are used to track the movement of the  $1.0 \text{ m s}^{-1}$  isotach representing onshore flow.

Cross-sectional moisture analysis (Figure 3.8b) shows a head has formed on the sea breeze front, in good agreement with that described by Simpson (1994) and observed by Finkle et al. (1995) with an instrumented aircraft. As the sea breeze moves inland, the leading edge of the front is now marked by the  $14.0 \text{ g kg}^{-1}$  isohume. Moist maritime is being advected inland by the sea breeze and is rising at the sea breeze front. Behind the front, drier air is being entrained from aloft, forming the head structure. Seaward of the sea breeze head is a much broader and weaker subsidence area associated with the return flow.

As the sea breeze matures over the next two hours, the landward portion has continued to move inland at speeds up to  $8 \text{ km hr}^{-1}$ . The seaward portion has advanced at

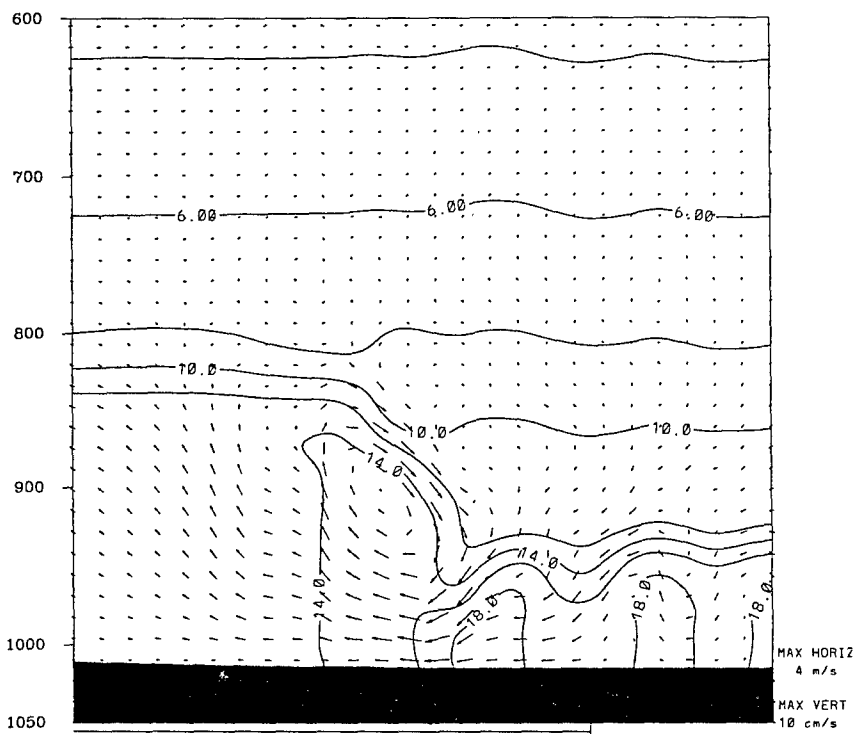
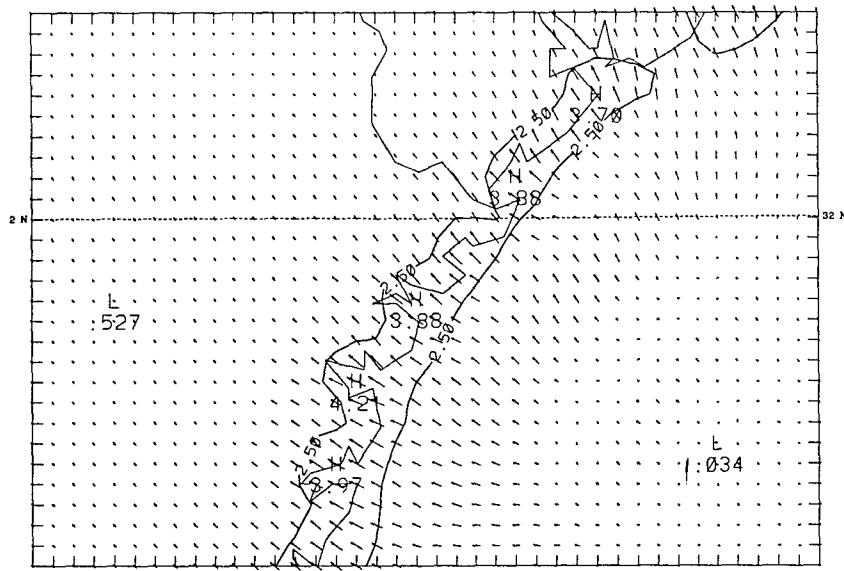


Figure 3.8. a: As in Figure 3.3a except for 01/17 UTC. b: As in Figure 3.3b except for 01/17 UTC.

15 km hr<sup>-1</sup> and coastal wind speeds have increased to 5 m s<sup>-1</sup> from 140° (Figure 3.9a). The sea breeze front propagates inland almost perpendicular to the surface with a relatively narrow, moist plume over the land and a dry, subsidence region over the water (Figure 3.9b). This subsidence region is creating a strong moisture gradient over the water that marks the top of the marine boundary layer. Thus as the sea breeze develops, it is also responsible for compacting the nearshore PBL, seaward of the sea breeze front.

The sea breeze reaches a maximum intensity of 6 m s<sup>-1</sup> at the shoreline by 01/21 UTC with a wind direction of 150°, slightly south of pure onshore (Figure 3.10a). The sea breeze has almost completely moved through the 4-km domain and through much of the 12-km domain. Maximum depth of the sea breeze circulation, to the top of the sea breeze head, is 220 mb (2300 m), as determined from the cross-sectional moisture analysis of the 12-km mesh (Figure 3.10b). The depth of the onshore flow of the sea breeze circulation, determined by examining the wind flow at the shoreline, is 50 mb (480 m). The maximum landward extent of the circulation is taken to be the landward edge 14.0 g kg<sup>-1</sup> isohume on the 12-km cross section, approximately 90 km. Note this inland penetration corresponds well with the landward edge of the 2.5 m s<sup>-1</sup> isotach (Figure 3.11a) and that the sea breeze has penetrated almost uniformly across the domain. The seaward extent is 130 km, using the 1 m s<sup>-1</sup> onshore isotach as the limit of the circulation (Figure 3.11b).

### **Day Two**

After 02/00 UTC, the sea breeze begins to decay. The winds gradually veer in time, turning past 180° by 02/03 UTC, marking the end of the sea breeze. By 02/08 UTC,

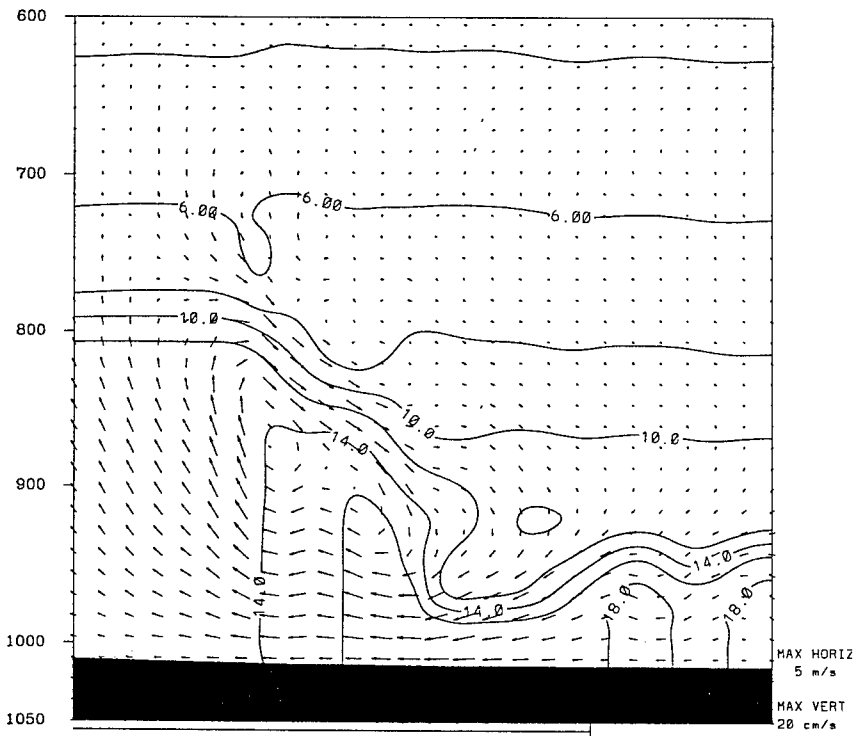
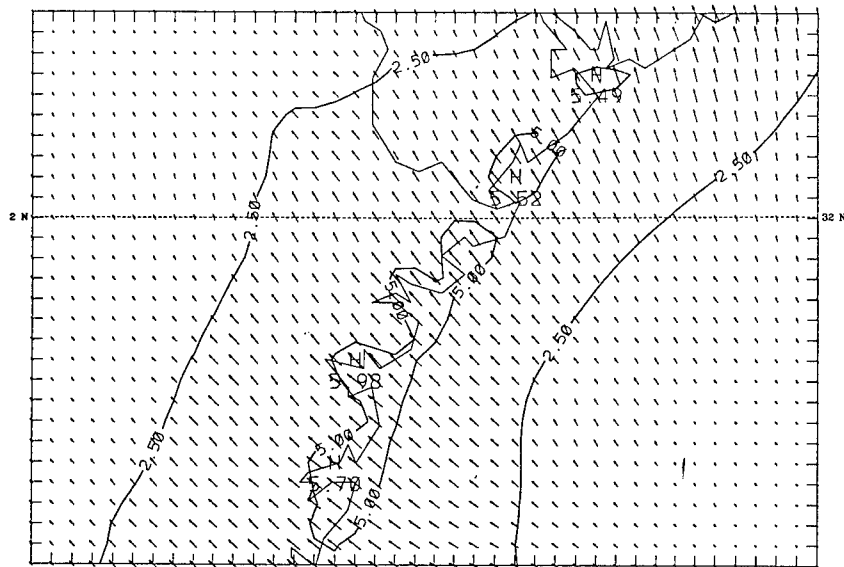


Figure 3.9. a: As in Figure 3.3a except for 01/19 UTC. b: As in Figure 3.3b except for 01/19 UTC.

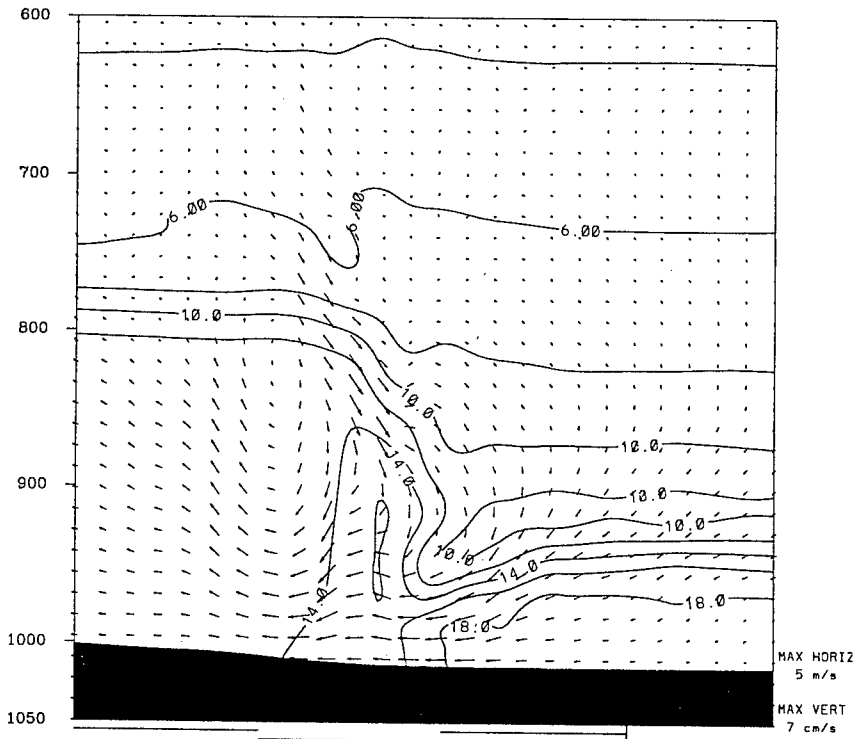
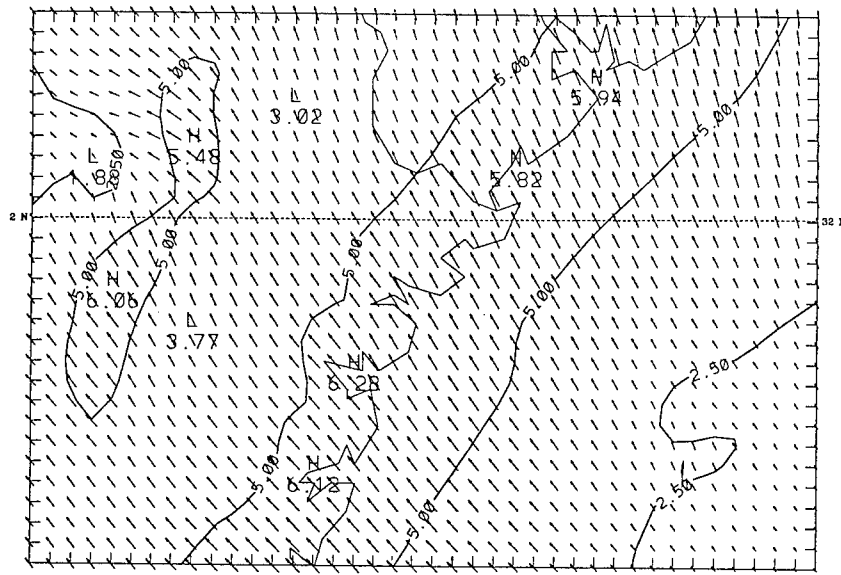


Figure 3.10. a: As in Figure 3.3a except for 01/21 UTC. b: As in Figure 3.3b except for the 12-km domain at 01/21 UTC along the solid line depicted in Figure 3.2a.

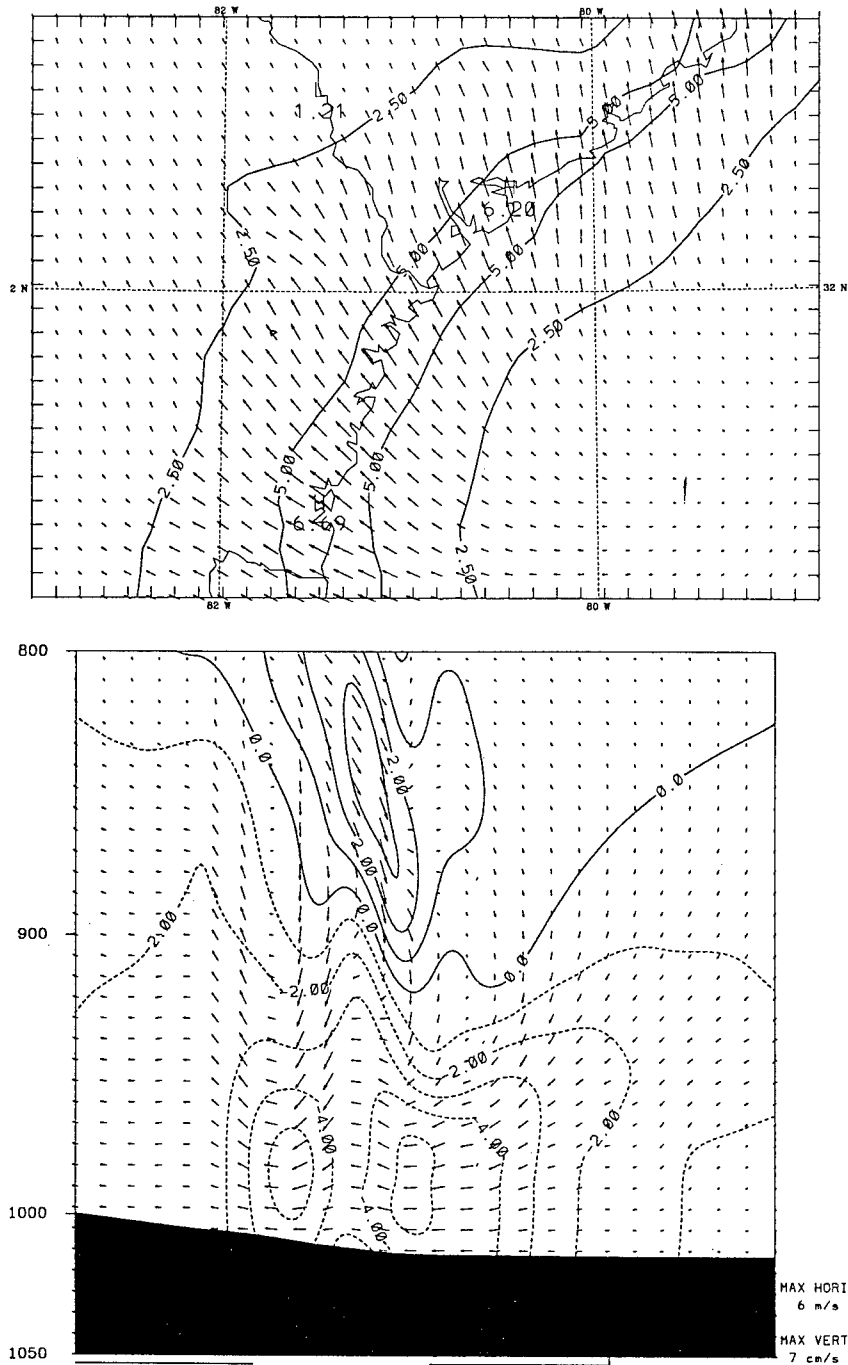


Figure 3.11. a: As in Figure 3.3a except for the 12-km domain at 01/21 UTC. b: 01/22 UTC cross-sectional analysis along the solid line depicted in Figure 3.2a. Arrows represent circulation vectors in the cross-sectional plane with strength indicated by relative size. Lines are isotachs of wind speed tangential to the cross section. Solid (dashed) lines are offshore (onshore) flow with a contour interval of  $1 \text{ m s}^{-1}$ .

the winds have become alongshore, blowing from  $220^\circ$  (Figure 3.12). During this veering period, the wind speeds decrease from the sea towards the land with time.

The transition to the land breeze is a continuous turning of the winds, not an abrupt change as in the sea breeze development. By 02/10 UTC, the winds have assumed the character of the land breeze with a maximum speed of  $1 \text{ m s}^{-1}$  from  $250^\circ$  (Figure 3.13a). The land breeze is again a compact circulation approximately 20 km wide, 12 km landward and 8 km seaward, with a total depth of 70 mb (730 m), and an offshore flow depth of less than 20 mb (200m) (Figure 3.13b). The initiation point of the land breeze is not defined for day two of the model simulation because of the gradual turning of the winds to assume the land breeze.

After 02/10 UTC, the wind speeds begin to decrease as the land breeze decays into the sea breeze transition. Again, the land breeze decays at the shoreline but still exists 4 km seaward, as in day one. By 02/15 UTC, the sea breeze has initiated across the Wassaw Sound with wind speed of approximately  $1 \text{ m s}^{-1}$  from  $120^\circ$ , almost perpendicular to shore (Figure 3.14a). Unlike the continuous transition to the land breeze, there was an abrupt transition from the almost calm conditions at the shoreline to the beginning of the sea breeze winds as in day one. Cross-sectional moisture analysis shows the beginnings of the sea breeze head and the leading edge of the marine air to be marked by the  $16.0 \text{ g kg}^{-1}$  isohume (Figure 3.14b). By 02/17 UTC, the sea breeze has reached wind speeds of  $3 \text{ m s}^{-1}$  from  $130^\circ$  and is advancing inland at speeds up to  $15 \text{ km hr}^{-1}$  and seaward at speeds up to  $15 \text{ km hr}^{-1}$  (Figure 3.15a).

The sea breeze has reached a maximum intensity of  $6 \text{ m s}^{-1}$  by 02/20 UTC and is



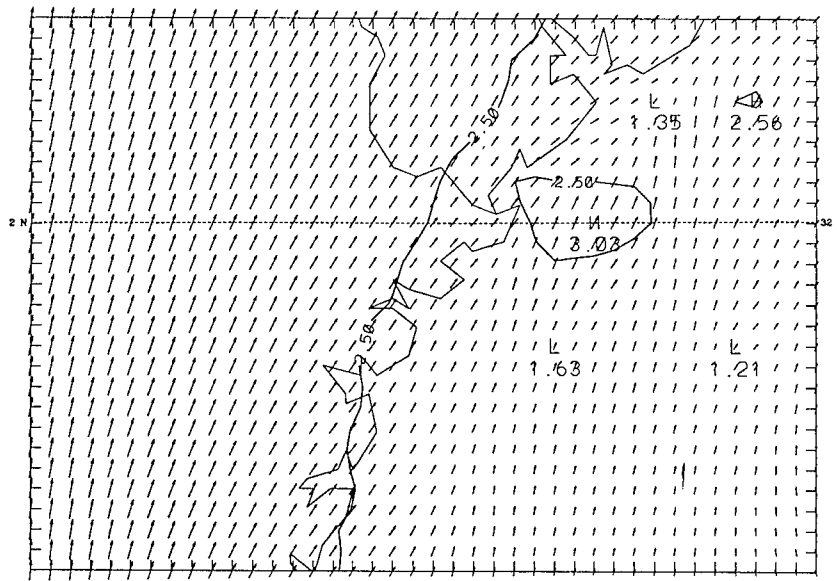


Figure 3.12. As in Figure 3.3a except for 02/08 UTC.

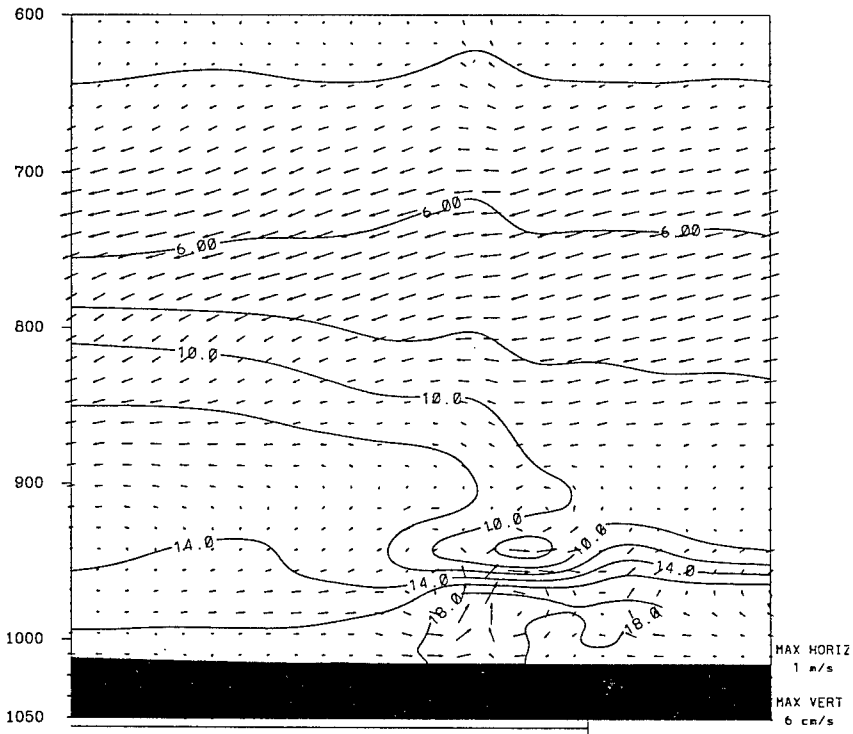
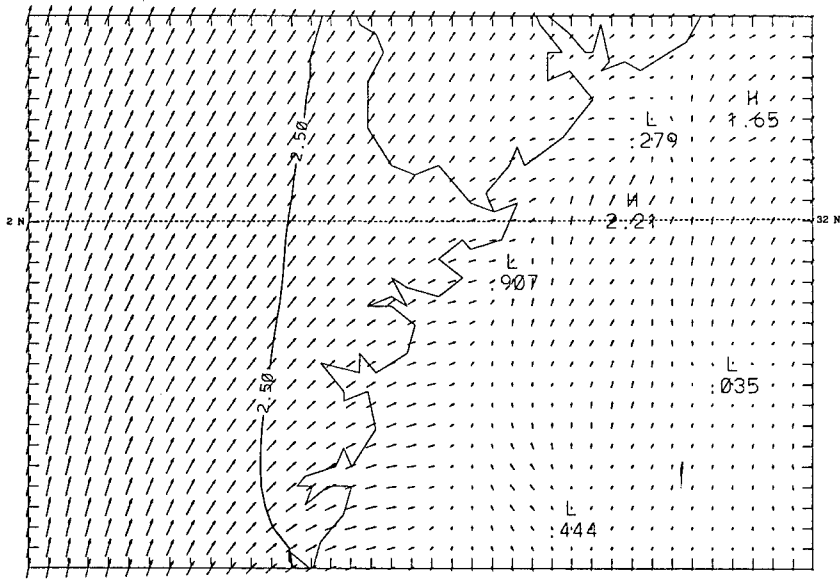


Figure 3.13. a: As in Figure 3.3a except for 02/10 UTC. b: As in Figure 3.3b except for 02/10 UTC.

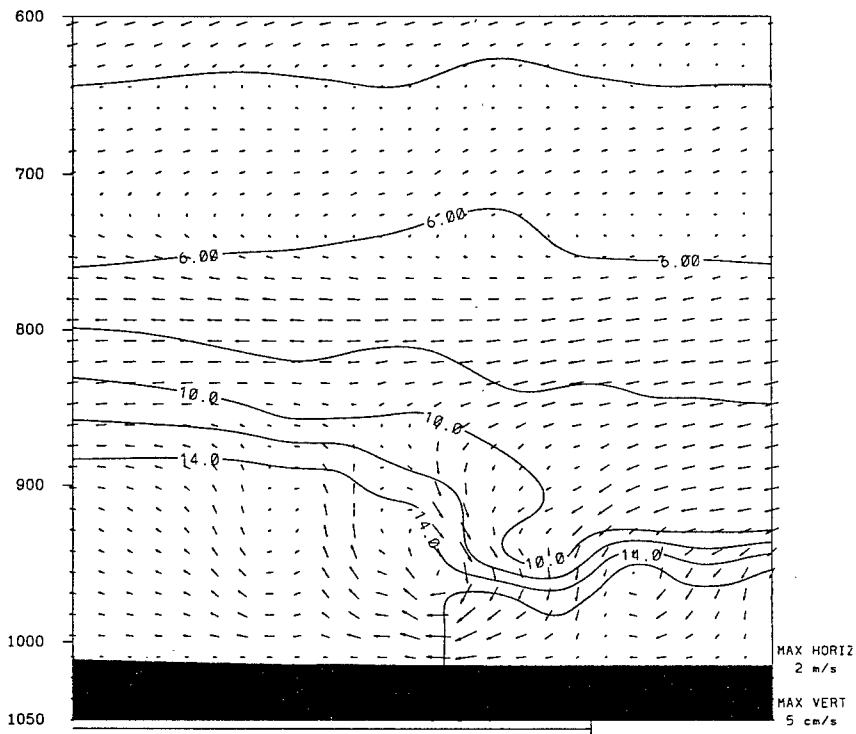
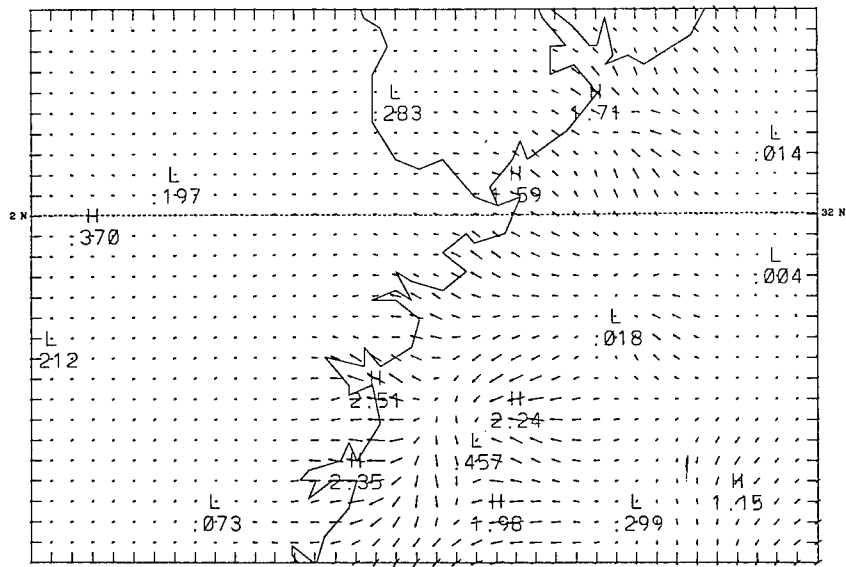


Figure 3.14. a: As in Figure 3.3a except for 02/15 UTC. b: As in Figure 3.3b except for 02/15 UTC.

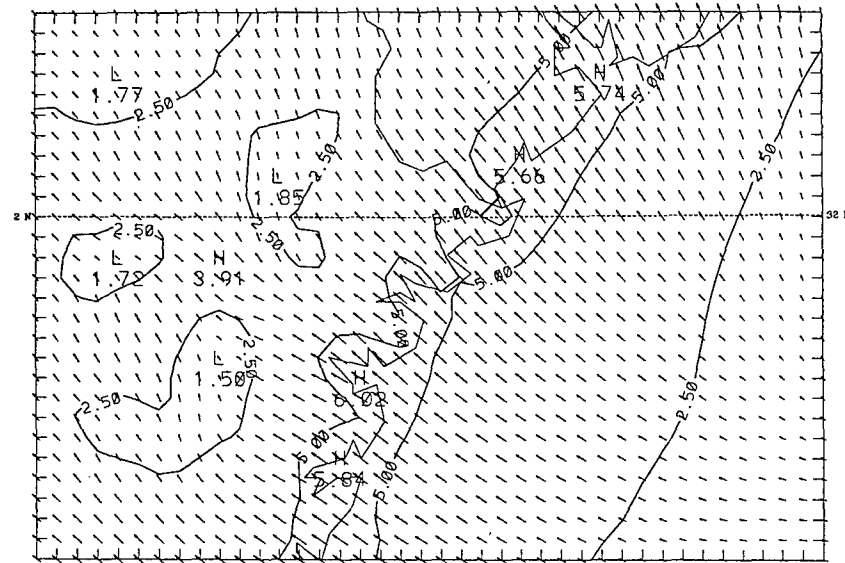
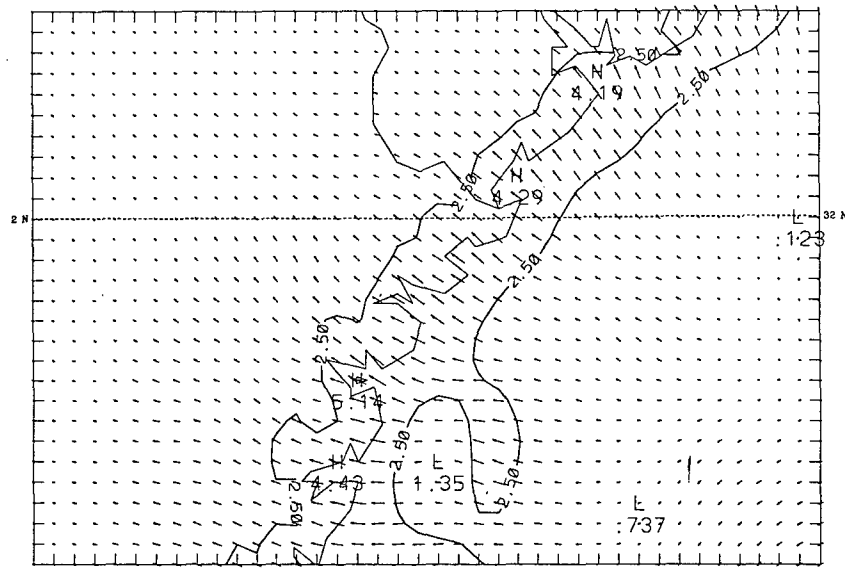


Figure 3.15. a: As in Figure 3.3a except for 02/17 UTC. b: As in Figure 3.3a except for 02/20 UTC.

flowing just slightly south of true onshore at  $140^{\circ}$  (Figure 3.15b). Again, the sea breeze has pushed through the most of the 4-km domain so to determine the maximum extent of the circulation, the larger domains must be examined. The 12-km domain cross-sectional moisture analysis shows a steep sea breeze front and head with the broad, drier subsidence region seaward (Figure 3.16a). The maximum depth of the sea breeze circulation is 220 mb (2300 m) with the depth of the onshore flow approximately 50 mb (480 m). By the end of the model run, the sea breeze has pushed well inland and the subsidence region originally over the water, has now also extended inland. The marine boundary layer over the water has been limited to a depth of 50 mb as a result of the sea breeze induced subsidence.

The maximum landward extent of the circulation on day two as marked by the  $14.0 \text{ g kg}^{-1}$  isohume, is 90 km. This again agrees well with inland penetration of the  $2.5 \text{ m s}^{-1}$  isotach in the 12 km domain. The seaward extent, as determined by the  $1 \text{ m s}^{-1}$  isotach representing onshore flow, is 150 km (Figure 3.16b).

Analysis of the diurnal pressure and temperature patterns lends some insight into the circulations that developed. Maximum land temperatures on day one reached  $32^{\circ}\text{C}$  while the daytime nearshore, over-water temperatures remained near  $25.6^{\circ}\text{C}$ . The pressure patterns show a thermal low developed over the land, reaching a minimum pressure of 1013 mb while the seaward pressures remained 1015 mb (Figure 3.17a). The pressure gradient that develops between these two features explain why the sea breeze in the Wassaw Sound tends to blow from a more southerly direction than straight onshore. The wind is adjusting to the larger-scale pressure gradients.

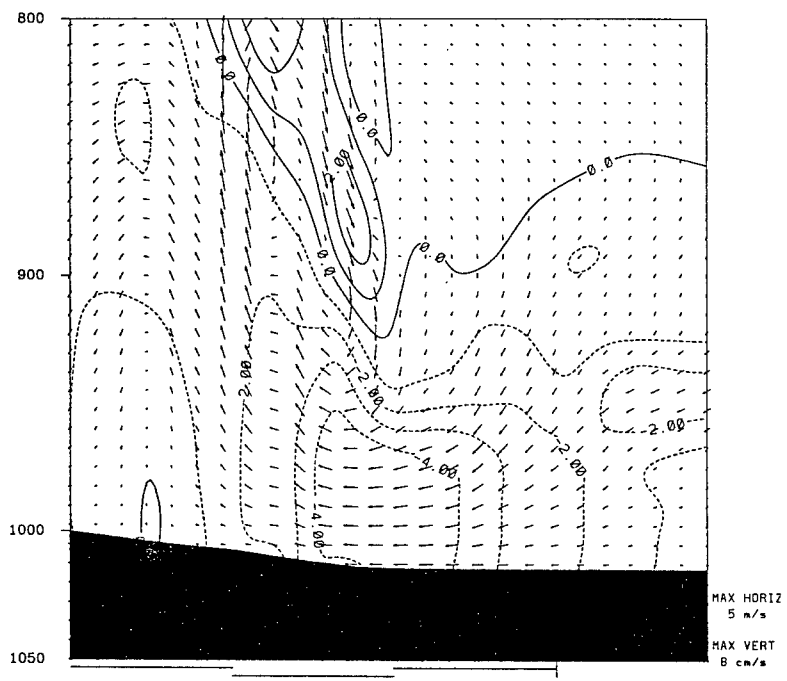
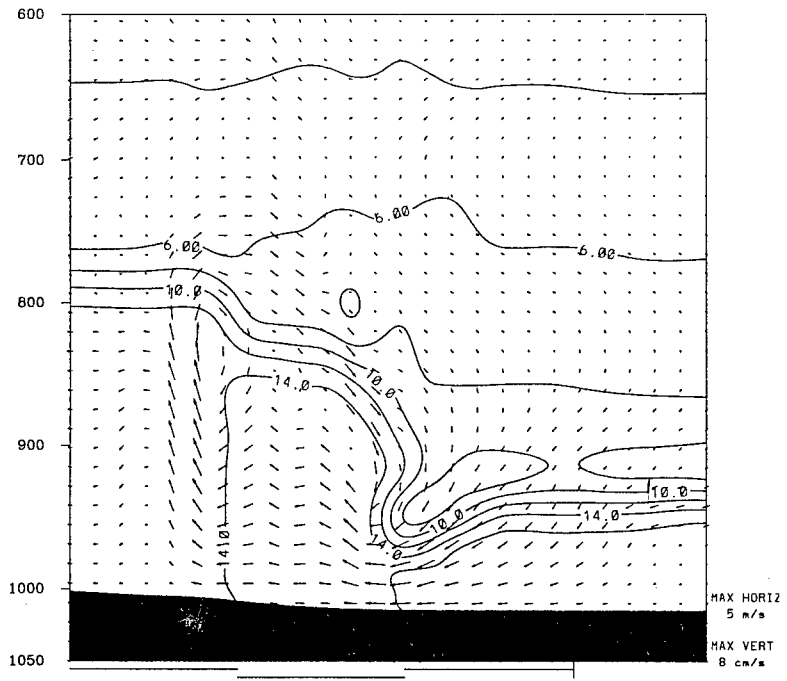


Figure 3.16. a: As in Figure 3.10b except for 02/20 UTC. b: As in Figure 3.11b except for 02/22 UTC.

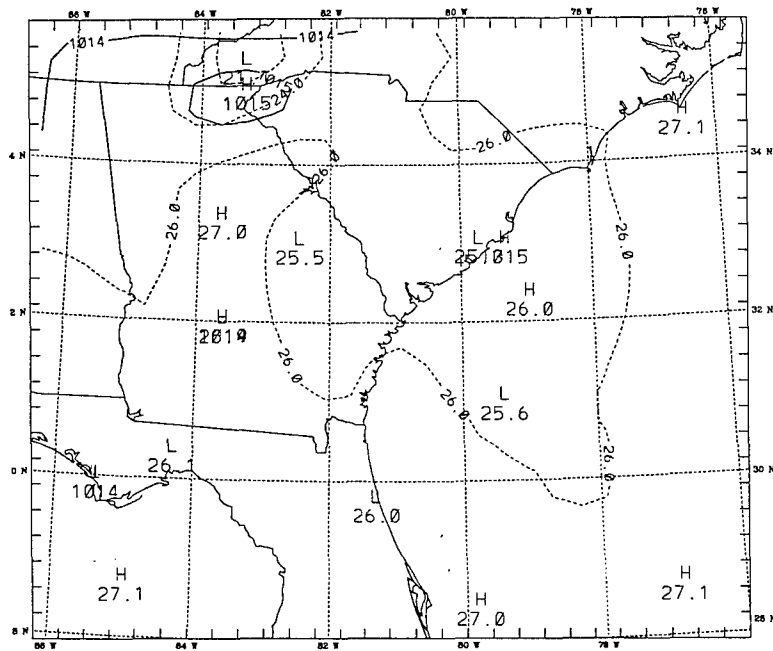
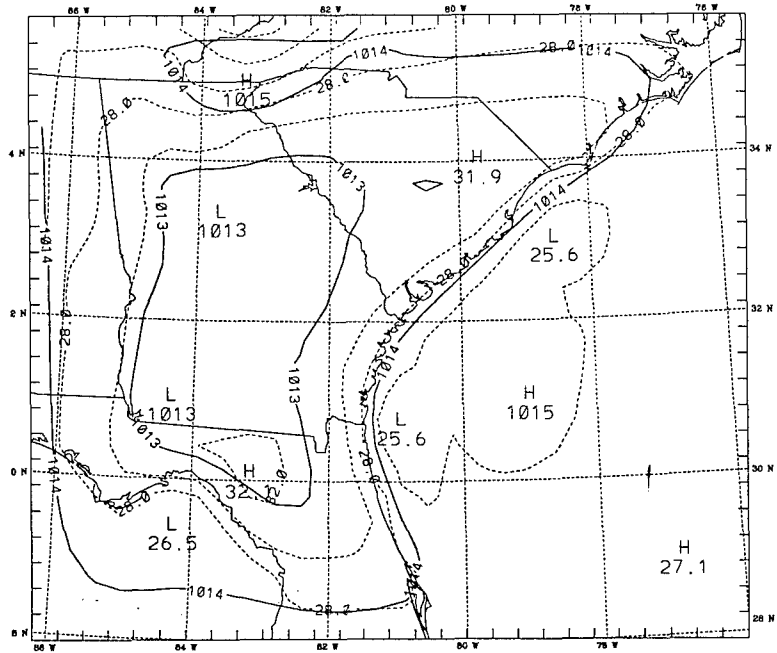


Figure 3.17. a: Pressure and temperature analysis for the 36-km domain at 01/20 UTC. Solid lines are pressure with a contour interval of 2 mb and dashed lines are temperature with a contour interval of 2 °C. b: As in Figure 3.17a except for 02/10 UTC.

Overnight, the land cools and a very weak pressure gradient forms across the domain. Only a very slight temperature contrast is responsible for the developing the land breeze (Figure 3.17b), leading to the very light land breeze wind speeds observed in the model. On day two, the same temperature and pressure patterns develop again during the daytime. Seaward pressures remain 1015 mb and landward pressures again fall to 1013 mb. Landward temperatures climb to 31 °C while nearshore seaward temperatures remain near 25.6 °C.

### **Average Initialization**

The second model run executed was the average initialization. This simulation was performed to see how the LSBS would develop under the average conditions expected during the 1996 Summer Olympic Games. This run used the same thermodynamic profile as the calm initialization but added the average wind profile computed from the CHS soundings (Figure 3.1a).

The initial flow field had 2.5 m s<sup>-1</sup> southerly flow at the surface veering with height until the flow becomes westerly at 2 m s<sup>-1</sup> by 850 mb. Above 850 mb, the flow continues westerly at 3 m s<sup>-1</sup> until above 400 mb, where the speeds increased to near 6 m s<sup>-1</sup>, with the direction veering slightly to become more northwesterly.

Unlike in the calm initialization, the sea and land breezes that develop will be influenced by this large-scale flow pattern, either tending to enhance the circulation or retard it. All three domains and boundary conditions were initialized to these average conditions.



## Day One

Throughout the early hours of the model run, there is no indication of a developing land breeze. The large-scale flow pattern over the Wassaw Sound is retarding its development. The initial conditions, with southerly winds at the surface and westerly winds aloft, closely matched those of a decaying sea breeze, inhibiting the early development of a land breeze as seen in the calm initialization.

By 01/08, there is evidence of the land breeze affecting the larger scale flow. The nearshore wind vectors have veered to become slightly offshore and decreased in speed, to less than  $1 \text{ m s}^{-1}$ , while the rest of the domain retains its southerly flow. This influence of the land breeze continues for the next four hours, having its maximum effect on the large-scale flow by 01/12 UTC (Figure 3.18a). At that time, its effects near the Wassaw Sound are confined to within 6 km of the coast and 6 km seaward.

Cross-sectional moisture analysis (Figure 3.18b) does show a very weak land breeze circulation 12 km wide with an offshore flow depth less than 10 mb (100 m) deep and a total depth of 100 mb (1000 m). This depth may be attributed in part to the large-scale flow being forced up and over the land breeze.

Over the next four hours, the transition from the land breeze to sea breeze occurs. Similar to the calm initialization, the land breeze effects decay and the winds at the shoreline become light. By 01/15 UTC (Figure 3.19a), the shoreline winds have switched direction to  $160^\circ$  and increased in speed to over  $1 \text{ m s}^{-1}$ . By 01/16 UTC, the sea breeze has increased in intensity to near  $4 \text{ m s}^{-1}$  (Figure 3.19b) and has moved inland up to 22 km. The circulation is expanding at speeds up to  $15 \text{ km hr}^{-1}$  landward while the seaward

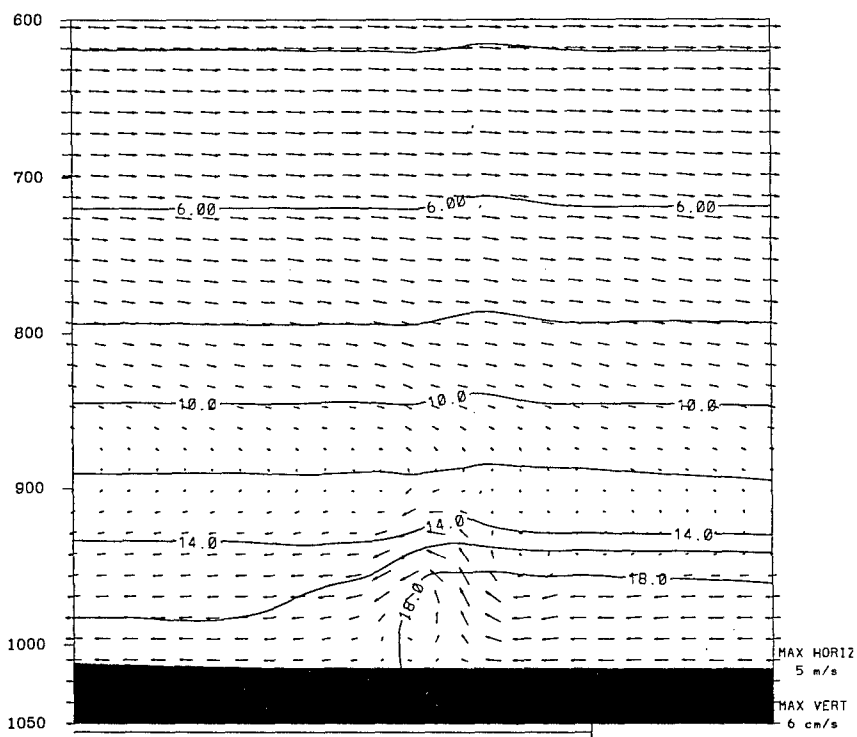
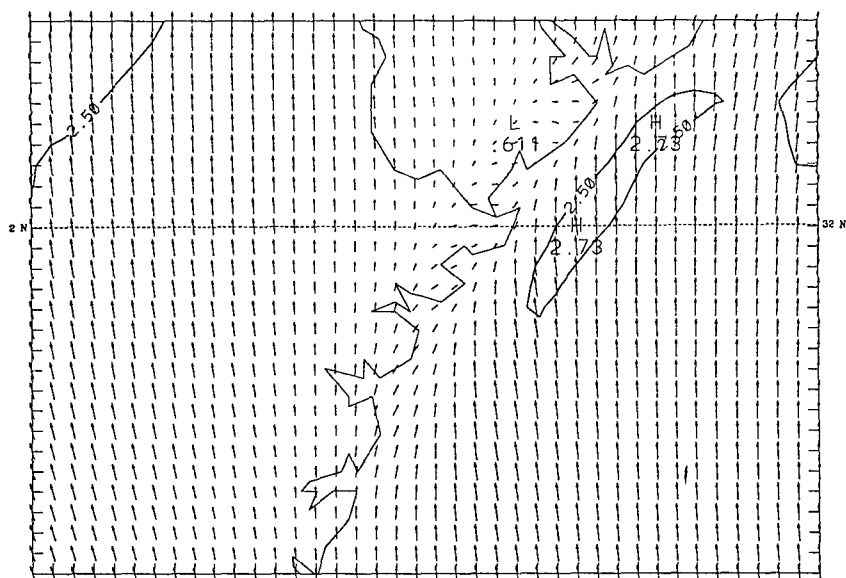


Figure 3.18. a: As in Figure 3.3a except for 01/12 UTC. b: As in Figure 3.3b except for 01/12 UTC.

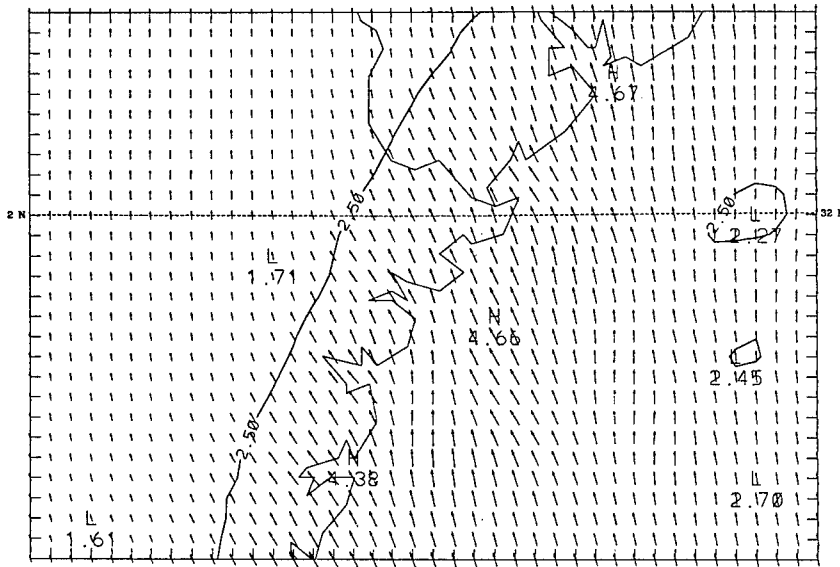
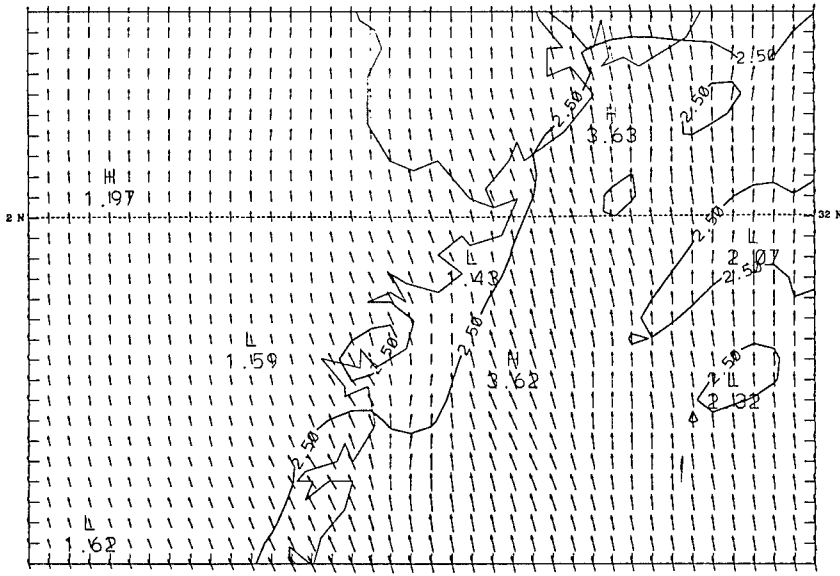


Figure 3.19. a: As in Figure 3.3a except for 01/15 UTC. b: As in Figure 3.3a except for 02/16 UTC.

expansion is being masked by the large-scale flow.

The sea breeze initiated with a direction south of pure onshore in response to the large-scale pressure gradient. In the calm initialization, the sea breeze began flowing perpendicular to the shore because there was no large-scale pressure gradient (Figure 3.20a). In this model run however, the winds veered slightly as they adjusted to the large-scale pressure gradient (Figure 3.20b).

The sea breeze front has moved through the entire 4-km domain by 01/20 UTC. Inland, temperatures reached over 32 °C while the over water temperatures remained near 26 °C. The sea breeze reaches a maximum wind speed across the Wassaw Sound of near 7 m s<sup>-1</sup> at 01/21 UTC from a direction of 160° (Figure 3.21a). Cross-sectional moisture analysis of the 12-km domain (Figure 3.21b) shows the onshore flow to be 40 mb (450 m) deep and the total depth of the circulation, to the top of the sea breeze head, to be 220 mb (2300 m). The maximum landward extent of the sea breeze, as marked by the 14.0 g kg<sup>-1</sup> isohume, is 112 km. This landward extent also closely corresponds to the landward edge of the 5 m s<sup>-1</sup> isotach on the 36-km domain (Figure 3.22a). The seaward extent of the circulation is masked by the background flow.

## **Day Two**

Overnight, the wind speeds decrease seaward to landward and the wind direction veers with time. The sea breeze decay, based on the wind direction veering past 180°, is masked by the background flow but can also be determined by examining the coastal temperature gradient. Using this criteria, the sea breeze decayed by 02/02 UTC as the temperature gradient has weakened significantly across the domain. By 02/10 UTC, the

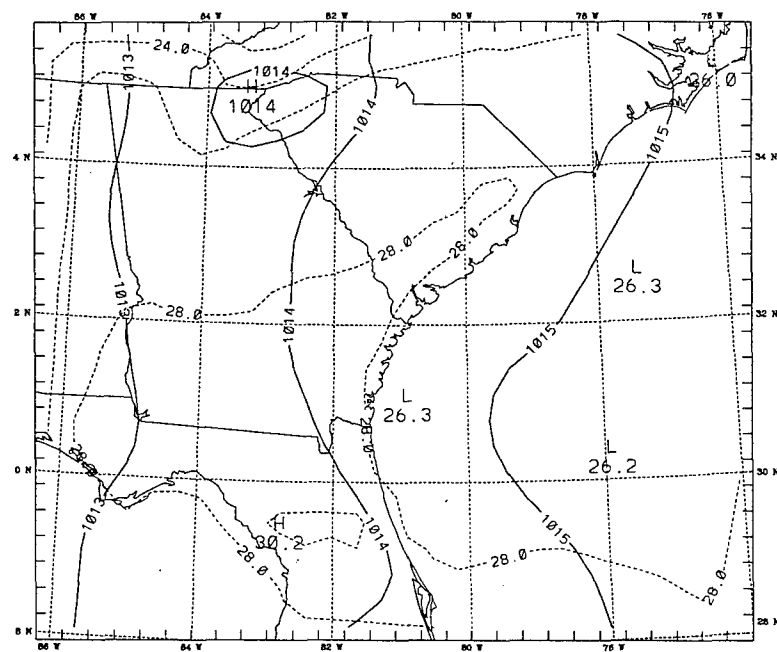
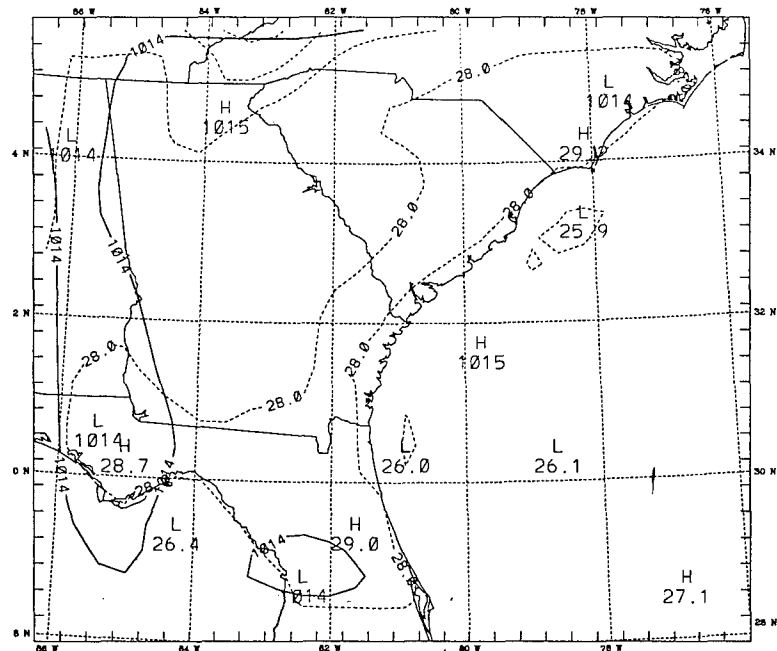


Figure 3.20. a: As in Figure 3.17a except for the calm idealization at 01/15 UTC. b: As in Figure 3.17a except for the average idealization at 01/15 UTC.

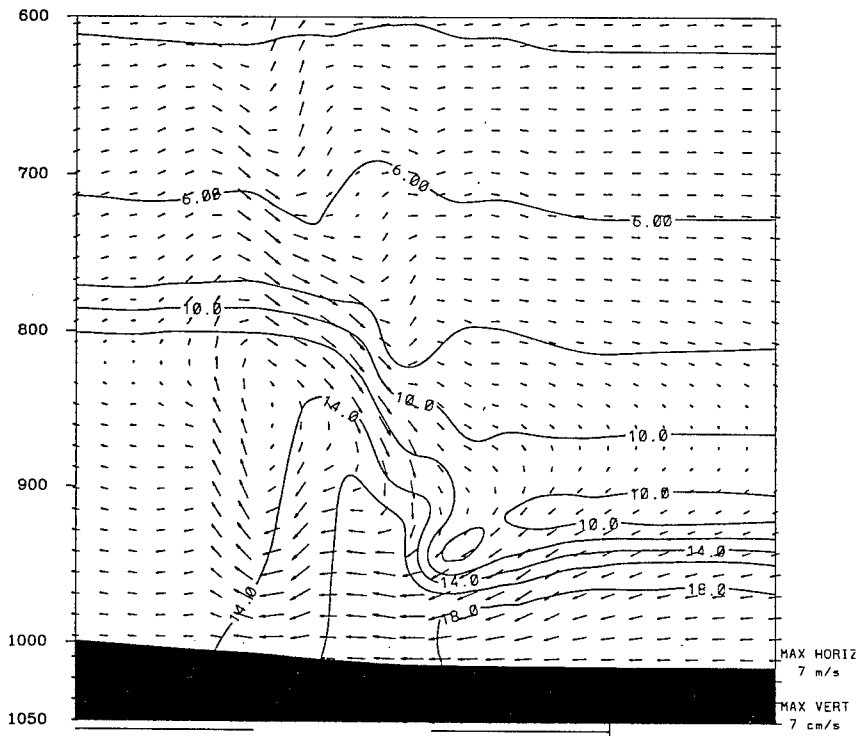
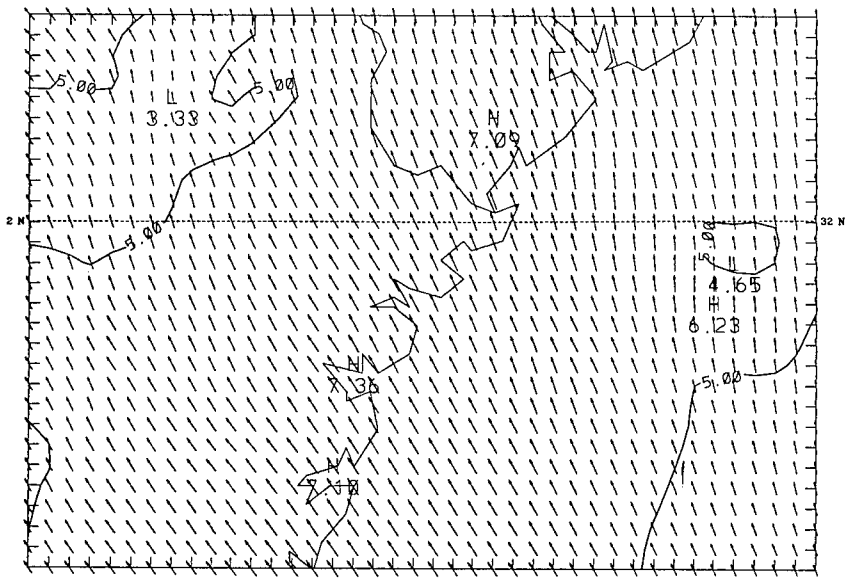


Figure 3.21. a: As in Figure 3.3a except for 01/21 UTC. b: As in Figure 3.10b except for 01/20 UTC.

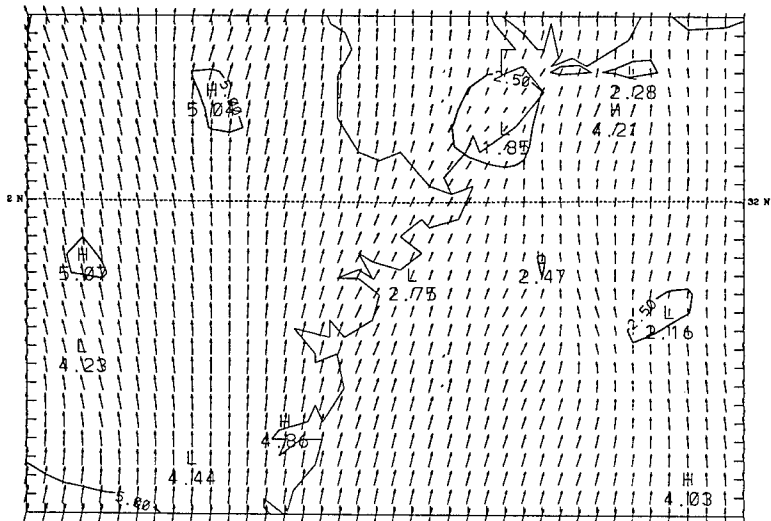
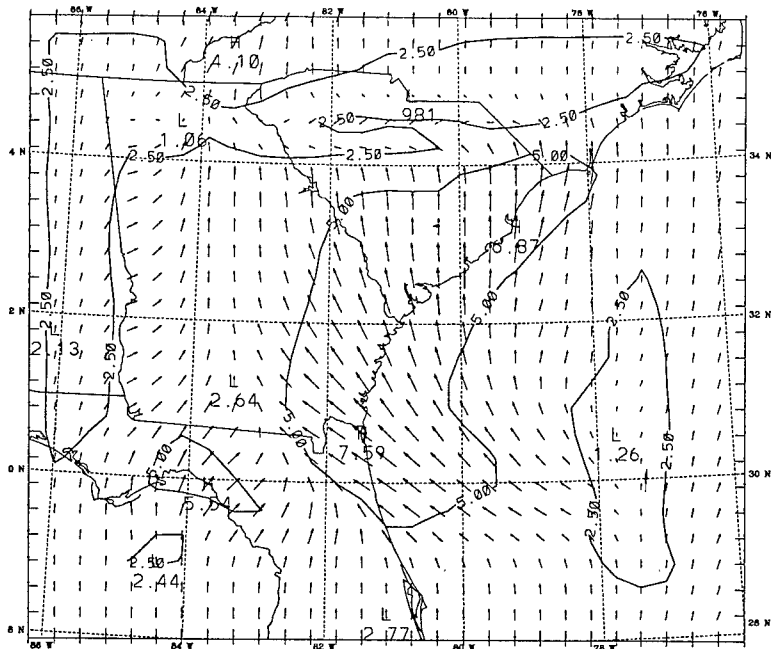


Figure 3.22. a: As in Figure 3.3a except for 36-km domain at 01/23 UTC. b: As in Figure 3.3a except for 02/10 UTC.

coastal winds have become almost alongshore, blowing from  $210^\circ$ , and the speeds have decreased to less than  $3 \text{ m s}^{-1}$  (Figure 3.22b). Over the inland areas, the winds have retained some of their onshore flow character but at the shoreline, the winds are approximately parallel to the coast. Most of the land areas of the domain are still experiencing relatively strong winds ( $4\text{-}5 \text{ m s}^{-1}$ ). By 02/12 UTC, there is no evidence of any effects on the flow field by the land breeze.

The land breeze did not develop on day two because of the temperature field. During the developmental period of the land breeze on day one of the simulation, the coastal temperature gradient was perpendicular to the shore (Figure 3.23a). Although the large-scale flow was southerly, the strong, normal to the coast temperature gradient developed a compact land breeze that effected the nearshore wind flow. On day two of the simulation, the large-scale flow was still southerly but the wind speeds were generally greater than  $2.5 \text{ m s}^{-1}$  across the entire domain. This produced a coastal temperature gradient that was parallel to the shoreline (Figure 3.23b). Thus the stronger large-scale flow forced the development of a temperature gradient which inhibited land breeze formation.

By 02/16 UTC, the winds across the Wassaw Sound have become onshore and the sea breeze has begun blowing from  $170^\circ$ , but this time with even stronger winds. Wind speeds across the area are near  $4 \text{ m s}^{-1}$  (Figure 3.24a) and the sea breeze front is rapidly advancing inland at speeds up to  $20 \text{ km hr}^{-1}$ . The leading edge of the sea breeze front has quickly moved inland 22 km (marked by the  $16.0 \text{ g kg}^{-1}$  isohume) and the head structure is already beginning to develop, much as on day one (Figure 3.24b). By 02/20 UTC, the



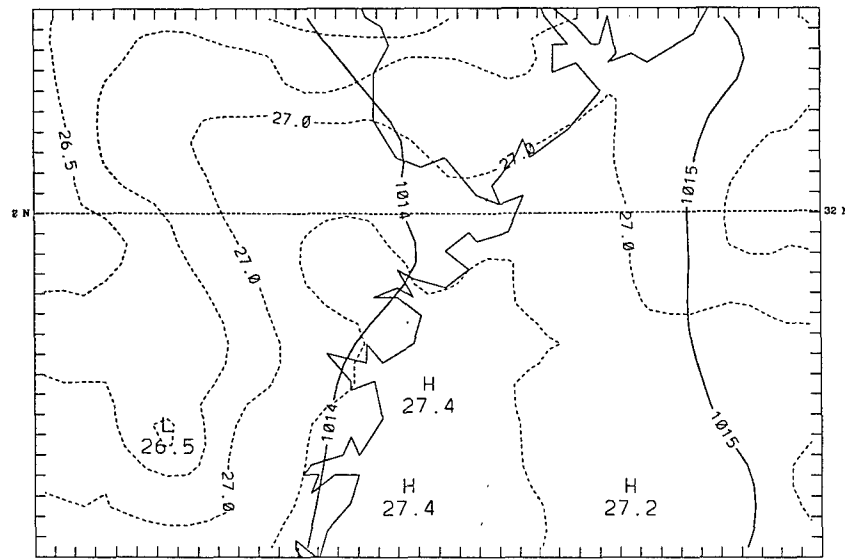
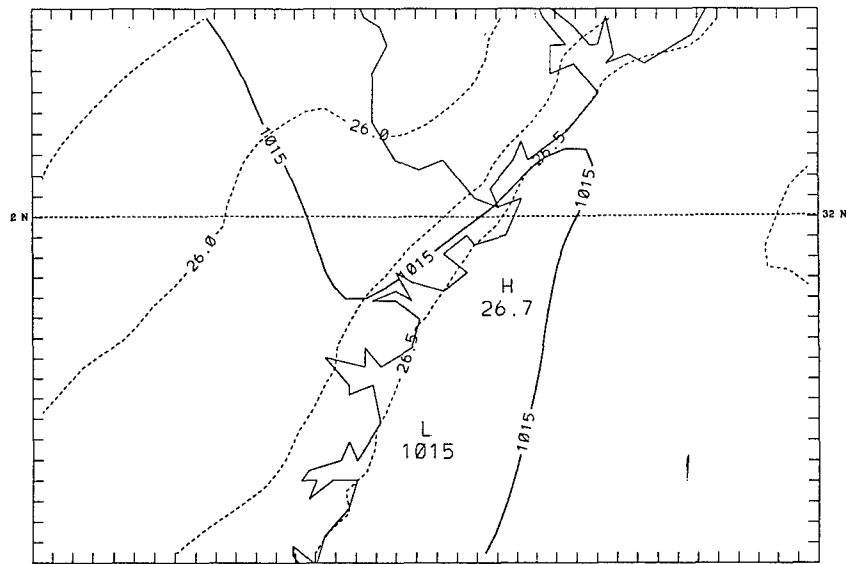


Figure 3.23. a: As in Figure 3.17a except for the 4-km domain at 01/12 UTC with a pressure contour interval of 0.25 mb and a temperature contour interval of 0.25 °C . b: As in Figure 3.24a except for 02/12 UTC.

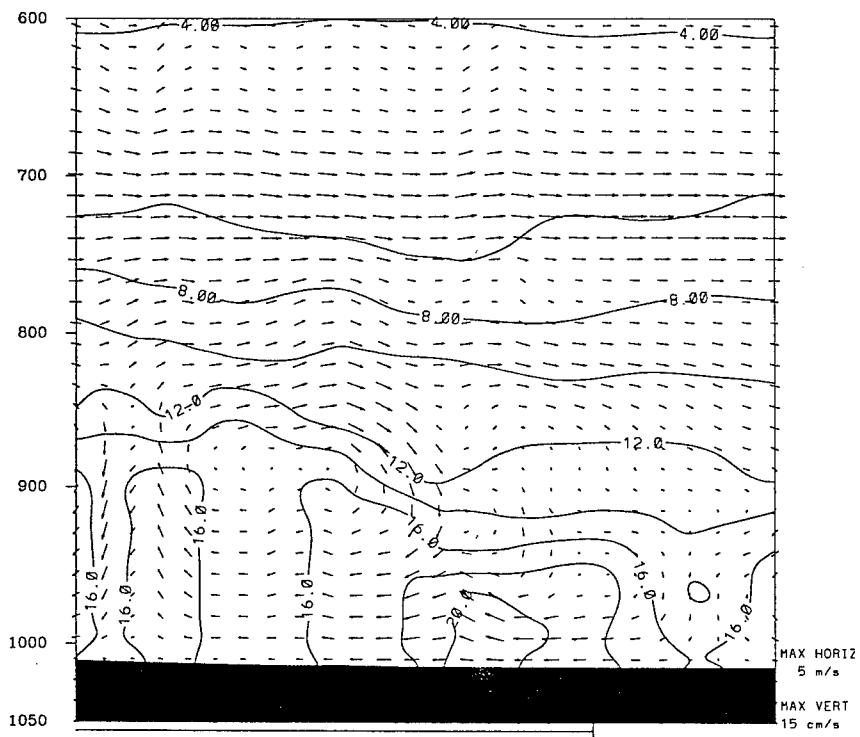
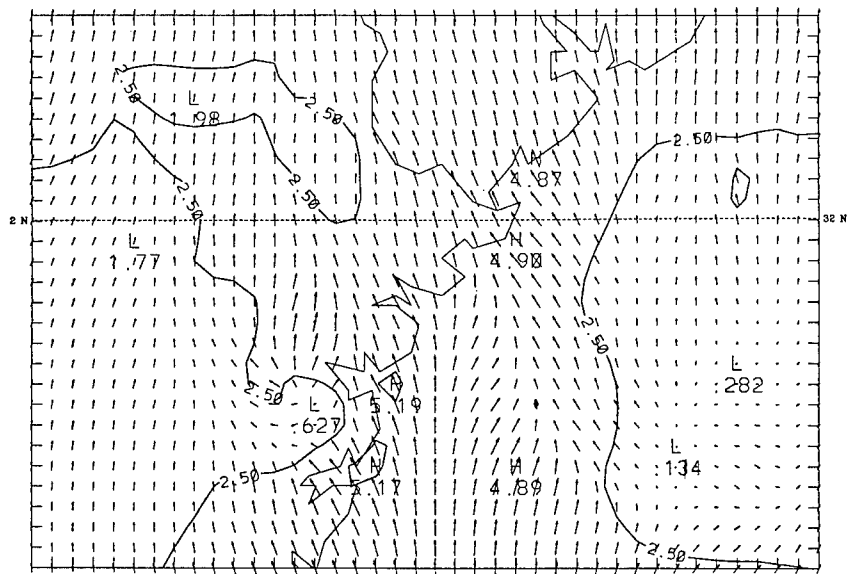


Figure 3.24. a: As in Figure 3.3a except for 02/16 UTC. b: As in Figure 3.3b except for 02/16 UTC.

sea breeze has reached a maximum strength of  $8 \text{ m s}^{-1}$  blowing from a direction of  $160^\circ$ . Inland, temperatures reached over  $33^\circ\text{C}$  while the over water temperatures again remained near  $26^\circ\text{C}$ .

As on day one, the sea breeze has propagated well inland moving through the 4-km domain and through much of the 12-km domain, reaching a maximum landward extent of 120 km. The circulation reached a maximum depth of 250 mb (2500 m) with the onshore flow approximately 40 mb (450 m) deep. The offshore extent is masked by the background flow. Pressure patterns for the average run, for both days of simulation, are similar to those presented for the calm initialization.

### **Offshore Initialization**

The third model run performed was the offshore initialization. This run was to simulate how the LSBS would develop with an offshore forcing. The thermodynamic and wind profile (Figure 3.25a) were compiled as described in Chapter 2, using the 850-mb and 700-mb winds to determine the flow regime. The initial flow field has surface winds from the southwest at  $3 \text{ m s}^{-1}$ , veering with height to become westerly at  $4 \text{ m s}^{-1}$ , and finally northwesterly at  $5 \text{ m s}^{-1}$  from 850 mb to the top of the sounding. This flow field is an example of allowing the boundary layer winds to vary, as discussed in Chapter 2, while still maintaining the large-scale forcing as offshore. All three domains and boundary conditions were initialized to these conditions.

### **Day One**

The initial near-surface flow field shows  $3 \text{ m s}^{-1}$  southwesterly winds across the entire domain (Figure 3.25b) which persists for the first 14 hours of the model run. No

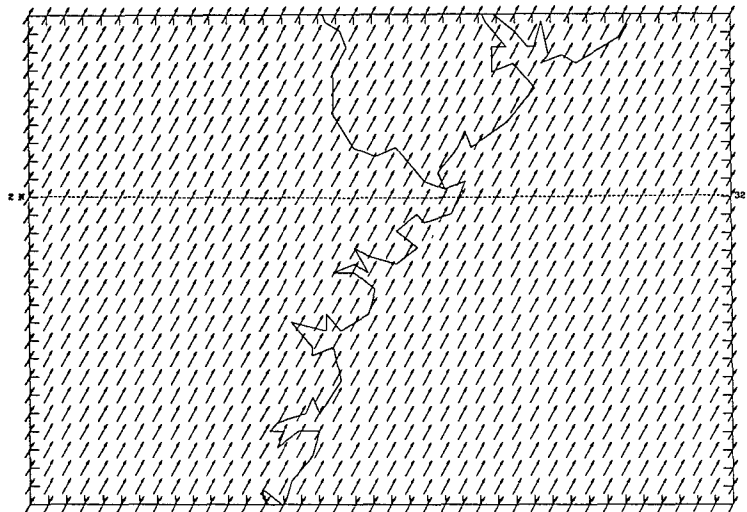
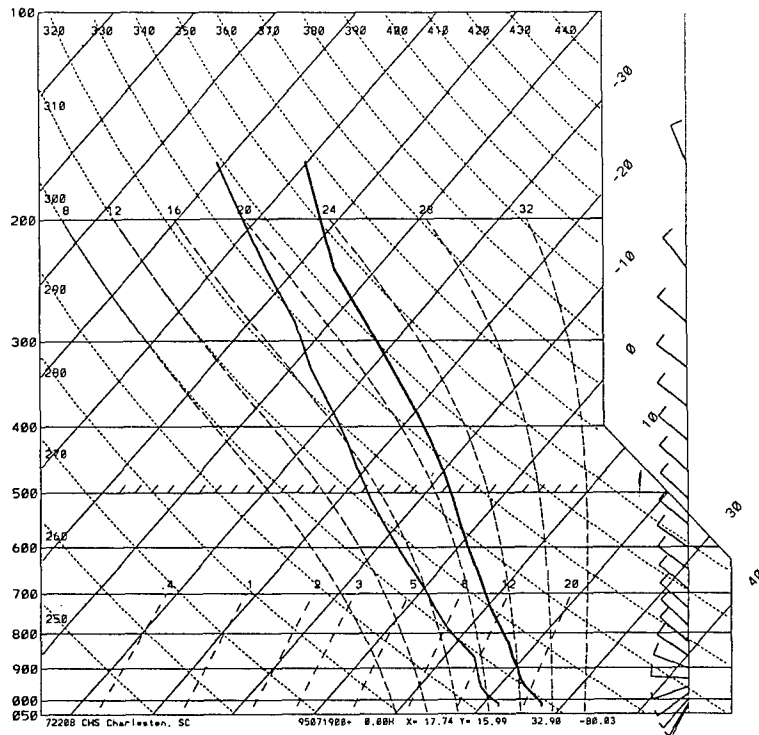


Figure 3.25. a: Thermodynamic and wind profile used to initialize the offshore idealization. Wind barbs are in knots. b: As in Figure 3.3a except for 01/00 UTC.

land breeze developed because the forcings were not conducive for development. The large-scale pressure gradient was promoting winds greater than  $2.5 \text{ m s}^{-1}$  at the lowest levels (Figure 3.26a) which prevented the development of a temperature gradient normal to the coast, required to drive the land breeze (Figure 3.26b).

By 01/15 UTC, inland heating forces a coastal temperature gradient to develop (Figure 3.27a). As a result, the sea breeze begins to form at the coastline, blowing at  $2.5 \text{ m s}^{-1}$  from  $170^\circ$  (Figure 3.27b). By the next hour, the sea breeze has moved inland 4 km and speeds across the Wassaw Sound have increased to  $5 \text{ m s}^{-1}$ , still blowing from  $170^\circ$ .

The sea breeze reaches a maximum at 01/21 UTC, with a speed of  $8 \text{ m s}^{-1}$  from  $170^\circ$  (Figure 3.28a). The sea breeze has propagated inland at speeds up to  $11 \text{ km hr}^{-1}$ , with a maximum inland penetration of 45 km. The circulation has a maximum depth of 240 mb (2450 m) with an onshore component reached 30 mb (300 m) deep.

Cross-sectional moisture analysis shows structure similar to the previous cases, with the sea breeze front being marked by the  $16.0 \text{ g kg}^{-1}$  isohume, and the broader, drier subsidence area seaward (Figure 3.28b). The offshore extent of the circulation reached 135 km and expanded at rates up to  $15 \text{ km hr}^{-1}$  (Figure 3.29a), aided by the offshore winds aloft.

## **Day Two**

Overnight, the winds continue to veer with time and speeds gradually decrease from the land to the sea. After 02/02 UTC, the winds lose their sea breeze character and by 02/11 UTC, the winds become almost parallel to the coast. Again, no land breeze developed on the second day because the large-scale forcings promoted wind speeds

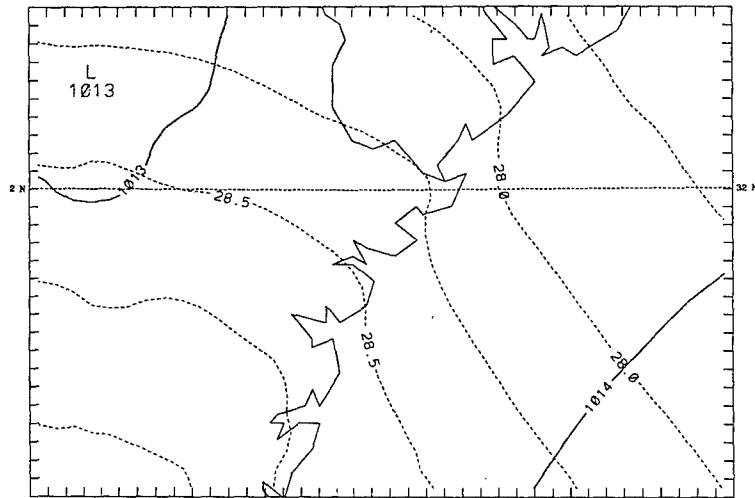
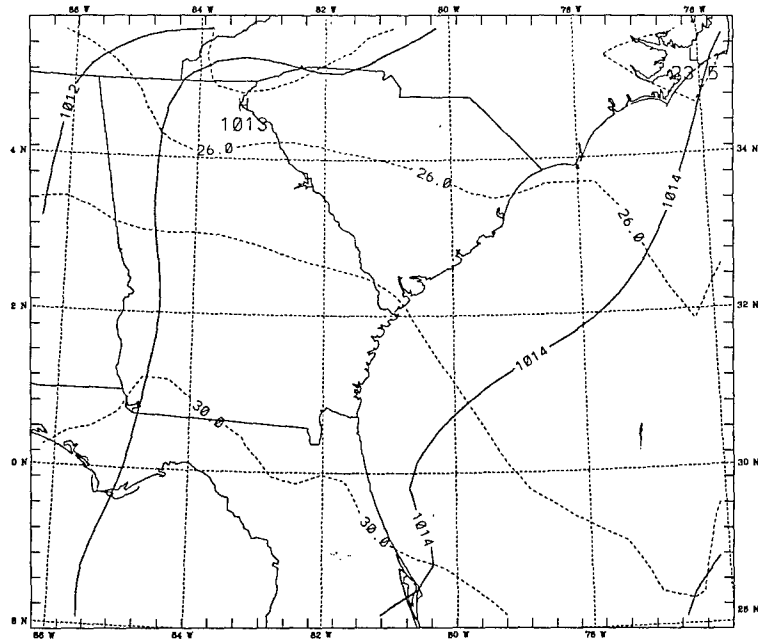


Figure 3.26. a: As in Figure 3.17a except for 01/11 UTC. b: As in Figure 3.23a except for 01/11 UTC.

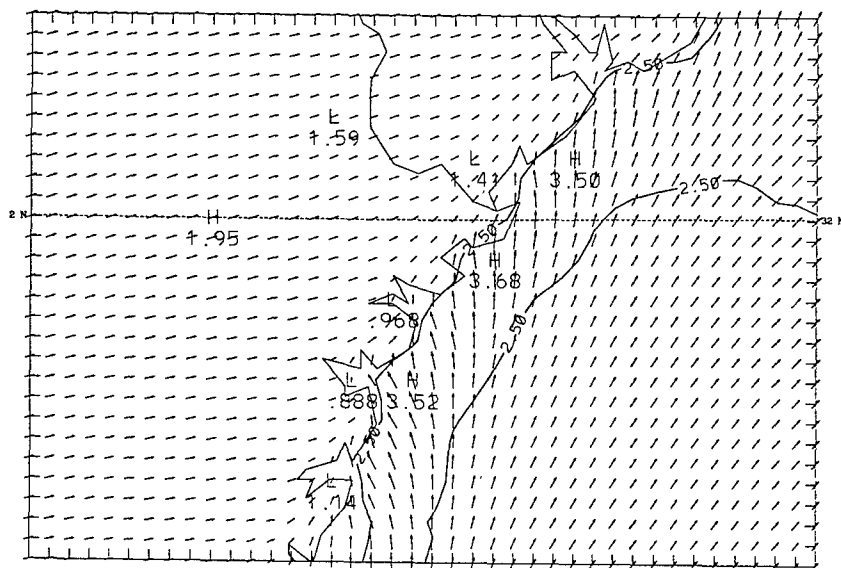
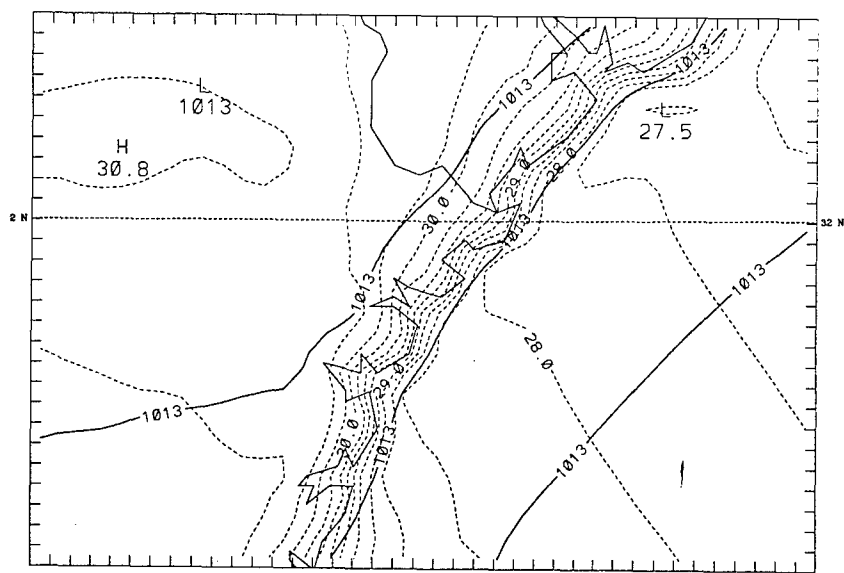


Figure 3.27. a: As in Figure 3.23a except for 01/15 UTC. b: As in Figure 3.3a except for 01/15 UTC.

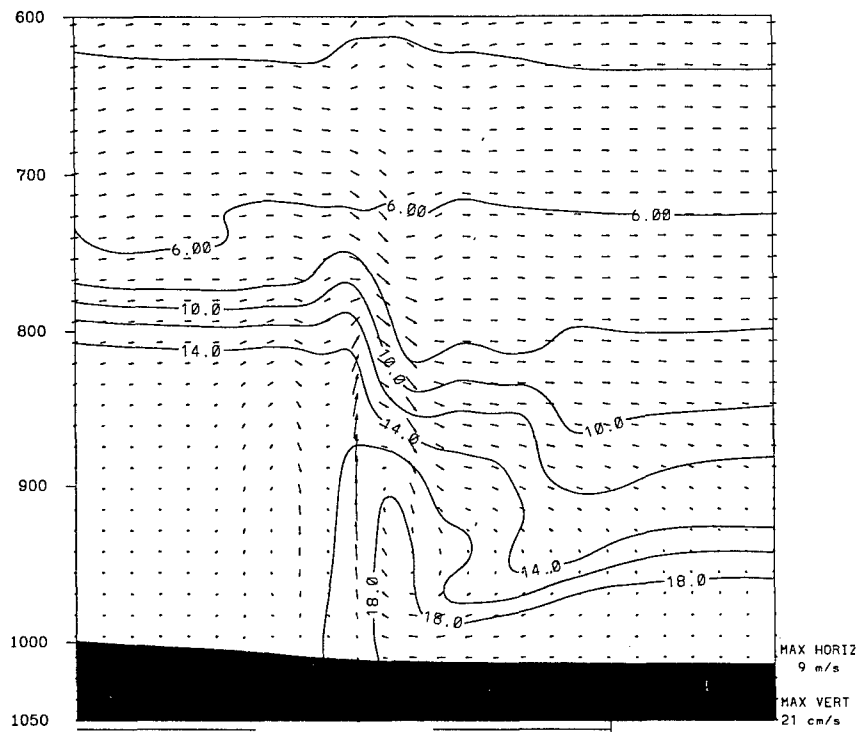
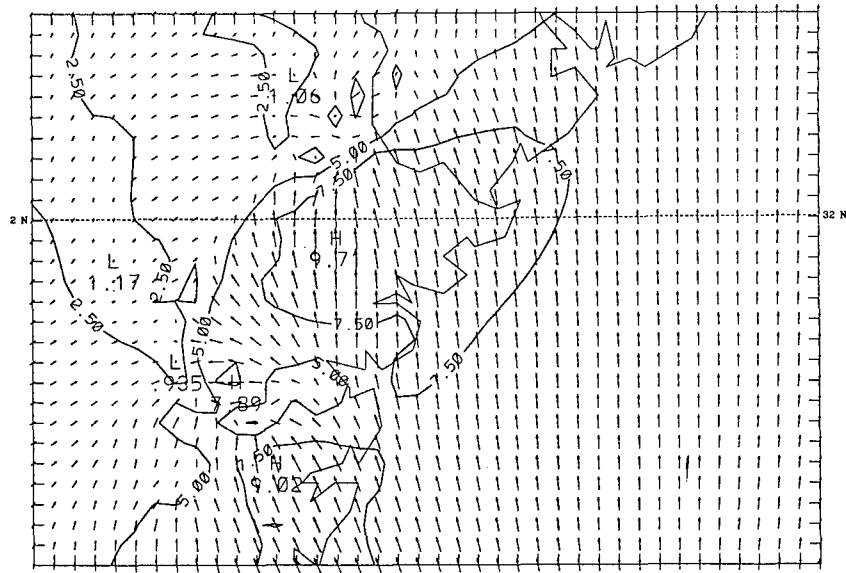


Figure 3.28. a: As in Figure 3.3a except for 01/21 UTC. b: As in Figure 3.10b except for 01/20 UTC.



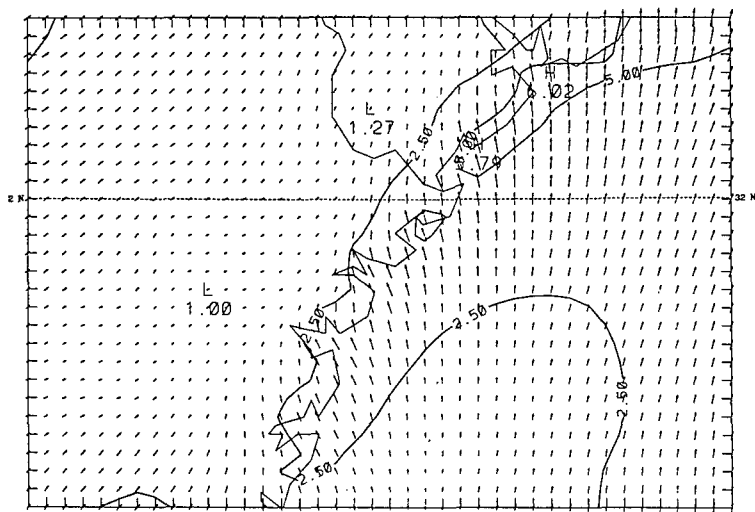
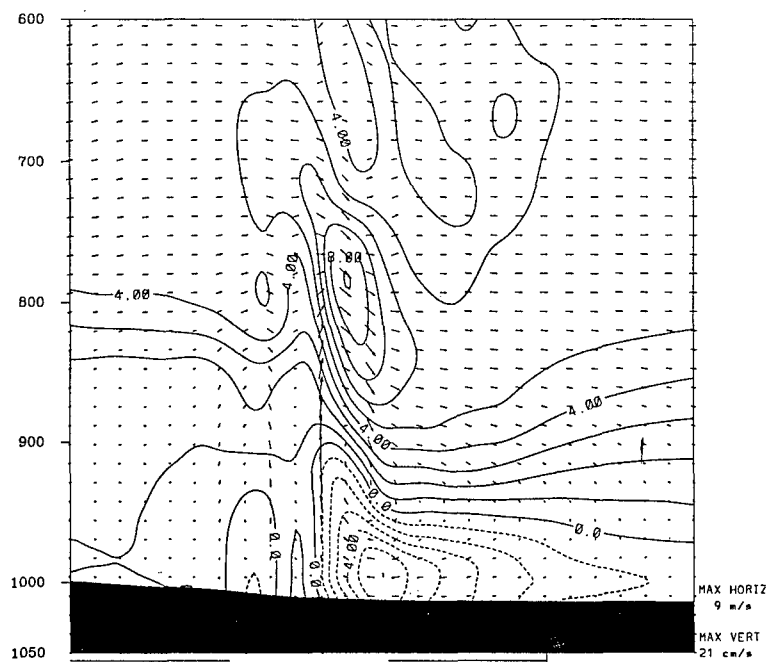


Figure 3.29. a: As in Figure 3.11b except for 01/20 UTC. b: As in Figure 3.3a except for 02/17 UTC.

greater than  $2.5 \text{ m s}^{-1}$ , not allowing a coastal temperature gradient to develop.

By 02/17 UTC, the sea breeze begins across the Wassaw Sound at  $2.5 \text{ m s}^{-1}$ , blowing from  $170^\circ$  (Figure 3.29b). Because no land breeze developed, there was not an abrupt transition to the sea breeze as seen in other simulations. Instead, the southwesterly winds from the previous hours backed and became onshore as the local forcings developed (Figure 3.30a). Within the next hour, the sea breeze quickly intensifies and wind speeds increase to near  $6 \text{ m s}^{-1}$ .

By 02/20 UTC, the sea breeze reaches its maximum speed,  $7 \text{ m s}^{-1}$  from  $170^\circ$  (Figure 3.30b). The sea breeze has moved inland at speeds up to  $11 \text{ km hr}^{-1}$ , reaching a maximum penetration of 40 km (Figure 3.31a). The maximum depth of the circulation is 270 mb (2800 m) with the onshore component 30 mb (300 m) deep. The seaward extent is 145 km and it advanced at speeds up to  $15 \text{ km hr}^{-1}$ . By the end of the model run, the winds have started to diminish across the Wassaw Sound to  $5 \text{ m s}^{-1}$  and veered to  $180^\circ$ .

The offshore initialization provides an excellent example of sea breeze induced convection. With the large-scale flow opposing the inland movement of the circulation, the sea breeze front can act as a focal point for convection. As a result, scattered convection initiates across the area as the sea breeze matures (Figure 3.31b).

### **Onshore Initialization**

The fourth model run executed was the onshore initialization. This run was to simulate how the LSBS would develop with an onshore forcing. The thermodynamic and wind profile (Figure 3.32a) were compiled as described in Chapter 2, using the 850-mb and 700-mb winds to determine the flow regime.

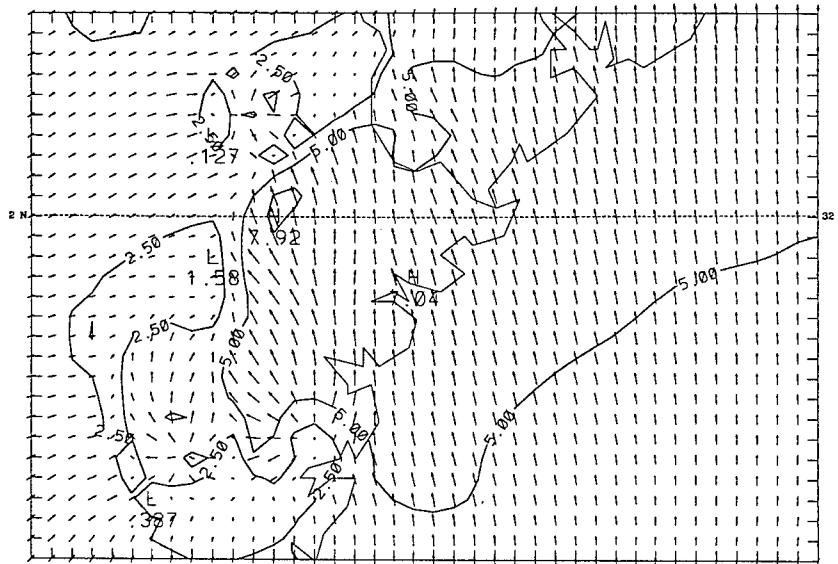
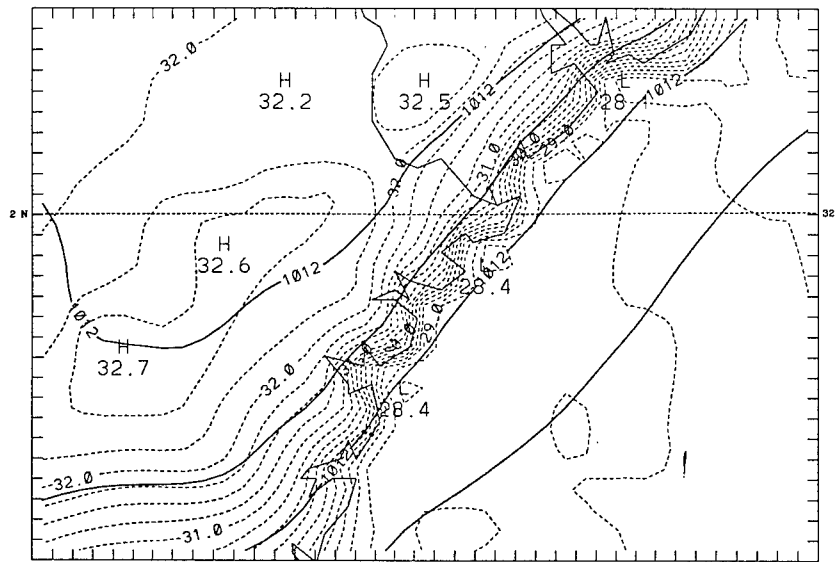


Figure 3.30. a: As in Figure 3.23a except for 02/17 UTC. b: As in Figure 3.3b except for 02/19 UTC.

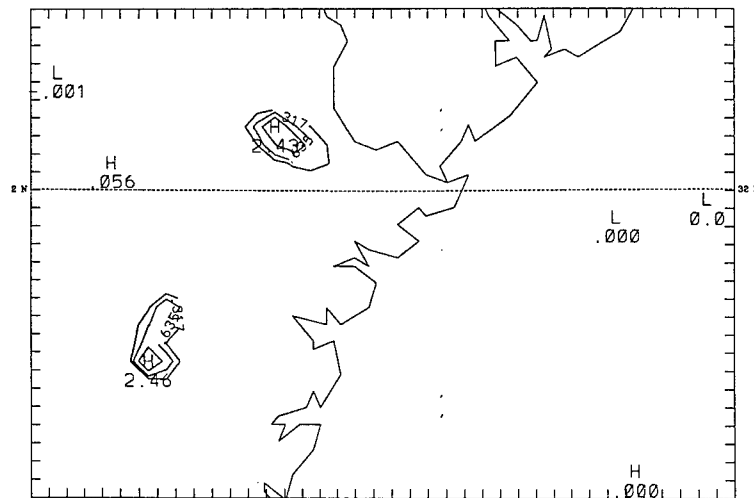
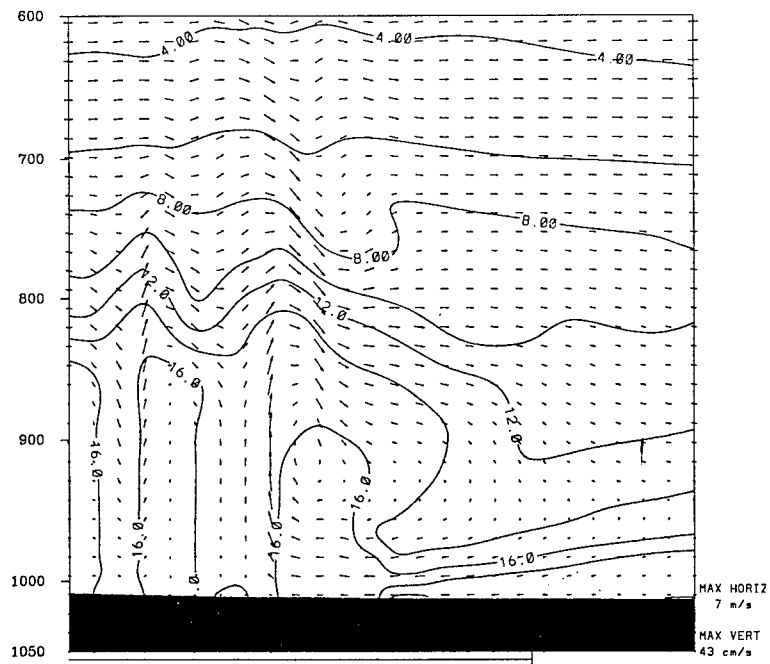


Figure 3.31. a: As in Figure 3.3b except for 02/20 UTC. b: Precipitation in cm across the 4-km domain for day one of the simulation.

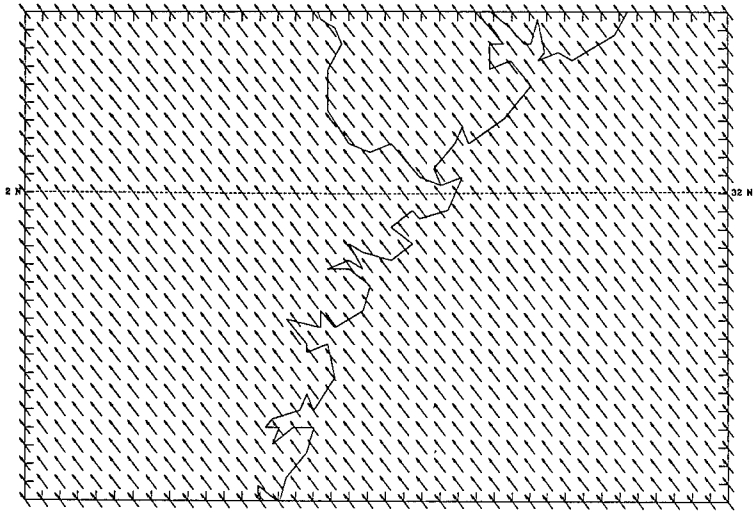
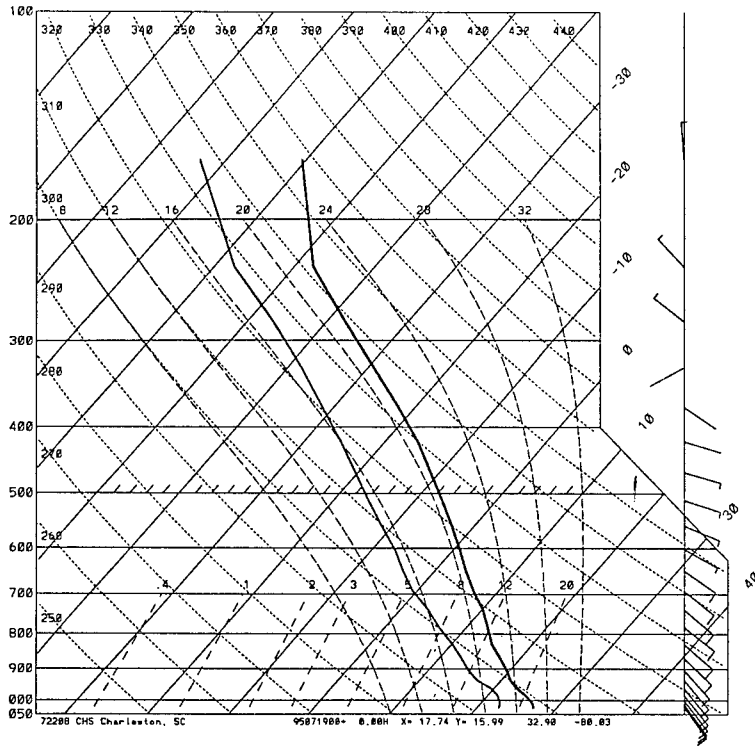


Figure 3.32. a: As in Figure 3.25a except for onshore idealization. b: As in Figure 3.3a except for 01/00 UTC.

The initial flow fields have  $3.5 \text{ m s}^{-1}$  southeasterly winds at the lowest model layer. The winds increase in speed to  $5 \text{ m s}^{-1}$  in the layer from 900 to 700 mb. Above 700 mb, the winds back slowly and decrease in speed, becoming easterly at  $3 \text{ m s}^{-1}$ . Above 400 mb, the winds become light and switch to northwesterly and then to northerly at  $3 \text{ m s}^{-1}$ . All three domains and boundary conditions were initialized to these conditions.

### **Day One**

The initial near-surface flow field shows  $3.5 \text{ m s}^{-1}$  winds from  $150^\circ$  across the entire domain (Figure 3.32b). Overnight, the winds continue southeasterly but speed decreases across the land to  $2.5 \text{ m s}^{-1}$  while the over-water speeds remain  $4\text{-}5 \text{ m s}^{-1}$ . Although an inland temperature gradient does form that could support the development of the land breeze, the large-scale forcings have formed the gradient inland and weakened it, preventing the land breeze formation (Figures 3.33a-b).

As the day progresses, inland heating does allow the development of a weak coastal temperature gradient (Figure 3.34a) however there is no evidence in the flow fields of the development of the sea breeze. Cross-sectional moisture analysis at the time of probable sea breeze initiation (01/16 UTC) does show the  $16.0 \text{ g kg}^{-1}$  isohume depicting a structure similar to those seen in the previous runs (Figure 3.34b), but the continued development of the sea breeze front and head using the  $16.0 \text{ g kg}^{-1}$  isohume is not supported by other plots. Cross-sectional wind analysis does show an area of increased speeds just inshore that may be the result of the sea breeze adding to the background flow (Figure 3.35a). Cross-sectional moisture analysis of the time of

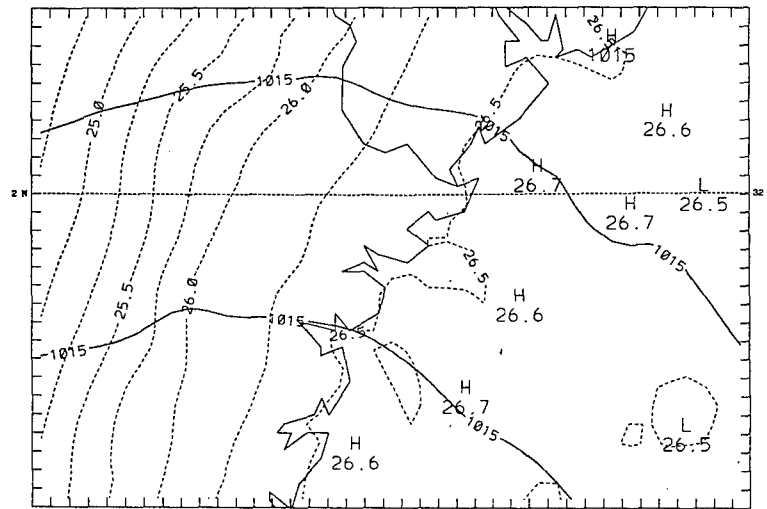
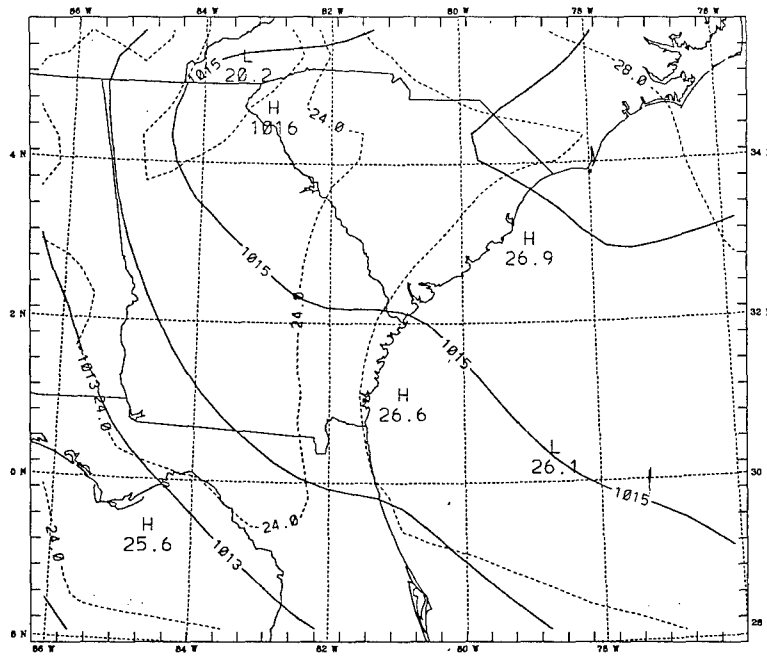


Figure 3.33. a: As in Figure 3.17a except for 01/11 UTC. b: As in Figure 3.23a except for 01/11 UTC.

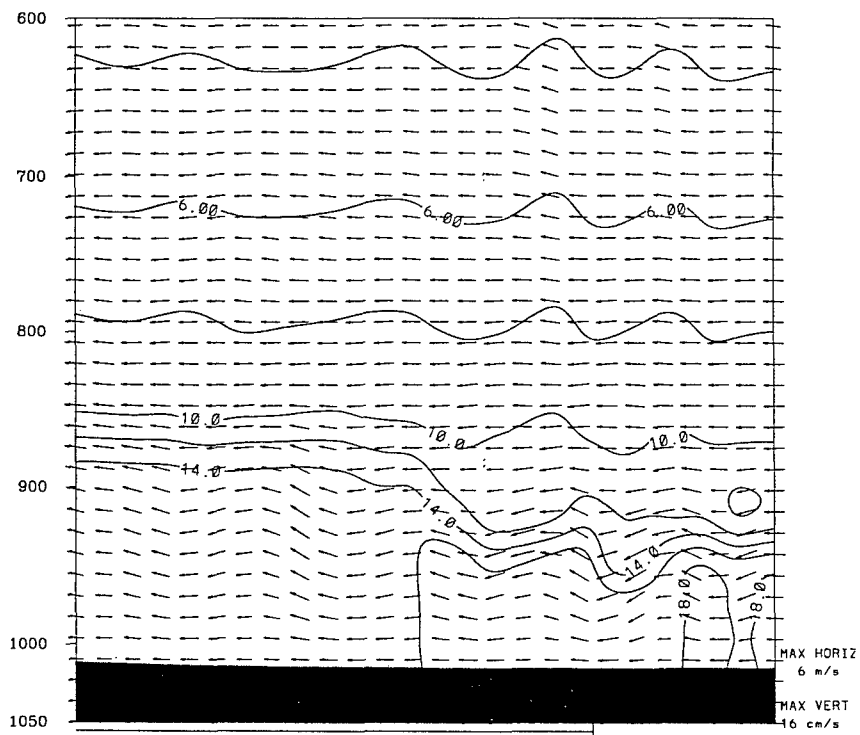
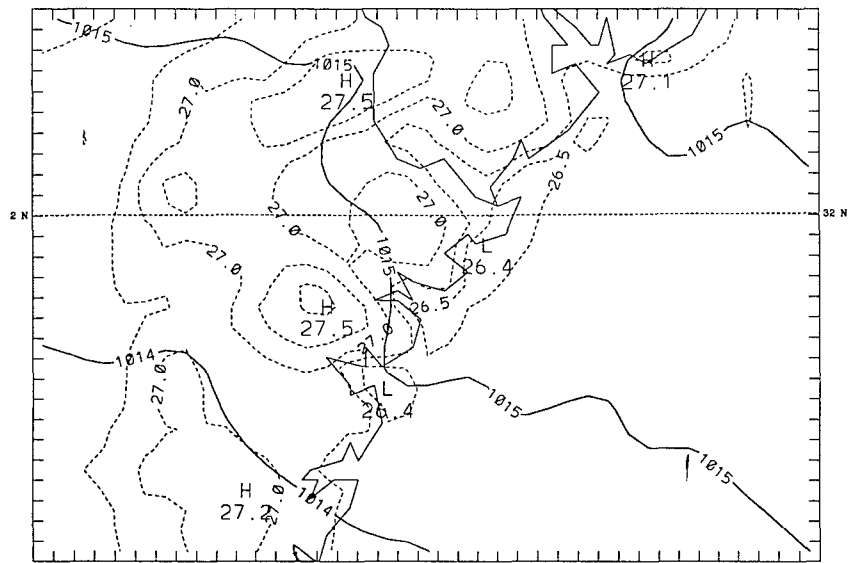


Figure 3.34. a: As in Figure 3.23a except for 01/16 UTC. b: As in Figure 3.3b except for 01/16 UTC.



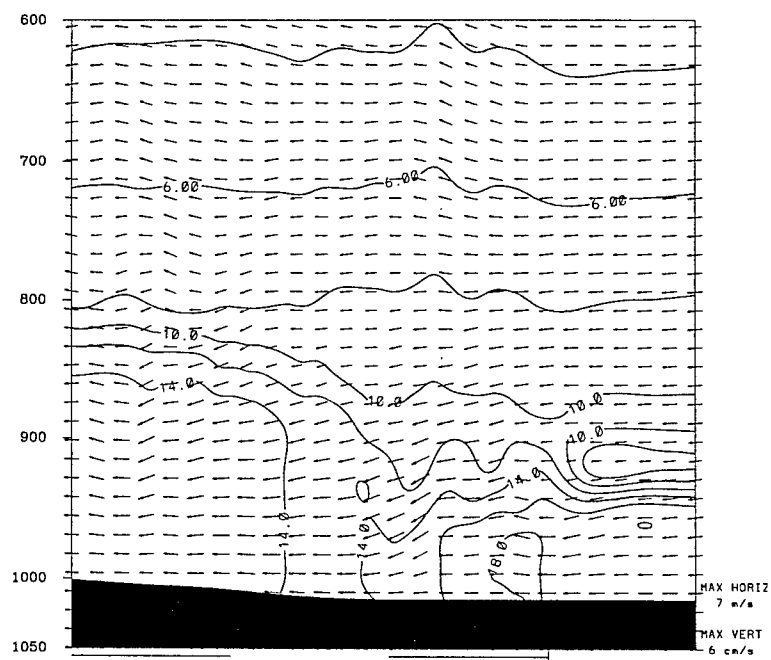
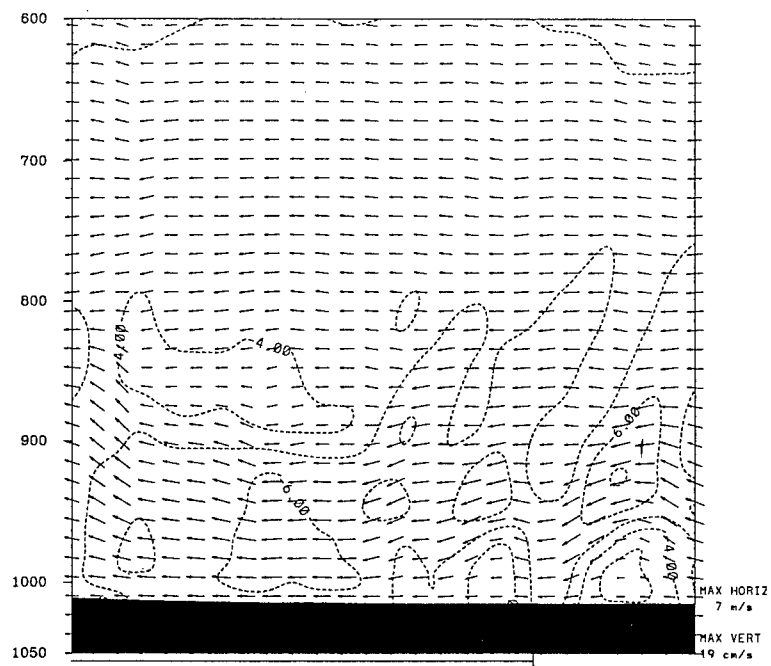


Figure 3.35. a: As in Figure 3.11b except for the 4-km domain at 01/18 UTC. b: As in Figure 3.10b except for 01/20 UTC.

probable maximum sea breeze strength (01/21 UTC) does show a compacted marine PBL with a dry area aloft, similar to the moisture structure observed in other model runs (Figure 3.35b) however there is no clear indication in any of the plots (horizontal wind fields or cross-sectional analyses) of the formation of the sea breeze as would normally be depicted. Sea breeze formation is being inhibited or masked by the background flow.

### **Day Two**

Overnight, the winds continue from the southeast. Decreased wind speeds, generally  $1-2.5 \text{ m s}^{-1}$  across the inland areas, allows a stronger coastal temperature gradient to develop (Figure 3.36a). As a result, by 02/11 UTC, there is evidence of the land breeze having an effect on the larger scale flow similar to that modeled in day one of the average idealization. Cross-sectional wind analysis shows an area of decreased wind speeds from the coast extending inland 10 km (Figure 3.36b). This area of decreased wind speeds may be a representation of the land breeze, an offshore flow, combining with the large-scale onshore flow. Seaward 5 km, the large-scale flow is deflected up and over this area of lighter wind speeds, reflected in the moisture analysis (Figure 3.37a). Maximum depth of this feature is 110 mb (1150 m). This impact by the land breeze on the large-scale coastal flow pattern continues until 02/13 UTC, when inland heating begins to reverse the coastal temperature gradient.

The rest of the model run is similar to day one, with predominately southeasterly flow across the entire domain (Figure 3.37b). A coastal temperature gradient again develops with a slight increase in wind speeds occurring just inland. Cross-sectional moisture analysis again shows a dry area aloft with a compacted marine PBL.

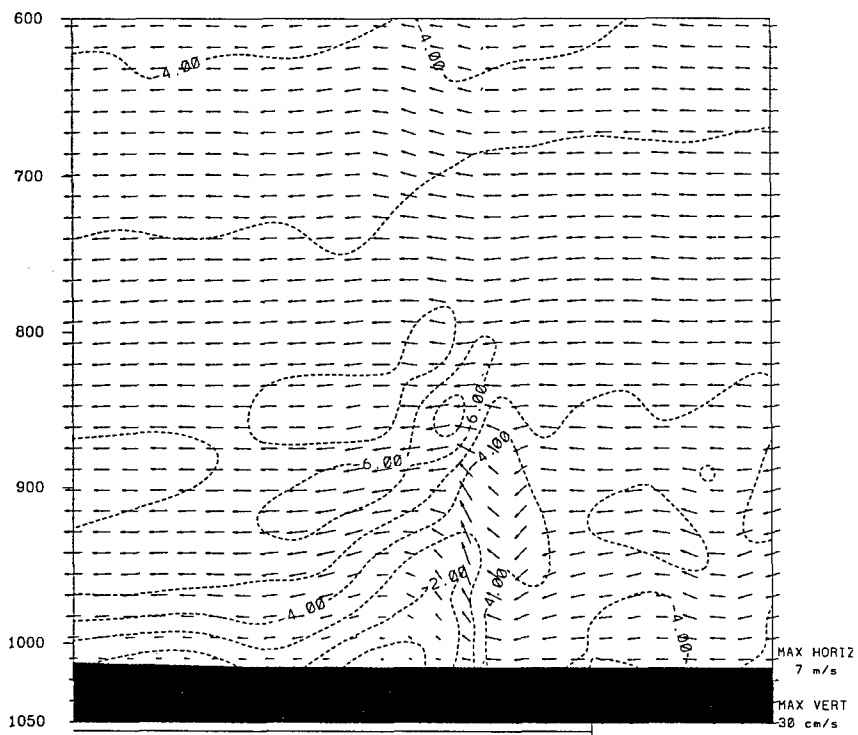
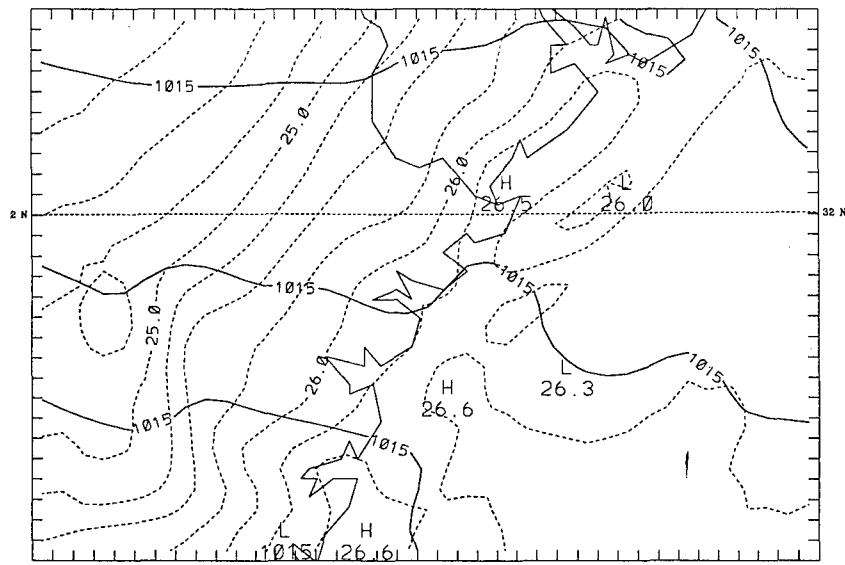


Figure 3.36. a: As in Figure 3.23a except for 02/11 UTC. b: As in Figure 3.35a except for 02/11 UTC.

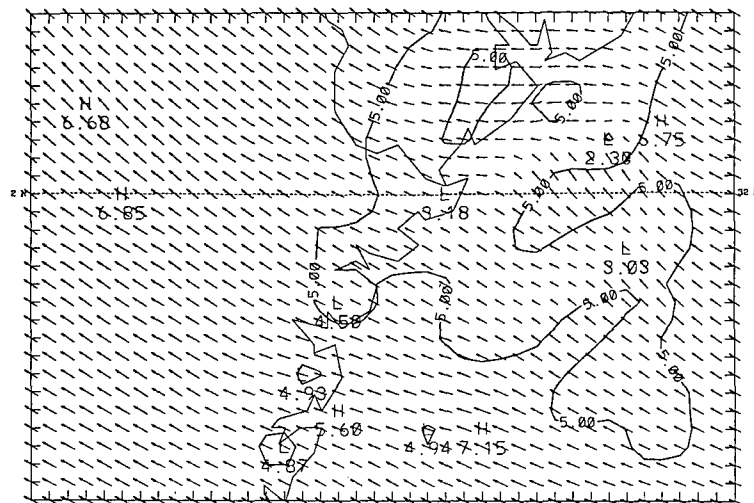
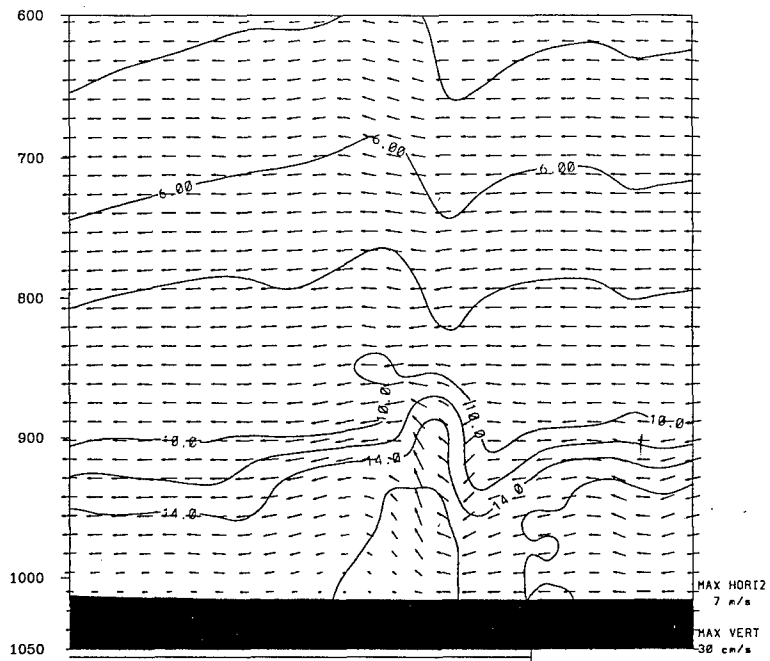


Figure 3.37. a: As in Figure 3.3b except for 02/11 UTC. b: As in 3.3a except for 02/21 UTC.

## Alongshore Initialization

The fifth and sixth model runs performed were the alongshore initializations. These runs were to examine how the LSBS develops with alongshore forcing, both from the northeast and from the southwest. The thermodynamic and wind profiles were compiled as described in Chapter 2, using the 850-mb and 700-mb winds to determine the flow regime.

The SW initialization (Figure 3.38a) has southwesterly winds from the surface veering slowly with height, becoming westerly by 300 mb. Wind speeds range from 3 m s<sup>-1</sup> at the surface to a maximum of 7.5 m s<sup>-1</sup> in a layer from 900 to 600 mb. Above 600 mb, winds speed decrease to 5 m s<sup>-1</sup>.

The NE initialization (Figure 3.38b) has southeasterly winds at the surface that back with height to become northeasterly above 900 mb, and northerly above 400 mb. This wind profile is again the result of allowing the boundary layer winds to vary while the large-scale forcing is still alongshore. Wind speeds range from 3 m s<sup>-1</sup> at the surface to a maximum of 10 m s<sup>-1</sup> at 150 mb. All three domains and boundary conditions were initialized to these respective conditions (SW and NE flows) for the two model runs.

### SW Day One

The initial near-surface flow field has southwesterly winds across the entire domain (Figure 3.39a). Over the next 11 hours, these winds veer with time to become alongshore and wind speeds decrease from the land to the sea. The large-scale forcing has allowed the establishment of a weak coastal temperature gradient (Figure 3.39b) which is driving the development of a weak land breeze.

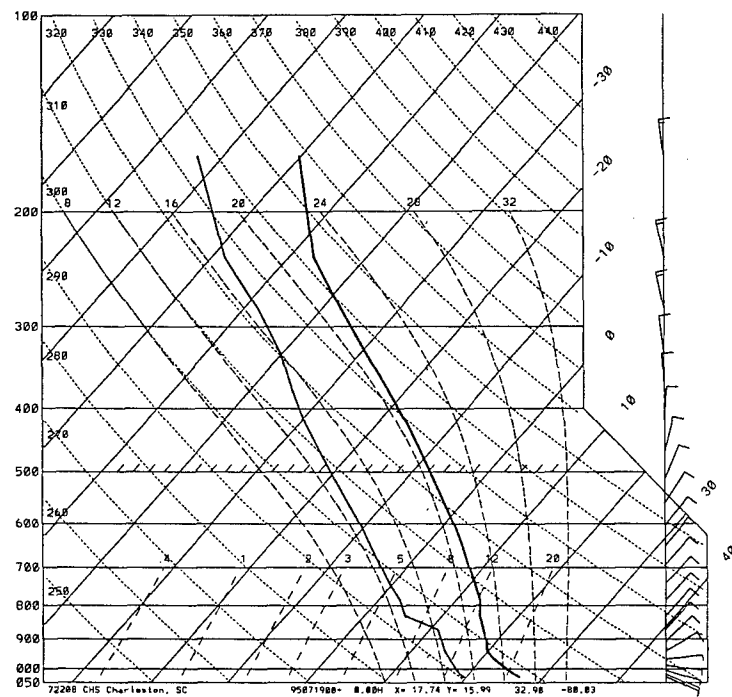
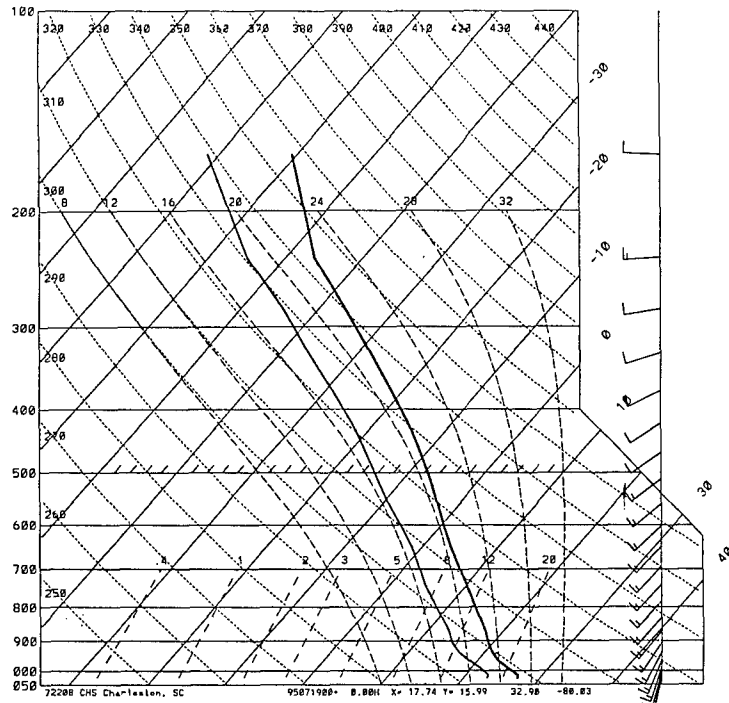


Figure 3.38. a: As in Figure 3.25a except for southwest alongshore initialization. b: As in Figure 3.25a except for northeast alongshore initialization.

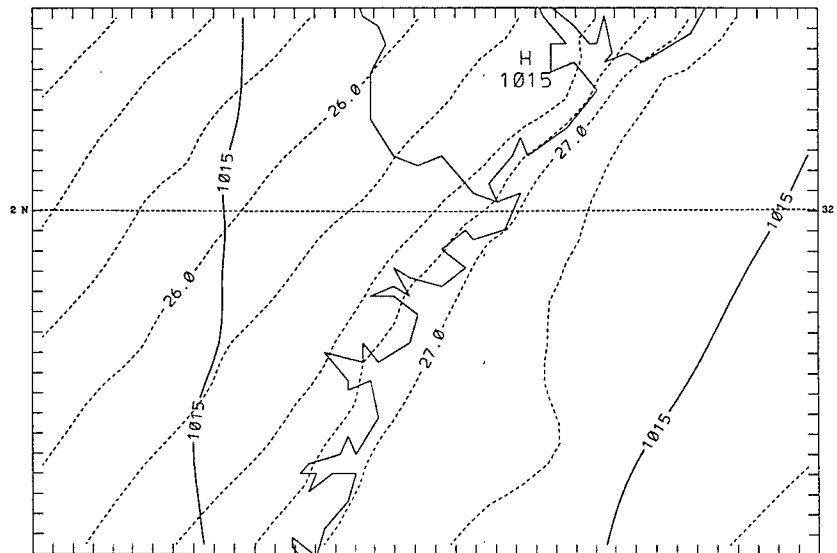
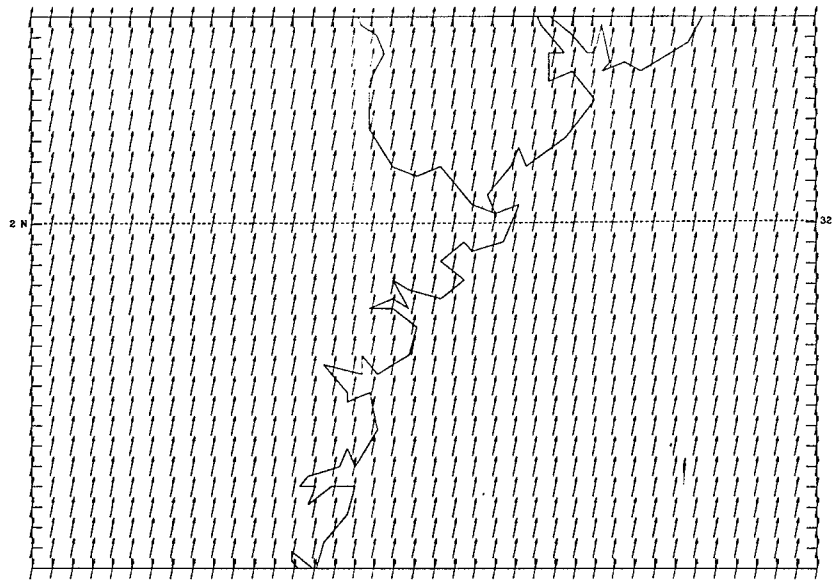


Figure 3.39. a: As in Figure 3.3a except for 01/00 UTC. b: As in Figure 3.23a except for 01/11 UTC.

Similar to that modeled in the onshore idealization, the developing land breeze is effecting the large-scale flow. Cross-sectional wind analysis shows a region at the shoreline extending inland 5 km with land breeze characteristics, counter to the large-scale flow. As before, this weak land breeze is creating a deflection in the large-scale flow, forcing it up and over. In turn, this is producing a relative speed maximum in the large-scale flow above the land breeze (Figure 3.40a). The maximum depth is 110 mb (1150 m) with offshore component confined to the lowest layer, less than 10 mb (50 m) deep. The extent of the effect is 5 km landward and less than 5 km seaward. Cross-sectional moisture analysis highlights the light land breeze circulation (Figure 3.40b).

By 01/16 UTC, the winds have assumed a sea breeze character, blowing from  $170^\circ$  at  $5 \text{ m s}^{-1}$ . Again, there is no abrupt transition to the sea breeze, only a backing of the winds to assume the sea breeze character. The sea breeze continues to intensify, reaching a maximum speed of over  $8 \text{ m s}^{-1}$  blowing from  $160^\circ$  by 01/20 UTC (Figure 3.41a). The circulation has reached a maximum depth of 230 mb (2300 m) with the onshore component 60 mb (600 m) deep (Figure 3.41b). Cross-sectional structure is as described in previous runs. The sea breeze front penetrated inland 80 km moving at speeds up to  $15 \text{ km hr}^{-1}$  but the seaward extent and movement was masked by the background flow.

## **Day Two**

The coastal temperature gradient loses its sea breeze character by 02/02 UTC. The winds continue to veer slowly and become alongshore by 02/07 UTC. Again, wind



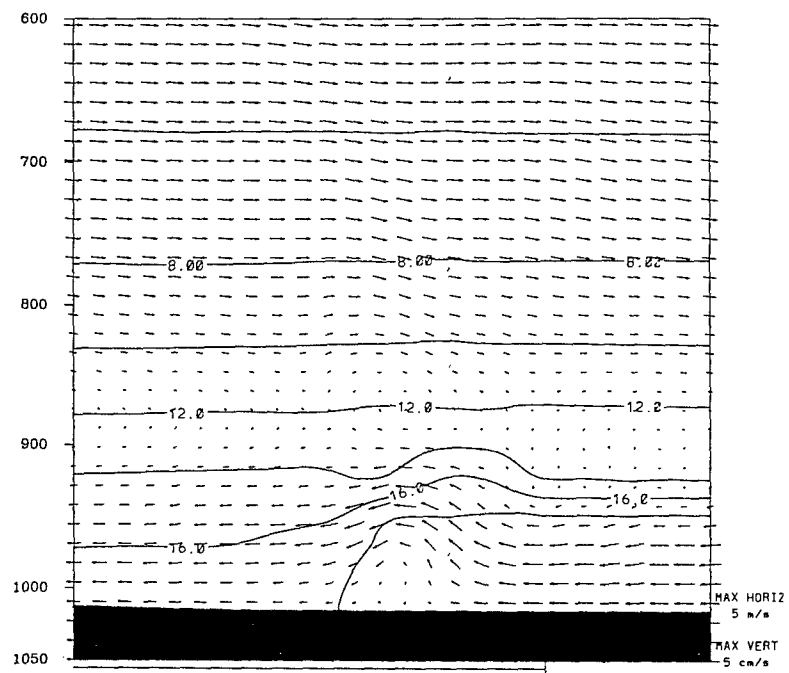
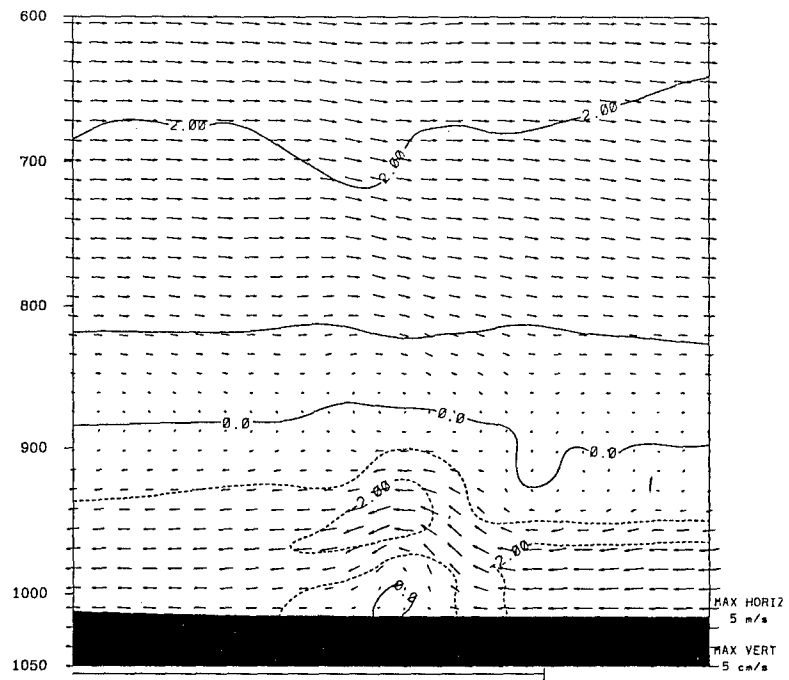


Figure 3.40. a: As in Figure 3.35a except for 01/12 UTC. b: As in Figure 3.3b except for 01/12 UTC.

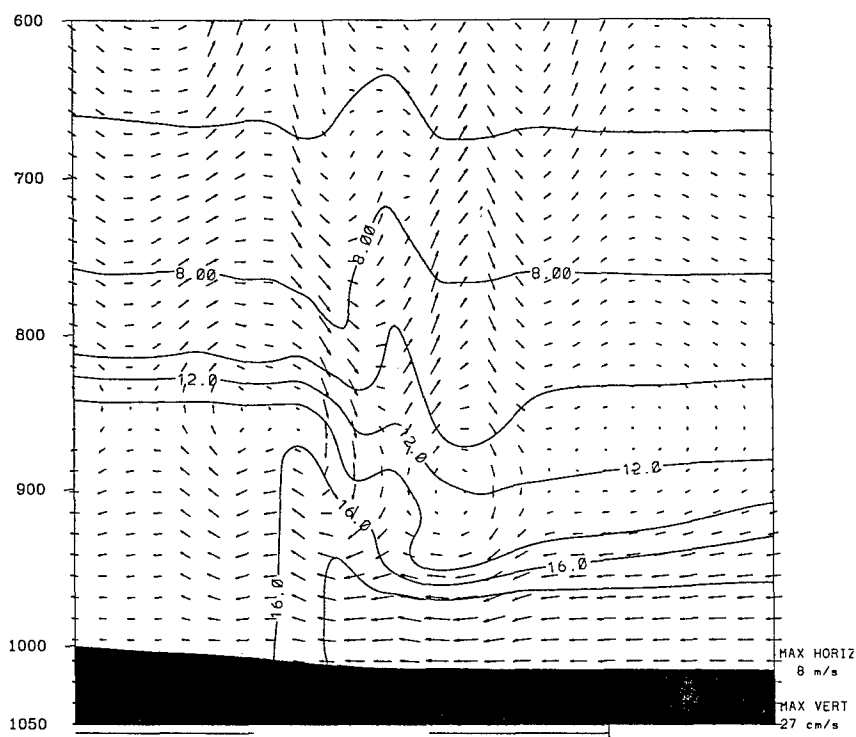
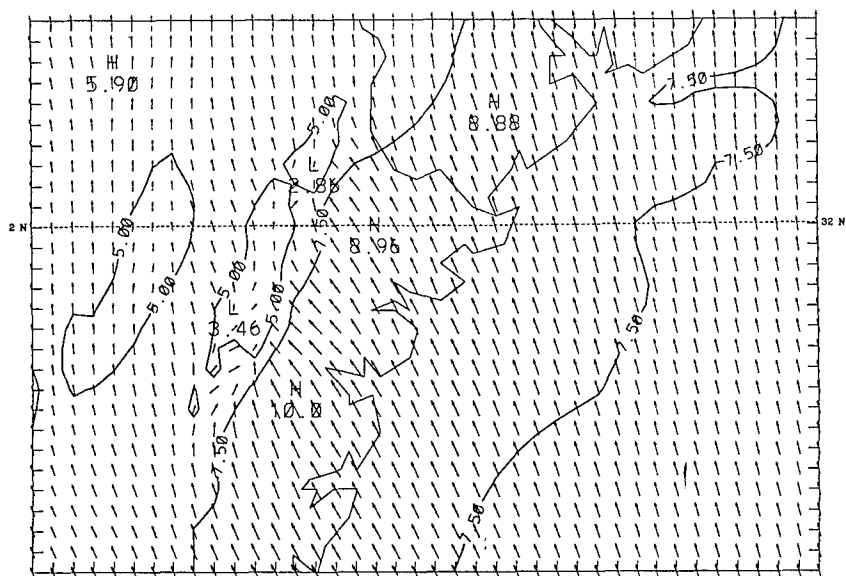


Figure 3.41. a: As in Figure 3.3a except for 01/20 UTC. b: As in Figure 3.10b except for 01/20 UTC.

speeds generally decrease from the land to the sea with time, however there is no evidence of any land breeze effects on the large-scale flow, either in the horizontal or cross-sectional fields.

The land breeze did not develop on day two because the local forcings changed. On day one, there was no local pressure gradient across the domain, just a weak temperature gradient that drove the formation of the land breeze. On day two, there is now a local pressure gradient across the Wassaw Sound, but it is directed opposite to the local temperature gradient effects (Figure 3.42a). Thus the local temperature and pressure gradient forcings for the land breeze are in opposition, so the large-scale flow across the domain is unaffected.

The winds assume a sea breeze character by 02/17 UTC, turning onshore at  $3 \text{ m s}^{-1}$  from  $170^\circ$  (Figure 3.42b). The sea breeze strength increases, reaching a maximum of  $7.5 \text{ m s}^{-1}$  blowing from  $170^\circ$  by 02/20 UTC (Figure 3.43a). The sea breeze front has moved inland 75 km moving at speeds up to  $15 \text{ km hr}^{-1}$ , has a maximum depth of 260 mb (2600 m) with an onshore component 60 mb (600 m) deep (Figure 3.43b). The seaward extent of the circulation is again masked by the large-scale flow.

### **NE Day One**

The initial near-surface flow field has southeasterly winds at  $3 \text{ m s}^{-1}$  across the entire domain (Figure 3.44a). Over the next 9 hours, the winds back due to the large-scale forcing and become alongshore by 01/09 UTC. The weak alongshore wind flow permits a coastal temperature gradient to develop (Figure 3.44b) and by 01/10 UTC, a land breeze forms with northerly flow at  $2.5 \text{ m s}^{-1}$  across the Wassaw Sound.

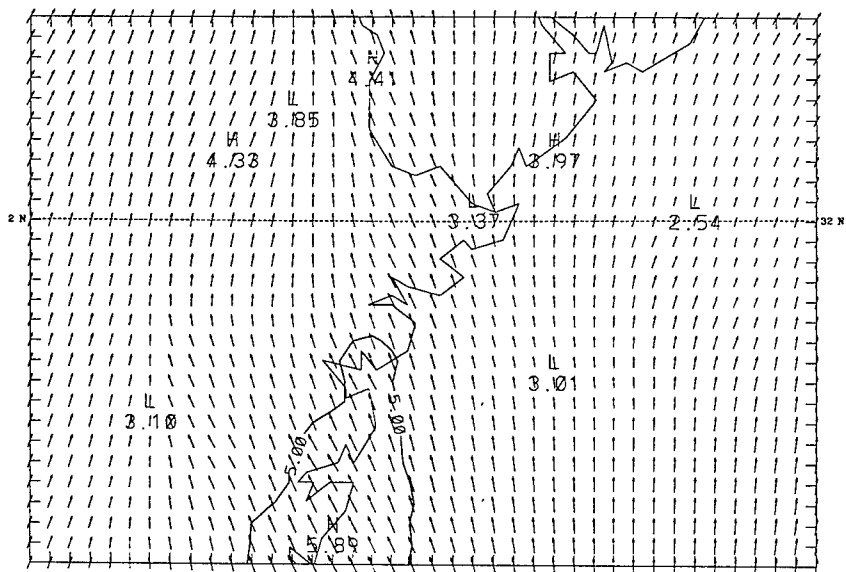
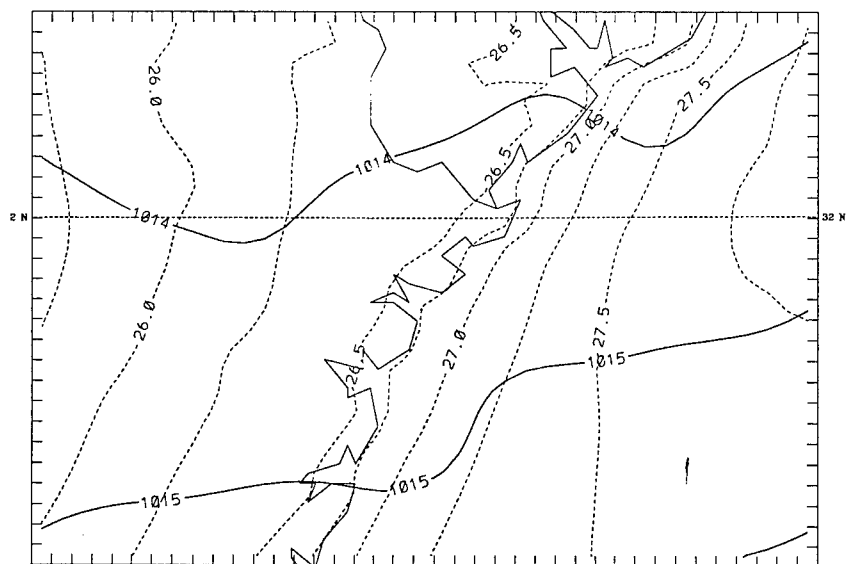


Figure 3.42. a: As in Figure 3.23a except for 02/11 UTC. b: As in Figure 3.3a except for 02/17 UTC.

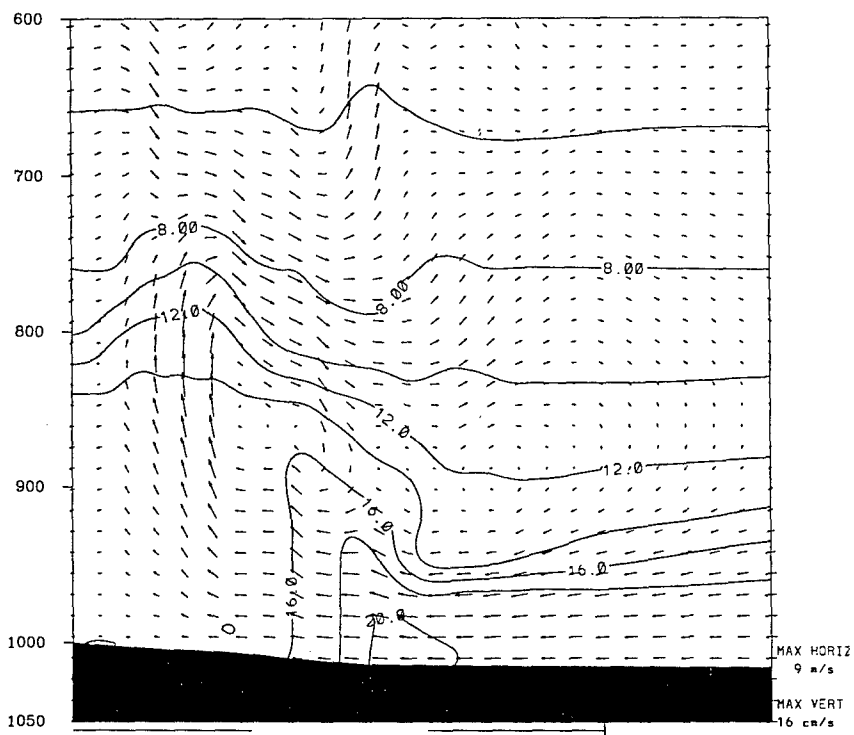
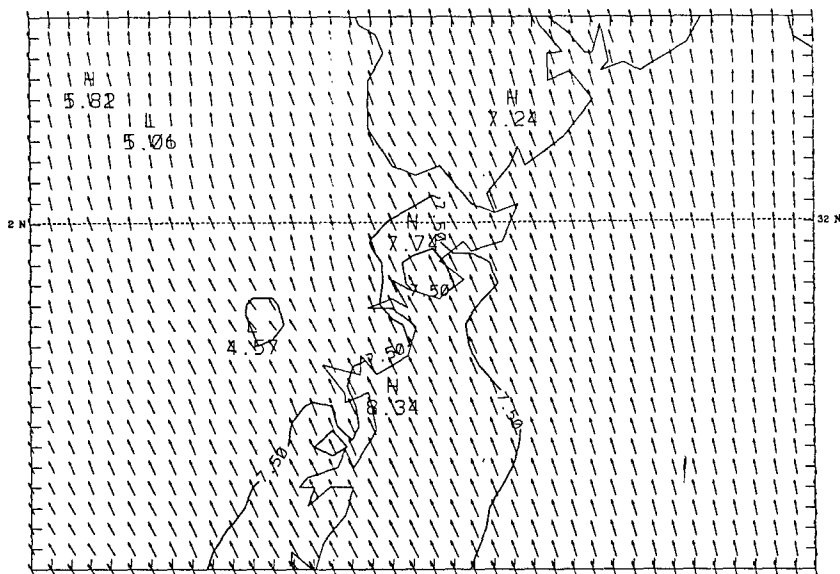


Figure 3.43. a: As in Figure 3.3a except for 02/20 UTC. b: As in Figure 3.10b except for 02/21 UTC.

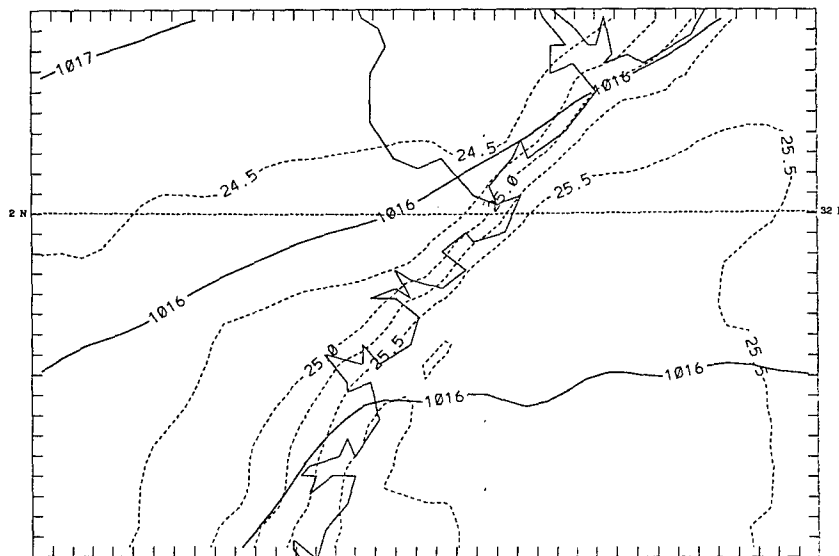
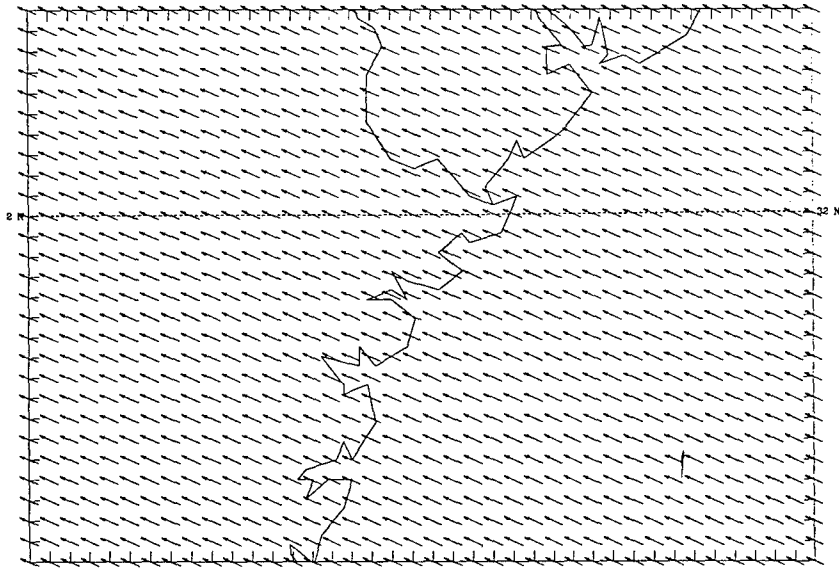


Figure 3.44. a: As in Figure 3.3a except for 01/00 UTC. b: As in Figure 3.23a except for 01/11 UTC.

Cross-sectional analysis shows a fully developed circulation that initiated at the shoreline, spread inland 11 km and seaward 5 km. Maximum depth of the circulation is 110 mb (1100 m) with the offshore component approximately 20 mb deep (220 m) (Figure 3.45a). As modeled in previous simulations, the center of the land breeze circulation moves seaward as it decays, persisting until 01/14 UTC.

The sea breeze initiates across the Wassaw Sound by 01/17 UTC, blowing at 2.5 m s<sup>-1</sup> from 100°. Unlike in previous simulations that had a fully developed land breeze, there was no abrupt transition to the sea breeze in this run. Instead, the winds veered with time in response to the large-scale forcing, assuming a sea breeze character as the local temperature gradient reversed. As the sea breeze strengthened, the winds continued to veer slightly, becoming more onshore.

The sea breeze reached its maximum strength at 01/21 (Figure 3.45b), flowing from 120° at 5 m s<sup>-1</sup>. Cross-sectional moisture analysis shows the sea breeze front marked by the 12.0 g kg<sup>-1</sup> isohume (Figure 3.46a). The front has moved inland at speeds up to 11 km hr<sup>-1</sup>, penetrating 85 km. The maximum depth of the circulation is 230 mb (2400 m) while the onshore component is 60 mb (600 m) deep. The seaward edge of the circulation moved at speeds up to 15 km hr<sup>-1</sup> and reached 120 km offshore.

## **Day Two**

Overnight, the seaward winds continued to blow onshore as the inland winds gradually decayed. After 02/02 UTC, the coastal temperature gradient has weakened significantly indicating the decay of the sea breeze. By 02/07 UTC, the inland winds have gone almost calm while the winds over the water continue to flow from 120° at

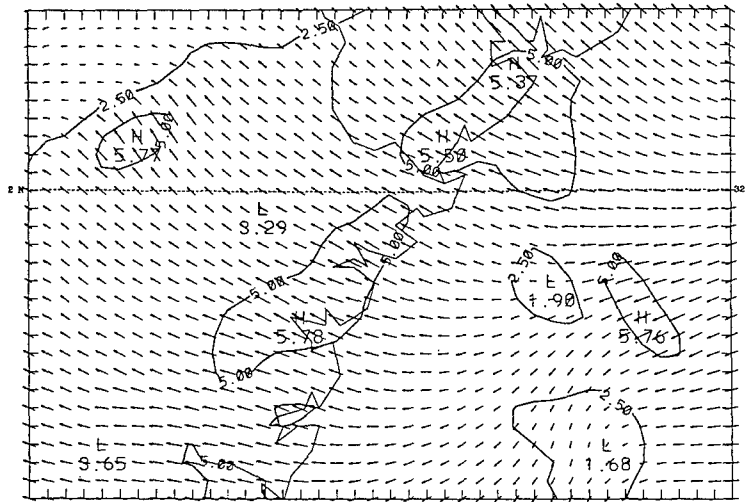
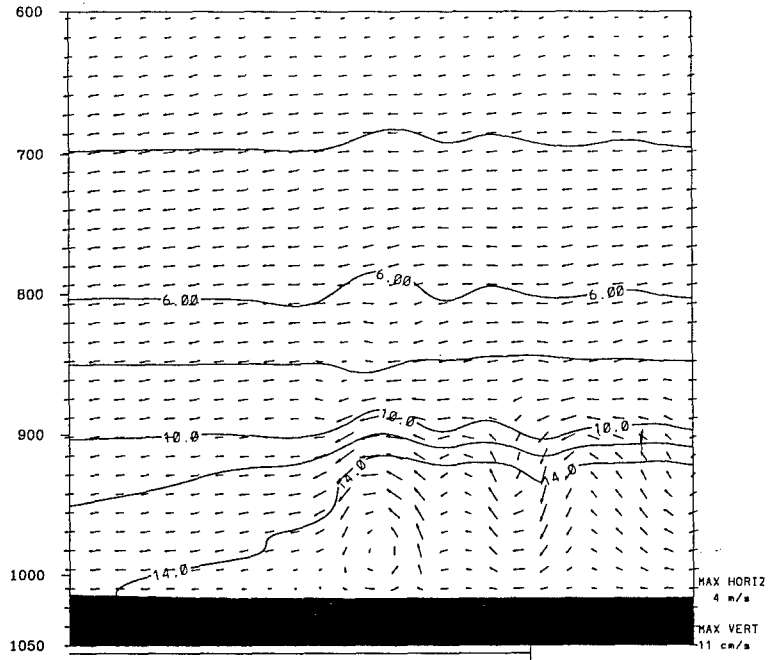


Figure 3.45. a: As in Figure 3.3b except for 01/12 UTC. b: As in Figure 3.3a except for 01/20 UTC.



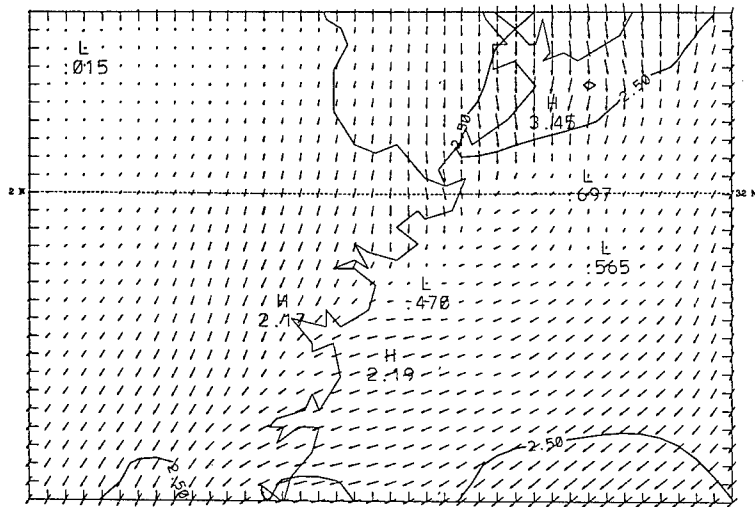
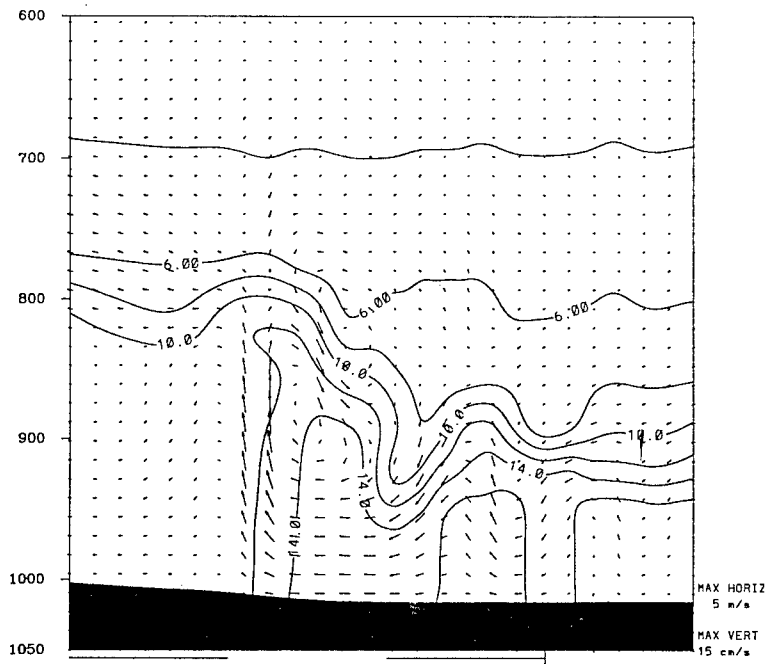


Figure 3.46. a: As in Figure 3.10b except for 01/22 UTC. b: As in Figure 3.3a except for 02/11 UTC.

1 m s<sup>-1</sup>. By 02/10 UTC, the land breeze has developed and winds across the Wassaw Sound have become slightly offshore, at less than 1 m s<sup>-1</sup>. In the next two hours, the land breeze becomes full developed and is flowing from the north at 2.5 m s<sup>-1</sup> (Figure 3.46b). Cross-sectional analysis shows a complete land breeze circulation, 100 mb deep (1050 m) with an offshore component 30 mb (300 m) deep (Figure 3.47a). The circulation extends 11 km inland and 5 km seaward.

The land breeze again decays by moving its circulation seaward while the sea breeze forms shoreward of it. Similar to day one, there is no abrupt transition to the sea breeze, instead the winds veer until assuming sea breeze character. By 02/17 UTC, the winds have become onshore from 90° at 2.5 m s<sup>-1</sup>. The sea breeze reaches its maximum strength by 02/20 UTC, flowing at 5 m s<sup>-1</sup> from 110°. Cross-sectional moisture analysis is similar to day one with the sea breeze has penetrating inland 60 km, moving at speeds up to 15 km hr<sup>-1</sup>. The maximum depth of the circulation is 210 mb (2100m) with an onshore component 30 mb (300 m) deep. Seaward, the circulation advanced at speeds up to 15 km hr<sup>-1</sup> and reached 135 km offshore (Figure 3.47b). By the end of the model run, the winds are still blowing onshore at 3 m s<sup>-1</sup> from 130°.

### **13 August 1995 Initialization**

The last model run performed was the test run. This run was done to examine how well the MM5, using the same set-up as used for the idealized simulations, would model the LSBS that developed across the Wassaw Sound during the period 13-15 August 1995. The model was initialized using NCEP gridded 2.5° resolution data. These archived data are available from NCAR and consists of meteorological information

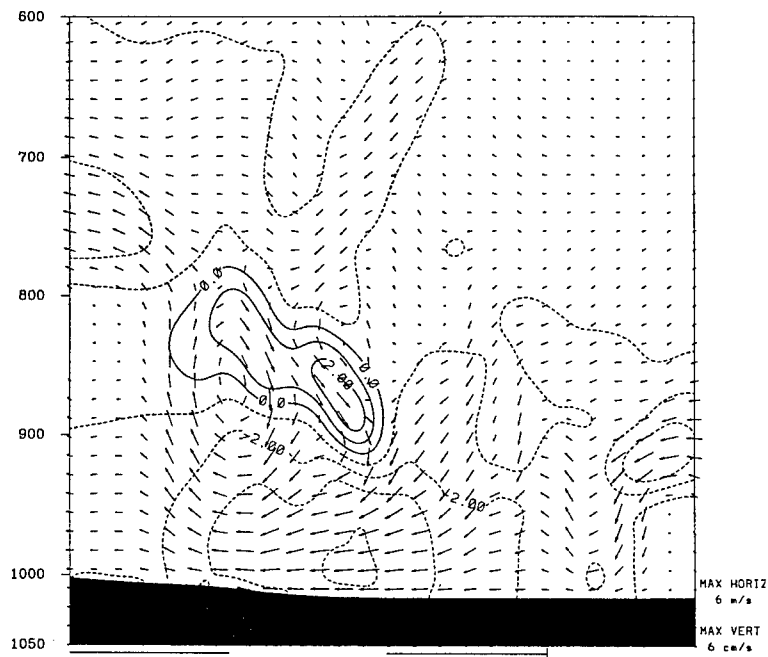
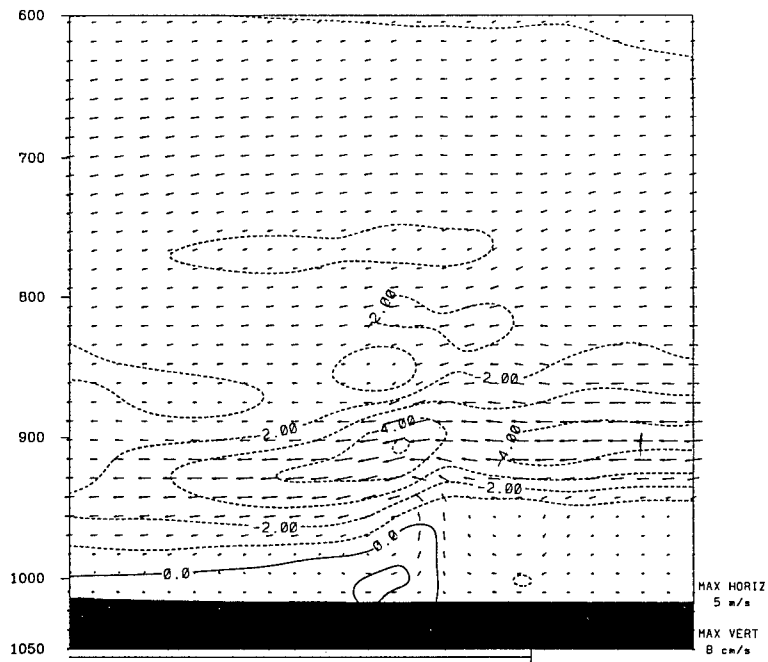


Figure 3.47. a: As in Figure 3.35a except for 02/11 UTC. b: As in Figure 3.11b except for 02/22 UTC.

(virtual temperature, heights, u and v wind components, and relative humidity) at standard pressure levels from the surface to 50 mb. These data were enhanced with surface and sounding information from stations that lie within the domains using the procedures outlined in Chapter 2.

The comparison data were collected by the Peachtree City, Georgia NWS during the same period. The collected data were not included in the large-scale data sets at NCAR so they were not ingested by the MM5 during initialization, and therefore represent an independent data set. The data consist of buoy observations from the Wassaw Sound area (buoy locations shown in Figures 1.3 and 3.48), limited Georgia Mesonet observations (Figure 3.48), and limited satellite imagery. A time series of buoy and station observational data is contained in the appendix. During this archival period at Peachtree City NWS, they had repeated equipment failures, thus limiting the available data.

### **Synoptic Setting**

The 13 August 1995 0000 UTC surface map (Figure 3.49b) shows high pressure over the Southeast U.S. This surface high pressure stays anchored over the region during the entire model run (Figure 3.50b). In the upper levels, there is ridging across the entire Southeast U.S. (Figure 3.49a). Through the model run, the ridge axis drifts slowly eastward from the Missouri-Kentucky border to the Tennessee-North Carolina border (Figure 3.50a). This synoptic pattern is typical of a strong summer high pressure ridge anchored across the Southeast U.S.

CHS soundings through the period show a dry atmosphere with a strong

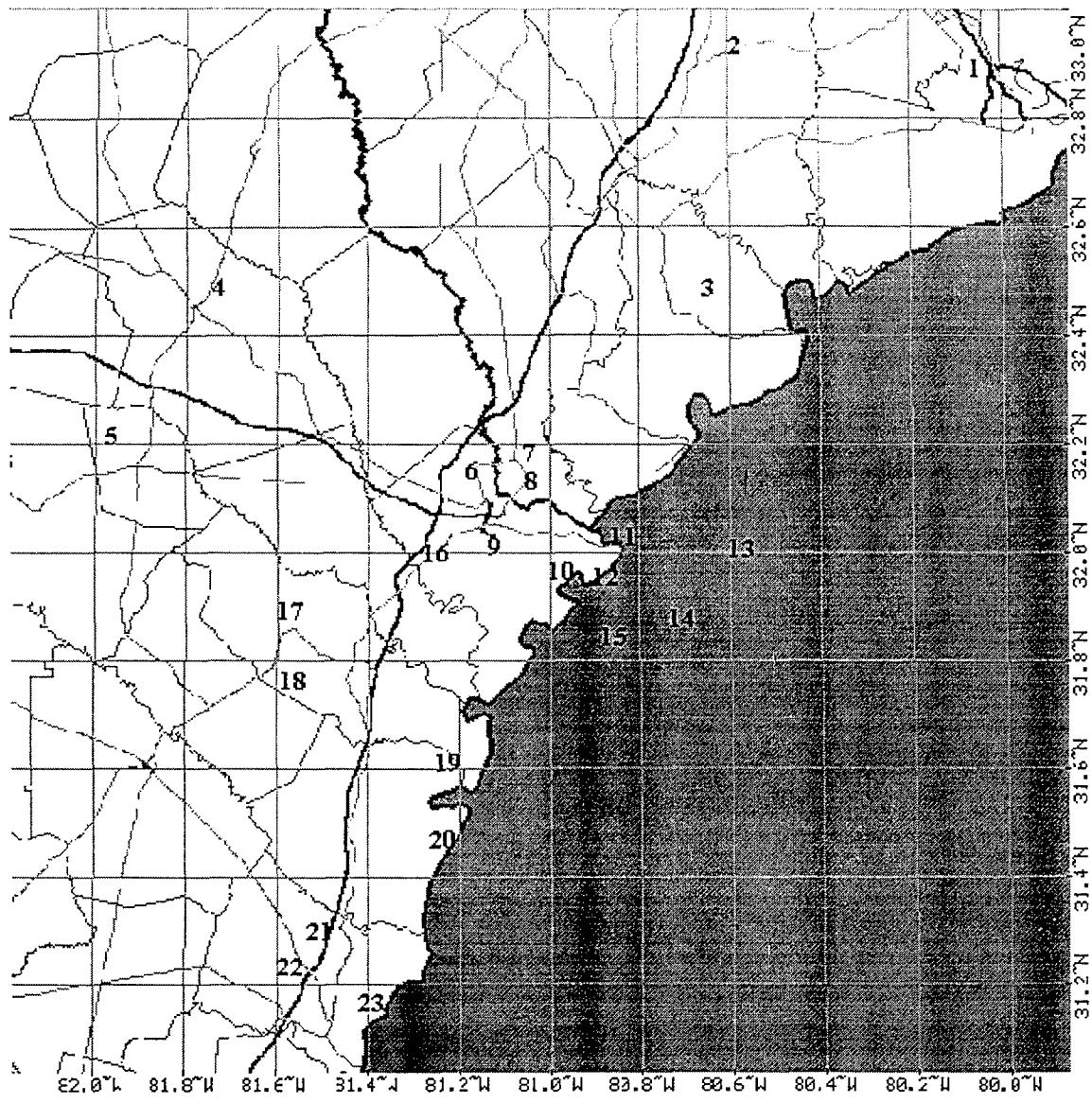


Figure 3.48. Observational mesonet sites found within the approximate bounds of the 4-km domain. Embedded numbers refer to site locations given in the Appendix.

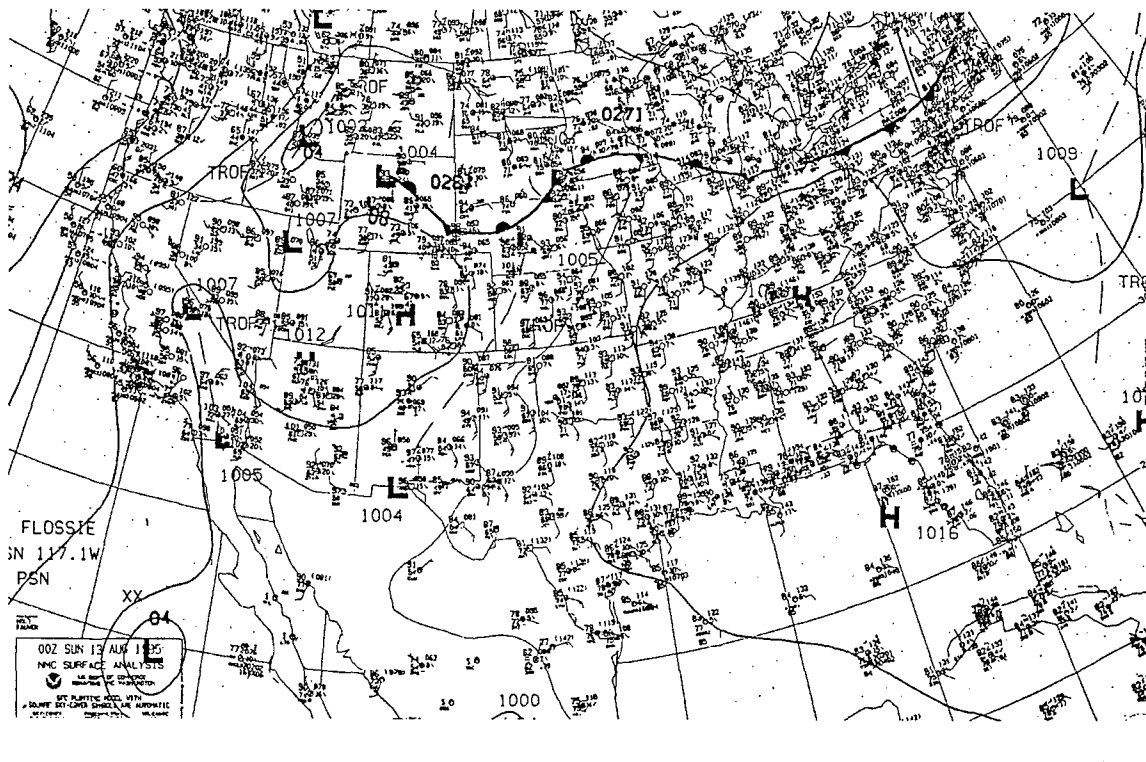
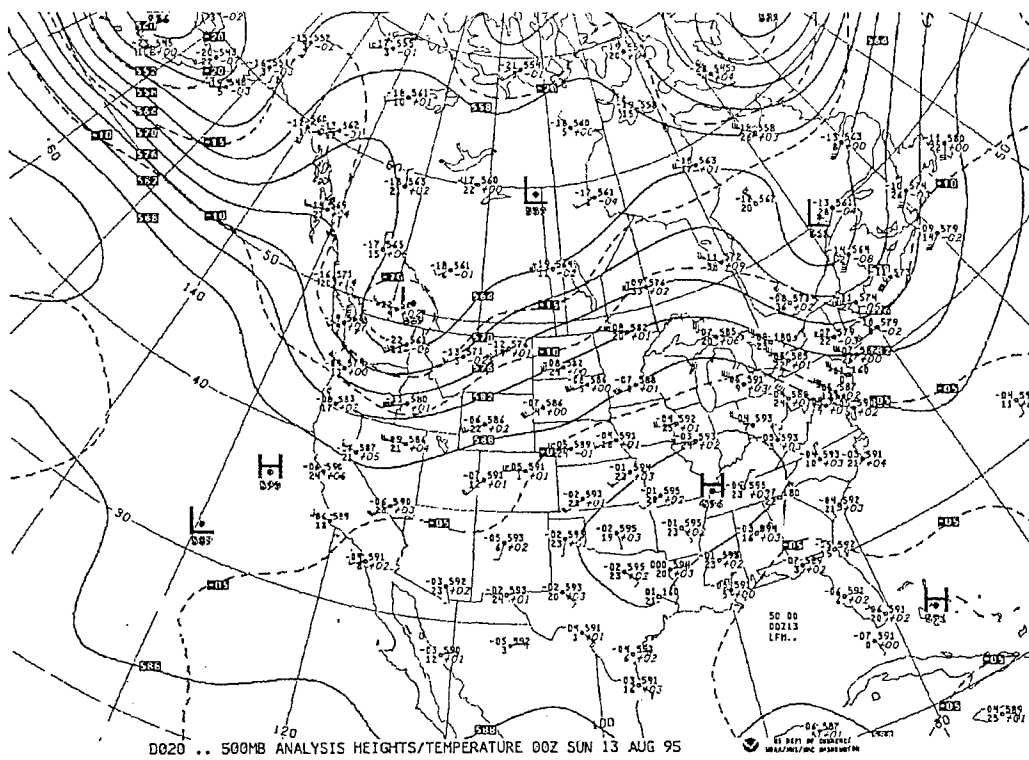


Figure 3.49. a: 500 mb chart for 13 August 1995 at 0000 UTC. b: Surface chart for 13 August 1995 at 0000 UTC.

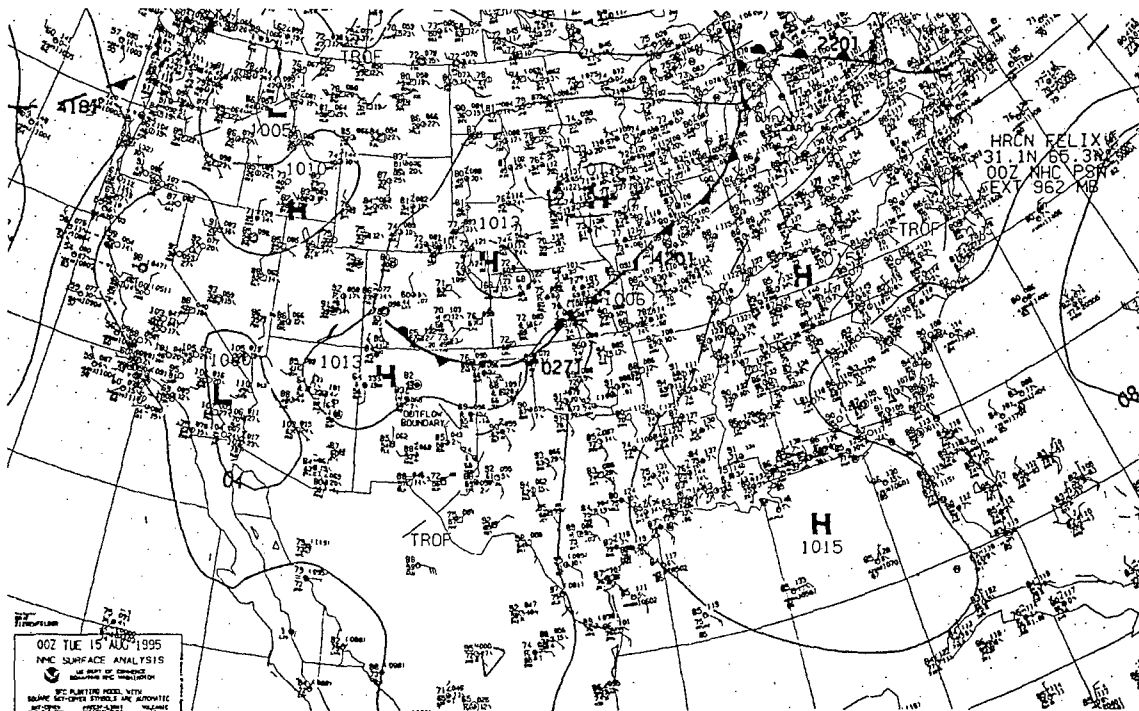
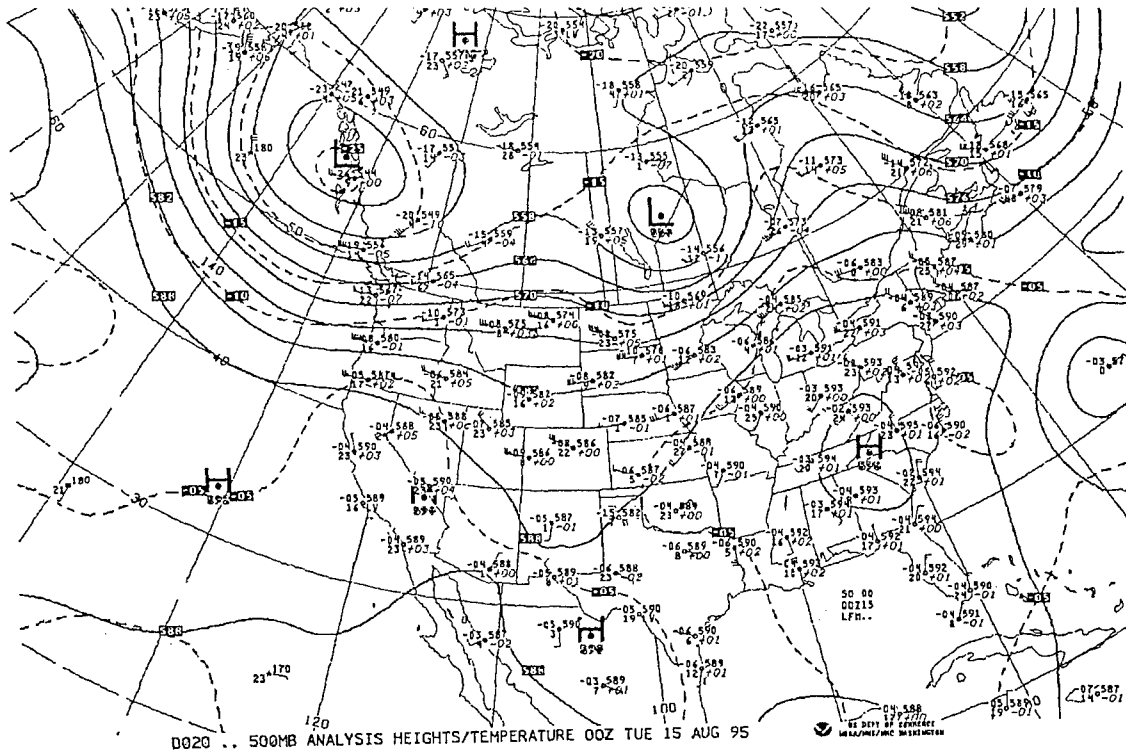


Figure 3.50. a: 500 mb chart for 15 August 1995 at 0000 UTC. b: Surface chart for 15 August 1995 at 0000 UTC.

subsidence inversion between 850 and 700 mb and strong radiational inversions overnight. Winds at the surface and lower layers are southwesterly to westerly veering with height to become predominately easterly above 500 mb. Wind speeds are  $5 \text{ m s}^{-1}$  at the surface, increasing to  $7 \text{ m s}^{-1}$  by 700 mb, decreasing again to  $5 \text{ m s}^{-1}$  above 650 mb, and increasing to  $25 \text{ m s}^{-1}$  by 200 mb (Figure 3.51a). This wind profile is most like the NE idealization but with stronger forcing.

### **Day One**

Upon initialization, the sea breeze is already decaying across the Wassaw Sound with  $5 \text{ m s}^{-1}$  southerly winds across the 4-km domain (Figure 3.51b). Over the next four hours, the winds veer to become parallel to the shore by 13/04 UTC and become offshore by 13/08 UTC. By 13/12 UTC, near-surface winds are from  $300^\circ$  at  $4 \text{ m s}^{-1}$  (Figure 3.52a).

Cross-sectional analysis at this time shows a layer 50 mb (550 m) deep across the entire domain with  $4 \text{ m s}^{-1}$  offshore flow, uncharacteristic of a land breeze (Figure 3.52b). Temperature and pressure analysis of the 4-km domain fail to show any temperature or pressure gradients across the domain indicating a land breeze. Because the layer is only 50 mb deep, it would not be reflected in the standard upper level charts. The CHS 13 August 1995 1200 UTC sounding (Figure 3.53b) however, does show a strong morning radiational inversion. Winds above this inversion become detached from the surface layer and thus increase from the lack of frictional effects.

The raw CHS sounding data (contained in the Appendix) also supports the modeled cross-sectional structure. Decoded sounding data shows  $4 \text{ m s}^{-1}$  westerlies at



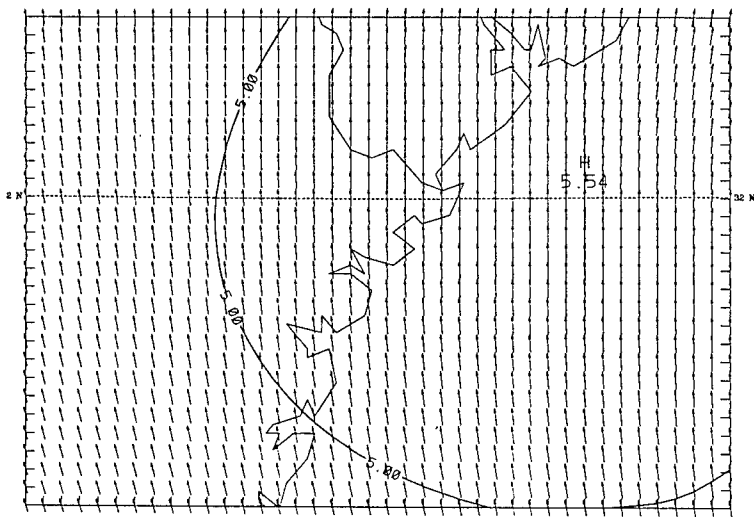
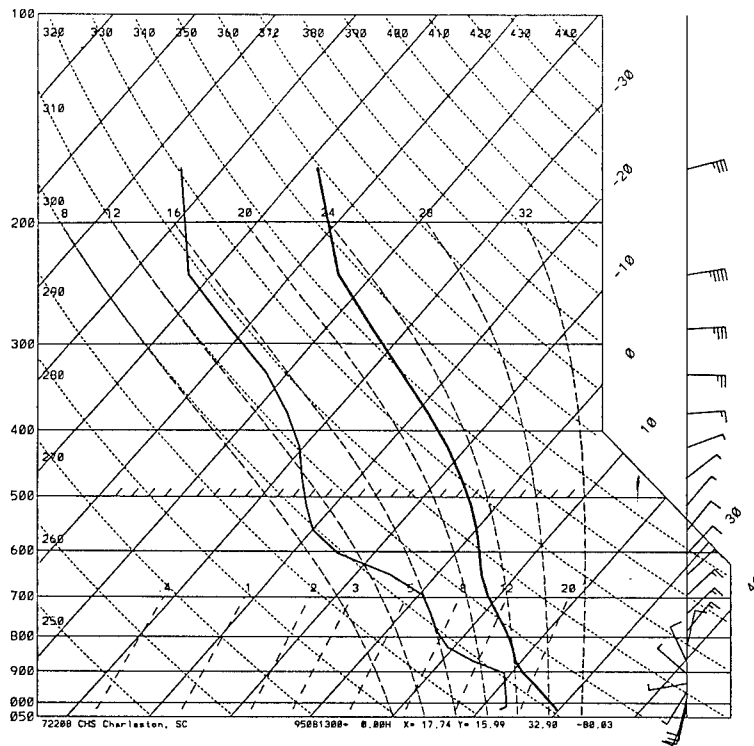


Figure 3.51. a: As in 3.25a except for CHS on 13 August 1995 at 0000 UTC. b: As in Figure 3.3a except for 13/00 UTC.

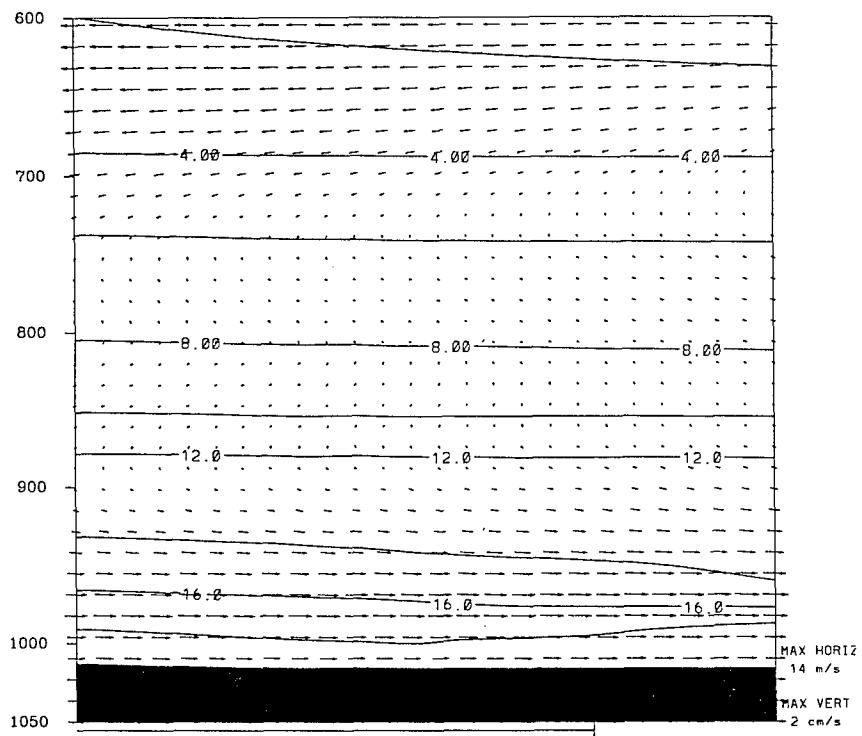
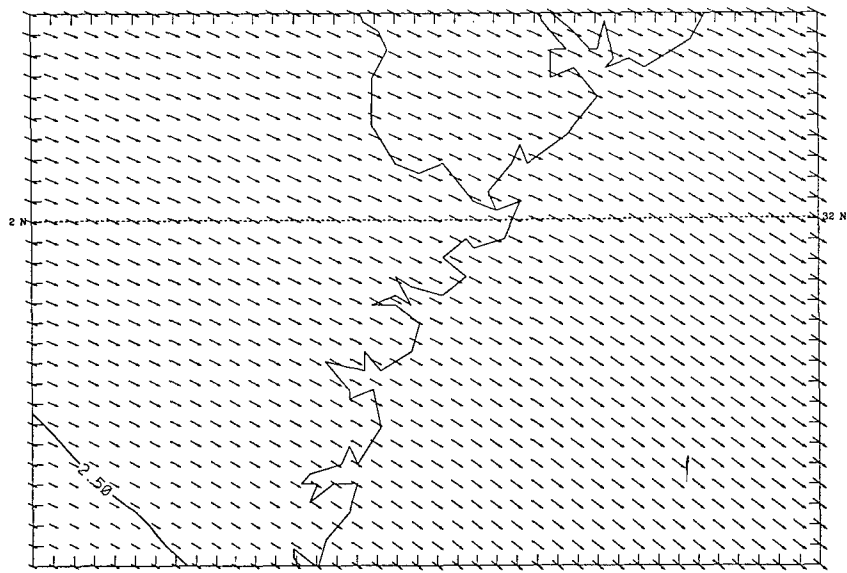


Figure 3.52. a: As in Figure 3.3a except for 13/12 UTC. b: As in Figure 3.3b except for 13/12 UTC.

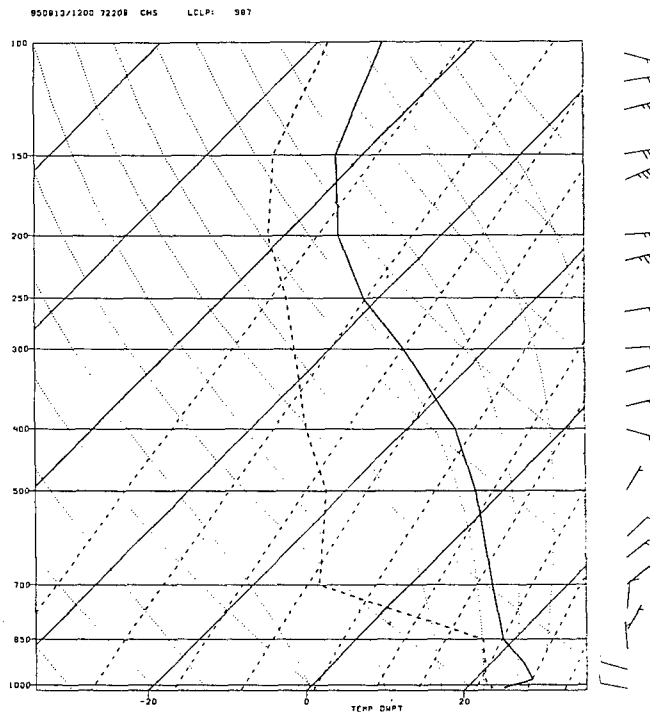
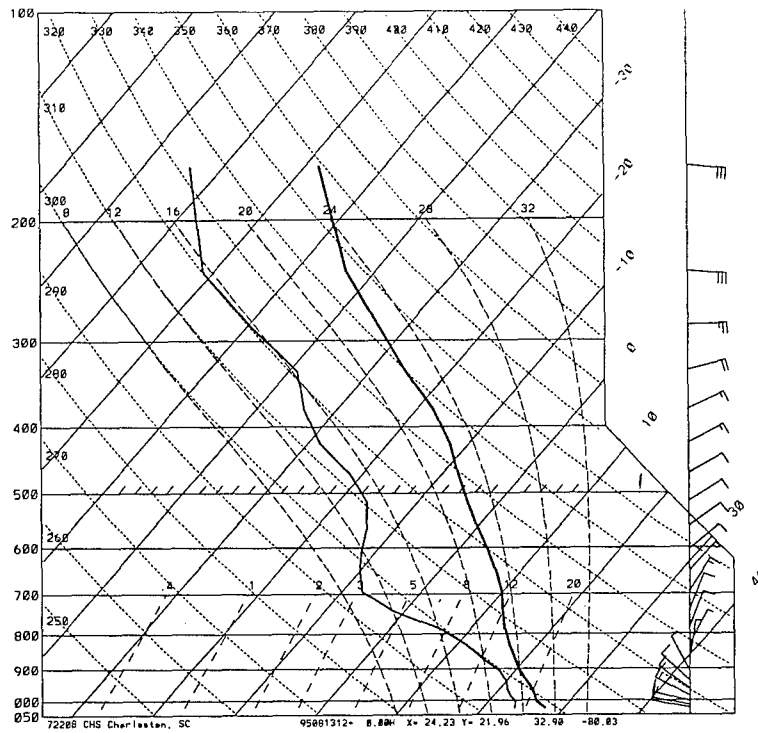


Figure 3.53 a: Modeled 13 August 1995 1200 UTC sounding for CHS. b: Observed 13 August 1995 1200 UTC sounding for CHS.

40 m above MSL. The model has represented these winds in its lowest model layer (0.995 sigma) approximately 40 m above MSL but it has failed to capture the surface conditions across the area because of the strong radiational inversion that formed from the surface to 40 m. Otherwise, the modeled sounding's thermodynamic and wind profiles closely match the observed sounding (Figure 3.53a).

Over the next three hours, the offshore flow decays until by 13/15 UTC, the winds over the Wassaw Sound have become almost calm (Figure 3.54a), indicating the transition to the sea breeze has begun. Within the next hour, the sea breeze begins with the coastal winds becoming onshore ( $150^\circ$ ) at  $2.5 \text{ m s}^{-1}$  (Figure 3.54b). By 13/19 UTC, the sea breeze has already obtained speeds of over  $5 \text{ m s}^{-1}$  from  $160^\circ$ . During these first hours, the sea breeze is advancing inland at  $5 \text{ km hr}^{-1}$  and seaward at  $11 \text{ km hr}^{-1}$ .

The sea breeze reaches its maximum strength across the Wassaw Sound, almost  $6 \text{ m s}^{-1}$  from  $170^\circ$ , by 13/20 UTC (Figure 3.55a). Cross-sectional moisture analysis (Figure 3.55b) shows the sea breeze with a narrow updraft at the sea breeze front (marked by the  $16.0 \text{ g kg}^{-1}$  isohume), the head structure, and the dry area associated with the broad subsidence area seaward. Over the water, this subsidence area has produced a very shallow marine boundary layer, approximately 25 mb (220 m) deep. The sea breeze has reached a maximum depth of 210 mb (2150 m) and the onshore component of the circulation has a depth of 30 mb (300 m). The maximum landward extent of the circulation is 33 km while the seaward extent is 55 km (Figure 3.56a).

Available observations from across the area on day one of the simulation show the sea breeze arriving at SSI, located approximately one km from the coast, by 13/17 UTC

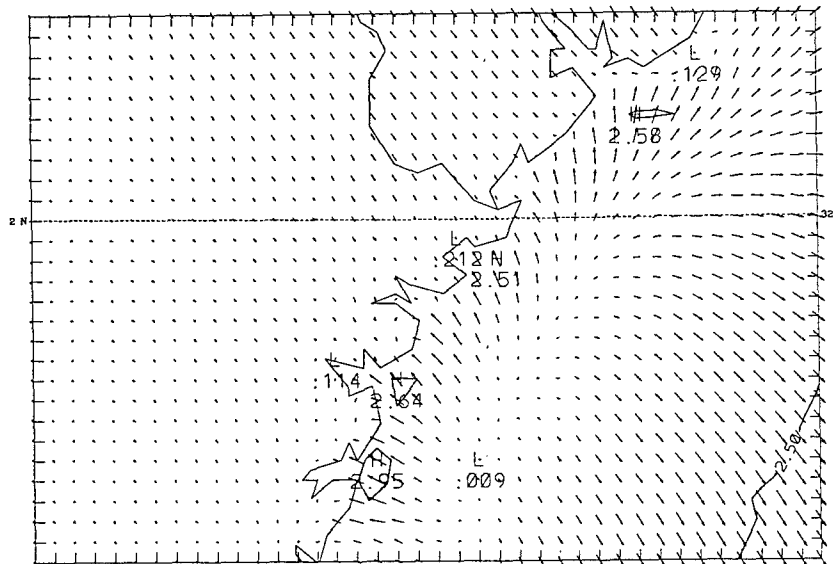
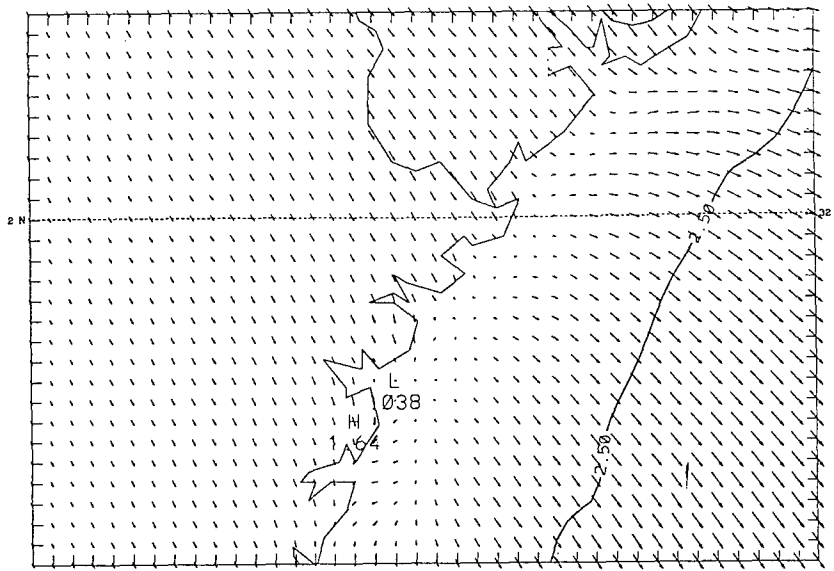


Figure 3.54. a: As in Figure 3.3a except for 13/15 UTC. b: As in Figure 3.3a except for 13/16 UTC.

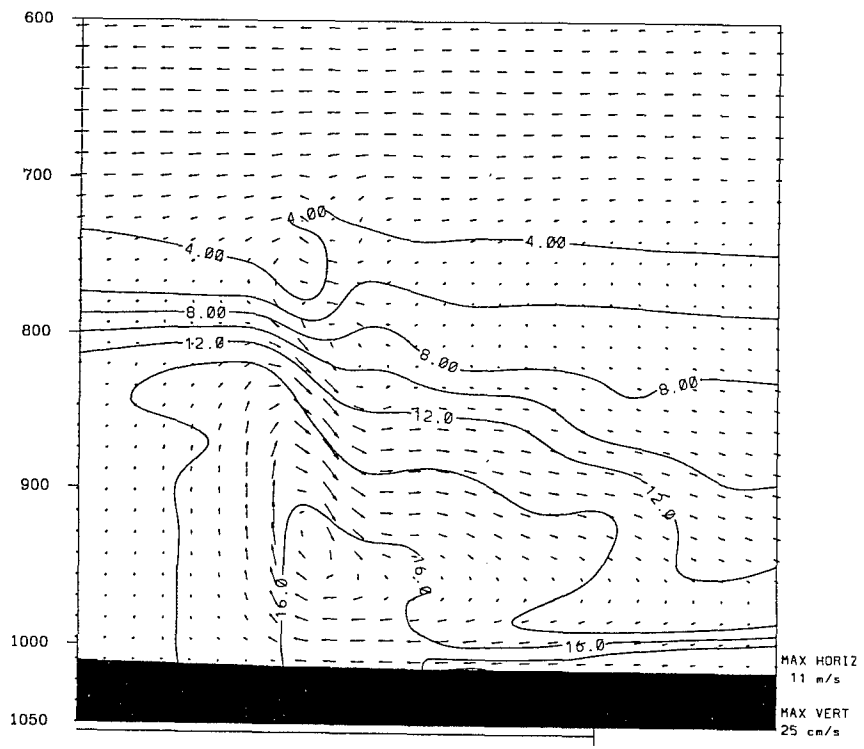
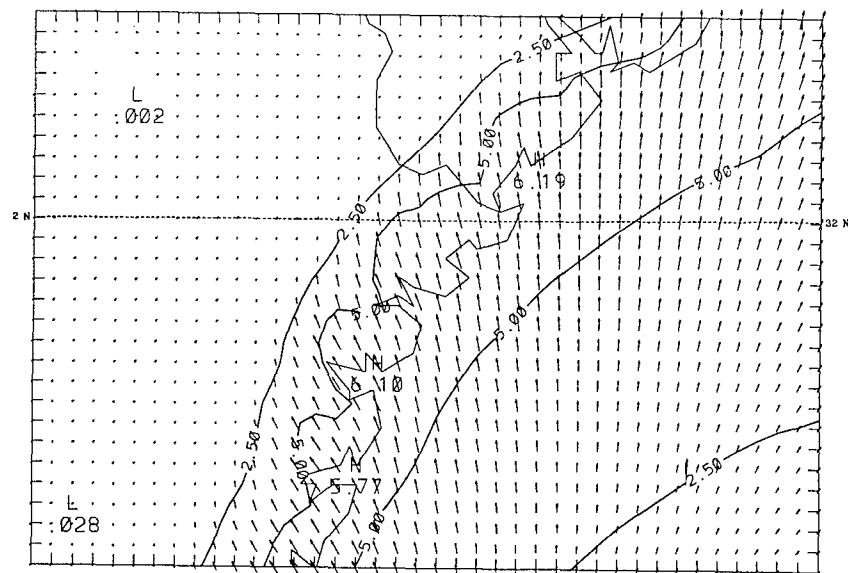


Figure 3.55. a: As in Figure 3.3a except for 13/20 UTC. b: As in Figure 3.3b except for 13/21 UTC.

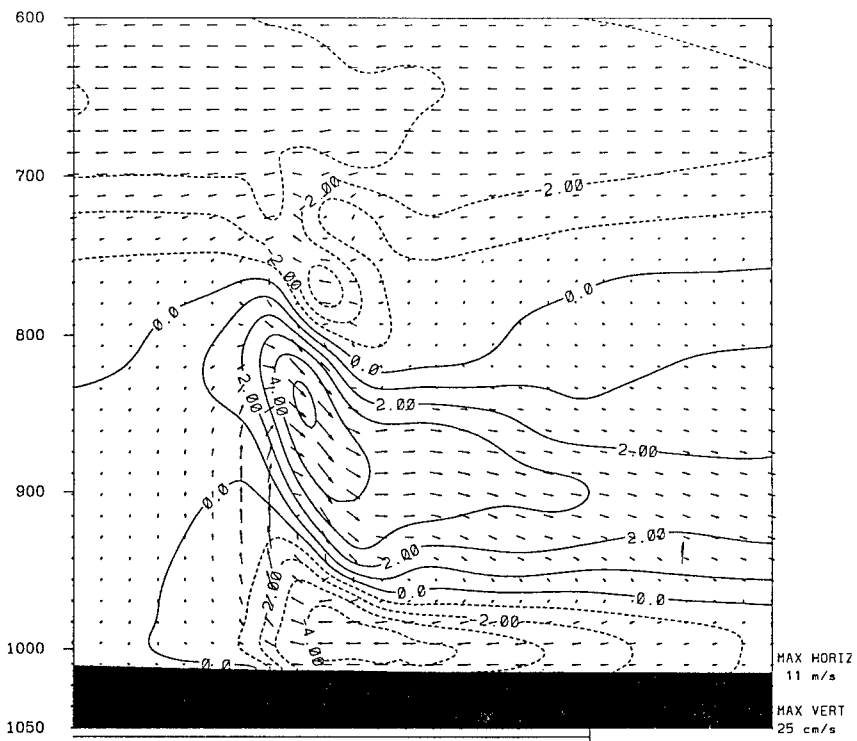


Figure 3.56. As in Figure 3.35a except for 13/21 UTC.

with winds from  $140^\circ$  at  $4 \text{ m s}^{-1}$ . Maximum wind speeds reached slightly greater than  $5 \text{ m s}^{-1}$  from  $170^\circ$  by 13/19 UTC. The sea breeze continued to blow across the area until at least 13/23 UTC when the data were no longer available. These observations of the sea breeze are in good agreement with the modeled sea breeze.

Observations from SAV, located approximately 40 km inland, show the sea breeze did not pass that station. Instead, the station experienced southwesterly flow at  $2\text{-}3 \text{ m s}^{-1}$  during the afternoon and early evening hours. Although the modeled wind speeds are lower than the observed, the observations are in good agreement with the sea breeze not penetrating past the station and the modeled wind directions are also in good agreement.

CHS observations, also located approximately 40 km inland, also did not show passage of the sea breeze in good agreement with the model. Further, the observed wind speeds and directions are in good agreement.

Observations from buoy 41021, located approximately 5 km seaward of the Wassaw Sound, shows the sea breeze initiating at 13/17 UTC from  $170^\circ$  at  $3 \text{ m s}^{-1}$  and reaching a maximum at 13/23 UTC of over  $5 \text{ m s}^{-1}$  from  $180^\circ$ . Both wind speed and directions are in excellent agreement with the model. Observations from the Savannah Light (SLVS1) Coastal Marine Automated Network (C-MAN) located approximately 12 km seaward of the mouth of the Savannah River, show the sea breeze at the station by 13/18 UTC, one hour later than the model. Otherwise, both the wind speeds and directions are in excellent agreement for the modeled sea breeze.

Comparisons between the observed 14 August 1995 0000 UTC CHS sounding



(Figure 3.57b) and the modeled (Figure 3.57a) show closely matching wind profiles. The thermodynamic profiles are similar except the modeled sounding's synoptically driven subsidence inversion is too low (820 versus 750 mb) and not as strong as the observed. Otherwise, the thermodynamic profiles match closely.

### **Day Two**

Overnight, the winds have veered, losing their sea breeze character by 14/01 UTC and become alongshore by 14/04 UTC. The winds continue to veer and by 14/12 UTC, they are blowing from  $280^\circ$  at  $5 \text{ m s}^{-1}$  across most of the 4-km domain (Figure 3.58a). Cross-sectional analysis again shows a layer approximately 70 mb (720 m) deep with the offshore flow (Figure 3.58b). The local temperature and pressure gradients across the Wassaw Sound are also combining to reinforce the offshore flow. As on the first day, there is no clearly defined land breeze circulation because the land areas did not become cooler than the water.

Observations overnight at SSI are in excellent agreement with the modeled winds while those at SAV closely match wind direction, but with modeled speeds too low, especially during the early morning hours. This again is the result of the model being unable to resolve the morning radiational inversion. The modeled wind, representative of the winds at approximately 40 m, continued to show winds speeds as high as  $5 \text{ m s}^{-1}$  while the SAV observations showed calm. CHS also had two hours where winds were not well represented by the model (14/02 UTC and 14/04 UTC), otherwise the CHS observations are in good agreement with the model. Buoy and C-MAN observations (41021 and SLVS1) are both in good agreement overnight.

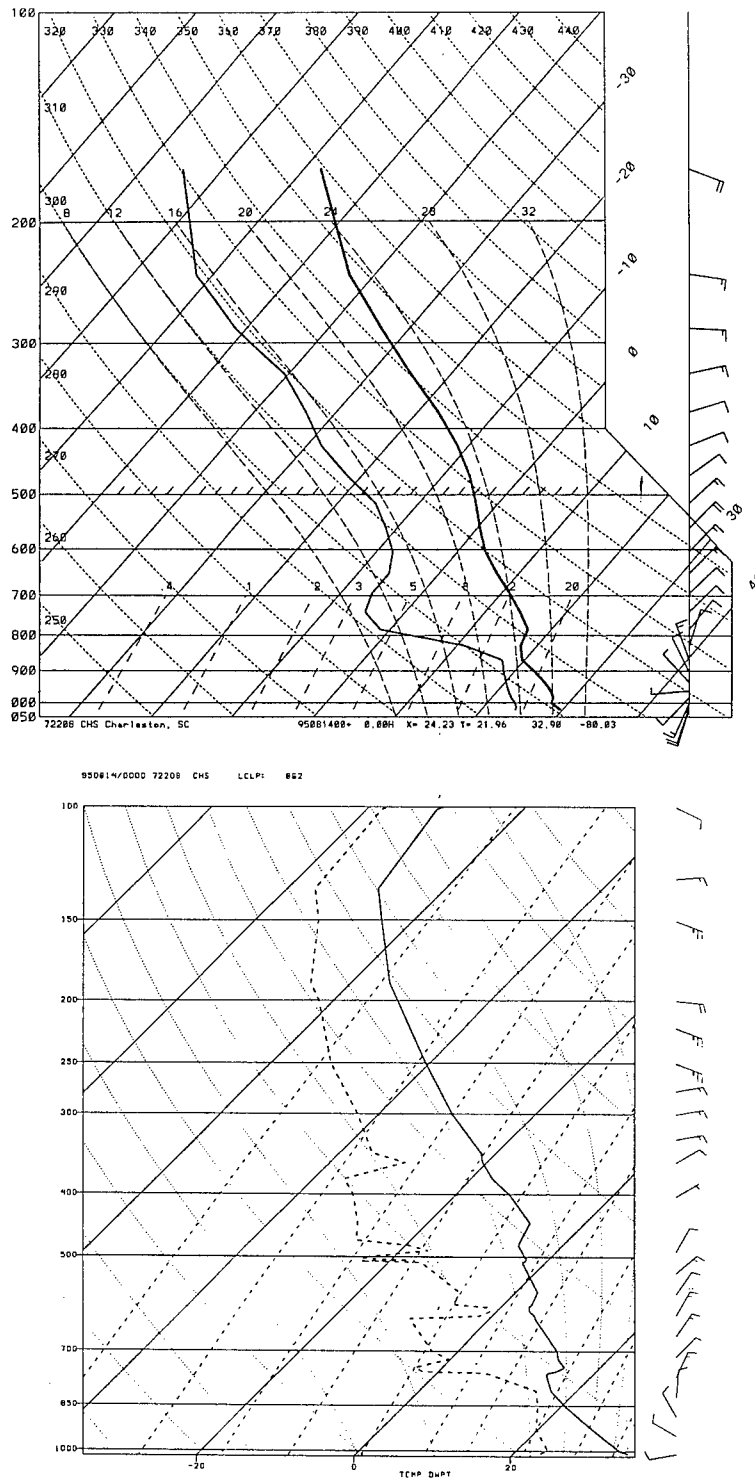


Figure 3.57. a: As in Figure 3.53a except for 14 August 1995 at 0000 UTC. b: As in Figure 3.53b except for 14 August 1995 at 0000 UTC.

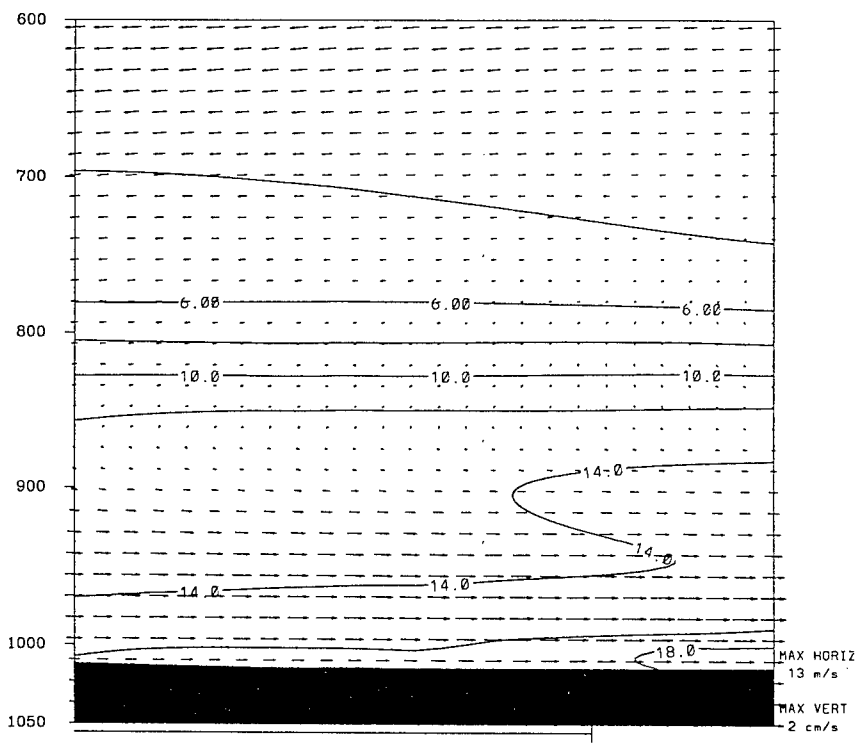
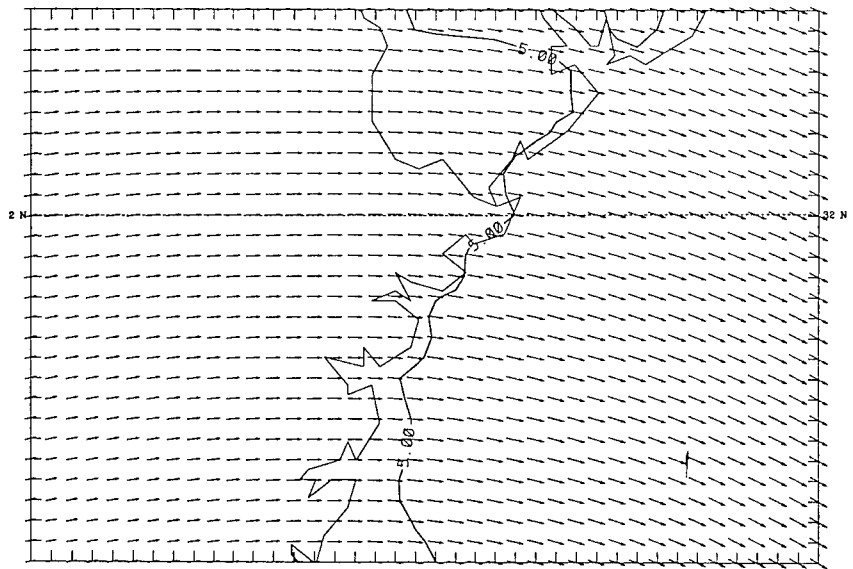


Figure 3.58. a: As in Figure 3.3a except for 14/12 UTC. b: As in Figure 3.3b except for 14/11 UTC.

The modeled 14/12 UTC sounding again closely matches the 14 August 1995 1200 UTC CHS sounding's wind profile (Figure 3.59a-b), however the model is unable to represent the strong surface radiational inversion that develops. Otherwise, the remainder of the thermodynamic profiles are similar.

The sea breeze transition does not occur until 14/17 UTC. First the coastal winds and the winds 4 km offshore decay to less than  $1 \text{ m s}^{-1}$  (Figure 3.60a). Then in the next hour, the sea breeze flow begins, but 4 km offshore (Figure 3.60b). Temperature analysis of the 4-km domain shows the strong, offshore flow created the temperature gradient offshore and weakened it, as compared to day one (Figures 3.61a-b). The sea breeze on day two developed first offshore in response to the offshore temperature gradient. Finally by 14/19 UTC, the sea breeze does begin across the Wassaw Sound, blowing from  $170^\circ$  at  $2.5 \text{ m s}^{-1}$ .

The sea breeze reaches its maximum strength of  $5 \text{ m s}^{-1}$  by 14/21 UTC, blowing from  $180^\circ$  (Figure 3.62a). Cross-sectional analysis shows structure as is discussed for day one. The sea breeze circulation has reached a maximum height of 180 mb (1800 m) with an onshore flow depth of less than 20 mb (170 m). The front moved inland at speeds up to  $5 \text{ km hr}^{-1}$  and only reached a maximum inland penetration of 11 km. Seaward, the circulation expanded at less than  $5 \text{ km hr}^{-1}$  during its first hours, then stopped. The maximum seaward extent was limited to less than 15 km (Figure 3.62b).

The sea breeze was inhibited because of the synoptic scale high pressure system inland, subsidence inversion aloft, and offshore wind flow. This combination produced an environment that prevented the circulation from growing both vertically and

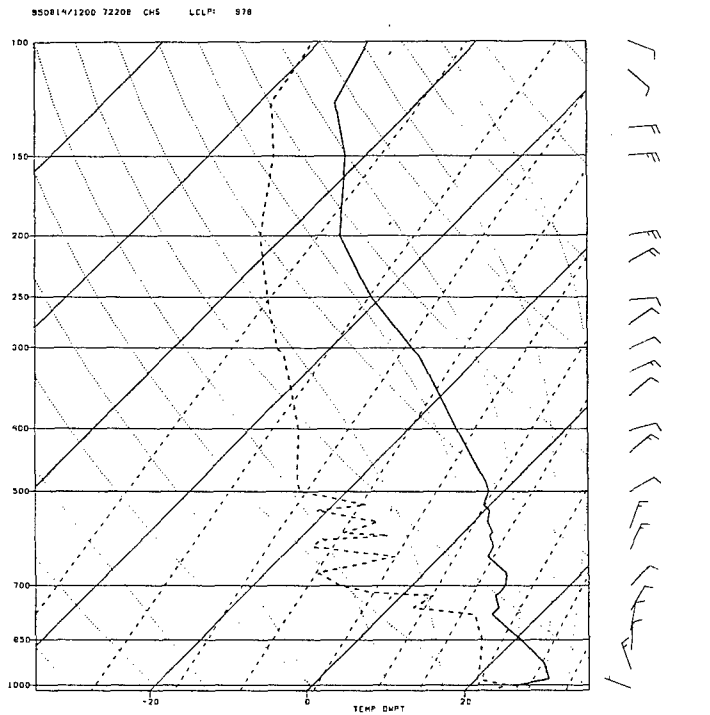
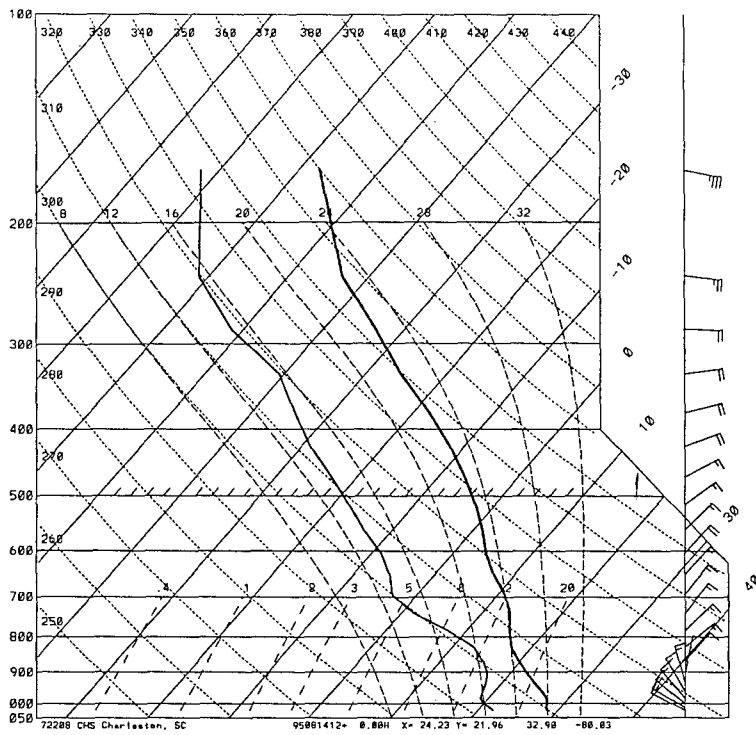


Figure 3.59. a: As in Figure 3.53a except for 14 August 1995 at 1200 UTC. b: As in Figure 3.53b except for 14 August 1995 at 1200 UTC.

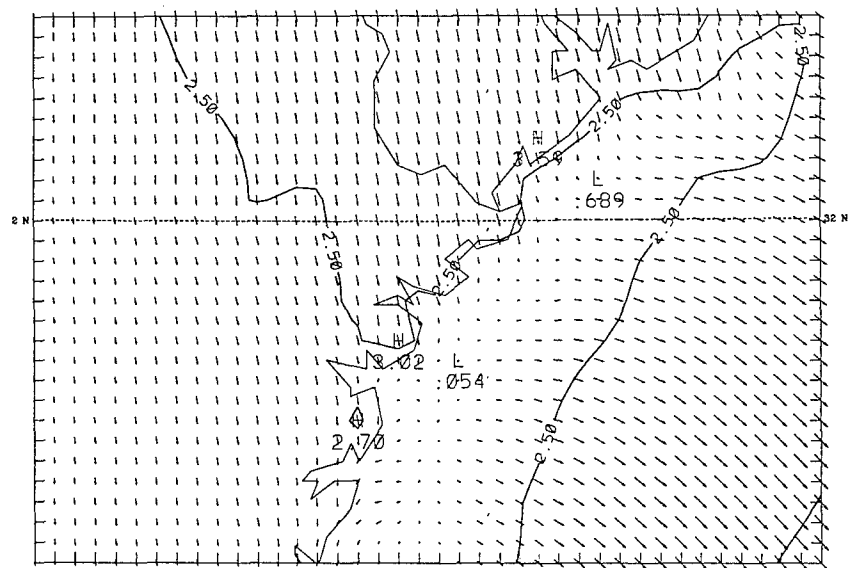
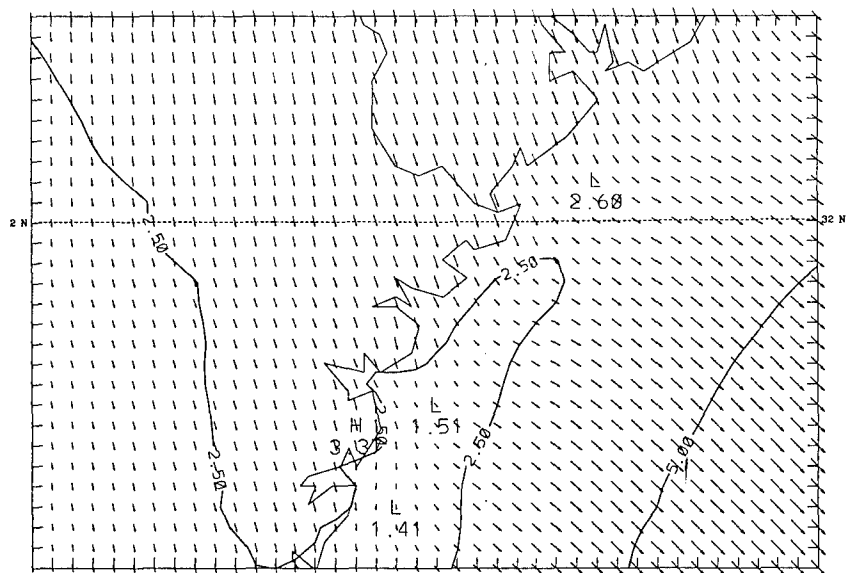


Figure 3.60. a: As in Figure 3.3a except for 14/17 UTC. b: As in Figure 3.3a except for 14/18 UTC.

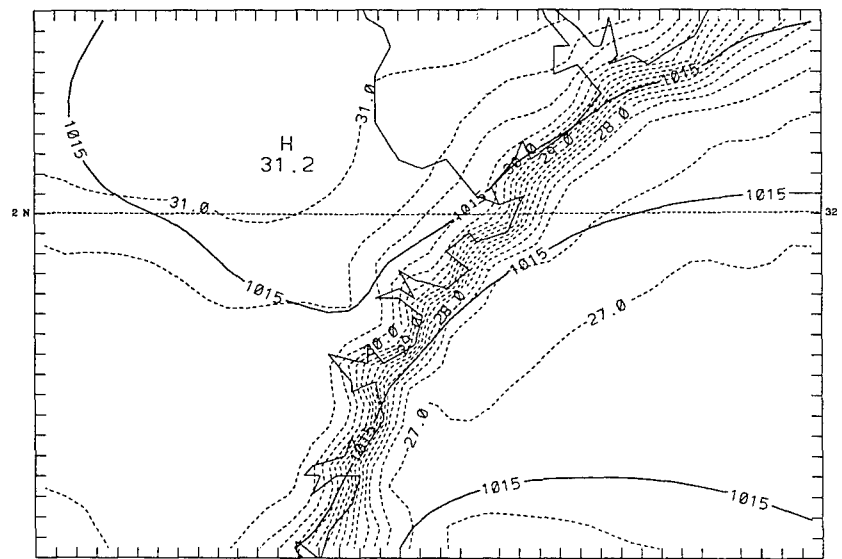
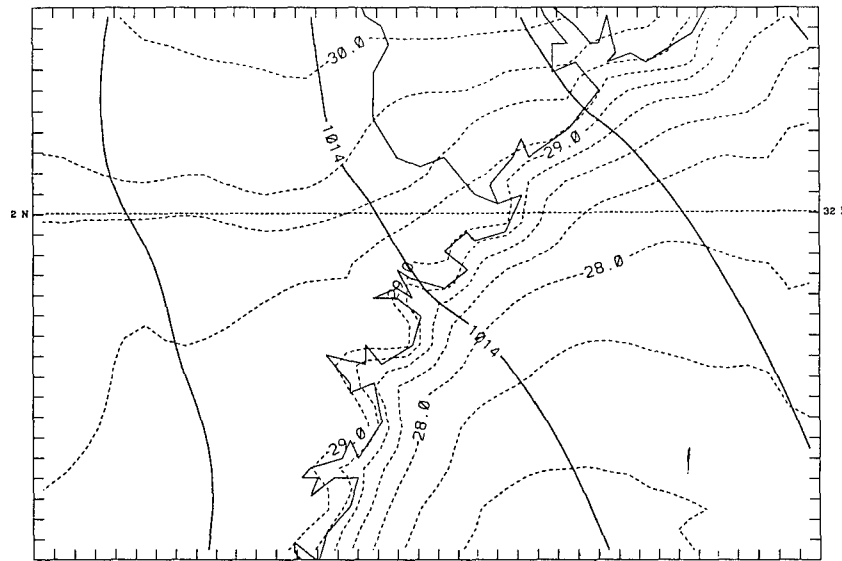


Figure 3.61. a: As in Figure 3.23a except for 14/15 UTC. b: As in Figure 3.23a except for 13/16 UTC.

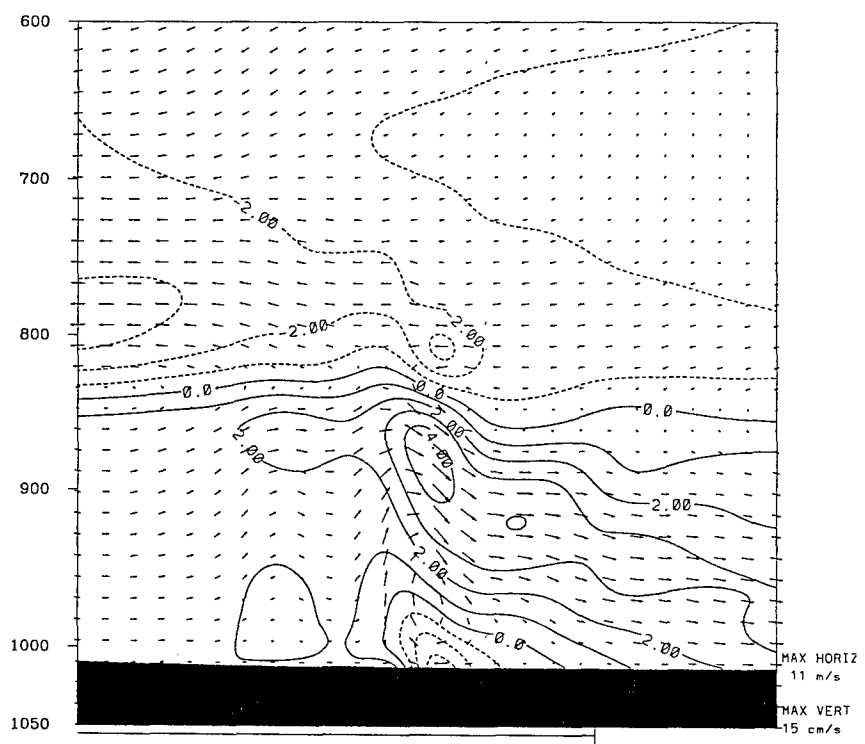
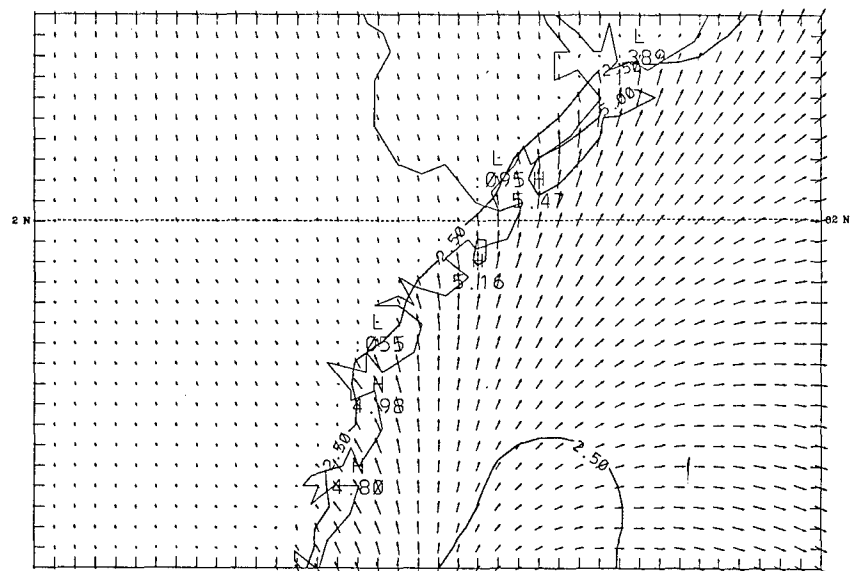


Figure 3.62. a: As in Figure 3.3a except for 14/21 UTC. b: As in Figure 3.35a except for 14/21 UTC.



horizontally. By 14/24 UTC, the winds have veered quickly and lost most of their sea breeze character.

Observations for the land stations during this period are similar to day one. SAV does not show passage of the sea breeze while SSI does, all in good agreement with the model output. At SSI, winds speeds are  $1 \text{ m s}^{-1}$  less than forecasted by the model but with wind directions in excellent agreement with the observed. At SAV, wind directions are in good agreement until 14/20 UTC, when the model continues with northwesterlies while the observed reported northeasterlies. Also, the model underforecast the wind speeds by up to  $2 \text{ m s}^{-1}$ . Comparison of the early afternoon CHS observations show similar results to the SAV observations except CHS does have passage of the sea breeze by 14/2000 UTC. This event is not forecasted by the model.

Buoy observations, like the land observations, agree well with the forecasted model output early in the development of the sea breeze. The buoy observations however, do not support the modeled seaward winds after the model has fully developed the sea breeze circulation.

Limited mesonet data are available for day two comparisons, generally from 1200-1500 UTC. These observations closely match the modeled the wind directions over these hours, but observed wind speeds are  $1\text{-}2 \text{ m s}^{-1}$  less than forecasted by the model.

## Discussion

### Land Breeze

From these simulations, the successful growth of a land breeze is closely tied to the establishment of a coastal temperature gradient. If the large-scale forcings are not

conducive for the formation of the gradient, no land breeze will develop, as modeled in many of the runs. For development, the large-scale winds must be less than  $2.5 \text{ m s}^{-1}$  and either alongshore or onshore. If the large-scale winds are stronger than  $2.5 \text{ m s}^{-1}$  or directed offshore, the land breeze will not form.

The maximum depths modeled in the simulations agree well with those described by Meyer (1971) in his radar observations of a land breeze off the Virginia coast. The modeled onshore component of the circulation however, ranged from less than 50 m to 300 m while Meyer's measured depth, for his two observed cases, was 90 m.

The wide range in modeled depths can be attributed to the land breeze being influenced by the large-scale flow. The two extremes of depth occurred with the alongshore simulations. In the NE case, a complete land breeze developed, the strongest of all the model simulations. A light onshore component of the over-water winds coupled with the offshore component of the inland winds acted together to compact the developing coastal temperature gradient, making a stronger land breeze. In the SW case, the land breeze did not fully develop and the depth represented the height of the onshore perturbation in the flow caused by the land breeze effects. In this case, the temperature gradient was not enhanced by the background flow.

The modeled horizontal extent of the circulation ranged from 12 km landward to 11 km seaward. Meyer observed the land breeze front 19-22 km seaward and made no observations of the landward extent.

The average land breeze modeled in this project initiated by 1000 UTC at the shoreline at less than  $1 \text{ m s}^{-1}$ . By 1200 UTC, the winds reached a maximum speed of

slightly greater than  $1 \text{ m s}^{-1}$  from  $320^\circ$ . The circulation had an offshore depth of 150 m, a maximum depth of 1000 m, a seaward extent of 6 km, and a landward extent of 9 km. After 1300 UTC, the land breeze begins to decay as the circulation translates seaward.

### **Sea Breeze**

The sea breeze is much less sensitive to the large-scale forcings than the land breeze. Although still dependent on the development of the coastal temperature gradient to drive the circulation, the gradient generally develops rapidly once inland heating occurs. Only when the large-scale forcings were onshore at speeds near  $5 \text{ m s}^{-1}$  did the sea breeze fail to clearly develop. This is in good agreement with Arritt (1993) who found that for large-scale onshore flow greater than  $3 \text{ m s}^{-1}$  the sea breeze was suppressed. The sea breeze was the strongest when the large-scale forcings were offshore or alongshore at speeds less than  $5 \text{ m s}^{-1}$ .

In simulations where the large-scale forcings were generally light, there was a clear transition from the land breeze to the sea breeze. As the land breeze decayed, its circulation migrated seaward. At the shoreline, the coastal temperature gradient would reverse, initiating the sea breeze. Within the next several hours, the sea breeze would expand both landward and seaward, eventually overcoming the decaying land breeze. When the forcings were stronger and the land breeze did not fully develop, there was not a clear transition to the sea breeze. The winds instead either veered or backed to assume a sea breeze character in response to the developing coastal temperature gradient.

The initiation point of the sea breeze was dependent on the location of the developing temperature gradient. In most simulations, this was located at the shoreline

but in one simulation, the circulation first initiated offshore as the gradient had formed seaward.

The prevailing direction of the sea breeze winds was also tied to the large-scale forcings. As the sea breeze matured, it would adjust to the large-scale pressure gradient and veer due to the Coriolis effects. Pure onshore flow was only modeled in the calm idealization while most of the model runs tended to have a flow south of true onshore in response to the large-scale pressure pattern.

Definable maximum landward and seaward extents varied widely. Inland penetrations ranged from as small as 11 km to as large as 120 km, but they are in good agreement with Williams' (1969) observational study. He noted the sea breeze could penetrate inland as much as 92 km or as little as 10 km, depending upon the prevailing synoptic conditions. The smallest inland penetration occurred on day two of the 13 August run as the sea breeze was inhibited by the strong synoptic-scale high pressure system inland and the strong subsidence inversion aloft. Although the land areas heated intensely and a strong temperature gradient formed at the coastline, the sea breeze was still unable to penetrate inland because of the higher overland pressures. The largest penetration occurred on day two of the average initialization and may be representative of a sea breeze becoming detached from the surface layer and surging inland (Simpson 1994).

The modeled inland penetration speeds are also in good agreement with Williams (1969) and those presented by Simpson (1994) and Atkinson (1981). Further, the seaward extensions and movement speeds are in good agreement with those presented by

Arritt (1989).

Maximum depths of the circulation also varied significantly from a maximum of 2600 m to a minimum of 1800 m with the onshore component depth varying accordingly (600 m to 170 m). Although this is a wide range, it is consistent with depths presented by Atkinson (1981).

The average sea breeze modeled in this project initiated by 1600 UTC at the shoreline with a speed of  $2.5 \text{ m s}^{-1}$  from  $150^\circ$ . By 2000 UTC, the winds had reached a maximum speed of  $6.5 \text{ m s}^{-1}$  from  $160^\circ$ . These model averages are in excellent agreement with the statistical averages developed by Powell (1996) using buoy and mesonet data for the area. The circulation had an onshore depth of 400 m, a maximum depth of 2300 m, a landward extent of 75 km, and a seaward extent of 110 km. After 0100 UTC, the circulation decayed as the winds veered and lost their sea breeze character.

### **Seaward Component**

Initiation of the sea breeze often occurred at the shoreline but frequently extended seaward. Onshore winds could initiate at the coastline and simultaneously seaward up to 11 km. The key to understanding where this development would take place was the location of the coastal temperature gradient. If the gradient was onshore or displaced offshore, the winds would initiate at the shoreline or seaward respectively.

Once the circulation did form, it rapidly expanded seaward at speeds of  $15 \text{ km hr}^{-1}$ , faster than the landward movement. This is in good agreement with Finkle's (1994) instrumented aircraft study that also found the seaward expansion faster than the landward.

Although the seaward extent was often greater than 100 km, the onshore component of the winds seaward would decrease quickly away from the coastline. The strongest winds of the circulations were usually tied to where the temperature gradient was the strongest, either the shoreline or the sea breeze front. As a result, unless forced by the background flow, the onshore component of the winds offshore decreased rapidly seaward in a developing sea breeze, as much as  $2 \text{ m s}^{-1}$  within 11 km. In a mature or decaying sea breeze, the offshore gradient of the onshore component of the winds was significantly less.

The sea breeze also directly impacted the depth of the marine PBL. As the circulation develops and matures, the return flow and associated subsidence acts to compact the boundary layer seaward of the sea breeze front. Over time, this creates a strong moisture gradient aloft, limiting the depth of the marine PBL. As the sea breeze moves inland, the associated subsidence area also moves, extending this effect overland.

## CHAPTER 4

### CONCLUSIONS

#### Summary

This study investigated the LSBS that develops in the waters off the Savannah, Georgia coast, using the PSU/NCAR MM5 model. This area was chosen because the 1996 Summer Olympic Games sailing competition will be held in the waters southeast of Savannah, in the Wassaw Sound. In addition, little work has been done to date on the seaward component of the sea breeze or on the Georgia coast LSBS.

The model was initialized using an average sounding and soundings that represented offshore, onshore, and alongshore flows. These soundings were derived from 1082 soundings from Charleston, South Carolina for the period 15 July through 15 August, 1946-1992. Data were sorted using the 850-mb and 700-mb winds to classify soundings into the appropriate regime.

In an effort to gain an understanding of both the land and sea breeze's initiation, intensity, duration, and decay under varying flow regimes, six idealized simulations (calm, average, onshore, offshore, and alongshore) were performed. The model set-up was tested with a real-data simulation of the LSBS that occurred across the Wassaw Sound during 13-15 August 1995.

Results show that the LSBS develops differently under varying flow regimes, agreeing well with previous findings (Bechtold et al. 1991; Arritt 1993, Herbster 1996). The calm initialization allowed the LSBS to develop with no large-scale forcings. As a result, the circulations initiated early in the model runs, penetrated long distances both inland and seaward, and showed clear transitions from the land breeze to the sea breeze.

The average initialization simulated how the diurnal circulations would develop with the average large-scale forcing expected to occur during the period 15 July through 15 August across the Wassaw Sound. The land breeze that developed was less intense than modeled in the calm idealization because of interaction with the large-scale forcings. On day two of the simulation, no land breeze occurred because the large-scale forcings did not permit the development of a coastal temperature gradient. The sea breezes that formed during this run flowed from south of pure onshore and had slightly higher speeds as the circulation adjusted to the large-scale pressure fields.

The offshore initialization showed how the LSBS would react to offshore forcings. As found by other researchers (Estoque 1962, Bechtold et al. 1991, Arritt 1993), the inland penetration of the sea breeze front was inhibited by the large-scale flow but the wind speeds were higher than the calm idealization because the forcings created a stronger coastal temperature gradient during the day. Overnight, the land breeze did not develop because the large-scale flow disrupted the formation of a coastal temperature gradient.

The onshore initialization modeled how the sea and land breeze would respond to large-scale onshore forcing. Again, as found by other researchers, (Estoque 1962,



Bechtold et al. 1991, Arritt 1993), onshore flow weakens the coastal temperature gradient. If the onshore flow is too strong, it does not permit the formation of either the land or sea breeze. In this simulation, there was very little clear indication of development of either the land or sea breeze, only hints of their influence on the large-scale flow.

The alongshore initialization simulated how the LSBS would respond to alongshore forcings. The large-scale forcings for the SW initialization did not allow the land breeze to develop fully. In the NE simulation, the large-scale forcings contributed to the development of the land breeze, allowing a land breeze to develop on both days of the simulation. Both idealizations did have full sea breeze circulation develop as the alongshore flows had generally little impact on the development of the daytime coastal temperature gradient. As a result, both had similar characteristics and structure.

The 13 August simulation was done to examine how the model, using the same set-up as the idealized simulations, would reproduce the LSBS that occurred during 13-15 August 1995 across the Wassaw Sound. Again, the large-scale forcings dominated the land breeze and did not allow it to develop. The sea breeze did develop on both days but was limited in both height and extent because of the surface high pressure system anchored inland and the synoptically forced subsidence inversion aloft. Overall, the model results compared favorably to the limited mesonet, satellite, and sounding data available for comparison.

These results are summarized in Tables 4.1 and 4.2 for the sea breeze and land breeze, respectively.

Table 4.1. Land breeze finding summary. Avg indicates the average idealization; NW (northwest) the offshore idealization; SE (southeast) the onshore idealization; SW (southwest) and NE (northeast) the alongshore idealizations; and 13 Aug the 13-15 August 1995 simulation. Onset time is defined as the time at which the winds over the Wassaw Sound first have an offshore component. Directions (dir) are degrees from true north and speeds (spd) are in  $\text{m s}^{-1}$ . Initiation point is defined as the point at which the winds first had an offshore component. Max refers to the time, direction and speed of the strongest land breeze. Landward (seaward) extents are in km and land-spd (sea-spd) is the maximum rate of advance in  $\text{km hr}^{-1}$  of the landward (seaward) boundaries of the circulation. Depth is the maximum height to the top of the circulation in meters and offshore is the depth of the offshore competent measured at the shoreline. Decay is defined as the time at which the winds across the Wassaw Sound lose their offshore component. Duration is the total time in hours the circulation existed. A indicates that the event had not occurred by the end of the model run. B indicates the winds backed to assume the land or sea breeze character. D indicates the circulation did not develop. E indicates the land breeze did not develop into a full circulation but still effected the large-scale flow across the area. M indicates the feature was masked by the background flow. V indicates the winds veered to assume the sea or land breeze character.

Regime	Calm	Calm	Avg	Avg	NW	NW	SE	SE	SW	SW	NE	NE	13Aug	13Aug
Day	1	2	1	2	1	2	1	2	1	2	1	2	1	2
Onset														
time	01/03	02/10	01/08	D	D	D	D	02/11	01/08	D	01/10	02/10	D	D
dir/spd	310/01	250/01	E	D	D	D	D	E	E	D	020/02	020/01	D	D
init. pt.	shore	shore	E	D	D	D	D	E	E	D	shore	shore	D	D
Max														
time	01/12	02/10	01/12	D	D	D	D	02/11	01/12	D	01/12	02/11	D	D
dir/spd	360/01	250/01	E	D	D	D	D	E	E	D	020/02	360/02	D	D
Extent														
landward	11	12	6	D	D	D	D	10	5	D	11	11	D	D
land-spд	<5	<5	<5	D	D	D	D	<5	<5	D	<5	<5	D	D
seaward	11	8	6	D	D	D	D	5	<5	D	5	5	D	D
sea-spд	<5	<5	<5	D	D	D	D	<5	<5	D	<5	<5	D	D
Depth														
time	01/12	02/12	01/13	D	D	D	D	02/12	01/12	D	01/12	01/11	D	D
max	1100	730	1000	D	D	D	D	1150	1150	D	1100	1050	D	D
offshore	200	200	<100	D	D	D	D	E	<50	D	220	300	D	D
Decay	01/13	01/12	01/13	D	D	D	D	02/13	02/12	D	01/14	02/14	D	D
Duration	10	2	5	D	D	D	D	2	4	D	4	4	D	D

Table 4.2. Sea breeze finding summary. As in Table 4.1 except onset time is defined as the time at which the winds over the Wassaw Sound first have an onshore component. Initiation point is defined as the point at which the winds first had an onshore component. Max refers to the time, direction and speed of the strongest sea breeze. Depth refers to the maximum height to the top of the circulation and onshore is the depth of the onshore component measured at the shoreline. Decay is defined as the time at which the winds across the Wassaw Sound lose their onshore component.

Regime	Calm	Calm	Avg	Avg	NW	NW	SE	SE	SW	SW	NE	NE	13Aug	13Aug
Day	1	2	1	2	1	2	1	2	1	2	1	2	1	2
Onset														
time	01/15	02/15	01/15	02/16	01/15	02/17	M	M	01/16	02/17	01/17	02/17	01/16	02/19
dir/spd	130/01	120/01	160/01	170/04	170/02	170/02	M	M	170/05	170/03	100/02	090/02	150/02	170/02
init. pt.	shore	shore	shore	B	B	B	M	M	B	B	V	V	shore	seaward
Max														
time	01/21	02/20	01/20	02/20	01/21	02/20	M	M	01/20	02/20	01/21	02/20	02/20	02/21
dir/spd	150/06	140/06	160/07	160/08	170/08	170/07	M	M	160/08	170/07	120/05	110/05	170/06	180/05
Extent														
landward	90	90	112	120	45	40	M	M	80	75	85	60	33	11
land-sp	15	15	15	20	11	11	M	M	15	15	11	15	5	5
seaward	130	150	M	M	135	145	M	M	M	M	120	135	55	15
sea-sp	15	15	M	M	15	15	M	M	M	M	15	15	11	5
Depth														
time	01/21	02/20	01/21	02/23	01/20	02/20	M	M	01/20	02/21	01/22	02/21	01/21	02/21
max	2300	2300	2300	2500	2450	2800	M	M	2300	2600	2400	2100	2150	1800
onshore	480	480	450	450	300	300	M	M	600	600	600	300	300	300
Decay	02/02	A	02/01	A	02/01	A	M	M	02/02	A	02/01	A	02/00	A
Duration	11	9+	10	8+	10	7+	M	M	10	7+	8	7+	8	4+

## Significant Results

The average land breeze modeled in this project initiated by 1000 UTC at the shoreline blowing at less than  $1 \text{ m s}^{-1}$ . By 1200 UTC, the circulation had reached a maximum speed of slightly greater than  $1 \text{ m s}^{-1}$  from  $320^\circ$ , had an offshore depth of 150 m, a maximum depth of 1000 m, a seaward extent of 6 km, and a landward extent of 9 km. After 1300 UTC, the land breeze begins to decay as the circulation translates seaward.

Under weak synoptic conditions, a clear transition occurs between the land breeze and sea breeze. As the land breeze decays, its circulation moves seaward. When the daytime inland heating reverses and intensifies the coastal temperature gradient, the sea breeze initiates at the coast while the land breeze still exists seaward. As the sea breeze intensifies, it expands both landward and seaward.

When stronger synoptic forcings do not allow the development of a land breeze, there is no clear morning transition to the sea breeze. Instead, the coastal winds either veer or back, in response to the developing coastal pressure gradient, to assume the character of the sea breeze.

The average sea breeze modeled in this project initiated by 1600 UTC at the shoreline with a speed of  $2.5 \text{ m s}^{-1}$  from  $150^\circ$ . The initiation point closely tied to the location of the developing coastal temperature gradient. Onshore winds could form at the coastline and simultaneously up to 11 km seaward.

As the sea breeze matures, the return flow and its associated subsidence region are responsible for compacting the marine PBL. As the circulation advances inland, this

effect can also penetrate inland. Seaward, the boundary of the circulation advanced faster than the landward edge and early in the sea breeze's development, the onshore component of the offshore wind speeds decreased quickly seaward.

By 2000 UTC, the average sea breeze had reached a maximum speed of  $6.5 \text{ m s}^{-1}$  from  $160^\circ$  with an onshore depth of 400 m, a maximum depth of 2300 m, a landward extent of 75 km, and a seaward extent of 110 km. After 0100 UTC, the circulation decayed as the winds generally veered and lost their sea breeze character.

### **Project Short-Comings**

The MM5 does not have the capability to alter soil moisture. Soil moisture is determined by the land-use type for a particular grid square. If rainfall develops over a grid box, the model is unable to change the soil moisture content. This can produce unrealistic latent and sensible heat fluxes over the rain-wetted, area which in turn will have a significant impact on the development of the sea breeze.

In the real-data test, the MM5 could not simulate a surface radiational inversion. Other researchers (Seaman et al. 1995) have also noted the model's inability to reproduce accurate surface layer temperatures when radiational cooling has occurred. Seaman et al. stated that this is due to the model's correlation between relative humidity and cloud cover. In certain settings, such as coastal simulations with high humidities, the model may tend to produce too much cloud cover overnight. In turn, this would inhibit any radiational cooling effects the model could have developed.

The LSBS is a mesoscale phenomenon with characteristics that can change significantly within one hour. This study used only hourly model output although the

MM5 set-up used in this project could output the data fields as often as every 108 seconds. While examining data every 1.8 minutes may not be feasible, analyzing a mesoscale feature every 15 or 30 minutes is realistic. Outputting the data every hour requires approximately 600 megabytes of storage space for a 48 hour run and increasing the frequency of model output would require a similar increase in archive space. The only limiting factors to prevent such a study are computer time, disk space, and additional man-hours required for analysis of the extra output.

### **Future Work**

This numerical study has provided some insight and new knowledge on the LSBS that develops in the Wassaw Sound, but other aspects may have a significant impact on the circulations in this area and future research that can be performed.

Little recent work has been done on the effects of the LSBS on coastal pollution transport and dispersion. Although Arritt (1989) noted the importance of the seaward component of the circulation on coastal pollution, the effect of the sea breeze induced compaction of the marine PBL, as found in this study, has not been addressed. This compaction could lead to higher concentrations of pollutants offshore, as they are advected seaward in the return flow. Then, these high concentrations could be recirculated overland, advected back onshore by the sea breeze.

The LSBS that develops along Georgia's barrier islands is unique because of the complex coastal terrain. The coastal area is a maze of salt water swamps and marshes with many embedded small rivers and streams. Compounding that, a 2.0 m tidal flux has currents as high as  $0.5 \text{ m s}^{-1}$ . Thus, the marshes are alternatingly moist or awash and



typically 50 to 100 m of additional beachline is exposed or covered by the changing tides. This changes the soil moisture characteristics of the coastal terrain, significantly altering the surface heat and moisture flux characteristics of the shoreline areas. The effects of tides on the LSBS and on changing the Wassaw Sound's coastal complexity are generally not well understood and beyond the scope of this modeling study.

Prior to the 1996 Summer Olympic Games, a copy of this thesis will be provided to the Marine Olympic Support Forecast Center (MOSFC) located in Savannah, Georgia. In addition, this author has been asked to brief the MOSFC on the results of this study.

The 1996 Summer Olympic Games will produce a unique and detailed data set for the Wassaw Sound area. A meso-network of observing systems is installed, three buoys from NDBC are scheduled to be in place for the competition, and additional soundings will be taken across the Southeast U.S. In addition, new technologies (Doppler radar and a profiler) will be used to provide high-resolution vertical wind profiles of the area. These data will be archived on CD-ROM and will provide a high-resolution data set ideal for further numerical and observational research into the Wassaw Sound LSBS.

**APPENDIX**  
**SUPPLEMENTAL DATA**

**Sounding Data**

**Idealization Soundings**

The following sections contain the sounding data used to initialize the model. Pressure (Press) is in mb, temperature is in °C, u and v wind components are in m s<sup>-1</sup>, relative humidity (RH) is in percent, wind direction (ddd) is in degrees from true north, and wind speed (ff) is in knots. Missing data are indicated by -9999.

**Offshore (Northwest)**

<u>Pressure</u>	<u>U</u>	<u>V</u>	<u>Temp</u>	<u>RH</u>	<u>ddd</u>	<u>ff</u>
1013.3	.9	2.5	29.3	72.0	200	5.1
1000.0	1.6	2.7	28.1	72.7	210	6.1
975.0	2.6	2.2	27.0	70.6	229	6.6
950.0	3.4	1.4	25.6	70.9	247.	7.2
925.0	4.4	0.0	23.9	72.3	270.	8.5
900.0	4.7	-1.3	22.2	73.3	286.	9.5
880.0	4.6	-2.2	20.9	72.4	296	10.0
860.0	4.7	-3.0	19.4	73.4	303	10.8
850.0	4.7	-3.4	18.7	74.4	306	11.2
840.0	4.7	-3.5	18.2	70.8	306	11.5
820.0	4.6	-3.9	17.0	66.0	310	11.7
800.0	4.5	-4.1	15.7	65.7	312	11.8
775.0	4.5	-4.2	13.9	63.9	313	11.8
750.0	4.6	-4.2	12.4	61.2	313	12.1
725.0	4.8	-4.1	10.4	60.8	310	12.2
700.0	4.9	-3.9	8.7	62.0	309	12.1
650.0	4.6	-3.7	5.5	55.3	309	11.4
600.0	5.0	-3.0	1.8	52.0	301	11.4
550.0	4.7	-3.9	-2.0	47.8	310	11.8
500.0	4.7	-4.4	-6.1	42.4	313	12.5
400.0	4.9	-3.9	-16.7	40.0	309	12.2
300.0	4.4	-3.1	-31.9	36.9	305	10.5
250.0	3.9	-4.0	-41.9	45.6	315	10.8
200.0	2.3	-4.0	-54.	-9999	335	10.4

150.0	1.9	-4.9	-66.6	-9999	339	10.3
100.0	2.1	-2.1	-68.1	-9999	44.	5.7

### Onshore (Southeast)

<u>Pressure</u>	<u>U</u>	<u>V</u>	<u>Temp</u>	<u>RH</u>	<u>ddd</u>	<u>ff</u>
1017.1	-2.1	2.9	27.4	74.3	144	7.1
1000.0	-2.6	3.4	25.8	77.8	142	8.3
975.0	-3.2	3.8	24.2	80.2	140	9.6
950.0	-3.6	4.2	22.5	83.3	139	10.8
925.0	-3.7	4.2	21.3	77.4	138	10.8
900.0	-3.6	4.0	20.2	73.0	137	10.4
880.0	-3.7	3.9	19.0	73.4	137	10.5
860.0	-3.8	3.8	17.7	72.0	165	10.3
850.0	-4.0	3.6	17.1	73.1	133	10.5
840.0	-4.0	3.6	16.6	73.1	132	10.4
820.0	-3.9	3.4	15.6	73.6	131	10.1
800.0	-3.8	3.0	14.3	70.5	129	9.4
775.0	-3.8	2.7	13.0	65.6	126	9.0
750.0	-3.6	2.6	11.5	64.0	125	8.7
725.0	-3.6	3.0	10.0	62.7	130	9.0
700.0	-3.7	3.1	8.0	59.5	130	9.4
650.0	-3.3	2.2	4.9	55.7	124	7.6
600.0	-3.2	1.8	1.4	56.7	119	7.1
550.0	-3.1	1.1	-2.3	50.0	110	6.4
500.0	-2.2	0.6	-6.8	48.0	106	4.5
400.0	-0.7	0.2	-17.5	42.7	108	1.4
300.0	0.6	0.2	-33.4	41.2	253	1.1
250.0	1.6	-2.0	-43.6	-9999	322	4.9
200.0	2.5	-2.4	-55.6	-9999	315	6.7
150.0	-0.6	-3.6	-65.5	-9999	10	7.0
100.0	-4.5	-2.4	-67.5	-9999	62	9.9

### Alongshore (Northeast)

<u>Pressure</u>	<u>U</u>	<u>V</u>	<u>Temp</u>	<u>RH</u>	<u>ddd</u>	<u>ff</u>
1015.7	-2.6	1.5	28.3	62.7	120	5.8
1000.0	-3.1	1.2	26.7	64.6	111	6.5
975.0	-3.7	0.6	24.6	66.5	100	7.3
950.0	-3.8	-0.3	23.0	69.1	86	7.4
925.0	-3.6	-2.1	21.4	69.5	60	8.2
900.0	-3.4	-3.2	19.8	70.2	46	9.1
880.0	-3.5	-3.7	18.6	66.0	43	9.9
860.0	-3.6	-4.0	17.5	63.9	41	10.4
850.0	-3.5	-4.1	16.9	67.4	41	10.6
840.0	-3.7	-4.3	16.1	61.7	41	11.0
820.0	-3.9	-4.4	15.1	52.6	41	11.5
800.0	-3.9	-4.5	14.2	44.7	41	11.5
775.0	-4.1	-4.6	13.3	48.2	42	12.0

750.0	-4.4	-4.7	11.9	49.2	43	12.5
725.0	-4.4	-4.5	10.5	43.6	44	12.2
700.0	-4.2	-4.5	8.9	46.7	43	11.9
650.0	-3.5	-4.8	5.7	40.4	36	11.4
600.0	-3.9	-4.3	2.0	40.7	42	11.2
550.0	-2.7	-4.3	-1.9	37.3	32	9.9
500.0	-2.1	-5.5	-6.5	35.2	21	11.4
400.0	0.1	-5.8	-17.9	30.2	359	11.2
300.0	1.1	-5.6	-33.4	35.0	349	11.0
250.0	2.0	-7.3	-43.2	-9999	345	14.7
200.0	1.5	-8.6	-54.5	-9999	350	16.9
150.0	1.4	-9.2	-65.7	-9999	352	18.0
100.0	-4.2	-5.0	-67.1	-9999	40	12.6

### Alongshore (Southwest)

<u>Pressure</u>	<u>U</u>	<u>V</u>	<u>Temp</u>	<u>RH</u>	<u>ddd</u>	<u>ff</u>
1014.8	0.5	3.4	27.5	75.8	188	6.7
1000.0	1.0	4.7	26.2	80.0	192	9.4
975.0	1.8	6.4	24.6	80.3	196	12.9
950.0	2.7	7.1	23.2	79.3	201	14.7
925.0	3.3	6.7	21.9	75.6	206	14.6
900.0	3.9	6.5	20.6	74.3	211	14.7
880.0	4.3	6.3	19.4	72.4	215	14.8
860.0	4.6	6.0	18.2	72.6	218	14.7
850.0	4.7	5.8	17.7	72.7	219	14.5
840.0	4.7	5.8	17.0	73.0	219	14.5
820.0	4.9	5.8	15.8	71.6	220	14.7
800.0	5.0	5.7	14.6	70.7	221	14.6
775.0	5.2	5.8	12.9	69.9	222	15.2
750.0	5.3	5.9	11.4	69.3	222	15.4
725.0	5.2	5.8	9.7	67.7	222	15.2
700.0	5.2	5.9	8.1	68.1	222	15.2
650.0	5.1	5.6	4.6	70.0	222	14.7
600.0	4.8	4.8	1.0	67.1	225	13.3
550.0	5.1	4.4	-2.6	60.3	230	13.1
500.0	5.1	3.9	-6.8	57.5	233	12.4
400.0	4.7	3.2	-17.2	52.7	236	11.1
300.0	5.8	1.4	-32.4	43.8	256	11.7
250.0	6.2	0.7	-42.5	42.72	63	12.0
200.0	6.8	0.3	-54.8	-9999	268	13.2
150.0	4.6	-0.4	-66.6	-9999	275	9.0
100.0	-1.0	0.0	-67.0	-9999	92	1.9

## CHS Soundings

The following sections contain the decoded sounding data from CHS for the period 13-15 August 1995. PRES is pressure in mb, TMPC is temperature in °C, DWPC is dew point temperature in °C, DRCT is wind direction in degrees from true north, SPED is wind speed in m s<sup>-1</sup>, MIXR is mixing ratio in g kg<sup>-1</sup>, and HGHT is height above MSL in m. Missing data are indicated by -9999.

### 13 August 1995 0000 UTC

<u>PRES</u>	<u>TMPC</u>	<u>DWPC</u>	<u>DRCT</u>	<u>SPED</u>	<u>MIXR</u>	<u>HGHT</u>
1013.00	31.40	23.40	200.00	5.00	18.27	14.00
1000.00	29.20	23.20	195.00	5.00	18.28	130.00
980.48	27.94	22.49	100.00	6.00	17.85	305.00
947.36	25.73	21.26	215.00	4.00	17.11	610.00
925.00	24.20	20.40	260.00	2.00	16.61	822.00
915.29	23.45	20.03	280.00	2.00	16.39	914.00
883.80	20.96	18.78	320.00	4.00	15.69	1219.00
867.00	19.60	18.10	329.84	4.49	15.32	1386.28
854.00	18.80	15.80	337.59	4.88	13.40	1516.61
850.00	18.80	12.80	340.00	5.00	11.04	1557.00
845.00	18.80	10.80	345.57	5.19	9.71	1607.73
823.41	17.72	9.34	10.00	6.00	9.03	1829.00
794.56	16.24	7.33	30.00	7.00	8.15	2134.00
790.00	16.00	7.00	32.39	7.00	8.01	2183.22
766.42	14.40	5.65	45.00	7.00	7.52	2438.00
739.11	12.48	4.03	50.00	8.00	6.96	2743.00
700.00	9.60	1.60	45.00	9.00	6.18	3200.00
662.20	6.39	-0.66	00.00	7.00	5.54	3658.00
660.00	6.20	-0.80	78.00	6.87	5.50	3685.40
644.00	5.60	-3.40	48.13	5.88	4.64	3886.31
638.00	5.40	-10.60	47.51	5.50	2.69	3962.77
625.00	5.20	-13.80	46.13	4.68	2.12	4130.68
614.57	4.45	-14.99	45.00	4.00	1.95	4267.00
579.00	1.80	-19.20	41.05	5.58	1.45	4749.95
574.00	1.20	-8.80	40.47	5.81	3.44	4819.73
569.92	1.08	-12.38	40.00	6.00	2.61	4877.00
560.00	0.80	-21.20	40.00	5.73	1.26	5018.01
549.00	0.00	-20.00	40.00	5.43	1.43	5176.86
537.00	-0.70	-11.70	40.00	5.09	2.92	5353.44
528.00	-1.50	-17.50	40.00	4.83	1.84	5488.12
518.00	-1.90	-15.90	40.00	4.54	2.15	5640.12
512.00	-2.50	-22.50	40.00	4.36	1.23	5732.54
500.00	-3.70	-24.70	40.00	4.00	1.04	5920.00
488.89	-4.97	-25.75	35.00	4.00	0.97	6096.00
453.00	-9.30	-29.30	28.49	5.95	0.75	6693.23
437.00	-9.70	-30.70	25.43	6.87	0.68	6971.69
434.82	-9.97	-30.80	25.00	7.00	0.68	7010.00
401.57	-14.29	-32.42	70.00	5.00	0.63	7620.00

400.00	-14.50	-32.50	70.00	5.00	0.63	7650.00
354.58	-21.37	-38.95	95.00	6.00	0.37	8534.00
326.28	-26.11	-43.40	95.00	9.00	0.25	9144.00
300.00	-30.90	-47.90	90.00	16.00	0.17	9760.00
263.06	-38.54	-53.38	85.00	26.00	0.10	10668.00
250.00	-41.50	-55.50	80.00	26.00	0.08	11020.00
200.00	-53.30	-65.30	75.00	25.00	0.03	12500.00
173.27	-59.39	-70.44	85.00	22.00	0.02	13411.00
172.00	-59.70	-70.70	84.23	21.74	0.02	13457.90
159.00	-60.30	-71.30	76.06	19.02	0.02	13948.98
150.00	-63.30	-73.30	70.00	17.00	0.01	14310.00
133.00	-70.10	-79.10	66.11	14.67	0.01	15036.47
128.50	-70.42	-79.27	65.00	14.00	0.01	15240.00
105.00	-72.30	-80.30	94.36	8.13	0.01	16433.04
104.54	-72.26	-80.35	95.00	8.00	0.01	16459.00
100.00	-71.90	-80.90	95.00	8.00	0.01	16720.00
94.90	-73.30	-81.30	90.60	8.00	0.01	17027.13
94.23	-73.07	-81.13	90.00	8.00	0.01	17069.00
85.00	-69.70	-78.70	60.04	8.00	0.01	17677.08
84.99	-69.69	-78.69	60.00	8.00	0.01	17678.00
78.90	-63.30	-73.30	69.58	8.38	0.02	18127.31
70.00	-64.50	-74.50	85.00	9.00	0.02	18860.00
55.20	-62.10	-72.10	100.80	12.16	0.04	20329.46
51.82	-59.93	-70.57	105.00	13.00	0.05	20726.00
50.00	-58.70	-69.70	105.00	12.00	0.06	20950.00
47.05	-57.46	-68.68	105.00	11.00	0.08	21336.00
38.00	-53.10	-65.10	88.38	12.42	0.16	22692.47
30.00	-53.90	-65.90	70.00	14.00	0.18	24210.00
29.21	-53.54	-65.61	70.00	14.00	0.19	24384.00
24.22	-51.05	-63.58	95.00	21.00	0.31	25603.00
20.00	-48.50	-61.50	105.00	17.00	0.49	26850.00
19.17	-49.01	-62.01	110.00	16.00	0.47	27127.00
18.30	-49.57	-62.57	105.00	16.00	0.46	27432.00
17.80	-49.90	-62.90	102.00	16.00	0.45	27614.17
16.68	-47.49	-61.06	95.00	16.00	0.62	28042.00
15.90	-45.70	-59.70	89.72	16.35	0.77	28359.07
14.55	-44.65	-58.45	80.00	17.00	0.99	28956.00
11.61	-41.96	-55.26	80.00	25.00	1.84	30480.00
10.61	-40.88	-53.99	80.00	27.00	2.34	31090.00
10.10	-40.30	-53.30	-9999	-9999	2.67	31419.47

13 August 1995 1200 UTC

<u>PRES</u>	<u>TMPC</u>	<u>DWPC</u>	<u>DRCT</u>	<u>SPED</u>	<u>MIXR</u>	<u>HGHT</u>
1013.00	25.00	23.20	280.00	4.00	18.04	14.00
1010.00	24.80	23.30	280.00	4.46	18.21	40.16
1000.00	25.60	22.40	280.00	6.00	17.39	128.00
982.00	27.40	21.40	280.00	6.91	16.64	289.12
980.24	27.30	21.33	280.00	7.00	16.60	305.00
947.01	25.46	20.07	285.00	6.00	15.87	610.00
925.00	24.20	19.20	305.00	4.00	15.38	818.00

<u>PRES</u>	<u>TMPC</u>	<u>DWPC</u>	<u>DRCT</u>	<u>SPED</u>	<u>MIXR</u>	<u>HGHT</u>
914.84	23.47	18.80	315.00	4.00	15.16	914.00
883.30	21.14	17.51	355.00	3.00	14.47	1219.00
850.00	18.60	16.10	25.00	4.00	13.73	1553.00
822.64	17.22	11.43	30.00	3.00	10.42	1829.00
793.43	15.69	6.27	15.00	4.00	7.59	2134.00
765.35	14.17	1.13	5.00	6.00	5.46	2438.00
738.18	12.64	-4.02	00.00	6.00	3.86	2743.00
700.00	10.40	-11.60	50.00	5.00	2.26	3191.00
660.83	8.02	-13.47	75.00	7.00	2.06	3658.00
636.52	6.47	-14.68	50.00	7.00	1.93	3962.00
613.03	4.92	-15.90	50.00	7.00	1.82	4267.00
590.41	3.37	-17.12	45.00	6.00	1.70	4572.00
568.62	1.81	-18.33	50.00	7.00	1.59	4877.00
500.00	-3.50	-22.50	30.00	3.00	1.26	5920.00
488.78	-4.56	-23.56	30.00	3.00	1.18	6096.00
401.55	-13.72	-32.72	105.00	7.00	0.61	7620.00
400.00	-13.90	-32.90	100.00	8.00	0.60	7650.00
369.59	-18.46	-36.09	75.00	11.00	0.48	8230.00
326.28	-25.65	-41.11	75.00	11.00	0.32	9144.00
300.00	-30.50	-44.50	85.00	10.00	0.24	9760.00
263.06	-38.72	-49.83	80.00	10.00	0.15	10668.00
250.00	-41.90	-51.90	80.00	11.00	0.13	11020.00
219.37	-48.46	-57.88	75.00	17.00	0.07	11887.00
200.00	-53.10	-62.10	85.00	15.00	0.04	12500.00
164.67	-60.13	-68.45	65.00	17.00	0.02	13716.00
150.00	-63.50	-71.50	80.00	15.00	0.02	14300.00
141.93	-64.62	-72.48	80.00	14.00	0.01	14630.00
128.14	-66.69	-74.30	75.00	12.00	0.01	15240.00
115.69	-68.75	-76.11	80.00	10.00	0.01	15850.00
104.47	-70.82	-77.92	105.00	8.00	0.01	16459.00
100.00	-71.70	-78.70	110.00	8.00	0.01	16720.00
99.26	-71.77	-78.77	110.00	8.00	0.01	16764.00
89.50	-72.70	-79.70	87.35	7.50	0.01	17374.50
81.50	-68.30	-75.30	66.85	7.04	0.02	17931.62
80.81	-67.90	-74.99	65.00	7.00	0.02	17983.00
73.60	-63.50	-71.50	83.67	8.87	0.03	18552.04
70.00	-64.50	-71.50	85.00	9.00	0.04	18860.00
50.00	-58.90	-66.90	85.00	15.00	0.09	20950.00
47.02	-58.16	-66.90	85.00	15.00	0.10	21336.00
46.00	-57.90	-66.90	85.00	15.00	0.10	21473.20
44.81	-57.08	-66.21	85.00	15.00	0.12	21641.00
37.50	-51.50	-61.50	97.49	14.38	0.26	22777.30
33.69	-51.88	-62.36	105.00	14.00	0.26	23470.00
30.00	-52.30	-63.30	100.00	13.00	0.26	24220.00
25.41	-52.14	-63.14	90.00	13.00	0.31	25298.00
20.00	-51.90	-62.90	80.00	20.00	0.40	26850.00
19.18	-50.98	-62.28	75.00	21.00	0.46	27127.00
18.31	-49.96	-61.61	75.00	23.00	0.52	27432.00
13.89	-43.86	-57.54	85.00	27.00	1.16	29261.00
13.30	-42.90	-56.90	-9999	-9999	1.31	29547.40

14 August 1995 0000 UTC

<u>PRES</u>	<u>TMPC</u>	<u>DWPC</u>	<u>DRCT</u>	<u>SPED</u>	<u>MIXR</u>	<u>HGHT</u>
1010.00	34.40	23.40	260.00	5.00	18.32	14.00
1000.00	33.00	24.00	265.00	5.00	19.21	107.00
978.16	31.24	22.81	275.00	4.00	18.25	305.00
945.44	28.54	20.98	300.00	4.00	16.84	610.00
925.00	26.80	19.80	315.00	3.00	15.98	806.00
913.67	25.87	19.39	320.00	4.00	15.77	914.00
882.42	23.23	18.24	330.00	4.00	15.18	1219.00
850.00	20.40	17.00	350.00	4.00	14.56	1547.00
822.63	18.18	15.71	5.00	5.00	13.83	1829.00
806.00	16.80	14.90	7.87	6.15	13.40	2004.92
793.86	16.11	12.87	10.00	7.00	11.89	2134.00
766.00	14.50	8.08	25.00	7.00	8.91	2438.00
761.00	14.20	7.20	26.82	6.82	8.44	2493.73
753.00	15.00	-2.00	27.50	6.52	4.41	2583.11
742.00	15.60	-3.40	33.84	6.12	4.03	2707.73
738.91	15.34	-2.93	35.00	6.00	4.19	2743.00
721.00	13.80	-0.20	41.79	6.00	5.26	2950.42
712.68	13.33	-1.46	45.00	6.00	4.85	3048.00
700.00	12.60	-3.40	45.00	6.00	4.27	3199.00
662.33	9.33	-6.67	35.00	7.00	3.52	3658.00
638.50	7.16	-8.84	30.00	7.00	3.08	3962.00
624.00	5.80	-10.20	30.00	7.62	2.83	4152.65
618.00	5.40	-1.60	30.00	7.88	5.54	4231.83
615.35	5.08	-1.39	30.00	8.00	5.65	4267.00
608.00	4.20	-0.80	30.80	7.68	5.97	4365.26
599.00	3.60	-1.40	31.80	7.28	5.80	4486.85
570.92	2.90	-7.10	35.00	6.00	3.95	4877.00
568.00	2.80	-7.20	36.02	6.14	3.94	4918.70
529.23	-0.94	-12.91	00.00	8.00	2.69	5486.00
510.00	-2.90	-15.90	46.74	7.35	2.18	5782.91
508.00	-2.70	-23.70	46.40	7.28	1.12	5814.09
506.00	-2.70	-17.70	46.05	7.21	1.89	5845.41
503.00	-2.90	-23.90	45.53	7.11	1.11	5892.59
500.00	-3.30	-23.30	45.00	7.00	1.18	5940.00
490.18	-4.37	-17.24	30.00	6.00	2.03	6096.00
489.00	-4.50	-16.50	30.37	5.95	2.16	6114.96
480.00	-5.50	-19.50	33.20	5.57	1.71	6260.48
471.00	-5.90	-26.90	36.08	5.19	0.90	6408.32
443.00	-6.90	-28.90	45.43	3.94	0.80	6885.62
402.61	-12.70	-32.83	60.00	2.00	0.60	7620.00
400.00	-13.10	-33.10	60.00	2.00	0.59	7670.00
379.00	-17.10	-36.10	60.00	3.88	0.46	8078.39
357.00	-20.50	-30.50	60.00	5.96	0.85	8524.79
356.56	-20.55	-30.70	60.00	6.00	0.84	8534.00
345.00	-21.90	-35.90	75.91	7.59	0.52	8777.62
342.09	-22.43	-36.31	80.00	8.00	0.50	8839.00
327.98	-25.08	-38.36	80.00	8.00	0.43	9144.00
300.00	-30.70	-42.70	80.00	7.00	0.30	9790.00



276.13	-35.16	-47.16	80.00	7.00	0.20	10363.00
264.21	-37.53	-49.53	110.00	10.00	0.16	10668.00
250.00	-40.50	-52.50	110.00	13.00	0.12	11050.00
241.55	-42.26	-53.95	110.00	15.00	0.10	11278.00
220.36	-46.95	-57.82	110.00	12.00	0.07	11887.00
210.46	-49.30	-59.75	95.00	11.00	0.06	12192.00
200.00	-51.90	-61.90	95.00	11.00	0.05	12530.00
188.00	-55.10	-65.10	98.25	11.22	0.03	12927.98
150.34	-64.01	-72.03	110.00	12.00	0.02	14326.00
150.00	-64.10	-72.10	105.00	11.00	0.02	14340.00
134.00	-68.50	-76.50	89.85	8.73	0.01	15024.44
129.24	-68.83	-76.70	85.00	8.00	0.01	15240.00
101.00	-71.10	-78.10	113.95	6.07	0.01	16710.94
100.10	-70.56	-77.56	115.00	6.00	0.01	16764.00
100.00	-70.50	-77.50	115.00	6.00	0.01	16770.00
95.10	-69.01	-76.75	110.00	5.00	0.01	17069.00
93.50	-68.50	-76.50	108.61	5.11	0.01	17170.17
89.00	-70.30	-78.30	104.58	5.43	0.01	17464.00
78.50	-69.90	-77.90	94.33	6.25	0.01	18209.26
70.02	-64.12	-72.12	85.00	7.00	0.03	18898.00
70.00	-64.10	-72.10	80.00	6.00	0.03	18900.00
66.00	-61.50	-70.50	88.40	6.72	0.04	19261.93
54.78	-59.89	-68.89	115.00	9.00	0.07	20422.00
50.00	-59.10	-68.10	105.00	8.00	0.08	20990.00
47.33	-58.80	-67.97	90.00	8.00	0.09	21336.00
42.97	-58.28	-67.73	75.00	10.00	0.10	21946.00
35.90	-57.30	-67.30	72.32	15.36	0.12	23080.61
30.72	-53.48	-64.35	70.00	20.00	0.22	24079.00
30.00	-52.90	-63.90	-9999	-9999	0.24	24230.00
29.00	-52.90	-63.90	-9999	-9999	0.24	24448.61

14 August 1995 1200 UTC

<u>PRES</u>	<u>TMPC</u>	<u>DWPC</u>	<u>DRCT</u>	<u>SPED</u>	<u>MIXR</u>	<u>HGHT</u>
1011.00	26.40	24.10	290.00	3.00	19.12	14.00
1000.00	26.00	24.80	298.17	3.65	20.19	112.00
979.00	29.20	20.20	314.02	4.92	15.47	300.73
945.52	27.61	19.22	340.00	7.00	15.06	610.00
925.00	26.60	18.60	350.00	5.00	14.80	805.00
913.57	25.75	18.19	355.00	5.00	14.60	914.00
882.32	23.36	17.04	5.00	5.00	14.04	1219.00
850.00	20.80	15.80	5.00	5.00	13.46	1546.00
822.39	18.33	14.35	10.00	5.00	12.66	1829.00
793.63	15.68	12.79	15.00	5.00	11.83	2134.00
776.00	14.00	11.80	24.45	4.37	11.33	2326.52
765.83	14.00	6.85	30.00	4.00	8.19	2438.00
758.00	14.00	3.00	34.26	3.72	6.30	2524.86
738.59	12.83	3.58	45.00	3.00	6.75	2743.00
725.00	12.00	4.00	45.00	3.69	7.08	2899.25
718.00	12.20	-3.80	00.00	4.05	4.04	2980.54
700.00	12.00	-9.00	45.00	5.00	2.78	3193.00

<u>PRES</u>	<u>TMPC</u>	<u>DWPC</u>	<u>DRCT</u>	<u>SPED</u>	<u>MIXR</u>	<u>HGHT</u>
669.00	10.60	-13.40	49.05	5.81	2.04	3570.45
661.94	9.80	-12.02	50.00	6.00	2.31	3658.00
631.00	6.20	-5.80	33.84	6.65	3.95	4052.94
614.69	5.76	-14.36	25.00	7.00	2.06	4267.00
609.00	5.60	-17.40	22.51	7.50	1.61	4343.10
595.00	4.60	-17.40	16.30	8.74	1.65	4532.58
592.12	4.37	-15.05	15.00	9.00	2.02	4572.00
585.00	3.80	-9.20	16.61	8.68	3.27	4670.30
579.00	3.80	-15.20	17.98	8.40	2.04	4753.96
570.25	3.01	-14.02	20.00	8.00	2.28	4877.00
557.00	1.80	-12.20	27.15	7.64	2.71	5067.09
535.00	0.60	-21.40	39.42	7.03	1.30	5390.89
524.00	-0.90	-15.90	4.74	6.71	2.12	5556.97
500.00	-1.90	-25.90	60.00	6.00	0.93	5930.00
489.66	-2.87	-26.87	65.00	6.00	0.87	6096.00
483.00	-3.50	-27.50	63.25	6.12	0.83	6204.91
435.46	-9.21	-31.02	50.00	7.00	0.66	7010.00
402.58	-13.55	-33.68	75.00	6.00	0.56	7620.00
400.00	-13.90	-33.90	75.00	6.00	0.55	7670.00
355.67	-20.19	-38.84	50.00	6.00	0.37	8534.00
341.22	-22.41	-40.59	65.00	7.00	0.33	8839.00
327.36	-24.63	-42.33	65.00	9.00	0.28	9144.00
308.00	-27.90	-44.90	65.00	6.81	0.23	9592.50
301.10	-29.45	-46.45	65.00	6.00	0.20	9754.00
300.00	-29.70	-46.70	65.00	6.00	0.19	9780.00
275.91	-35.03	-50.19	55.00	6.00	0.14	10363.00
264.09	-37.81	-52.01	75.00	5.00	0.12	10668.00
252.78	-40.60	-53.84	85.00	6.00	0.10	10973.00
250.00	-41.30	-54.30	80.00	7.00	0.10	11050.00
220.36	-47.97	-59.28	60.00	10.00	0.06	11887.00
200.00	-53.10	-63.10	80.00	12.00	0.04	12530.00
191.54	-54.51	-64.36	85.00	13.00	0.03	12802.00
150.00	-62.50	-71.50	85.00	12.00	0.02	14340.00
135.91	-66.65	-75.13	85.00	10.00	0.01	14935.00
129.21	-68.77	-76.99	95.00	9.00	0.01	15240.00
124.00	-70.50	-78.50	104.31	8.20	0.01	15488.23
110.69	-72.29	-79.77	130.00	6.00	0.01	16154.00
105.09	-73.12	-80.35	120.00	4.00	0.01	16459.00
100.00	-73.90	-80.90	110.00	4.00	0.01	16750.00
99.76	-73.86	-80.86	105.00	4.00	0.01	16764.00
92.20	-72.70	-79.70	89.79	5.52	0.01	17225.56
89.94	-71.20	-78.42	85.00	6.00	0.01	17374.00
82.10	-65.70	-73.70	85.00	8.69	0.02	17918.91
81.24	-65.58	-73.70	85.00	9.00	0.02	17983.00
75.40	-64.70	-73.70	-9999	-9999	0.02	18437.63
70.00	-66.10	-75.10	-9999	-9999	0.02	18890.00

15 August 1995 0000 UTC

<u>PRES</u>	<u>TMPC</u>	<u>DWPC</u>	<u>DRCT</u>	<u>SPED</u>	<u>MIXR</u>	<u>HGHT</u>
1011.00	33.00	24.00	160.00	4.00	19.00	14.00
1000.00	31.60	23.60	165.00	4.00	18.74	113.00
978.75	30.39	22.94	175.00	5.00	18.39	305.00
945.93	28.46	21.89	215.00	3.00	17.83	610.00
925.00	27.20	21.20	260.00	2.00	17.47	810.00
914.12	26.30	20.92	285.00	2.00	17.37	914.00
882.93	23.68	20.10	330.00	2.00	17.09	1219.00
850.00	20.80	19.20	345.00	3.00	16.77	1553.00
832.00	19.40	18.70	1.74	3.67	16.60	1738.59
823.26	18.93	17.28	10.00	4.00	15.32	1829.00
794.44	17.35	12.51	30.00	6.00	11.60	2134.00
766.71	15.78	7.75	40.00	9.00	8.70	2438.00
750.00	14.80	4.80	43.07	9.00	7.24	2626.61
700.00	10.60	-3.40	00.00	11.00	4.27	3206.00
694.00	10.00	-3.00	39.21	11.31	4.44	3277.59
683.00	10.00	-10.00	37.76	11.90	2.63	3410.27
662.69	8.48	-11.77	35.00	13.00	2.35	3658.00
615.29	4.73	-16.12	40.00	15.00	1.78	4267.00
604.00	3.80	-17.20	35.07	13.77	1.65	4418.97
570.75	2.90	-19.22	20.00	10.00	1.47	4877.00
546.00	2.20	-20.80	11.21	8.83	1.34	5235.57
529.18	0.74	-21.90	5.00	8.00	1.26	5486.00
500.00	-1.90	-23.90	1.00	10.00	1.12	5940.00
490.27	-2.61	-24.61	10.00	10.00	1.07	6096.00
473.00	-3.90	-25.90	12.75	10.37	0.98	6380.52
403.11	-13.82	-33.91	25.00	12.00	0.54	7620.00
356.03	-21.10	-39.48	35.00	12.00	0.35	8534.00
327.62	-25.96	-43.18	25.00	10.00	0.26	9144.00
300.00	-31.10	-47.10	35.00	8.00	0.18	9790.00
264.21	-37.93	-52.54	25.00	8.00	0.11	10668.00
250.00	-40.90	-54.90	45.00	9.00	0.09	11050.00
201.00	-52.44	-63.50	110.00	9.00	0.04	12497.00
200.00	-52.70	-63.70	110.00	9.00	0.04	12530.00
178.00	-57.90	-67.90	114.20	9.84	0.02	13273.55
174.12	-58.54	-68.42	115.00	10.00	0.02	13411.00
165.80	-59.97	-69.56	100.00	9.00	0.02	13716.00
150.34	-62.83	-71.85	115.00	7.00	0.02	14326.00
150.00	-62.90	-71.90	115.00	8.00	0.02	14340.00
130.00	-68.50	-76.50	71.57	5.10	0.01	15209.28
129.33	-68.56	-76.56	70.00	5.00	0.01	15240.00
122.87	-69.15	-77.15	60.00	6.00	0.01	15545.00
105.37	-70.90	-78.90	80.00	6.00	0.01	16459.00
100.10	-71.49	-79.49	85.00	6.00	0.01	16764.00
100.00	-71.50	-79.50	85.00	6.00	0.01	16770.00
93.70	-71.90	-79.90	88.00	6.55	0.01	17153.00
81.60	-71.50	-79.50	97.00	7.71	0.01	17967.70
69.91	-63.46	-72.47	100.00	10.00	0.03	18898.00
63.20	-60.10	-70.10	93.98	9.70	0.05	19523.71

<u>PRES</u>	<u>TMPC</u>	<u>DWPC</u>	<u>DRCT</u>	<u>SPED</u>	<u>MIXR</u>	<u>HGHT</u>
56.50	-62.50	-71.50	87.29	9.36	0.04	20220.30
50.00	-60.10	-70.10	80.00	9.00	0.06	20980.00
47.25	-59.66	-69.77	85.00	10.00	0.07	21336.00
38.95	-58.14	-68.63	70.00	11.00	0.10	22555.00
32.10	-56.63	-67.50	85.00	17.00	0.14	23774.00
30.00	-56.10	-67.10	-9999	-9999	0..15	24200.00

### Observations

### Mesonet

**Station Locations.** The following are the locations of the mesonet and synoptic stations depicted in Figure 3.48. Number refers to the number embedded in the figure.

<u>Number</u>	<u>Name</u>	<u>Location</u>
1	Charleston, SC	32.90 N 80.03 W
2	Walterboro, SC	32.91 N 80.62 W
3	Beaufort MCAS, SC	32.48 N 80.72 W
4	Statesboro, SC	32.47 N 81.77 W
5	Pulaski, GA	32.29 N 81.98 W
6	Savannah, GA	32.13 N 81.20 W
7	Port Wentworth, GA	32.17 N 81.98 W
8	Savannah Refuge, GA	32.10 N 81.08 W
9	Hunter AAF, GA	32.02 N 81.15 W
10	Skidaway Island, GA	31.95 N 81.00 W
11	Tybee Island, GA	32.03 N 80.90 W
12	Williamson Island, GA	31.94 N 80.93 W
13	SLVS1 C-MAN	31.57 N 80.00 W
14	41021 Buoy	31.90 N 80.80 W
15	41022 Buoy	31.90 N 80.90 W
16	Savannah CRS, GA	32.00 N 81.27 W
17	Ft. Stewart, GA	31.88 N 81.57 W
18	Liberty County, GA	31.78 N 81.61 W
19	Harris Neck Refuge, GA	31.62 N 81.25 W
20	Fish and Wildlife, GA	31.49 N 81.20 W
21	Midway, GA	31.28 N 81.44 W
22	Sterling, GA	31.26 N 81.61 W
23	Saint Simons Island, GA	31.15 N 81.38 W

**Data.** Due to equipment outages at Peachtree City NWS, the following are the only Georgia Mesonet observations that were archived during the period 13-15 August 1995. GSKI is Skidaway Island (number 10), GHNR is Harris Neck Refuge (number 19), GTYB is Tybee Island (number 11), GSVH is Savannah CRS (number 16), and GSTA is Statesboro (number 4).

GSKI 1200 AMOS 80/M/3202/M PK WND 02  
GHNR 1200 AMOS 80/M/2803/M PK WND 03  
GTYB 1200 AMOS 83/M/2600/M PK WND 01  
GSVH 1200 AMOS 74/M/2401/M PK WND 01  
GSTA 1200 AMOS 78/M/2902/M PK WND 04  
GSKI 1215 AMOS 81/M/3202/M PK WND 02  
GHNR 1215 AMOS 80/M/2902/M PK WND 03  
GTYB 1215 AMOS 85/M/2100/M PK WND 01  
GSVH 1200 AMOS 74/M/2401/M PK WND 01  
GSTA 1200 AMOS 78/M/2902/M PK WND 04  
GSKI 1230 AMOS 82/M/3102/M PK WND 02  
GHNR 1230 AMOS 82/M/2901/M PK WND 03  
GTYB 1230 AMOS 86/M/2600/M PK WND 01  
GSKI 1245 AMOS 83/M/3202/M PK WND 03  
GHNR 1245 AMOS 83/M/3001/M PK WND 03  
GTYB 1245 AMOS 87/M/2500/M PK WND 01  
GSKI 1300 AMOS 84/M/3304/M PK WND 04  
GHNR 1300 AMOS 84/M/2902/M PK WND 03  
GTYB 1300 AMOS 88/M/2100/M PK WND 01  
GSVH 1300 AMOS 80/M/3201/M PK WND 03  
GSTA 1300 AMOS 81/M/3103/M PK WND 05  
GSKI 1315 AMOS 85/M/3302/M PK WND 03  
GHNR 1315 AMOS 86/M/2702/M PK WND 02  
GTYB 1315 AMOS 89/M/2400/M PK WND 01  
GSVH 1300 AMOS 80/M/3201/M PK WND 03  
GSTA 1300 AMOS 81/M/3103/M PK WND 05  
GSKI 1330 AMOS 86/M/3303/M PK WND 04  
GHNR 1330 AMOS 87/M/2802/M PK WND 03  
GTYB 1330 AMOS 89/M/2402/M PK WND 03  
GSKI 1400 AMOS 88/M/3203/M PK WND 04  
GHNR 1400 AMOS 89/M/2701/M PK WND 02  
GTYB 1400 AMOS 90/M/2500/M PK WND 02  
GSVH 1400 AMOS 85/M/3203/M PK WND 04  
GSKI 1415 AMOS 89/M/3302/M PK WND 04  
GHNR 1415 AMOS 90/M/2701/M PK WND 02  
GTYB 1415 AMOS 91/M/2900/M PK WND 03  
GSVH 1400 AMOS 85/M/3203/M PK WND 04  
GSTA 1400 AMOS 84/M/3104/M PK WND 06  
GSKI 1430 AMOS 90/M/3304/M PK WND 04  
GHNR 1430 AMOS 91/M/2603/M PK WND 03  
GTYB 1430 AMOS 92/M/2401/M PK WND 02  
GSKI 1445 AMOS 91/M/3403/M PK WND 04  
GHNR 1445 AMOS 92/M/3002/M PK WND 04  
GTYB 1445 AMOS 93/M/2801/M PK WND 03  
GSKI 1500 AMOS 91/M/3204/M PK WND 05

GHNR 1500 AMOS 93/M/2802/M PK WND 03  
 GTYB 1500 AMOS 93/M/2503/M PK WND 03  
 GSVH 1500 AMOS 89/M/3503/M PK WND 04  
 GSKI 1515 AMOS 92/M/3304/M PK WND 05  
 GHNR 1515 AMOS 94/M/2700/M PK WND 04  
 GTYB 1515 AMOS 92/M/0303/M PK WND 04  
 GSVH 1500 AMOS 89/M/3503/M PK WND 04  
 GSTA 1500 AMOS 88/M/3304/M PK WND 06  
 GSKI 1530 AMOS 92/M/3405/M PK WND 05  
 GHNR 1530 AMOS 95/M/2101/M PK WND 03  
 GTYB 1530 AMOS 92/M/0302/M PK WND 04  
 GSKI 1545 AMOS 93/M/3303/M PK WND 05  
 GHNR 1545 AMOS 95/M/2101/M PK WND 03  
 GTYB 1545 AMOS 92/M/0603/M PK WND 04

### Synoptic

The following are the synoptic observations from Charleston, South Carolina (CHS, number 1); Savannah, Georgia (SAV, number 6); and Saint Simons Island, Georgia (SSI, number 23) during the period 13-15 August 1995. SKC is sky cover in eighths, TMPC is temperature in °C, DWC is dew point in °C, SPD is wind speed in m s<sup>-1</sup>, DRCT is the direction the wind is blowing from in degrees from true north, and PMSL is pressure reduced to mean sea level in mb. Missing data are indicated by -9999.

<u>STN</u>	<u>DATE</u>	<u>SKC</u>	<u>TMPC</u>	<u>DWC</u>	<u>SPD</u>	<u>DRCT</u>	<u>PMSL</u>
CHS	950813/0200	3.00	10.00	10.00	3.09	30.00	1008.80
CHS	950813/0400	8.00	11.11	11.11	1.03	300.00	1011.10
CHS	950813/0500	0.00	26.11	24.44	2.57	250.00	1014.60
CHS	950813/0600	0.00	26.11	24.44	3.09	240.00	1014.60
CHS	950813/0700	0.00	25.56	24.44	2.57	230.00	1014.30
CHS	950813/0800	0.00	25.56	23.89	3.09	260.00	1014.10
CHS	950813/0900	0.00	25.00	23.89	3.60	250.00	1014.10
CHS	950813/1000	0.00	24.44	23.33	4.12	260.00	1013.90
CHS	950813/1100	0.00	25.00	23.33	4.12	280.00	1014.40
CHS	950813/1200	0.00	25.56	23.33	4.12	280.00	1014.90
CHS	950813/1300	0.00	27.78	23.33	4.63	290.00	1015.30
CHS	950813/1400	0.00	30.56	23.89	3.09	290.00	1014.90
CHS	950813/1500	0.00	32.22	23.89	4.12	280.00	1014.90
CHS	950813/1600	0.00	33.89	22.78	4.12	300.00	1014.60
CHS	950813/1700	0.00	35.00	23.33	3.09	310.00	1014.30
CHS	950813/1800	3.00	36.11	21.67	3.09	310.00	1013.90
CHS	950813/1900	3.00	36.67	21.67	2.57	320.00	1013.20
CHS	950813/2000	3.00	36.67	22.22	3.09	270.00	1012.90
CHS	950813/2100	3.00	37.22	22.78	5.66	270.00	1012.20
CHS	950813/2200	3.00	36.67	23.33	5.14	300.00	1012.20
CHS	950813/2300	3.00	35.00	23.33	4.63	260.00	1011.90
CHS	950814/0200	0.00	26.11	22.78	0.00	0.00	1011.50
CHS	950814/0400	0.00	13.89	12.78	1.54	110.00	1013.20
CHS	950814/0500	3.00	27.78	24.44	3.60	250.00	1013.40

<u>STN</u>	<u>DATE</u>	<u>SKC</u>	<u>TMPC</u>	<u>DWC</u>	<u>SPD</u>	<u>DRCT</u>	<u>PMSL</u>
CHS	950814/0600	0.00	27.78	24.44	4.63	250.00	1013.60
CHS	950814/0700	0.00	27.78	24.44	5.14	270.00	1013.20
CHS	950814/0800	3.00	27.78	24.44	4.12	270.00	1012.90
CHS	950814/0900	0.00	26.67	24.44	3.60	270.00	1012.60
CHS	950814/1000	0.00	26.11	24.44	3.60	270.00	1012.60
CHS	950814/1100	0.00	26.67	24.44	2.57	290.00	1012.60
CHS	950814/1200	0.00	27.22	24.44	3.60	280.00	1013.20
CHS	950814/1300	0.00	29.44	24.44	4.63	310.00	1013.20
CHS	950814/1400	0.00	31.67	25.00	4.12	330.00	1013.60
CHS	950814/1500	0.00	33.89	25.00	4.12	350.00	1013.60
CHS	950814/1600	0.00	36.11	25.00	4.12	320.00	1013.20
CHS	950814/1700	3.00	37.78	22.22	6.69	330.00	1013.20
CHS	950814/1800	3.00	37.78	21.11	6.17	330.00	1012.60
CHS	950814/1900	3.00	38.33	21.67	4.12	340.00	1011.90
CHS	950814/2000	3.00	38.89	22.22	1.54	10.00	1011.50
CHS	950814/2100	8.00	35.56	24.44	3.60	180.00	1011.20
CHS	950814/2200	8.00	33.89	24.44	4.12	170.00	1011.20
CHS	950814/2300	7.00	33.33	24.44	3.60	160.00	1010.90
SAV	950813/0200	6.00	14.44	7.78	0.00	0.00	-9999
SAV	950813/0400	6.00	21.67	20.56	3.09	90.00	1006.90
SAV	950813/0500	0.00	26.11	23.33	2.57	210.00	1015.40
SAV	950813/0600	0.00	25.56	23.89	2.57	240.00	1015.20
SAV	950813/0700	0.00	25.00	23.33	2.06	210.00	1015.00
SAV	950813/0800	0.00	25.00	23.33	0.00	0.00	1014.70
SAV	950813/0900	0.00	24.44	23.33	0.00	0.00	1014.50
SAV	950813/1000	0.00	24.44	22.78	0.00	0.00	1014.50
SAV	950813/1200	0.00	25.00	23.33	0.00	0.00	1015.50
SAV	950813/1300	0.00	26.67	23.33	2.57	310.00	1015.50
SAV	950813/1400	0.00	29.44	24.44	1.54	320.00	1015.90
SAV	950813/1500	0.00	31.67	24.44	2.57	310.00	1015.90
SAV	950813/1600	0.00	33.33	23.33	2.57	0.00	1015.90
SAV	950813/1700	3.00	35.56	23.33	1.54	240.00	1015.20
SAV	950813/1800	3.00	35.00	23.33	1.03	290.00	1014.90
SAV	950813/1900	3.00	36.11	23.89	2.57	220.00	1014.50
SAV	950813/2000	3.00	35.56	22.78	2.57	250.00	1013.80
SAV	950813/2100	3.00	36.11	23.33	3.60	230.00	1013.50
SAV	950813/2200	3.00	35.00	23.33	3.09	250.00	1013.30
SAV	950813/2300	0.00	34.44	22.78	3.09	240.00	1013.20
SAV	950814/0200	-9999	10.00	10.00	0.51	290.00	1008.30
SAV	950814/0400	6.00	21.11	16.11	0.00	0.00	-9999
SAV	950814/0500	0.00	26.67	23.89	2.57	230.00	1014.50
SAV	950814/0600	0.00	26.11	23.89	2.57	230.00	1014.40
SAV	950814/0700	0.00	26.11	23.89	2.06	240.00	1014.20
SAV	950814/0800	0.00	25.56	23.33	0.00	0.00	1013.50
SAV	950814/0900	0.00	25.56	23.33	0.00	0.00	1013.20
SAV	950814/1000	0.00	25.00	23.33	0.00	0.00	1013.00
SAV	950814/1100	0.00	25.00	23.33	0.00	0.00	1013.20
SAV	950814/1200	3.00	25.56	23.89	2.06	290.00	1013.70
SAV	950814/1300	0.00	27.78	23.33	2.06	310.00	1013.80

<u>STN</u>	<u>DATE</u>	<u>SKC</u>	<u>TMPC</u>	<u>DWC</u>	<u>SPD</u>	<u>DRCT</u>	<u>PMSL</u>
SAV	950814/1400	0.00	30.56	23.89	2.06	320.00	1014.20
SAV	950814/1500	0.00	33.33	23.89	2.57	350.00	1014.50
SAV	950814/1600	0.00	35.00	24.44	3.09	350.00	1014.50
SAV	950814/1700	0.00	36.11	24.44	3.09	350.00	1014.20
SAV	950814/1800	0.00	36.11	24.44	3.09	350.00	1013.50
SAV	950814/1900	3.00	36.11	24.44	4.12	340.00	1012.80
SAV	950814/2000	3.00	37.78	25.56	2.06	10.00	1012.50
SAV	950814/2100	3.00	37.22	25.00	3.09	30.00	1012.10
SAV	950814/2200	3.00	36.67	23.89	3.09	0.00	1012.00
SAV	950814/2300	0.00	36.11	23.33	3.09	40.00	1011.60
SSI	950813/0200	-9999	23.33	20.56	1.54	220.00	-9999
SSI	950813/0400	3.00	20.56	13.89	2.06	120.00	-9999
SSI	950813/0500	3.00	28.33	23.89	3.09	220.00	1015.60
SSI	950813/0600	3.00	28.33	23.89	3.09	220.00	1015.60
SSI	950813/0700	0.00	26.67	22.78	2.57	260.00	1014.90
SSI	950813/0800	0.00	25.56	23.33	1.54	290.00	1014.60
SSI	950813/0900	0.00	25.56	22.78	1.03	300.00	1014.60
SSI	950813/1000	0.00	25.00	22.78	2.06	250.00	1014.60
SSI	950813/1100	0.00	25.00	23.33	1.54	320.00	1014.90
SSI	950813/1200	0.00	25.56	23.33	2.06	300.00	1015.60
SSI	950813/1300	0.00	26.67	23.33	2.57	230.00	1015.90
SSI	950813/1400	0.00	29.44	23.33	3.09	350.00	1016.30
SSI	950813/1500	0.00	31.67	23.89	2.06	0.00	1016.30
SSI	950813/1600	0.00	33.33	23.33	2.06	30.00	1015.90
SSI	950813/1700	3.00	32.78	23.89	4.12	140.00	1015.60
SSI	950813/1800	3.00	33.89	25.00	5.14	150.00	1015.20
SSI	950813/1900	3.00	33.89	25.00	5.14	170.00	1014.90
SSI	950813/2000	3.00	33.33	23.89	5.14	130.00	1014.20
SSI	950813/2100	3.00	32.22	23.89	4.63	140.00	1013.90
SSI	950813/2200	0.00	33.33	24.44	5.14	160.00	1013.90
SSI	950813/2300	0.00	32.22	25.00	4.12	180.00	1013.50
SSI	950814/0200	-9999	7.22	5.00	0.00	0.00	1015.70
SSI	950814/0400	6.00	20.56	18.33	2.57	220.00	-9999
SSI	950814/0500	0.00	28.33	24.44	3.09	210.00	1014.60
SSI	950814/0600	0.00	28.33	24.44	4.12	210.00	1014.60
SSI	950814/0700	0.00	27.78	25.56	4.12	240.00	1014.20
SSI	950814/0800	0.00	27.22	24.44	3.09	270.00	1013.90
SSI	950814/1000	0.00	26.67	24.44	3.60	270.00	1013.50
SSI	950814/1100	0.00	26.67	23.89	3.09	280.00	1013.50
SSI	950814/1200	0.00	-9999	24.44	2.57	290.00	-9999
SSI	950814/1300	0.00	28.33	24.44	3.09	310.00	101420
SSI	950814/1400	0.00	30.56	25.00	3.60	340.00	1014.20
SSI	950814/1500	0.00	32.22	24.44	3.60	330.00	1014.20
SSI	950814/1600	0.00	34.44	25.56	3.60	330.00	1014.20
SSI	950814/1700	0.00	36.11	24.44	4.63	330.00	1014.20
SSI	950814/1800	3.00	35.56	22.78	4.12	340.00	1013.90
SSI	950814/1900	3.00	36.11	24.44	2.57	100.00	1012.90
SSI	950814/2000	3.00	35.56	23.33	3.09	150.00	1012.50
SSI	950814/2100	3.00	35.00	22.78	2.57	150.00	1012.20



<u>STN</u>	<u>DATE</u>	<u>SKC</u>	<u>TMPC</u>	<u>DWC</u>	<u>SPD</u>	<u>DRCT</u>	<u>PMSL</u>
SSI	950814/2200	3.00	33.89	24.44	3.09	180.00	1011.90
SSI	950814/2300	3.00	33.33	23.89	2.06	150.00	1011.50

### Buoy

The following are observations from buoy 41022 (number 15) and C-MAN station SLVS1 (number 13) for period 13-15 August 1995 . YY is year, MM is month, DD is day, HH is hour, WD is wind direction in degrees from true north, WSPD is wind speed in  $m s^{-1}$ , GST is wind gusts in  $m s^{-1}$ , BAR is barometric pressure in mb, ATMP is atmospheric temperature in  $^{\circ}C$ , and WTMP is water temperature in  $^{\circ}C$ . Missing data are indicated by 999.0.

#### SVLS1

<u>YY</u>	<u>MM</u>	<u>DD</u>	<u>HH</u>	<u>WD</u>	<u>WSPD</u>	<u>GST</u>	<u>BAR</u>	<u>WTMP</u>
95	08	13	00	183	6.8	7.2	1014.1	29.3
95	08	13	01	194	6.5	6.9	1014.4	29.1
95	08	13	02	201	6.6	7.1	1014.8	29.0
95	08	13	03	206	6.2	6.5	1015.0	29.1
95	08	13	04	214	7.5	7.9	1015.1	29.0
95	08	13	05	227	7.7	8.2	1015.0	29.0
95	08	13	06	231	7.5	8.2	1014.9	29.1
95	08	13	07	250	6.7	7.5	1014.5	29.1
95	08	13	08	259	6.1	6.7	1014.2	28.9
95	08	13	09	261	5.4	5.7	1014.2	28.9
95	08	13	10	263	4.3	4.8	1014.2	28.9
95	08	13	11	292	5.1	5.4	1014.7	28.9
95	08	13	12	301	5.0	5.3	1015.2	28.9
95	08	13	13	322	5.5	5.7	1015.2	28.9
95	08	13	14	312	4.3	4.8	1015.4	28.9
95	08	13	15	291	2.2	2.4	1015.6	29.0
95	08	13	16	276	1.2	1.5	1015.5	29.0
95	08	13	17	211	1.2	1.5	1015.2	29.1
95	08	13	18	191	3.1	3.6	1015.0	29.1
95	08	13	19	196	4.4	4.7	1014.4	29.4
95	08	13	20	195	3.9	4.1	1013.9	30.1
95	08	13	21	191	4.6	4.9	1013.5	29.7
95	08	13	22	192	5.2	5.6	1013.1	29.7
95	08	13	23	197	6.0	6.3	1013.1	29.7
95	08	14	00	197	5.7	6.2	1013.1	29.4
95	08	14	01	194	6.3	6.6	1013.2	29.4
95	08	14	02	204	5.9	7.0	1013.5	29.4
95	08	14	03	210	6.7	7.1	1013.8	29.5
95	08	14	04	216	6.7	7.0	1014.0	29.2
95	08	14	05	222	7.4	8.0	1014.0	29.3
95	08	14	06	236	6.5	7.1	1013.9	29.4
95	08	14	07	241	6.3	6.6	1013.6	29.4

<u>YY</u>	<u>MM</u>	<u>DD</u>	<u>HH</u>	<u>WD</u>	<u>WSPD</u>	<u>GST</u>	<u>BAR</u>	<u>WTMP</u>
95	08	14	08	249	6.4	7.0	1013.1	29.4
95	08	14	09	244	5.8	6.1	1012.7	29.1
95	08	14	10	260	4.8	5.2	1012.6	29.2
95	08	14	11	270	4.8	5.3	1012.8	29.2
95	08	14	12	303	4.6	5.0	1013.2	29.1
95	08	14	13	304	4.7	5.0	1013.5	29.1
95	08	14	14	325	3.7	4.0	1013.5	29.1
95	08	14	15	333	2.9	3.0	1013.8	29.1
95	08	14	16	312	1.2	1.3	1013.7	29.2
95	08	14	17	283	1.2	1.4	1013.5	29.3
95	08	14	18	290	1.4	1.5	1013.1	29.3
95	08	14	19	0	0	.0	1012.5	29.3
95	08	14	20	88	.2	.3	1011.9	29.4
95	08	14	21	70	1.5	1.9	1011.7	29.6
95	08	14	22	109	1.8	1.9	1011.5	29.5
95	08	14	23	118	2.6	2.8	1011.2	29.5
95	08	15	00	133	3.8	4.0	1011.1	30.0

41021

<u>YY</u>	<u>MM</u>	<u>DD</u>	<u>HH</u>	<u>WD</u>	<u>WSPD</u>	<u>GST</u>	<u>BAR</u>	<u>ATMP</u>	<u>WTMP</u>
95	08	13	00	177	5.8	6.8	1013.6	29.0	29.0
95	08	13	01	191	5.5	6.5	1013.8	28.9	29.0
95	08	13	03	201	5.9	7.0	1014.5	28.9	28.5
95	08	13	04	200	6.2	7.2	1014.8	28.5	28.5
95	08	13	05	218	6.2	7.1	1014.8	28.2	28.4
95	08	13	06	233	5.4	6.3	1014.8	27.7	28.2
95	08	13	07	234	6.1	7.6	1014.6	27.5	28.2
95	08	13	08	248	4.7	5.6	1014.2	26.8	28.2
95	08	13	09	258	4.4	5.2	1014.2	26.9	28.3
95	08	13	10	266	4.6	5.5	1014.0	26.8	28.3
95	08	13	11	303	4.4	5.4	1014.5	26.1	28.3
95	08	13	12	297	4.4	5.4	1014.9	26.1	28.2
95	08	13	13	314	3.3	4.3	1015.0	26.8	28.2
95	08	13	14	311	2.3	2.9	1015.0	28.1	28.2
95	08	13	15	283	1.6	2.3	1015.4	28.9	28.4
95	08	13	16	22	1.2	1.7	1015.1	29.7	28.4
95	08	13	17	190	2.0	2.3	1015.0	29.8	29.8
95	08	13	18	170	3.1	3.6	1014.8	29.7	30.0
95	08	13	19	175	4.2	4.7	1014.3	29.7	29.7
95	08	13	20	176	4.1	4.9	1014.1	29.7	29.3
95	08	13	21	176	4.4	5.3	1013.4	30.0	29.7
95	08	13	22	175	4.8	5.4	1012.9	29.8	29.4
95	08	13	23	186	5.4	6.2	1012.7	29.7	29.2
95	08	14	00	180	5.4	6.5	1012.7	29.7	29.2
95	08	14	01	191	5.4	6.2	1012.7	29.2	29.2
95	08	14	03	199	6.0	7.4	1013.4	29.2	29.2
95	08	14	04	201	5.8	6.7	1013.4	29.2	29.0
95	08	14	05	210	6.2	7.4	1013.5	29.2	28.9

<u>YY</u>	<u>MM</u>	<u>DD</u>	<u>HH</u>	<u>WD</u>	<u>WSPD</u>	<u>GST</u>	<u>BAR</u>	<u>ATMP</u>	<u>WTMP</u>
95	08	14	06	222	5.6	6.3	1013.7	28.9	28.5
95	08	14	07	229	4.5	5.5	1013.6	28.5	28.4
95	08	14	08	240	4.6	5.7	1013.3	28.4	28.4
95	08	14	09	231	4.4	5.1	1012.8	28.2	28.4
95	08	14	11	257	3.3	4.1	1012.7	27.4	28.4
95	08	14	12	294	3.9	4.9	1013.1	27.4	28.4
95	08	14	13	307	3.0	3.9	1013.3	27.6	28.5
95	08	14	14	329	3.5	4.3	1013.4	29.2	28.5
95	08	14	15	318	2.0	2.7	1013.5	30.0	28.9
95	08	14	16	17	.6	1.2	1013.4	31.2	29.8
95	08	14	19	348	.2	.8	1012.6	999.0	31.7
95	08	14	20	76	1.0	1.4	1011.9	999.0	31.7
95	08	14	22	145	2.0	2.6	1011.2	999.0	31.7
95	08	15	00	126	3.2	3.9	1011.0	31.7	30.7

## REFERENCES

- Abbs, D. J., 1986: Sea breeze interactions along a concave coastline in Southern Australia: observations and numerical modeling study. *Mon. Wea. Rev.*, **114**, 831-848.
- Anthes, R. A., 1977: A cumulus parameterization scheme utilizing a one-dimensional cloud model. *Mon. Wea. Rev.*, **105**, 270-286.
- Arakawa, A. and V. R. Lamb, 1977: Computational design of the basic dynamical process of the UCLA general circulation model. *Methods in Comput. Phys.*, **17**, 173-265.
- Arritt, R. W., 1989: Numerical modeling of the offshore extent of sea breezes. *Quart. J. Roy. Meteor. Soc.*, **115**, 547-570.
- \_\_\_\_\_, 1993: Effects of the large scale flow on characteristic features of the sea breeze. *J. Appl. Meteor.*, **32**, 116-125.
- Atkinson, B.W., 1981: *Meso-Scale Atmospheric Circulations*. Academic Press, 495 pp.
- Bechtold, P. J-P. Pinty and P. Mascart, 1991: A numerical investigation of the influence of large-scale winds on sea-breeze and inland-breeze type circulations. *J. Appl. Meteor.*, **30**, 1268-1279.
- Bedford, C. D. and R. L. Davis, 1987: Mesoscale analysis and forecasting for the 1987 America's Cup, Freemantle, Western Australia'. *Mesoscale Analysis and Forecasting: Proceedings of an International Symposium*, 669-675.
- Blanchard, D. O. and R. E. Lopez, 1985: Spatial patterns of convection in South Florida. *Mon. Wea. Rev.*, **113**, 1282-1299.
- Cautenet, S. and R. Rosset, 1989: Numerical simulation of sea breezes with vertical shear during the dry season at Cape of Three Points, West Africa. *Mon. Wea. Rev.*, **117**, 329-339.

- Chen, S., J. Dudhai, D. Gill, Y. Guo, K. Manning, D. Stauffer, and D. Witman, 1995: PSU/NCAR Mesoscale Modeling System Tutorial Class Notes. NCAR, 139 pp.
- Estoque, M. A., 1961: A theoretical investigation of the sea breeze. *Quart. J. Roy. Meteor. Soc.*, **87**, 136-146.
- \_\_\_\_\_, 1962: The sea breeze as a function of the prevailing synoptic situation. *J. Atm. Sci.*, **19**, 136-146.
- Finkele, K., J. Hacker, H. Kraus, and R. Byron-Scott, 1995: A complete sea-breeze circulation cell derived from aircraft observations. *Bound.-Layer Meteor.*, **73**, 299-317.
- Forecast Systems Lab. and National Climatic Data Center, 1993: Radiosonde Data of North America 1946-1992, CD-ROM Version 1.0.
- Garza, C., S. Rinard, M. Powell, and P. Hart, 1996: Developing a comprehensive climatological publication for use by the participants during the 1996 Olympic Yachting events. *Conf. on Coastal Oceanic and Atmos. Pred.*, Atlanta, GA, pp 334-335.
- Gould, K. J., 1993: Analysis of the Florida sea breeze circulation using operational doppler weather radar. M.S. Thesis, Dept. of Meteorology, Florida State University, 144 pp.
- Grell, G. A., 1993: Prognostic evaluation of assumptions used by cumulus parameterizations. *Mon. Wea. Rev.*, **121**, 764-787.
- \_\_\_\_\_, J. Dudhia and D. R. Stauffer, 1994. A Description of the Fifth-Generation Penn State/NCAR Mesoscale Model (MM5). NCAR Technical Note NCAR/TN 398 + STR, 121 pp.
- Herbster, C. G., 1996: An observational and modeling study of the Florida Panhandle and Big Bend sea breezes. Ph.D. dissertation, Florida State University, number of pages to be determined.
- Itoh, H. and H. Sugimura, 1989: Numerical experiments on the interaction of ocean and bay breezes. *J. Met. Soc. Japan*, **67**, 411-428.
- Kuo, Y. H. and R. A. Anthes, 1984: Semiprognostic tests of Kuo-type cumulus parameterization schemes in an extratropical convective system. *Mon. Wea. Rev.*, **112**, 1498-1509.

- Lambert, S., 1974: High resolution numerical study of the sea-breeze front. *Atmosphere*, **12**, 97-105.
- Lindsey, C. G., T. S. Dye, P. T. Roberts, and S. E. Ray, 1996: Characteristics of the sea breeze-land breeze circulation observed over the Gulf of Mexico. *Conf. on Coastal Oceanic and Atmos. Pred.*, Atlanta, GA, pp 344-349.
- Lu, R. and R. P. Turco, 1994: Air pollutant transport in a coastal environment. Part I: Two dimensional simulations of sea-breeze and mountain effect. *J. Atmos. Sci.*, **51**, 2285-2297.
- Mahrer, Y., 1985: A numerical study of the effects of sea surface temperature on the sea and land breeze circulation. *Israel J. Earth Sci.*, **34**, 91-95.
- Mahrer Y. and R. A. Pielke, 1977: The effects of topography on the sea and land breezes in a two-dimensional numerical model. *Mon. Wea. Rev.*, **105**, 1151-1162.
- McPherson, R. D. 1970: A numerical study of the effect of a coastal irregularity on the sea breeze. *J. Appl. Meteor.*, **9**, 767-777.
- Meyer, J. H., 1971: Radar observations of land breeze fronts. *J. Appl. Meteor.*, **10**, 767-777.
- Naval Oceanography Command Detachment Asheville, 1992: Marine Climatic Atlas of the World, CD-ROM Version 1.0.
- Naval Oceanography Command Detachment Asheville, USAFETAC OL-A, and National Climatic Data Center, 1992: International Station Meteorological Climate Summary, CD-ROM Version 2.0.
- Neumann, J. and Mahrer, Y., 1974: Evolution of a sea breeze front; a numerical study. *J. Atmos. Sci.*, **28**, 532-542.
- Nicholls, M. E., R. A. Pielke, and W. R. Cotton, 1991: A two-dimensional numerical investigation of the interaction between sea breezes and deep convection over the Florida peninsula. *Mon. Wea. Rev.*, **119**, 298-316.
- Pearce, R. P., 1955: The calculation of a sea breeze circulation in terms of the differential heating across the coast line. *Quart. J. Roy. Meteor. Soc.*, **81**, 351-381.
- Pielke, R. A., 1974: A three-dimensional numerical model of the sea breezes over South Florida. *Mon. Wea. Rev.*, **102**, 115-139.
- \_\_\_\_\_, 1984: *Mesoscale Meteorological Modeling*, Academic Press, 612 pp.

- \_\_\_\_\_ and R. P. Pearce, 1994: Mesoscale Modeling of the Atmosphere. American Meteorological Society, 168 pp.
- Physick, W. L., 1980: Numerical experiments on the inland penetration of the sea breeze. *Quart. J. Roy. Meteor. Soc.*, **106**, 735-746.
- Powell, M. D., 1993: Wind forecasting for yacht racing at the 1991 Pan American Games. *Bull. Amer. Meteor. Soc.*, **74**, 5-16.
- \_\_\_\_\_, S. Rinard, C. Garza, and G. Hoogenboom, 1996: Wind forecasting for the sailing events of the Summer Olympic Games. *Conf. on Coastal Oceanic and Atmos. Pred.*, Atlanta, GA, pp 336-343.
- Rinard, S., M. Powell, C. Garza and G. Hoogenboom, 1996: Marine weather support during the 1996 Olympic Games. *Conf. on Coastal Oceanic and Atmos. Pred.*, Atlanta, GA, pp 331-333.
- Segal, M., R. T. McNider, R. A. Pielke, and D. S. McDougal, 1982: A numerical model simulation of the regional air pollution meteorology of the Greater Chesapeake Bay area - summer day case study. *Atmos. Environ.*, **16**, 1381-1397.
- Seaman, N. L., D. R. Stauffer, and A. M. Lario-Gibbs, 1995: A multiscale four-dimensional data assimilation system applied in the San Joaquin Valley during SARMAP. Part I: Modeling design and basic performance characteristics. *J. Appl. Meteor.*, **34**, 1739-1761.
- Sherman, O. T., 1880: Observations on the height of land and sea breezes, taken at Coney Island. *Amer. J. Sci.*, **119**, 300-302.
- Staff, WSFO Los Angeles, 1983: Background climatological, meteorological, and oceanographic information for the 1984 Olympic Games sailing events. NOAA National Weather Service Western Region, Scientific Services Division, Los Angeles, California, 60 pp.
- Stauffer, D. R. and N. L. Seaman, 1990: Use of four-dimensional data assimilation in a limited-area mesoscale model. Part I: Experiments with synoptic-scale data. *Mon. Wea. Rev.*, **118**, 1250-1277.
- Simpson, J. E., 1994: *Sea Breeze and Local Winds*. Cambridge University Press, 234 pp.
- Steyn, D. G. and I. G. McKendry, 1988: Quantitative and qualitative evaluation of a three-dimensional mesoscale model simulation of a sea breeze in complex terrain. *Mon. Wea. Rev.*, **116**, 1914-1926.

- Stull, R. S., 1993: *An Introduction to Boundary Layer Meteorology*. Kluwer Academic Publishers, 666 pp.
- Wexler, R., 1946: Theory and observations of land and sea breezes. *Bul. Amer. Meteor. Soc.*, **27**, 272-287.
- Williams, D. T., 1969: A preliminary report on 1968 spring season sea breeze fronts that passed the Project Theo basic surface network. Unpublished report from the U.S. Forest Service, obtained from the Savannah, GA National Weather Service Office.
- Yan, H. and R. A. Anthes, 1987: The effect of latitude on the sea breeze. *Mon. Wea. Rev.*, **115**, 936-956.
- Xian, Z. and R. A. Pielke, 1991: The effects of width of landmasses on the development of sea breezes. *J. Appl. Meteor.*, **30**, 1280-1304.
- Zhang, D. and R. A. Anthes, 1982: A high-resolution model of the planetary boundary layer-sensitivity tests and comparisons with SESAME-79 data. *J. Appl. Meteor.*, **21**, 1594-1609.
- Zhong, S. and E. S. Takle, 1993: The effects of large-scale winds on the sea-land-breeze circulations in an area complex coastal heating. *J. Appl. Meteor.*, **32**, 1181-1194.



